UNIVERSITÉ DE STRASBOURG

ECOLE DOCTORALE MSII (ED n° 269)
INSA de Strasbourg (ICUBE)-UMR 7357

PhD-Thesis presented by:

Mrs Loba SAGNOL

Defence: December 15th, 2017

To obtain the title of: **Docteur de l'université de Strasbourg**

Discipline: Civil Engineering

in cotutelle with Hochschule Karlsruhe - Technik und Wirtschaft

---

EXPERIMENTAL AND ANALYTICAL STUDY OF THE REINFORCEMENT OF PAVEMENTS BY GLASS FIBRE GRIDS

Doctoral supervisors:

Mr CHAZALLON Cyrille	Professor, INSA de Strasbourg
Mr STÖCKNER Markus	Professor, Hochschule Karlsruhe

Jury Members:

Examinator:

Mrs HATTAB Mahdia	Professor, Université de Lorraine
Mr. QUEZADA Juan Carlos	Maître de conférences, INSA de Strasbourg

Reviewers:

Mr PARTL Manfred	Professor, EMPA Zürich
Mr HORNYCH Pierre	Directeur de recherches (HDR), IFSTTAR, Nantes

Guest:

Mr DOLIGEZ Daniel	6D Solutions

-

Loba SAGNOL

Experimental and numerical study of the reinforcement of infrastructure by glass fibre grids

Résumé

Cette thèse traite de l'effet des grilles en fibre de verre, utilisées pour renforcer les structures routières, sur la liaison entre deux couches d'enrobés bitumineux, la durée de vie en fatigue et le module de rigidité des éprouvettes cylindriques renforcées, ainsi que sur les déflexions mesurées sur une section de route renforcée in situ.

Des essais de cisaillement (LEUTNER) ainsi que de module et de fatigue (ITT) ont été conduit sur des éprouvettes renforcées et non renforcées en utilisant différentes grilles, différentes emulsion ainsi que différentes quantités d'emulsion. Pour ces essais, une surface de test a été construite in-situ, de laquelle les éprouvettes ont été extraites.

Une section de route in-situ a également été construite, renforcée avec 3 différentes grilles et avec deux sections de références. Les deflexions de la chaussée ont été déterminées avant et après les travaux. Une modélisation de la strucutre a été faites basée sur les résultats des mesures de déflexion.

Mots-clés: Grille en fibre de verre, renforcements, cisaillement, fatigue, module de rigidité, deflexions

Résumé en anglais

This PhD-study evaluates the impact of glass fibre grids, used to reinforced asphalt structures, on the bonding between two asphalt layers, the fatigue life and the stiffness modulus of reinforced cylindrical specimens as well as on the deflections measured on a reinforced in-situ road section.

Shear tests (LEUTNER) as well as modulus-tests and fatigue-tests (ITT) were conducted on reinforced and unreinforced specimens, using different grids, different emulsions and different emulsion quantities. For this tests, an outdoor test-surface was constructed, from which the specimens were extracted.

A in-situ road test section was also constructed, reinforced with 3 different grids and having two reference sections. The deflections of the road were determined before and after the construction works. A modelisation of the structure, based on the deflection measurements, was made.

Kewords: Flexible pavements, glass fibre grids, reinforcement, shear strength, fatigue life, stiffness modulus, deflections

-

Abstract

This PhD-study evaluates the impact of glass fibre grids, used to reinforced asphalt structures, on the bonding between two asphalt layers, the fatigue life and the stiffness modulus of reinforced cylindrical specimens as well as on the deflections measured on a reinforced in-situ road section.

Investigation on bonding, fatigue life and stiffness modulus were done with laboratory tests. The specimens used for the tests were extracted from a two-layered outdoor test surface, consisting of an AC 16 lower layer with a 25/55-55RC bitumen and an AC 11 upper layer with the same bitumen, both layers being quite typical for German road structures. Altogether, 24 different interface options were constructed, using two different emulsions, three to four different emulsion application rates, 4 grids (1, 5, W, N) and reference sections. The determination of the bonding strength was done with the Leutner test, a static destructive shear test implying the shearing of one layer of the specimen with a constant displacement rate of 50 mm/min while the other layer is held. The determination of the fatigue life and the stiffness modulus was made only on the specimens reinforced with grid 1 and 5 with the highest coating as well as on the unreinforced reference sections, also with the highest coating rate. The test used for fatigue and stiffness modulus investigation was the indirect tensile test, during which a cylindrical asphalt specimen is submitted to sinusoidal a cyclic compressive stress on its vertical diametric plane, causing the rupture of the specimen through splitting along the centre in vertical direction.

Regarding the bonding, it was shown that the tests without reinforcement grid reached more important shear strength, that higher application rates resulted in higher shear strengths for the reinforced specimens and that larger strand sections of the grids led to greater shear resistances. Regarding the stiffness modulus, it was shown that the specimens reinforced with grid 5 gave constantly higher results for temperatures from -20 °C to +30 °C compared to unreinforced specimens. It was also observed that the influence of the interface at low temperature caused strongly weakened stiffness modulus compared to uni-layered specimens. Regarding the fatigue life, it was shown that reinforced specimens were able to achieve a longer life cycle compared to unreinforced specimens, but that the difference depends from the test temperature, being more constant for 10 °C than for 20 °C.

Deflections were measured on a French road with a traffic of 300 trucks per day before and after maintenance works, implying the construction of a new AC 10 surface course on the old road structure. Parts of the road were reinforced with different glass fibre grids and overbuilt with 4 cm of the new surface layer, two unreinforced reference sections were built with 6 cm of the new surface layer. Deflections measured after the maintenance work showed an improvement of the deflections on all parts of the roads. Special distinctions of a section, showing that its characteristics (e.g. reinforcement) brought especially good or bad improvements in comparison to the deflections measured on the old structure, could

not be observed.

The deflection results as well as the known characteristics of the layers of the structure were used to model the structure. It was shown that the structures modelled with BISAR gave results near to the actual measured deflections for the unreinforced parts, but that the results calculated on the reinforced parts were higher than the actually measured values. This led to the assumption that the grids had an positive effect on the deflections.

Kewords: Flexible pavements, glass fibre grids, reinforcement, shear strength, fatigue life, stiffness modulus, deflections

Zusammenfassung

Diese Thesis beschäftigt sich mit der Wirkung von Glasfasergittern, die zur Verstärkung von Asphaltbefestigungen für Verkehrsflächen verwendet werden, auf den Verbund zwischen zwei Asphaltschichten, die Ermüdungslebensdauer und den Steifigkeitsmodul von verstärkten zylindrischen Probe-körpern und auf die Auslenkung, die an einem verstärkten in-situ-Straßenabschnitt gemessen werden.

Die Untersuchung des Verbundes, der Ermüdungslebensdauer und des Steifigkeitsmoduls erfolgten durch Labortests. Die hierfür verwendeten Proben wurden aus einer zweischichtigen Außen-Testfläche extrahiert, bestehend aus einer unteren AC 16 Schicht mit einem 25/55-55 RC-Bitumen und einer oberen AC 11 Schicht mit dem gleichen Bitumen, zwei durchaus geläufige Deck- und Binderschichten in Deutschland. Insgesamt wurden 24 verschiedene Grenzflächenvarianten, bestehend aus zwei verschiedenen Emulsionen, drei bis vier verschiedenen Emulsionsquantitäten, 4 Glasfasergittern (1, 5, W, N) und Referenzabschnitte hergestellt und untersucht. Die Bestimmung des Verbunds erfolgte bei allen Probevariation mit dem Leutner-Test, einem zerstörenden Schertest, bei der eine Schicht der Probe mit einer konstanten Geschwindigkeit von 50 mm / min abgeschert, während die andere Schicht gehalten wird. Die Bestimmung der Ermüdungslebensdauer und des Steifigkeitsmoduls erfolgte nur auf den mit Gitter 1 und 5 verstärkten Probekörper mit der höchsten Emulsionsmenge sowie auf den unverstärkten Referenzprobekörper, ebenfalls mit der höchsten Emulsionsmenge. Der Test, der für die Ermüdungs- und Steifigkeitsmoduluntersuchung verwendet wurde, war der indirekte Spaltzugschwellversuch, bei dem eine zylindrische Asphaltprobe einer sinusförmigen zyklischen Druckspannung auf ihrer vertikalen diametralen Ebene unterworfen wurde, wodurch der Bruch der Proben durch die Aufspaltung entlang der Mitte in vertikaler Richtung bewirkt wurde.

Hinsichtlich des Verbundes wurde gezeigt, dass die Ergebnisse von der Referenzproben höhere Scherfestigkeiten aufwiesen als verstärkte Probekörper, dass höhere Emulsionsmengen zu höheren Scherfestigkeiten bei verstärkten Probekörpern führen und dass die Form der Stränge der Gitter die Scherfestigkeit positiv beeinflussen kann. Hinsichtlich des Steifigkeitsmoduls wurde gezeigt, dass die mit dem Gitter 5 verstärkten Proben bei Temperaturen von - 20 °C bis + 30 °C immer höhere Ergebnisse erzielten als die Referenzproben. Es wurde auch beobachtet, dass der Einfluss der Grenzfläche bei niedriger Tem-

peratur zu einem stark geschwächten Steifigkeitsmodul im Vergleich zu homogenen Proben führte. In Bezug auf die Ermüdungslebensdauer zeigte sich, dass verstärkte Proben einen längeren Lebenszyklus als Referenzproben erreichen konnten, dass aber der Unterschied auch von der Testtemperatur abhängt und für 10 °C konstanter als bei 20 °C war.

Die Einsenkungsmessungen wurden auf einer französischen Landstraße mit einem Verkehr von 300 Lkw pro Tag vor und nach einer Erhaltungsmaßenahme gemessen, wobei die Arbeiten den Bau einer neuen AC 10 Asphaltdeckschicht auf dem alten Straßenaufbau als 'Verstärkung im Hocheinbau' bedeutete.

Dabei wurden Teile der Straße mit verschiedenen Glasfasergittern verstärkt und mit 4 cm der neuen Deckschicht überbaut, zwei unverstärkte Referenzabschnitte wurden mit 6 cm der neuen Deckschicht gebaut. Die nach der Erhaltungsmaßnahme gemessene Einsenkung zeigte eine Verminderung der Einsenkungen auf allen Teilen der Straßen. Besondere Unterscheidung eines Abschnitts, der zeigt, dass seine Eigenschaften (z. B. Verstärkung) besonders gute oder schlechte Verbesserungen im Vergleich zu den Auslenkungen gemessen an der alten Struktur hervorgebracht haben, konnte nicht beobachtet werden.

Die Ergebnisse der Einsenkungsmessungen sowie die bekannten Eigenschaften der Schichten des Aufbaus wurden verwendet, um den Aufbau zu modellieren. Es wurde gezeigt, dass der mit BISAR modellierte Aufbau Ergebnisse in der Nähe der tatsächlichen gemessenen Auslenkungen für die unverstärkten Teile lieferte, aber dass die auf verstärktem Teil berechneten Ergebnisse höher waren als die tatsächlich gemessenen Werte. Dies führte zur Annahme, dass die Gitter einen wichtigen positiven Effekt auf den Auslenkung haben können.

Schlüsselworte: Glasffasergitter, Straßenverstärkung, Scherkraft, Ermüdung, Steifigkeitsmodul, Einsenkungsmessung

Résumé

Cette thèse traite de l'effet des grilles en fibre de verre, utilisées pour renforcer les structures routières, sur la liaison entre deux couches d'enrobés bitumineux, la durée de vie en fatigue et le module de rigidité des éprouvettes cylindriques renforcées, ainsi que sur les déflexions mesurée sur une section de route renforcée in situ.

L'étude de la liaison entre les couches, de la durée de vie en fatigue et du module de rigidité a été effectuée en laboratoire. Les éprouvettes utilisées pour cela ont été extraites d'une surface d'essai extérieure à deux couches, consistant en une couche inférieure AC 16 avec un bitume 25/55-55 RC et une couche supérieure AC 11 avec le même bitume, représentant deux structures plutôt typique en Allemagne. Au total, 24 interfaces différentes ont été construites, en utilisant deux émulsions différentes, trois à quatre taux d'application d'émulsion différents, 4 grilles (1, 5, W, N) et des sections de référence. La détermination de la résistance au cisaillement a été effectuée sur toutes les variantes avec le test Leutner, un test de cisaillement destructif impliquant le cisaillement d'une couche de l'échantillon avec un taux de déplacement constant de 50 mm/min tandis que l'autre

couche est maintenue. La détermination de la durée de vie en fatigue et du module de rigidité a été faite uniquement sur les éprouvettes renforcées avec la grille 1 et 5 et le taux d'émulsion le plus élevé ainsi que sur les sections de référence non renforcées également avec le taux d'émulsion le plus élevé. Le test utilisé pour la mesure de la fatigue et de la rigidité a été l'essai en traction indirecte, au cours duquel un échantillon cylindrique est soumis à une contrainte de compression cyclique sinusoïdale sur son plan diamétral vertical, ce qui provoque la rupture des éprouvettes par le biais du milieu dans la direction verticale.

En ce qui concerne le collage, il a été démontré que les essais sans grille de renforcement ont atteint des valeurs de résistance au cisaillement plus importantes, que les taux d'application plus élevés entraînent une résistance au cisaillement plus élevée pour les éprouvettes renforcées et que les grilles ayant des fils avec une section plus hautes peuvent atteindre de plus grandes résistances au cisaillement. En ce qui concerne le module de rigidité, il a été démontré que les éprouvettes renforcées avec la grille 5 donnaient des résultats plus élevés pour des températures de - 20 °C à + 30 °C que les éprouvettes non renforcées. Il a également été observé qu'à basse température, l'influence de l'interface provoque un module de rigidité fortement affaiblie par rapport aux éprouvettes homogènes. En ce qui concerne la durée de vie en fatigue, il a été démontré que les éprouvettes renforcées atteignaient une durée de vie plus longue que les éprouvettes non renforcées, mais que la différence dépend également de la température d'essai, étant plus constante pour 10 °C que pour 20 °C.

Des déflexions ont été mesurées sur une route française avec un trafic de 300 poids lourds par jour avant et après les travaux d'entretien, impliquant la construction d'une nouvelle couche de surface BBSG TM et M classe 3, 0/10 sur l'ancienne structure routière. Quelques parties de la route ont été renforcées avec différentes grilles en fibre de verre sur lesquelles 4 cm de nouvelle couche de surface ont été posée, deux sections de référence non renforcées ont été construites avec 6 cm de nouvelle couche de surface. Les déflexions mesurées après les travaux de maintenance ont montré une amélioration des déflexions sur toutes les parties de la route. La distinction particulière d'une section, montrant que ses caractéristiques (par exemple, le renforcement) aient apporté une amélioration particulièrement bonne ou mauvaise par rapport aux déflexions mesurée sur l'ancienne structure, n'a pas pu être observée.

Les résultats des déflexions ainsi que les caractéristiques connues des couches de la structure ont été utilisés pour modéliser la structure. Il a été montré que la structure modélisée avec BISAR donnait des résultats proches des déflexions mesurées en temps réel sur les sections non renforcées, mais que les résultats calculés sur les parties renforcée étaient supérieurs aux valeurs réellement mesurées. Il en a été conclu que les grilles devaient avoir un effet positif sur les déflexions.

Mots-clés: Grille en fibre de verre, renforcements, cisaillement, fatigue, module de rigidité, deflexions

Acknowledgement

This thesis would not have been possible without the help and support of many people, some of whom I would sincerely like to thank here.

Sincere thanks are due to my doctoral supervisors Professor Cyrille CHAZALLON, INSA de Strasbourg and Professor Dr.-Ing. Markus STÖCKNER, Hochschule Karlsruhe - Technik und Wirtschaft. It was a pleasure for me to work with both of them, as they encouraged me to always give my absolute best, helping me with their useful suggestions, their valuable contributions, their always competent remarks and their guidance before and during the time of my PhD, making the work with both of them inspiring and motivating.

Special thanks also to Juan Carlos QUEZADA GUAJARDO, INSA de Strasbourg, and Daniel DOLIGEZ, 6D Solutions, for their precious mentoring and support, their interesting work, their helpful contributions and the constructive discussions we had.

I am also very grateful to the former and actual members of the GC-E team of the INSA de Strasbourg, comprising Georg KOVAL, Saïda MOUHOUBI, Hossein NOWAMOOZ, Ioana Maria ARSENIE, Andrea THEMELI, Kai LI, Xiaofeng GAO, Peng JING, Quoc Tuan TRINH, Saeid NIKOOSOKHAN, Anicet DANSOU, Laura GAILLARD, Guixian LIU, Xuan Nam HO, Ba Danh LE, Hossein ASSADOLLAHI and Fujiao TANG, as well as to the teams of the institutes IGS and IVI of the Hochschule Karlsruhe, comprising Jochen KÄRCHER, Hartmut HERB, Manuel NIEVER, Sonja CYPRA, Elke HÄUßLER, Tim REUBER and Jan WACHSMANN and the laboratory technicians Kai WÄCHTER, Kevin MÜLLER, Daisy WIEDE and Jan SCHULTE. Thank you for your great work, your friendly advices, your valuable support, your encouragements and the very interesting discussions we were able to have.

Thanks also to Reif GmbH & Co KG for the allocation of space and their help in the construction of the test surface, from which the specimens for the laboratory tests were extracted, and who enabled thereby important parts of the work done in this thesis.
My appreciations also go to the Cerema, and especially to Alain HEBTING and Celine PLATZ, for their precious work, their interesting suggestions and their help for the work on the test road RD4.

I owe my greatest gratitude to my mother Emmanuelle GUERIN for her review of the thesis and the corrections that she provided, and to my whole family and friends, especially Aliénor SAGNOL, Pascal SAGNOL and Julian RYCHERT, for their tireless support and warm encouragements. Without them, this thesis would not have been possible.

I dedicate this thesis to Mr. Frieder ULMER.

Contents

List of Figures

List of Tables

General Introduction

Keeping in mind sustainable development, the building and maintenance of road pavements should take into account the fact that in time some raw materials such as oil by-products are going to be more difficult to find and to extract. In view of the existing road network in Europe, maintenance is becoming a major issue. The ageing road network requires developing affordable ecological solutions to allow a partial, total or graduate rehabilitation of the road.

Grids, especially glass fibre grids, represent an effective and economic solution to reinforce the asphalt structure, increasing its lifetime and slowing down crack propagation. Grids can be installed in new roads or in existing ones. Grids are used as reinforcement to enhance the existing road properties against traction and their resistance to cracking.

Yet, using grids means inserting an additional layer between the two asphalt layers. This additional layer may have a strong impact on the bonding between the two asphalt layers and may lead to a loss of adhesion.
A feeble bonding may lead to a bad transmission of traffic-induced stresses and strains through the layers as each layer must be considered independently instead of having all layers working as a whole. Consequently tensions can occur in the lower parts and compression in the upper parts of every layer.

The subject of this thesis is to study the positive impact of the glass fibre grids on the reinforcement of asphalt structures, the containment of reflective cracks and the increase of the road lifetime, as well as negative impacts of the grids on the bonding between road layers, which may reduce the life time of asphalt structures.

For this investigation, this study is built on five different pillars:

1. A general introduction, explaining the general behaviour of roads and road materials under traffic loads, climate changes and passing time, as well as possible rehabilitation methods for aged pavements

2. A literature review about effects and impacts of glass fibre grids inserted into asphalt structures in order to reinforce them. The review looks at laboratory tests as well as in-situ observations.

3. Three different laboratory tests carried out during this study:

   (a) On the bonding between two aspahlt layer, with and without glass fibre grids at their interface. In this part of the study, the effect of different grids as well as different emulsions and different emulsion application rates is observed.

(b) On the stiffness modulus of reinforced and unreinforced two-layered specimens, determined with cyclic indirect tensile tests

(c) On the fatigue life of reinforced and unreinforced specimens during cyclic indirect tensile tests.

4. Observations made on an in-situ road section before and after maintenance works, during which different grids were installed between the old road structure and the new surface layer.

5. The modelling of the in-situ road section in order to recognize the effect of the glass fibre on the deformations of the road.

Part I

Generals

I.1 Road pavements: Materials and structures

A road usually consists of different layers, bonded to each other to give a complex unit. Each layer has its own function, enabling the structure to reduce the stresses and strains induced by traffic loads and movements.

Basically road structure differentiates between rigid and flexible types. Rigid pavements are generally built using Portland cement as a hydraulically binding agent. This agent enables them to withstand tensions through the strong bonds between particles. The advantages of this pavement type are its stiffness, tensile strength, fatigue resistance and its good resistance to permanent deformation. The strong vulnerability of hydraulically bound materials to temperature change can easily create cracks on its surface and obliges the adding of joints in the concrete.

With 90 % of bitumen bound paved highways [THO 14], this pavement type constitutes the most used form of road structures. Bitumen is a highly viscous liquid or semi-solid form obtained from petroleum. Unlike hydraulic binders, bitumen enables deformations in the structure without breaking the bond between the particles and can afterward find back to its original form, enabling self-healing properties of the bitumen. The advantage of bitumen bound pavements are their stiffness, their resistance to deformation under repeated load and their main insensitivity against temperature changes [THO 14] . Bitumen mixed with aggregates is named asphalt concrete. In this study, the pavement type considered and used is asphalt concrete.

I.1.1 Asphalt concrete

Asphalt concrete is a composite material consisting of bitumen or bituminous binders and aggregates. This mixture can be technically made or found in nature (for example Trinidad asphalt). When technically made, it is important to mix the components in a water free environment with mixing temperature in the range of 150 °C, depending on the bitumen used for the mixture [LAV 03].

I.1.1.1 Bitumen

Bitumen is a dark, heavy-transient complex mixture of different organic substances [STR 09], which is extracted during the reconditioning of different crude oils. Bitumen consists largely of hydrocarbons with small amounts of sulphur, oxygen and nitrogen and traces of

halogens, phosphor, and metals. Bitumen has a colloidal structure where the asphaltene particles are dispersed in the maltene matrix. This colloidal structure gives the bitumen its characteristics such as its temperature dependency and its bond. The elastoviscous properties and the degree of hardness depend on the crude oil used. Bitumen can be modified with polymers such as elastomers and thermoplastics.

I.1.1.2 Aggregates

Aggregates used for asphalt concrete are classified in three groups, depending on their size:

- Coarse aggregate, going from a minimum diameter of 2 mm to a maximal diameter of 45 mm

- Fine aggregates, going from a minimum diameter of 0.063 mm to a maximal diameter of 2 mm.

- Filler, aggregates with a diameter smaller than 0.063 mm.

The shape of the particles is important for the resistance against deformation. An angular shape will lead to a greater resistance.
In order to ensure a water free environment during the mixing with bitumen, the aggregates are preheated in a dryer.

I.1.2 Road structure

I.1.2.1 Different layers of the structure

The different layers of a road structure are shown in figure I.1.1.
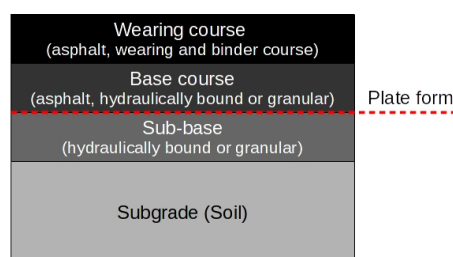
Figure I.1.1: Example of a typical asphalt pavement structure

Starting from the top, the upper layer can consist of two different courses: the wearing course and the binder course.
The task of the wearing course is to enable a safe trafficability of the road. For this, the wearing course has to:

- Ensure a good friction between the surface and the tyres

- Seal the surface against water ingress through the prevention of cracking

- Have a cross slope important enough to discharge water

- Have a stiffness high enough to prevent the creation of rutting.

Some of these points, however, request opposite measures: the prevention of cracks requires flexible and elastic pavement, which however is unfavorable for the prevention of rutting. Finding the appropriate mixture for the wearing course is, therefore, an important task during the road design.

The binder course is used for strongly trafficked pavements and ensures the transmission of the stresses created by traffic loads and movements from the wearing course to the lower base courses. Furthermore, the binder course shall correct unevennesses and irregularities of the base course.

The base course is mainly responsible for the strength of the structure. Its most important task is the absorption of vertical and horizontal stresses caused by traffic. The base course can be divided into different layers, which can be bound hydraulically or by the bitumen or consisting of unbound materials. Layers of unbound materials would be positioned at the bottom of the base course. They can favour the draining or rerouting of water through the course and so be a protection against freezing. In unbounded courses, compressive forces are absorbed through the contacts between the particles. However the absence of cohesion between the particles prevent a good absorption of tensile stresses.
In bitumen bounded base course, the existing cohesion between the particles due to the bitumen as well as the indentation between the particles are responsible for the stability and deformation resistance.

The subbase course is a compacted unbound granular layer whose upper surface serves as plateform for the superstructure. The subbase can help reducing traffic stresses as well as work as a drainage layer. A particular sustainable subbase course can enable a thinner superstructure.

The subgrade is the lowest part of the structure. Usually it is only made of compacted soils. In cases of a soil with low bearing capacity, an exchange or a treatment with lime, cement or other hydraulic binders may be necessary.

I.1.2.2   Interlayer bonding

The bonding between two layers is of crucial importance for the transmission of strains and stresses through the structure and so for the apparent stiffness of the road. The following three major factors constitute the bonding between two layers (see also figure I.1.2):

A) Indentation

Indentation describes the interlocking between grains of the upper and lower layers. The indentation between the layers is created during the compaction of the layers when the aggregates of the upper layer are pressed in the depressions and voids of the lower layer

B) Adhesion

Adhesion depends on the binder type and content of the layers as well as on the emulsion or tack coat used between the layers. Adhesion is particularly important at lower temperature.Its importance decreases at higher temperatures, as the bitumen softens and/or melts

C) Friction

Friction takes place through the contacts of the aggregates of the upper and lower layer and can be impeded by bitumen at the interface [AIF 07]
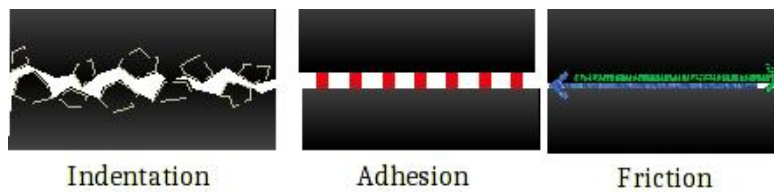
Figure I.1.2: Three factors of bonding: Indentation, adhesion and friction

In case of a debonded interface, as modelised by Wellner and Ascher [AIF 07] (see figure I.1.3), every layer works as a unique layer. This can lead to compressions at the upper part and tensions at the lower part of each layer,thereby inducing the creation of cracks at the bottom of each layer.
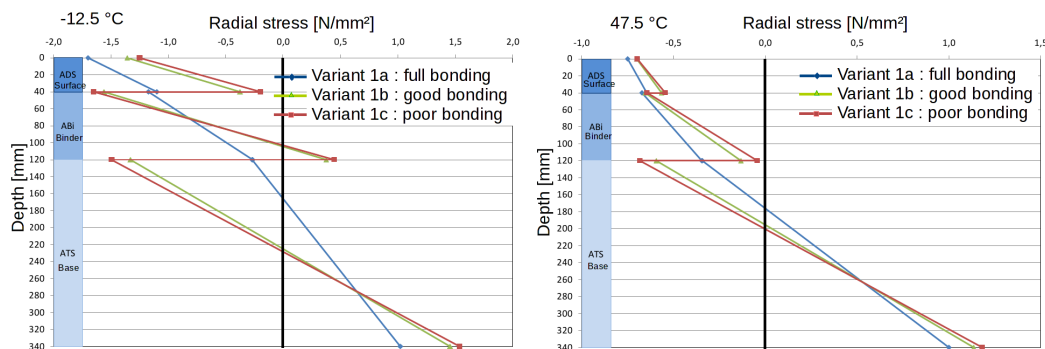
Figure I.1.3: Modelling of the loss of interlayer bonding in a three layered asphalt structure at two different temperatures [AIF 07]

A debonded interface can also enable the intrusion of water between the courses.

A poor interlayer bonding can have several different factors, as summerized Canestrari et al. in their work from 2013 [CAN 13]. These factors can be specific type of base course materials, low compaction of the base course, the sub-base course or the sub-grade, segregation in the base course, the type of bitumen used in the surface course, the climatic conditions during construction, the contamination with dust of the lower layer surface, a water flow between the layers or a poor or excessive tack-coat application.

To ensure a good bonding, different measures can be taken.
The most common form is to use tack coats such as bitumen emulsions on the interlayer, which provides for a better adhesion in addition to the existing indentation. Yet too much tack coat or emulsion can lead to the formation of slip planes on the interface, which can hinder the proper functioning of the indentation.
Bonding can also be improved by milling the lower courses to enhance the indentation or the construction of the layers in hot-on-hot manner, using the compact asphalt method.

I.1.3   Damage mechanisms on road structures

The most important causes of damage to road structures are:

- Traffic: load and movements

- Weather and climate change

- Time

Each of these causes will lead to different sorts of damages which can cause the deterioration of a road.

I.1.3.1   Traffic loads and movements

Traffic loads have two different effects on the structure:

1. Vertical loads through the weight of the vehicles. Vertical loads are transmitted via the tyres of the vehicles and have therefore shapes similar to an ellipse or a circle. A small car can have a wheel load of 1 kN while the maximum wheel load for a truck in Germany is of 57.5 kN (maximum axle load of 11.5 tonnes) and of 67.5 kN in France (maximum axle load of 13.5 tonnes with double wheels). For moving vehicles, the vertical load operates as a dynamic load. The dynamic load proportion is dependent on different factors such as irregularities of the road surface, speed of the vehicles and vehicle construction (suspension, damping and tyres) [VEL 13].

2. Horizontal loads through acceleration and deceleration as well as in ascents and curves

Damages caused by traffic loads and movements induce principally deformation of the road surface and the formation of cracks.

Deformation will appear mostly in form of ruts (see figure I.1.4), describing a longitudinal surface depression of the asphalt in the wheel path. Rutting can have multiple causes, as traffic compaction or displacement of unstable asphalt, base or subgrade consolidation, a low air void design, excessive amounts of asphalt binder, sand, mineral filler or rounded aggregate particles or an insufficient structural strength [LAV 03].

The form of the ruts can show the probable cause: ruts with a small radius are mostly caused by a disorder in the bituminous layers, ruts with a larger radius are mostly the result of a disorder in the soil.

Figure I.1.4: Ruts on a road [AP9 15]

The roads most subject to deformation are the ones with frequent, slow driving or standing heavy traffic as for example the heavy traffic lane of a motorway, the bus lane or parking places for trucks.

The use of certain materials can prevent or retard rutting, for example crushed aggregates, harder binder and polymer modified bitumen. A small bitumen content in the upper layer can also have a positive effect.

The flowing of the materials can also cause deformations due to horizontal movements. Damages caused this way can be observed as slippages at stop lines of junctions, as a result of decelerations.

Cracks are the direct results of traffic caused tensile strains which exceed the tensile strength of the structure. This may be due to a wrongly designed road structure having to bear heavy loads or a great repetition of load passages.

Therefore the most important and decisive factors for the design of a road structure are:

1. Traffic load and number of passages

2. Stiffness modulus of the layers

3. Thickness of the layers

4. Stiffness of the subgrade soil

Cracks induced by traffic passages will mostly appear in or beneath the wheel path and have a longitudinal form with many junctions. In cases of too thin asphalt layers or too soft foundations, the cracks will appear as so called crocodile or alligator cracks.

Cracks appearing in the wheel path are mostly caused by the tension at the bottom of the pavement structure and are cracks that evolve from bottom to the top. The surface directly under the wheel path is subject to compression. Cracks appearing beneath the wheel path are cracks starting from the surface and working their way down.

The distribution of compressions and tensions due to traffic load on a road structure is sketched in figure I.1.5.
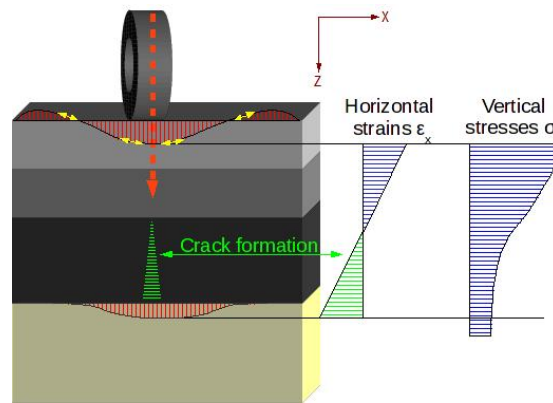
Figure I.1.5: Repartition of stress and strains in a road structure under traffic loading

Cracks appearing on the surface can enable the intrusion of water in the pavement structure. In case of low temperature, this water can become ice. During freezing, the volume of the water expands which can lead to the burst of the pavement, creating potholes.

I.1.3.2   Weather and climate change

Cracks induced by temperature changes can have different causes.

When the temperature drops, the material shrinks. This results in tensions which lead to stresses in the structure. The lack of relaxation ability caused through the non-effective viscous properties of the bitumen at cold temperature induces a slow reduction of these stresses. Tensions and stresses appearing this way are called cryogenic.

When traffic load is applied to the structure, these two types of stress combine to generate cracks appearing as transversal cracks across the full width of the pavement. To prevent such damages, the use of softer or modified bitumen can be useful.

At low temperatures the frost impermeability of the unbound granular layers under the pavement structure is crucial. Otherwise, the capillary action of the granular base course will lead to an increase of water directly under the pavement structure. The result

can be deformations of the upper structure due to the formation of ice packs under it.

Warm temperature can have a negative influence on the deformation properties of bitumen, as described before.

I.1.3.3   Time

Ageing means principally the oxidation of bitumen. This oxidation takes place between polar molecules within the bitumen and free oxygen of the air. It leads in additional cross-linking between the molecules and so to a higher stiffness and an increase in viscosity of the bitumen.

The ageing process can be split into two different time frames. The first one is a short-term frame taking place during the mixing, transportation, installation and compaction of the asphalt and before it is exposed to the traffic. In this first time frame, the bitumen is exposed to high temperatures from blending with the rock aggregates in the asphalt mixing equipment to the completion of the asphalt layers.

The second one is long-term ageing during which the bitumen is exposed to the air on the surface and through the voids inside the structure.

Aged bitumen are accountable for a faster formation of cracks under fatigue loading, as well as a weaker adherence between grains and bitumen. This may result in pull-outs at the surface, affect the adhesion between two layers and weaken the interlayer bonding.

I.1.4   Road maintenance methods

Road maintenance can be differentiate between

1. Superficial repairs

2. Rehabilitation work

3. Renewal of one or more layer

This section only deals with maintenance works carried out on bituminous layers and specifically excludes processing on concrete roads.

I.1.4.1   Superficial repairs

Superficial repairs on asphalt roads are performed in order to maintain acute road safety through minor and preferably fast repairs.

Gritting   Gritting describes the procedure of spraying emulsion and approximately 3 mm size particles on a road. This surface treatment is used to improve the grip between the tyres and the road and can be used to eliminate crocodile cracks and the loss of material.

Use of bituminous sludge's and pore filling mixtures   Bituminous sludge's are products made of bituminous emulsions, filler, additives and water and are used against the loss of material as a result of abrasion.

Asphalt patching and emergency pothole repairs   In these cases, the affected surface is cut out of the road and backfilled with suitable material. This method can be used for surfaces with an excessive accumulation of binder, surfaces showing a loss of granular materials and around potholes.

Crack sealing   The sealing of cracks, open joint and open gaps is done with a bituminous mastic (bitumen and filler) which is poured in the opening, as represented in figure I.1.6. The most effective way to seal a crack is to cut it with a saw first, in order to ensure a good infiltration of the sealing material in the crack. The sealing can be done by hand or using a pump unit.

Crack,
evtl. widened
through sawing

Asphalt surface layer
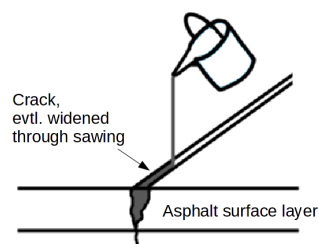
Figure I.1.6: Crack sealing

Roughening of the surface   To roughen or abraide the surface, different methods can be used as precision milling, bush hammering, shot blasting, use of rotating discs and high pressure of water jets. All these measures are used to increase the grip of the surface.

Reprofiling   Reprofinling can be used in case of rutting. The shoulders of the road are levelled by milling a thin part of the surface, as can be seen in figure I.1.7.
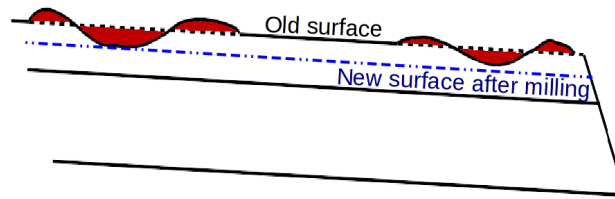
Figure I.1.7: Reprofiling of a surface with deformation due to rutting

Straube and Krass [STR 09] represents the suitability of the used method for different damage forms as shown in table I.1.1.

Table I.1.1: Suitability of repair methods for different damage forms [STR 09]

Condition assessment	Cause	Repair method					
		Gritting	Use of bituminous sludges	Asphalt patching	Sealing	Roughening	Reprofiling
Evenness length profile	Deformation	-	-	0	-	-	+
Evenness length profile	Bearing capacity	-	-	-	-	-	-
Evenness cross profile	Deformation	-	-	0	-	-	+
Evenness cross profile	Bearing capacity	-	-	-	-	-	-
Grip	Binder accumulation	-	-	+	-	+	-
Grip	Polished grain surface	-	-	-	-	+	-
Crocodile cracks		+	0	-	-	-	-
Loss of material		+	+[1]	+	-	-	-
Mends		-	-	+	-	-	-
Pull-outs		-	-	+	-	-	-
Single cracks		-	-	-	+	-	-
+ : suitable; -: limitedly suitable; 0: not suitable [1]: For the improvement of the condition assessment 'Loss of material through abrasion', the process of application of pore filling mixtures is not suitable							

I.1.4.2   Rehabilitation works

Rehabilitation work consists in construction actions made on the existing road surface. It implies surface treatments as surface dressing and the adding of very thin overlays as well as hot in-situ recycling.

Surface dressing   Surface dressing consists in spraying bitumen on the road surface, on which coarse aggregates are then spread. The aggregates are then pressed by using a rubber wheeled roller. The working procedure is outlined in figure I.1.8.
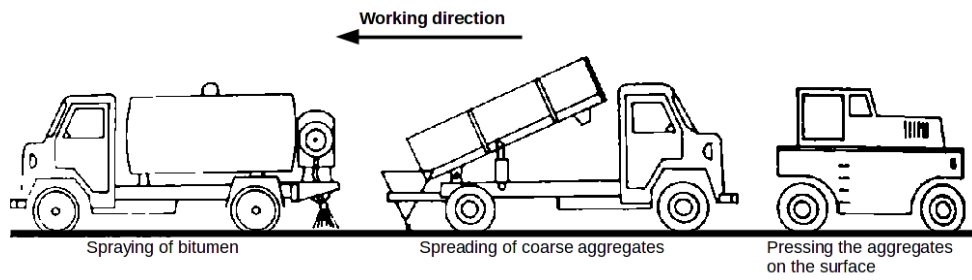
Figure I.1.8: Sketch of the surface dressing [STR 09]

Hot in situ recycling   This methods consists in the repaving of asphalt layers with the already existing materials. For this, the apshalt layer is warmed up, then loosened and then compacted again. In some cases, the existing material is mixed with another, new material during the loosening step. The working procedure is shown in figure I.1.9.
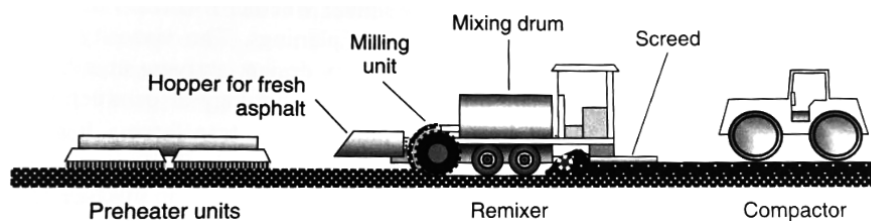
Figure I.1.9: Schematic figure of hot in-situ recycling of asphalt [THO 14]

I.1.4.3   Renewal

Renewal works implies the new construction of one or more layers with a minimal thickness of 4 cm, either on the old structure, or after milling one or more layers of the old structure.
After renewal works, the new surface shows no damages it had before. The quality of the new surface is at it's highest.

I.1.4.4   Alternative maintenance methods: Use of interlayers

The use of interlayer system as increased in the last few decades, as interlayer systems have been showed able to delay crack initiation and propagation through an asphalt structure, even though their mechanical behaviour is mostly not fully understand. In his book 'Principles of Pavemant Engineering' [THO 14], Nick Thom lists the five following interlayer options:

- A geogrid or strong geotextile, prviding actual enhanced strength

- A standard geotextile, acting as a separation layer

- A high durability asphalt layer

- A granular interlayer

- An open-graded asphalt layer

Speaking of geogrids and strong geotextiles, he explains that they can slow down the rate of crack propagation almost by a factor 4. Particularly in the case of thin overlays, most geotextiles are capable of providing a significant degree of reinforcement.

One type of geogrid is the glass fibre grids, a composite material made of glass fibre surrounded by a resin. Glass fibre grids can be installed between a cracked asphalt or concrete structure and a new surface layer. Their purpose is to stop the propagation of the crack through the new layer thus increasing the lifetime of the new pavement.

I.2   Glass fibre grids

Glass fibre grids are composite materials. A composite material is a material consisting of at least two materials, a reinforcement and a matrix, connected in a non-miscible manner and having properties and performances different of the individual component.

I.2.1   Reinforcement

The reinforcement ensures the mechanical strength and the rigidity of the composite material through a strong atomic bond. Typical reinforcements are different types of fibres as for example:

- Glass fibre, with a high resistance against traction and a relatively low density.

- Carbon fibres, with a low density hence a reduced weight and high tensile strengths, which enable their use for example in wind turbines and aerospace market.

- Organic fibres, with mostly a rather low elasticity modulus but sometimes with a very high melting temperature, enabling their use for protective clothing against fire. They are also found in rubber and in pressurized structures.

Fibre reinforcements offer often greater strength and stiffness than the original materials in a compact form. This is mainly due to the difference in size between the fibres and the compact shape, as larger volumes will rather show weak or weakened links. It can also be observed that the size of a defect in a smaller volume can not be as great as in a larger volume.

The reinforcement used in the grids of this study is glass fibre. Glass fibre is an inorganic material whose strength is derived from strong covalent bonds between silica and oxygen. Different types of glass can be used as reinforcing fibres:

- Type E (abbreviation for 'electric'): This type is most often used because of its good value for money, its relatively high Young modulus its good tensile strength.

- Type S (abbreviation for 'strength') & R (abbreviation for 'resistance'). These types have a high young modulus and are mostly used for high performance structures.

- Type C (abbreviation for 'corrosion'): This type has a good resistance to corrosion in acid environments, but has a rather low resistance to traction.

- Type D (abbreviation for 'dielectric')

The glass used in the grids studied in this report is of type E. Some of the properties of glass fibres of this type are shown in table I.2.1:

Table I.2.1: Properties of glass fibres, type E. [RIC 11]

Density	Young modulus	Resistance to traction of one fibre
2.62 g/m^3	73,500 N/mm^2	3450 N/mm^2

To manufacture the fibres, the silica is mixed with other components in order to reduce the melting temperature of the mixture to about 1200 ° C. The liquid glass is then poured into a die with several hundred holes with a diameter of 1 to 2 mm. The filaments exiting this die are then wound rapidly, allowing to stretch them to reduce their section to a diameter of 5 to 15 μm. This rapid change in diameter causes a massive movement in the material from the core to the surface, which helps to remove most of the faults.

I.2.2   Matrix

The matrix plays two key roles: First as a binder between the various components of the material, ensuring the transmission and the distribution of the stresses acting on the material to the reinforcement, secondly as a protection for the reinforcements against possible external aggressions as moisture and to a certain extent against abrasion.

Three types of matrices can be distinguished: the polymer matrix, the ceramic matrix and the metal matrix [BAT 09]. Polymer resins are the most commonly used for the manufacture of composite materials. They can have a viscoelastic behaviour, enabling them to have the properties of a fluid and a solid at the same time.

Polymer resins can be classified into two categories: thermoplastics and thermosetting.

Thermoplastic resins are composed of very rigid chains, due to strong covalent bonds between them. Typical examples of thermoplastics are polyethylene, which is used inter alia for garbage bags, cleaning bottles or insulation for high voltage cables, and polystyrene, used, for example, for yogurt containers or as an insulator.

Thermosetting resins are of relatively low cost. Their manufacturing temperature is rather low, which facilitates their implementation. As they are generally in liquid form, they can easily impregnate the fibres.

Typical examples of thermosetting resins are unsaturated polyesters, also known as UP, epoxides having a very high strength, vinyl esters having a good resistance to corrosion and phenols having a very good resistance to high temperature.

The resin used in the glass fibre grids studied here is a reticulated thermosetting resin of the styrene butadiene type. Some properties of the resin are listed in table I.2.2 .

Table I.2.2: Properties of the resin given by the manufacturer

Resistance to traction	Young modulus	Elongation at break	Bulk density
75 N/mm^2	3200 N/mm^2	1.5 %	1 g/m^3

Part II

Literature Review

II.1 Effect of glass fibre grids and other geosynthetics on fatigue life of the road structure

II.1.1 Prevention of reflective cracks using geosynthetics

Reflective cracking describes the propagation of cracks from an old pavement to a new overlay. According to Nejad et al. [NEJ 14], this is mainly due to the following three types of stresses:

1. Stress due to cyclic thermal expansion and contraction

2. Stress caused by thermal gradient variations

3. Stress due to the loading, which plays the most important part in overlay damage

Zamora-Barraza et al. [ZAM 11] complete the listing by adding as other reflective cracking catalysts differential consolidations and ground contraction. They describe a crack as a discontinuity in a structure which reduces the bending strength of the structure and creates an area of stress concentration, thus leading to a greater magnitude of movements above a crack.

II.1.1.1 Laboratory tests

In their study of 2014, Nejad et al [NEJ 14] investigated the effect of several geosynthetics on the crack propagation by building a multi-layered slab made of an artificially cracked lower layer (made with a fibre saw), an asphalt overlayer with a thickness varying between 50 mm, 75 mm and 100 mm and a geosynthetic positioned between the two layers.
The geosynthetics used in this study were different geocomposites, polypropylene non-woven geotextiles and polyethene non-woven geotextiles.
The slab was loaded under cyclic condition through a circular plate positioned on the top of the slab, above the crack, with a maximum load of 6.79 kN at 10 Hz and with a rest period of 50 ms between the loadings. The test device is illustrated in figure II.1.1.
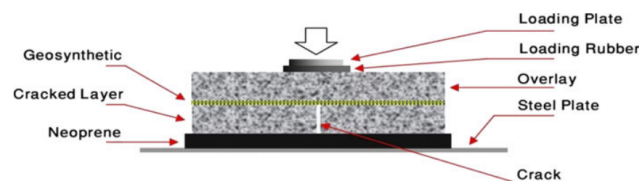
Figure II.1.1: Schematic test set-up used by Nejad et al.

Nejad et al. showed that the use of geotextiles and geocomposites of different moduli was able to improve the pavement resistance against bending mode, which is counted as the most effective mode of failure in reflective cracking. They observed that an increase in geosynthetic modulus in asphalt structures with an overlay of 75 mm to 100 mm could delay crack initiation and reduce vertical crack growth rate, compared to results achieved with unreinforced specimens.

In a thin overlayer (50 mm), the crack growth rate stayed relatively high for all specimens.

Zamora- Barraza et al. [ZAM 11] evaluated the durability of different types of geo-textiles and geogrids as anti-reflective cracking systems and compared them to reference systems without interlayer, using a test device similar to the device in the study of Nejad et al. [NEJ 14].

A slab consisting of two 50 mm thick asphalt layers and an interlayer was subjected to cycling loading through a beam load on the top of the structure, while the lower asphalt layer was cut in order to simulate a 40 mm high crack.

The asphalt layers used in this study were made of an AC16 surf mix with a 60/70 bitumen. The interlayer used were polyester geogrids with and without non-woven geotextiles with non-woven and with un-woven polypropylene fibres and a SAMI. The emulsion used as tack coat was a C69B3, the residual binder content used to coat the interlayer was modified to observe its influence on the durability of the structures.

The test was conducted at 20°C with a frequency of 10 Hz. The loading range went from a maximum load of 19 kN to a minimum load of 3 kN. The failure criterium was chosen as to be the breach of the crack through the surface course.

Zamora- Barraza et al. showed that all anti reflecting cracking systems performed better than the reference system. The most effective interlayer was the geogrid systems, which withstand three to six times more cycles than the reference specimens. It was also observed that geogrids with higher modulus showed better performances and that an increasing geogrid stiffness provided higher resistance to deformations.

Regarding the tack coat content, Zamora- Barraza et al. observed that for structures with polyester geogrids and without reinforcements an optimum content of residual binder could be determined. For contents higher than the determined optimum, the specimens showed lower durabilities. On the other hand, polypropylene geotextiles showed no optimum binder content, but a low influence regarding the tack coat application rate.

Zamora- Barraza et al. reminded that crack propagation is closely related to deformations. This could be seen as reflective cracks could reach the surface of reinforced specimens whereas the geosynthetic materials inside the structure remained unbroken.

Romeo et al [ROM 14] observed the mechanical response of flexible pavements reinforced with fibre glass. To do so, they built multi-layered slabs and beams consisting of a 20 mm thick asphalt lower layer, a glass fibre grid at the interlayer and a 40 mm asphalt

wearing course. The reinforced pavements were subjected then to a static three point bending test.

The nominal maximum aggregate size of the asphalt mixture was 12.5 mm. The bitumen used had a penetration grade of 68-28. The three fibre glass grids used had different mechanical and geometrical properties.

The static three point bending test performed in the study was conducted at a constant application speed of 0.084 mm/s and at a test temperature of 20 °C. The stresses and strains were measured during the test and strain maps of the specimens were drawn.

It was observed that the failure load reached by reinforced specimens was significantly higher than the failure load reached by unreinforced specimens. The use of reinforcements resulted in a strength increase of about 50 %, showing that the reinforcement was able to improve the resistance of the specimens.

The strain maps showed that for reinforced specimens, the strains were mainly concentrated at the bottom layer, showing that the reinforcements acted like a barrier to the crack, as represented in figure II.1.2.
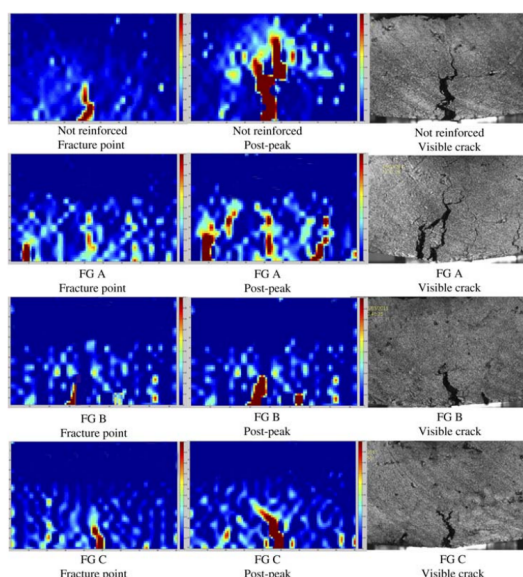
Figure II.1.2: Strain maps of [ROM 14]

Speaking of fracture energy, it was shown that the reinforcement was able to increase the pavement cracking resistance from three to ten times.

Romeo et al. observed that at least three meshes had to be present in the interlayer to achieve representative responses.

To sum up, Romeo et al. showed that the mechanism of reinforcement can occur if the reinforcing material has a stiffness higher than the asphalt mixture and when the reinforcing material has sufficient cross sectional area to strengthen the overlay.

II.1.1.2   Full-scale observations

In their study of 2013, Nguyen et al. [NGU 13] showed inter alia the results of their investigation made on the IFSTTAR APT facility, consisting in testing new reinforced pavements in a full-scale test.

The IFSTTAR APT facility is a large pavement fatigue carousel in Nantes shown in figure II.1.3.

Figure II.1.3: Pavement fatigue carousel at IFSSTAR in Nantes, France [NGU 13]

Two sections were built for the test: one reinforced with high strength open fibre glass grid coated with a patent-pending elastomeric polymer and self-adhesive glue and one reference section without a grid. The pavement structure consisted of a 20 + 60 mm thick bituminous 0/10 wearing course with a 35/50 bitumen, which was built on a granular subbase. The grid was positioned on the 20 mm thick lower layer and the grid sections, as well as the reference sections, were coated with 300 g/m^2 before adding the 60 mm thick upper layer.

The pavement was loaded with 1 million cycles at 65 kN and 200 000 cycles at 70 kN. During the tests, the crack propagation on the two sections was monitored and given as a percentage of the ratio between the length of pavement with cracks and the initial length. After 600 000 cycles, the first cracks were observed on the unreinforced section. After 1.2 million cycles, the extent of cracking on the unreinforced sections reached 70 %, while the reinforced sections showed no cracks at all.

Deflection measurement made with a Benkelman beam at different numbers of load cycles showed no significant differences in deflection between the reinforced and unreinforced sections.

Another part of their study consisted in regarding the reinforcement of a cracked structure achieved through various maintenance methods. For this purpose, Nguyen et al. built three types of new overlays on an old structure consisting of an unbound granular layer, an 80 mm thick, cracked binder course and a 60 mm cracked bituminous course, which had been milled before the installation of the new sections.

The first of these three sections consisted in adding a 40 mm thick surface course to the old

structure. The second structure consisted in placing a glass fibre grid on the interlayer on which a 25 mm thick surface layer was built. The third sections consisted in adding of a 25 mm thick surface layer to the old structure. Both unreinforced sections were coated with a residual binder application rate of 300 g/m^2, the reinforced section with an application rate of 500 g/m^2.

Here again, the crack propagation was monitored. The first cracks appeared after 430 000 loads on the third section (25 mm overlayer, without reinforcement). After 530 000 loads, cracks appeared in the second section (25 mm overlayer, with reinforcement), followed by the first section after 600 000 loads.

The test ended after 3.3 millions of loads. At that point, the first and third sections (both without reinforcements) were totally cracked, whereas section 2 showed only 10 % of cracked surface, indicating that under traffic loading, the reinforcement through the grid is mainly activated during crack propagation, and not during the first crack initiation phase.

II.1.2   Ability of geosynthetics to prevent separation

In their paper of 2012, Vismara et al. [VIS 12] present the results of monotonic indirect tensile strength tests conducted on two-layered cylindrical specimens (of 100 mm diameter and 84 mm height), reinforced in two cases with different polypropene non-woven with glass fibres, horizontally (as shown in figure III.3.3) and a third case were only tack coat was applied on the interface. The asphalt mixture used for the specimens was composed of granular with a nominal maximum size of 11 mm and a bitumen with a penetration grade of 60 [1/10 mm].

The specimens were loaded with a constant displacement of 0.85 mm/sec, while the responding force was measured during 5 seconds. The aim was to destroy all specimens. The tests were carried out at 5 °C and 25 °C.

The force-time graphs obtained showed a steep slope leading to a peak showing the fracturing point of the specimens. The peak is higher and the slope steeper for the specimens without reinforcement.
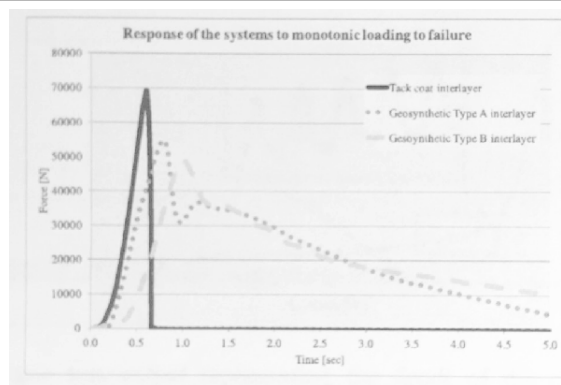
Figure II.1.4: Example of a monotonic indirect tensile tests carried out on reinforced and unreinforced specimens of the study of Vismara et al. [VIS 12]

For unreinforced specimens, the slope after the peak, representing the loss of resistance after fracture, is also very steep, which is typical for brittle fracture.

The slope of the reinforced specimens after the peak is much flatter, showing a rest-resistance of the reinforcement even after fracturing of the asphalt materials. This effect is caused by a bridging effect, showing the ability of the geosynthetic to keep the specimen together.

These tests show that an effect of the grid on indirect tensile tests is visible even for small specimens.

II.1.3   Fatigue life

Virgili et al. [VIR 09] published 2009 a study devoted to repeated load test on bituminous systems reinforced by geosynthetics, in which they compare the flexion behaviour and resistance to repeated loading cycles of reinforced and unreinforced specimens, using a conventional four point bending test.

The slabs tested during the test were two-layered specimens made of the same asphalt mixture with a 12 mm maximum aggregate size and a 70/100 bitumen. The lower layer is a 30 mm thick, the upper layer is a 45 mm thick. The reinforcing materials used were a glass fibre geogrid, a polyester geogrid and a geomembrane. All geogrids were fixed with a cationic emulsion.

Virgili et al. were able to observe that the geomembrane was able to extend service life while keeping low vertical displacement values (measured at mid-length of the beam), which confirmed the stress absorbing function of the geomembrane. They also observed that the glass fibre geogrid as well as the polyester geogrid reached high vertical displacement values, showing that both grids only begin to work when high tensile stresses reach the interface or when a crack grows up to the geogrid. This is the reason why the geogrid should be positioned at places where high tensile stresses are acting.

In their study of 2012, Ferrotti et al. [FER 12] conducted inter alia four point bending tests on reinforced and unreinforced double-layered slabs, using fibre glass grids coated with different treatments as reinforcements.

The layers of the slabs were made with two asphalt mixtures consisting of aggregates with a maximum aggregate size of 10 mm and 14 mm and in both cases an asphalt binder classified as 50/70.

During the test, loading cycles were repeatedly performed on the beams in a stress controlled mode. The load applied on the beam ranged between 0 kN and 3 kN with a frequency of 1 Hz and a test temperature of 20 °C.

Ferrotti et al. observed that the provided resistance of the reinforced specimens was considerably higher than the resistance provided by the unreinforced specimens. They also showed that a better interlayer shear resistance between the layers of the double-layered slabs, due to the different coating treatments, guaranteed a better resistance performance to repeated loading cycles.

In their study of 2016, Arsenie et al. [ARS 16] tested the fatigue behaviour of glass fibre grid-reinforced asphalt concrete beams using 4 point bending tests (4PB tests) and compared it to the behaviour of unreinforced grids.

To do so, they built three-layered asphalt concrete beams consisting of two 25 mm thick asphalt layers on the sides and a 75 mm thick layer in-between. The asphalt mixture used had a nominal aggregate size of 0/10 mm and a bitumen with a 35/50 penetration grade. For the reinforced beams, glass fibre grids were installed on both interfaces, using 600 g/m^2 of residual binder as tack coat.

The total dimensions of the beams were 630 mm x 100 mm x 100 mm.

The 4PB tests were performed under sinusoidal alternating loading conditions and were displacement controlled. The force response and the phase angle were measured.

Arsenie et al. observed that the geogrid was able to increase the fatigue life N_f by 50 % based on individual tests to 62 % based on fatigue curves. They also observed that the tensile strains of the reinforced specimens increased by 10.52 % and the fatigue curve slope increased by 11.55 %.

II.2   Effect of glass fibre grids on the interlayer bonding

In the same study, Ferrotti et al. [FER 12] conducted ASTRA shear tests on unreinforced and reinforced specimens. The ASTRA device ('Ancona Shear Testing Research and Analysis') is a direct shear box in which the cylindrical, double-layered asphalt specimen is positioned so, that the interlayer is positioned in the unconfined interlayer shear zone (see figure II.2.1).
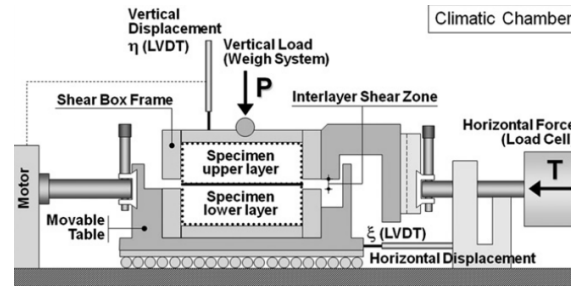
Figure II.2.1: ASTRA device [FER 12]

A constant horizontal displacement rate of 2.5 mm/min is applied to the specimens. The materials used for the tests are the same as before.

Ferrotti et al. were able to observe that the specimens without the grid offered the highest pure shear resistance values, showing that the presence of a grid generated a reduction in interlayer resistance. As Ferrotti et al. also varied the different coating treatments, they could also observe that some surface coatings were able to maximize the interlayer bonding of reinforced specimens.

With this results, Ferrotti et al. were able to confirm other studies showing that the insertion of a geotextile or a grid had a negative influence on the bonding between two layers.

Vismara et al. [VIS 12] characterized in 2012 the effect of geosynthetics in Asphalt pavements at different temperatures.
The samples used for the tests were built under laboratory conditioned and consisted in building cylindrical two-layered asphalt specimens using an asphalt mixture with a nominal maximum aggregate size of 11 mm and a bitumen with a 60 penetration grade. The reinforcement installed in the interlayer were polypropylene non-woven and glass fibres with a tensile strength of 50 kN/mm^2 resp. 100 kN/mm^2.
The investigation of the shear strength was done with the Leutner test, a monotonic shear testing device described in section III.2.1, at 5 °C and 25 °C.
Vismara et al. observed that for both test temperature, the shear strength values of unreinforced specimens were higher than the shear strength values of reinforced specimens.

Dietlind Jacobs summarized in his paper of 2010 [JAC 10] the results of some shear tests made in Switzerland on reinforced and unreinforced specimens, using researches done by Sokolov in 2007 [SOK 07], Raab in 2007 [RAAB 07] and Raab and Partl in 2004 [RAAB 04]. The device used in all tests was an LPDS, standing for 'Layer-Parallel Direct Shear', which function is similar to the Leutner test device.
The two layered specimens used in the tests were made of two asphalt layer (Sokolov 2007) or of an asphalt layer laid on a concrete superstructure (Raab 2004 and 2007). Different

types of reinforcement were used, as carbon fibre grids, steel grids and glass-non-woven. No informations were given regarding the application of tack coat.

He observed that reinforcement at the interlayer reduced the interlayer bonding, showing that only one reinforced specimen was able to reach the required shear force of 15 kN whereas all unreinforced specimens were able to exceed it (see figure II.2.2).
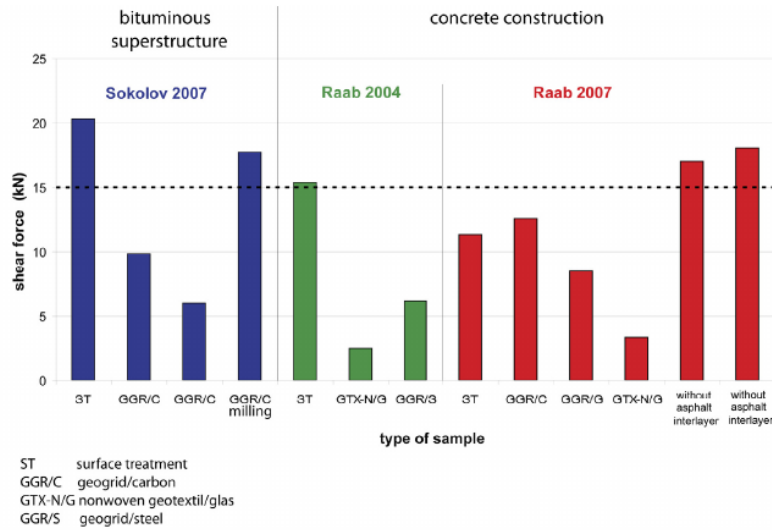
Figure II.2.2: Overview of measured shear forces in different analysis [JAC 10]

In 2016, Raab et al. [RAAB 16] investigated the interlayer bonding of reinforced asphalt pavements and compared values of specimens built in a laboratory to specimens extracted from in-situ surfaces.

The slabs constructed in a laboratory were made of two layers of AC 8 and AC 11 with a thickness of 30 mm each. The cores extracted from the in-situ surface were made of a 40 mm thick AC 11 layer on a 65 mm AC 22 layer. Three types of interlayer were installed between the layers: a glass fibre grids installed with a SAMI (A), a polyester grid (B) and a glass and carbon fibre grid (C). The testing device used for the investigation was the LPDS. The tack coat application rate was not mentioned

The tests of the laboratory cores showed that all specimens were able to exceed a shear strength of 15 kN, while grid B even surpassed the unreinforced specimen.

However, when looking at the in-situ cores, it was observed that, although the ranking of the systems remained similar, the shear strength was weakened.

2010, Zamora-Barraza et al. [ZAM 10] investigated new procedures for measuring the adherence between geosynthetic materials and asphalt layers. To do so, they decided to develop a new test, consisting of 3 layered slabs made of the same asphalt mixture. Geotextiles and tack coat were applied on both interlayers between the asphalt layer. The test consisted of applying a load with a deformation rate of 5 mm/min on the middle

layer, while holding the two other layers (see figure II.2.3).
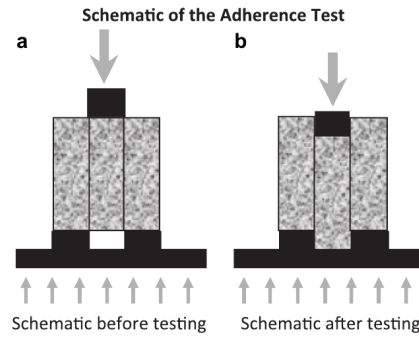
Figure II.2.3: Test device of Zamora-Barraza et al. to investigate the interlayer bonding

The tests were carried out at 15 °C, the asphalt mixture used for the slab manufacturing was an AC 16 with a binder content of 5 %. Five interlayer options were chosen: a reference interlayer without geosynthetic material, a polyester geogrid with unwoven geotextile material, a polyester geogrid material, a glass fibre geogrid material, and a geotextile material. In order to investigate also the influence of the tack coat, the tack coat application rate was varied.

It was observed that the highest shear resistance was obtained for the reference material, followed by the polyester geomesh. For these options, an optimum amount of residual binder was determined, being of about 0.5 kg/m^2 for the unreinforced structure and of 0.35 kg/m^2 for the polyester geomesh (see figure II.2.4). For the other reinforcements, no optimum binder content was found, which was assumed to be so because the test was less sensitive to binder content.
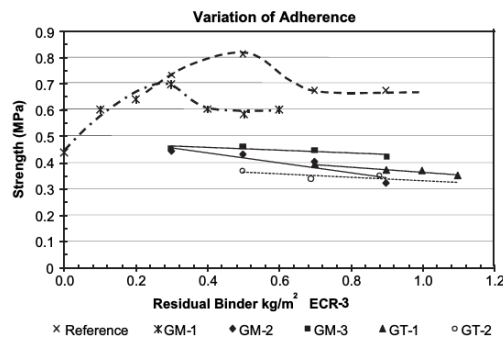
Figure II.2.4: Variation of adherence stress for the reference specimens and the reinforced specimens

2010, Plug and de Bondt [PLUG 10] investigated the adhesion of reinforcement grids in asphalt overlays over the time. Two trial sections were built for this purpose. The first section was built over an existing asphalt pavement, on which a first AC 11 levelling layer was laid, followed by a glass grid coated with two different emulsions and topped with an

AC 16 layer. The second section was also constructed on an existing surface, on which an AC 8 levelling layer was laid, followed by the application of the grids using two different emulsions with two different application rates each and topped with an AC 16 surface course.

Cores with a diameter of 150 mm were extracted 1 month and 1 year after the construction of the test structures. The interlayer bonding of the cores was tested using the Leutner shear test device.

Plug and de Bondt were able to observe that the shear strength could increase up to 3 times over long time observations. They also observed that a high viscosity emulsion can lead to higher interface shear strength and shear stiffness.

II.3   Conclusion: Literature Review

The literature review showed that glass fibre grids and other geotextiles have proven their positive effect on life prolongation and crack prevention.

But it was also observed that the insertion of a glass fibre grid or other geotextile had mostly a negative impact on the shear resistance of an interlayer.

Yet a debonded interface can shorten the lifetime of bitumen, as a working together of the layer is hindered and with it an effective reduction of the stresses induced by traffic loads.

Therefore, the purpose of the following study is to investigate the effects of the different glass fibre grids on the shear strength, the fatigue life, the stiffness modulus and the in-situ comportment.

Part III

Laboratory testing

III.1 Preparation of specimens for laboratory testing

The laboratory testing shall give us information about the characteristics of asphalt specimens reinforced with different grids. The investigation mainly focuses on:

- Influence of the reinforcement on the shear strength:
  These tests are aimed at showing the effects of four different glass fibre grids reinforcements in asphalt specimens submitted to shear strength and compare them to unreinforced specimens, while coated with two different emulsions and with three to four different amount of emulsions. The specimens used for these tests are two-layered cylindrical specimens with a 150 mm diameter and a minimum height of 2 x 40 mm.

- Influence of the reinforcement on the stiffness modulus:
  The specimens tested in this tests were two-layered cylindrical specimens (of 100 mm diameter) with and without glass fibre reinforcement, where the interlayer lays perpendicular to the loading direction.

- Influence of the reinforcement on the fatigue life:
  The specimens tested in this tests are identical to the ones used for the stiffness modulus.

As the number of specimens required to carry out all tests with a minimum amount of 5 repetitions per shear test, 4 per fatigue and cyclic test was very large, it was decided that the specimens should be extracted from an outdoor test surface, built in in-situ conditions.

III.1.1 Characteristics of the glass fibre grids used on the test surface

The test surface was reinforced with four different grids, whose characteristics are listed in table III.1.1.

Table III.1.1: Characteristics of the glass fibre grids installed on the test surface

Grid Name	Non-woven	Resin	Tensile strength	Mesh size
			kn/m	cm^2
1	Light polyester fibre	A	100	4 x 4
5	Light polyester fibre	A	50	4 x 4
W	-	A	50	4 x 4
N	Light polyester fibre	B	50	4 x 4

All grids are from the same manufacturer. The resin of grids 1, 5 and W are the same, whereas the resin of grid N differs slightly, leading to a different form of the strands. The polyester used on grids 1, 5 and N is the same. Grid W is identical to grid 5 but without non-woven, as it was removed from the manufacturing process before the non-woven was glued to it.

A drawing of the grids is shown in figure III.1.1.
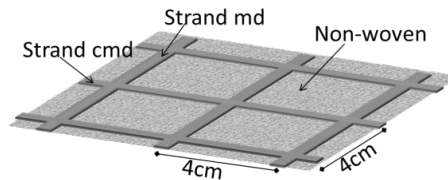
Figure III.1.1: Draft of a grid installed on the test surface

III.1.2   Characteristics of the emulsion C60B4-S and C40B5-S used on the test surface

The two emulsion types used on the test surface are typical bonding emulsion for use between two asphalt layers. The main difference between both emulsions is the content of the residual binder, which is of 40 % for C40B5-S and 60 % in C60B4-S. The lower residual binder content of C40B5-S is compensated through a harder bitumen with a penetration grade of 100 [0.1 mm] and the adding of a fluxing agent which reduces the viscosity.

Table III.1.2: Characteristics of the emulsions used on the test surface

Emulsion		C40B5-S	C60B4-S
Content of residual binder	[%]	40	60
Breaking value		> 180	122
Penetration grade	[0.1 mm]	100	172
Softening point ring and ball	[°C]	46.2	42.8
Fluxing agent to reduce the viscosity	[%]	2 to 3	< 2

For asphalt interlayers, the quantity of C40B5-S which is to be used for the bonding is identical to C60B4-S, independent from the amount of residual binder. The use of C40B5-S is not recommended for the use on interlayers with glass fibre grids, yet is not advised against.

Results of initial tests made by the manufacturer of the emulsions are shown in appendix I.

III.1.3   Dimensions of the test surface

The test surface was 22 m large and 5.8 m wide and was divided in 5 different lanes of 1 m each with a border of 40 cm in the breadth and at least 1 m in the length. An outline of the test surface is shown in figure III.1.2.
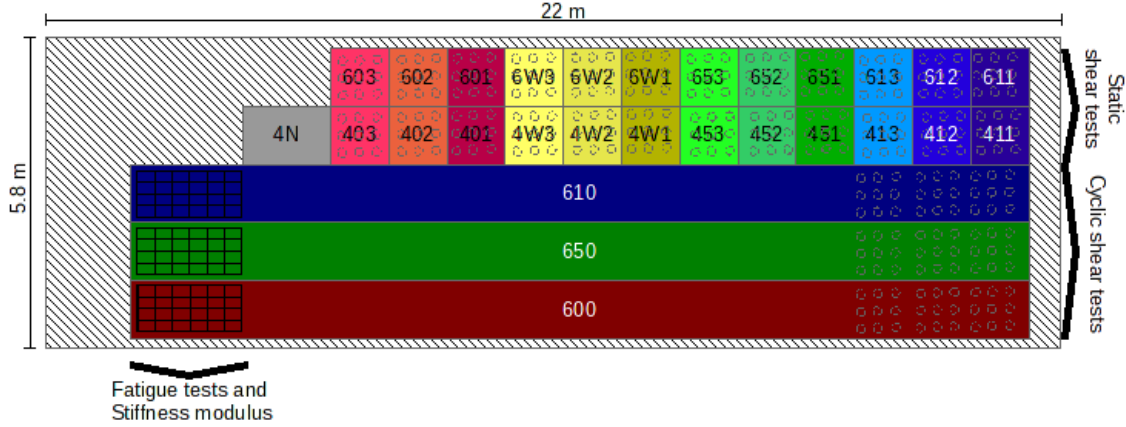
Figure III.1.2: Outline of the test surface

The two upper lanes were planned for the extraction of two-layered cylindrical cores with a 150 mm diameter for static shear tests (Leutner). The lanes were divided respectively into 12 and 13 sections of 1m² with different types of grids as well as different amounts of emulsion used for coating. 3 of the 12 or 13 sections of each lane were prepared as reference sections without grids. 3 different coating variations of types 1, 2 and 3 were used for each grid except for grid N which had only one emulsion application rate and was used only with the emulsion C40B5-S. The application rates varied depending on the grid used in each section, to get under- and over-dosages of the reinforced sections. The application rates used for the unreinforced sections were based on the instructions taken from the German directive ZTV Asphalt-StB 2013 [ZTV 13] except for section 600 which was overdosed. The recommended application rates of the reinforced sections were given by the manufacturer of the grids.

The different application rate corresponding to each section are listed in table III.1.6. The two lanes differed from each other in the emulsion used for the coating. The upper lane was coated with a C60B4-S, the lower lane with C40B5-S. Information about the emulsions are given in table III.1.2

The right parts of the three lower lanes were planned for the extraction of two-layered cylindrical specimens with a 150 mm diameter for cyclic shear tests. The lower layer was made without a grid, the middle layer with grid 1 and the upper layer with grid 5. The emulsion used for coating was C60B4-S. The cyclic shear test was not carried out during this study.

The left parts were for the extraction of rectangular cores (300 mm x 200 mm), from which

cylindrical cores of a 100 mm diameter were to be extracted. These cores were planned for fatigue and modulus testing. The grids and emulsion used in this section were identical to the ones used in the right part of the lanes.

III.1.4 Construction of the test surface

Unbound granular base course The test surface was constructed on an unused space on the premises of the company REIF GmbH & Co KG in Rastatt, Germany.

Four dynamic plate load tests were conducted on the existent unbound granular base course, on which the test surface was to be constructed. These tests were performed with a plate of 300 mm diameter and a load of 10 kg. The results of these tests are listed in table III.1.3.

Table III.1.3: Results of dynamic plate load tests on test surface

	Test 1	Test 2	Test 3	Test 4
Average sinking of the plate [mm]	0.463	0.400	0.406	0.402
Evd [MN/m^2]	48.6	56.3	55.4	56.0
Ev2 [MN/m^2] (= Evd * 2)	97.2	112.6	110.8	112.0

Lower layer - binder course The first layer was made June, 3rd 2015, directly on the unbound granular base course and had the characteristics shown in table III.1.4 (see also appendix I):

Table III.1.4: Characteristics of the lower asphalt layer of the test surface

Lower layer: AC 16 BS - Asphalt concrete, binder course					
		Maximum nominal granular size	[mm]	16
Bitumen type		25/55-55 RC	Void content	[%]	4.9
Ring and Ball	[°C]	63	Bulk density	[g/cm^3]	2.463
Penetration grade	[0.1 mm]	25 to 55	Height of the layer	[mm]	60

Compaction was measured on 4 different points with a TROXLER 4640-B. The final compaction values obtained were as follows: 97.3 %, 97.4 %, 97.8 % and 98.3 %. Pictures of the construction of the lower layer are shown in figure III.1.3.

Coating and application of the different glass fibre grids The coating of the two lower lanes was started on the day of the construction of the binder course. The application of the emulsion was done using a spraying machine. The objective was to spray a quantity of 250 g/m^2 of C60B4-S on the lowest lane and 1000 g/m^2 of C60B4-S on the second lowest lane. However, the application with the spraying machine turned out

Figure III.1.3: Construction of lower layer: Finisher on unbound granular base course, test surface, compaction of the surface

to be more difficult and much less exact than anticipated. The quantities sprayed on the two lanes was much bigger than required. The lowest lane was coated with 1360 g/m² of C60B4-S, the second lowest lane with 2730 g/m² of C60B4-S, which represented a strong over dosage on both lanes. Therefore coating with the spraying machine was suspended. Grid 5 was applied on the second lowest lane before the emulsion broke and pressed on the binder course using brooms.

The coating of the three other lanes took place on June 5th. In order to have a more accurate spreading, the emulsion was applied with painter roller on the middle lane. Grid 1 was applied directly after the spreading of the emulsion and pressed on the binder course using brooms.

For the smaller sections of the upper two lanes, the different amount of emulsion had been weighed and filled in smaller boxes before the construction (emulsion which would remain in the boxes was taken into account in the weighting). In a first step, 2/3rd of the emulsion in the boxes were applied on the respective sections with brushes. The grids were directly applied on the unbroken emulsion. The last third of the emulsion was then spread on the top of the grids and the grids were pressed on the asphalt with brushes.

Upper layer: Surface course   The surface course was made June 6th, 2015. As it had rained during the weekend, the surface of the lower layer was cleared of rainwater with compressed air. The characteristics of the surface course are listed in table III.1.5(see also appendix I). Measurements made with the TROXLER 4640-B gave an average compaction of 97.7 %.

Table III.1.5: Characteristics of the upper asphalt layer of the test surface

Upper layer: AC 11 DS - Asphalt concrete, surface course					
		Maximum nominal granular size	[mm]		11
Bitumen type		25/55-55 A	Void content	[%]	5.59
Ring and Ball	[°C]	63	Bulk density	[g/cm³]	2.288
Penetration grade	[0.1 mm]	25 to 55	Height of the layer	[mm]	60

Extraction of the specimens   The extraction of the different specimens started on June, 10th 2015 with the drilling of the cores with 150 mm diameter. 9 cores were drilled in each section of the two upper lanes and 123 cores were extracted from each other lane. For some cores in the two upper lanes, the drilling broke the bonding between the upper and lower layer, so that the specimens fell apart. This was the case for the following cores:

- Section 4W1: 1 core
- Section 4W2: 2 cores
- Section 4W3: 5 cores
- Section 6W3: 2 cores
- Section 451: 2 cores
- Section 452: 4 cores
- Section 453: 2 cores
- Section 412: 4 cores
- Section 411: 3 cores
- Section 613: 2 cores

Due to this loss, the minimal amount of 5 repetitions for the shear tests could not be met in section 4W3. Here, the missing test was counted with a shear strength of 0 MPa.

The rectangular specimens extracted on the right side of the lower 3 lanes had a width of 20 cm and a length of 30 cm and were cut using a circular saw.

Figure III.1.4 shows pictures of the test surface after drilling and sawing.

Figure III.1.4: Test surface after the extraction of the specimens

The drilling and the resulting loss of specimens gave first impressions about the effects of the glass fibre grids as well as of the emulsion noted. It was noted that the destroyed specimens were all reinforced. It was also noted that most destroyed specimens had been coated with C40B5-S.

Nomenclature   The name of each section is based on the applied emulsion (4 for C40B5-S and 6 for C60B4-S) for the first number, the grid (0 = no grid, 1, 5, W and N) for the second number. The third number represents the emulsio application rate from 0 (highest) to 3 (lowest). All sections with the same grid and the same emulsion are summarized in a section group and have an X instead of an application rate number.

For example:

<p style="text-align:center">6   W   1</p>
<p style="text-align:center">Emulsion C60B4-S Grid W Application rate 1</p>

III.1.5   Characteristics of each section

Table III.1.6: Characteristics of the sections of the test surface

Section group	Name of the sections	Emulsions	Grids	Application rate, residual binder	Recommended application rate (residual binder)
				g/m^2	g/m^2
60X	600 601 602 603	C60B4-S	Reference structure, no grid	816 210 150 90	90-150
61X	610 611 612 613	C60B4-S	1	600 420 360 300	600
65X	650 651 652 653	C60B4-S	5	1636 360 300 240	500
6WX	6W1 6W2 6W3	C60B4-S	W	270 210 150	350
40X	401 402 403	C40B5-S	Reference structre, no grid	140 100 60	80-120
41X	411 412 413	C40B5-S	1	280 240 200	-
45X	451 452 453	C40B5-S	5	240 200 180	-
4WX	4W1 4W2 4W3	C40B5-S	W	180 140 100	-
4N	4N	C40B5-S	N	200	

III.2 Shear tests on reinforced and unreinforced specimens

The shear resistance describes the mechanical resistance of an interface between two layers against stresses acting in the parallel direction. The shear resistance, as well as the shear strength, are used to characterize and quantify the bonding strength between two asphalt layers (see also section I.1.2.2: Interlayer bonding).

Investigation over the interlayer bonding strength can be conducted with different test devices, which can be split into two different groups: destructive tests and nondestructive tests.

The destructive tests can be divided in following subgroups (see also figure III.2.1):

- Torque tests: During this test, both layers are glued to a metal plate. One of them is held while the other is subjected to a twisting load.

- Tensile tests: In this test, one layer is fixed while the other is pulled off in the axial direction. One limitation of this test is its impossibility of measuring any kind of interlocking or friction between the aggregates.

- Wedge splitting tests: This test consists in pushing a wedge in a pre-made notch at the height of the interlayer of the specimen.

- Shear test (with or without normal stress): The shear test consists in holding one layer of the specimen while the other layer is loaded with a constant displacement speed until failure occurs. This test can be conducted with a normal stress applied to the specimen, which is more representative of in-situ loads. An example of a device enabling the application of normal stress can be found in [AIF 07].
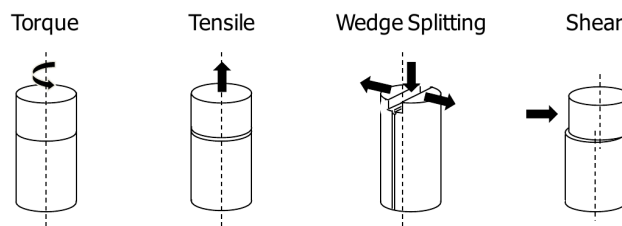
Figure III.2.1: Destructive tests to investigate the interlayer bonding strength [CAN 13]

Non-destructive tests are the Portable Seismic Pavement Analyzer (PSPA), the Colibri Test, the Hammer Test and the Falling Weight Deflectometer.

The test used in this study is the Leutner shear test which is a destructive, monotonic shear test and will be described below.

III.2.1   Leutner shear test

The Leutner shear test is a destructive monotonic shear test with pure interlayer shearing carried out on cylindrical, two-layered specimens with a diameter of (150 ± 2) mm. During the test, the binder course of the core is fixed while the wearing course is loaded with a constant shear displacement rate of 50 mm/min until failure occurs. The displacement, shear force and shear stress are measured during the tests. A schematic sketch, as well as a picture of the machine, are displayed in figure III.2.2.
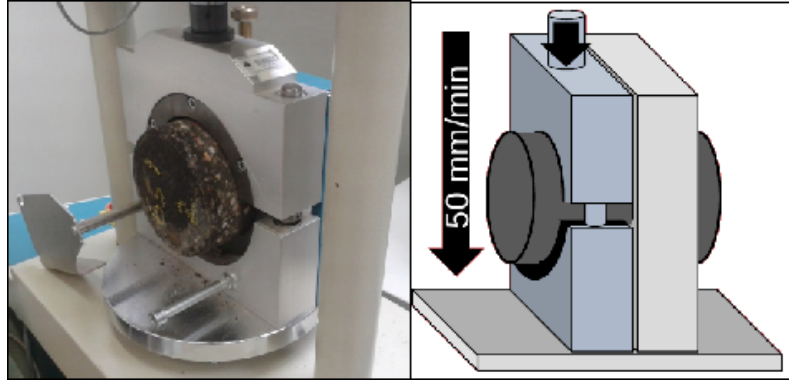
Figure III.2.2: Leutner test: picture and schematic sketch of the machine

The tests were performed according to the German directive TP Asphalt StB Teil 80 - Abscherversuch 2012 [TP-A 12], except for the test temperature which was performed at laboratory conditions at (25 ± 3) °C, as no climatic chamber was available.

III.2.2   Temperature adjustment

In order to enable the comparison of the shear stress results, the temperatures of the different tests were analytically adjusted to 25 °C using the relation proposed by Canestrari et al. [CAN 13] represented by the equation:

$$\tau = 10^{a*T+b} \tag{1}$$

where τ is the shear strength in MPa, T the temperature in °C and a, b coefficients. As the coefficients a and b depend on material parameters, Leutner tests at different test temperatures varying from 4.5 °C to 30 °C were carried out on the specimen types 600, 610 and 650. To ensure the temperature conditioning, the cores were tempered at test temperature for at least 12 hours before the test. The number of tests done for the temperature adjustment is listed in table III.2.1. Figure III.2.3 shows the different results and the regression curve for each section, based on equation 1.

Table III.2.1: Shear tests at different temperatures

Section	Number of tests carried out at different temperatures			
	4.5 °C	10 °C	20 °C	30 °C
600	-	-	4	4
610	3	-	4	4
650	-	2	4	4
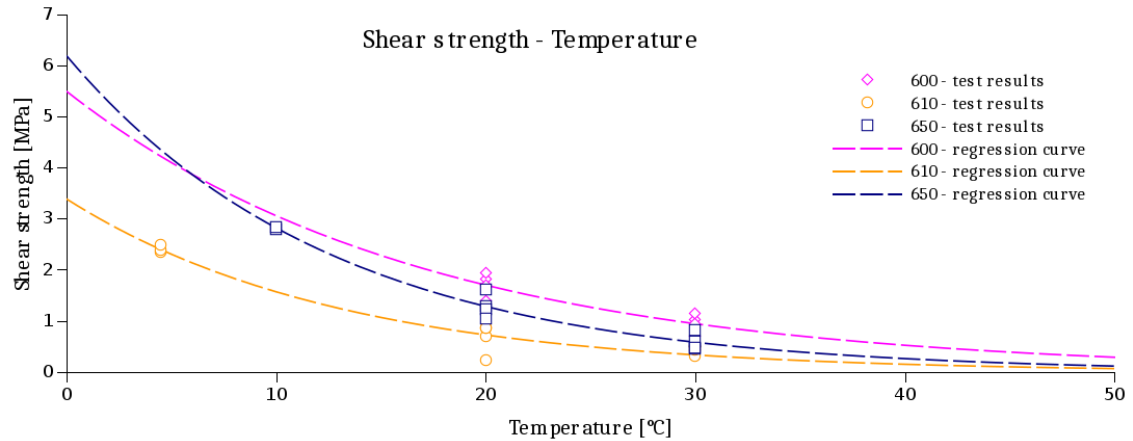
Figure III.2.3: Shear stress determined at different temperature, for sections 600, 610 and 650, with regression curve

The equation of the regression curves obtained were the followings:

- 600: $\sigma = 10^{-0.025*T+0.740}$; $R^2 = 0.81$

- 610: $\sigma = 10^{-0.033*T+0.529}$; $R^2 = 0.96$

- 650: $\sigma = 10^{-0.034*T+0,791}$; $R^2 = 0.96$

The result of 610 and 650 show very similar slopes of -0.033 respectively -0.034. On the other hand, the unreinforced specimens show a very different slope of -0.025. This shows a greater temperature influence on the shear strength of reinforced specimens, meaning that for lower temperatures, the shear resistance is higher when the interface is reinforced with a grid.

The temperature adjustment was performed on all test results which had not been carried out at 25 °C, using for reinforced specimens the mean value of the 610 and 650 slopes, being a = -0.0335 and for unreinforced the slope value a = -0.025.

The difference between the results before and after the temperature adjustment is shown in figure III.2.4.
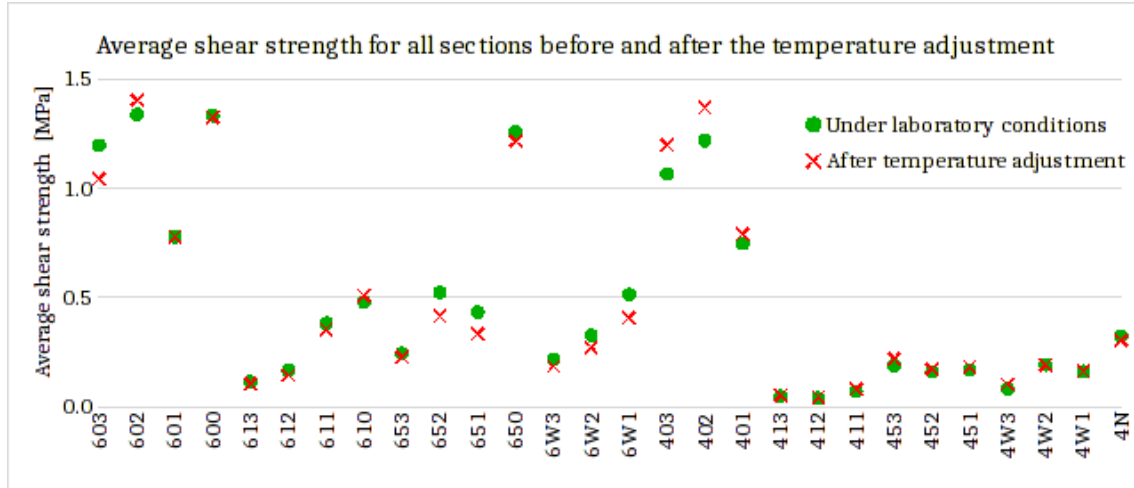
Figure III.2.4: Difference in average shear strength achieved under laboratory conditions and after temperature adjustment

III.2.3   Results after temperature adjustment

The average shear strength of each section, as well as the standard deviation and the coefficient of variation, are listed in table III.2.2 (specimens coated with C60B4-S) and table III.2.3 (specimens coated with C40B5-S). The result of each test can be found in appendix II.

Table III.2.2: Shear strength results of specimens coated with C60B4-S

C60B4-S		Grid	Residual Binder	Number of tests	Average shear strength	Standard deviation	Coefficient of variation
			[g/m^2]		[MPa]	[MPa]	
60X	603		90	5	1.04	0.116	0.112
	602	-	150	5	1.40	0.129	0.092
	601		210	6	0.78	0.183	0.235
	600		816	6	1.32	0.129	0.097
61X	613		300	6	0.11	0.037	0.349
	612	1	360	6	0.14	0.058	0.406
	611		420	6	0.35	0.110	0.311
	610		600	5	0.51	0.059	0.117
65X	653		240	6	0.23	0.041	0.180
	652	5	300	6	0.41	0.121	0.292
	651		360	6	0.33	0.094	0.281
	650		1638	8	1.22	0.312	0.257
6WX	6W3		150	6	0.18	0.109	0.594
	6W2	W	210	6	0.27	0.083	0.308
	6W1		270	6	0.41	0.072	0.176

Table III.2.3: Shear strength results of specimens coated with C40B5-S

C40B5-S		Grid	Residual binder	Number of tests	Average shear strength	Standard deviation	Coefficient of variation
			[g/m^2]		[MPa]	[MPa]	
	403		60	6	1.20	0.230	0.192
40X	402	-	100	6	1.37	0.362	0.265
	401		140	6	0.79	0.256	0.324
	413		200	5	0.05	0.043	0.820
41X	412	1	240	5	0.04	0.026	0.603
	411		280	6	0.08	0.031	0.382
	453		160	6	0.22	0.048	0.22
45X	452	5	200	5	0.17	0.046	0.269
	451		240	5	0.18	0.031	0.170
	4W3		100	5	0.10	0.085	0.822
4WX	4W2	W	140	6	0.19	0.127	0.663
	4W1		180	6	0.16	0.095	0.589
4N	4N	N	200	6	0.30	0.073	0.242

III.2.3.1   Graphical representation of the results

The average shear strengths achieved by each section for a given quantity of residual binder are shown in figure III.2.5 (see also appendix II). The orange curves represent the sections coated with C40B5-S and the blue curves the sections coated with C60B4-S.
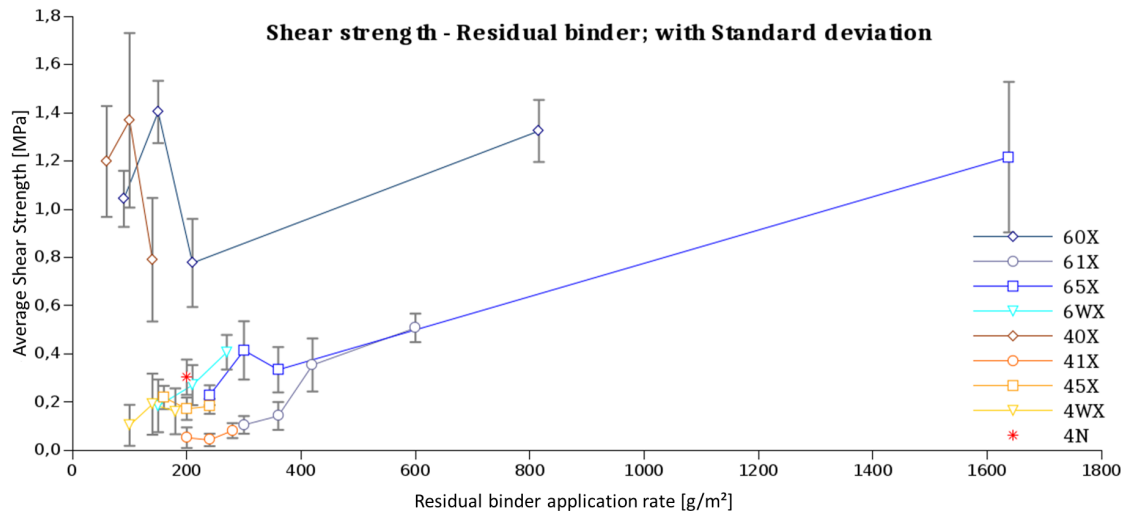
Figure III.2.5: Average shear strengths against residual binder application rates with standard deviation

A first glance shows a considerable difference in shear strength between the unreinforced specimens on the left upper side and the reinforced specimens on the left lower side.

It can also be observed that only section 650 can reach values as high as the maximum of the unreinforced sections.

In the following study, the results will be observed under different aspects:

- Influence of the glass fibre grids

- Influence of the emulsion application rate

- Influence of the emulsion type

- Influence of the non-woven

- Influence of the resin respectively the form of the strands

III.2.3.2   Observations made on the interfaces of the specimens after the tests

After the tests, the specimens were broken apart in order to analyse the interface. Observations were made on the state of the interface (evenness, presence of dirt) and on the positioning of the grids and non-woven for reinforced specimens.

A successful shear test is recognizable by the appearance of the interface which should be even and clean as well as by the appearance of the specimens halves, which should show no pressure area on their sides. Examples of the described phenomenon can be found in figure III.2.6.

(a) Interface as it should be (Specimen 601-1)

(b) Pullout on the side of a specimen (602-4)

Figure III.2.6: Interfaces after testing: (a) smooth interface, (b) Pull out on the side, sign of a pressure area next to the actual interface

The existence of a pressure area beside the interface is also visible in the test result of the specimens, as the shear strength varies considerably from the other specimens of the same section. The specimen 602-4, for example, achieved a shear strength of 0.89 MPa, whereas the other specimens of the section achieved an average shear strength of 1.40 MPa. Specimen 413-8, on the contrary, achieved a shear strength of 0.58 MPa whereas

the average shear strength of section 413 is 0.05 MPa.

The results of specimens showing a pressure area beside the interface were removed and not taken into account in further investigation.

Behaviour of the grid   In 81.5 % of the cases, it was observed that the grid stayed glued to the binder course (lower layer). Only 16.1 % of the reinforced specimens had the grid glued on the surface course (upper layer) and 2.4 % of the reinforced specimens had parts of the grids on both sides. The specimens in which the grid was glued to the surface layer were specimens from the section 4N (6 of 6 specimens), 650 (8 of 8 specimens), 610 (4 of 5 specimens) and 611 (2 of 6 specimens).
Specimens showing parts of the grid on both sides were from the section 4W1 (2 of 6 specimens) and 4W2 (1 specimen).
Examples of the described interfaces are shown in figure III.2.7.

(a)Grid on BC: 651, left SC, right BC   (b)Grid on both sides: 4W1, left SC, right BC

(c)Grid on SC: 610, left SC, right BC   (d)Grid on SC: 4N, left SC, right BC
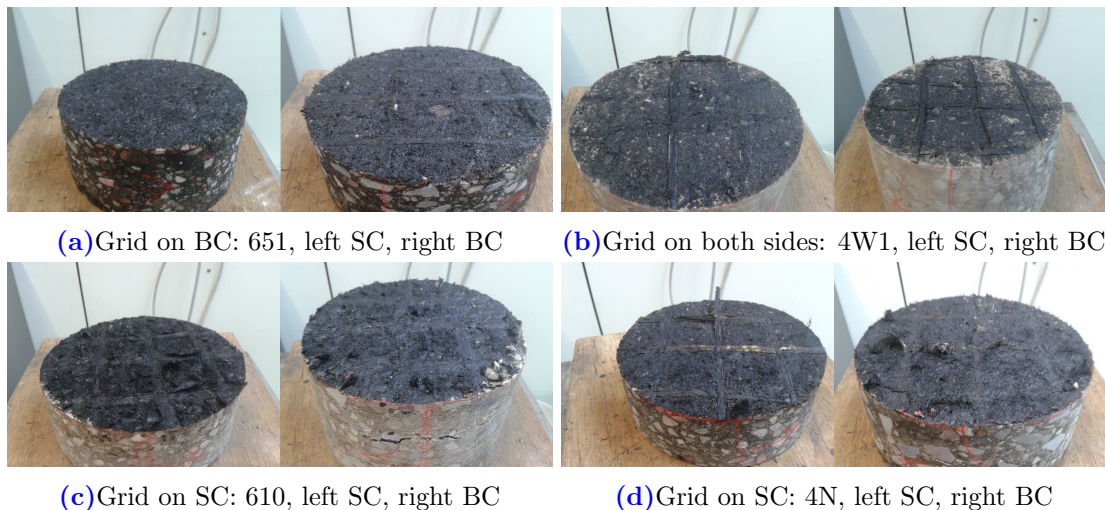
Figure III.2.7: Position of grids on the interfaces of different specimens: (a): Grid glued on BC (81.5% of the specimens), (b): Grid on both sides (2.4 %), (c) and (d): Grid on surface course (16.1 %)

Behaviour of the non-woven   In most cases, the non-woven stayed glued on the binder course. 17 specimens (13.7 % of the reinforced specimens) however showed the non-woven torn between the surface and the binder course. An example of a torn non-woven can be seen in figure III.2.7d.
Torn non-woven were found especially on specimens of section 411 (4 of 6 specimens), 4N (6 of 6 specimens) and 611 (4 of 6 specimens). The sections 413, 451 and 650 showed each 1 specimen with a torn non-woven.

Dirt on the interface   Dirt and dust found on the interface of the specimens could come from two possible sources:

- Dirt came on the interface during construction, e.g. with construction machines

- Dirt came into the specimen during drilling because of a porous interface.

The spread of dirt in the interface gives indication on its source.

Dirt that was already on the binder course before the surface course was made is positioned on the whole surface while dirt coming from drilling is mainly positioned at the edge of the interface, letting the middle largely dirt-free.

The specimens tested in this study showed only signs of dirt coming from drilling. Some example are shown in figure III.2.8. A degree of dirt-contamination ($^{\circ}_{DC}$)was established, with degree 0: no contamination, degree 1: light contamination, degree 2: medium contamination and degree 3: strong contamination. Intermediate degrees were also possible.

(a)Dirt on BC of specimen 452-7: degree 1   (b)Dirt on BC of specimen 453-3: degree 2   (c)Dirt on BC of specimen 4W3-1: degree 3

Figure III.2.8:   Dirt on the interface of some specimens with respective dirt-contamination degree

Table III.2.4 as well as appendix II lists all specimens showing some dirt on their interface and their respective dirt contamination degree. It was observed that the specimens with high dirt-contamination degrees ($^{\circ}_{DC} \geq 1.75$) were mostly bound with the C40B5-S emulsion (63 %).

It was also observed that 91.6 % of the specimens, in which dirt was found, were reinforced specimens. This amount increased to 100 % when looking only at high dirt-contamination degrees ($^{\circ}_{DC} \geq 1.75$).

When looking at the emulsion application rate, it can be noted that 23.6 % of specimens showing a dirty interface had the application rate 1, 34.7 % the application rate 2 and 41.7 % the application rate 3. When looking only at the higher degrees ($^{\circ}_{DC} \geq 1.75$), we find 24.5 % of application rate 1, 34.7 % of application rate 2 and 40.8 % of application rate 3.

Keeping in mind that the intrusion of dirt during drilling is mainly due to voids at the interface, we can already conclude that the amounts of voids at the interface is especially high for reinforced specimens coated with emulsion C40B5-S and an application rate 3. In contrast, high application rate (application rate 0), as well as unreinforced specimens, are not represented or under-represented in the listing.

Table III.2.4: Specimens and their respective dirt contamination degree $^\circ_{DC}$

$^\circ_{DC}$	Specimens						
3	4W3-1						
2	412-4	412-9	413-1	413-2	413-3	413-7	4W1-4
	4W2-4	4W2-7	4W3-2	4W3-7	611-7	612-4	612-5
	613-2	613-5	6W3-1	6W3-4			
1.75	412-8	613-7					
1.5	411-5	411-6	452-7	4W3-6	603-4	612-9	
1.25	453-5	4W1-2	4W1-6	612-2			
1	403-4	412-3	412-6	451-2	451-5	453-8	4W1-5
	4W1-7	4W2-1	611-1	611-2	612-3	612-8	6W2-8
0.75	4W2-9	653-2					
0.5	413-5	603-3	603-6	613-6	613-9	651-4	652-1
	653-4	6W2-9	6W3-9				
0.25	452-8	453-2	4W1-9	4W2-2	4W2-3	601-6	603-2
	651-7	652-6	653-9	6W1-6	6W2-4	6W2-5	

Residual binder quantity Interfaces of section 600 and 603, 610 and 613 and 650 and 653 are shown in III.2.9.
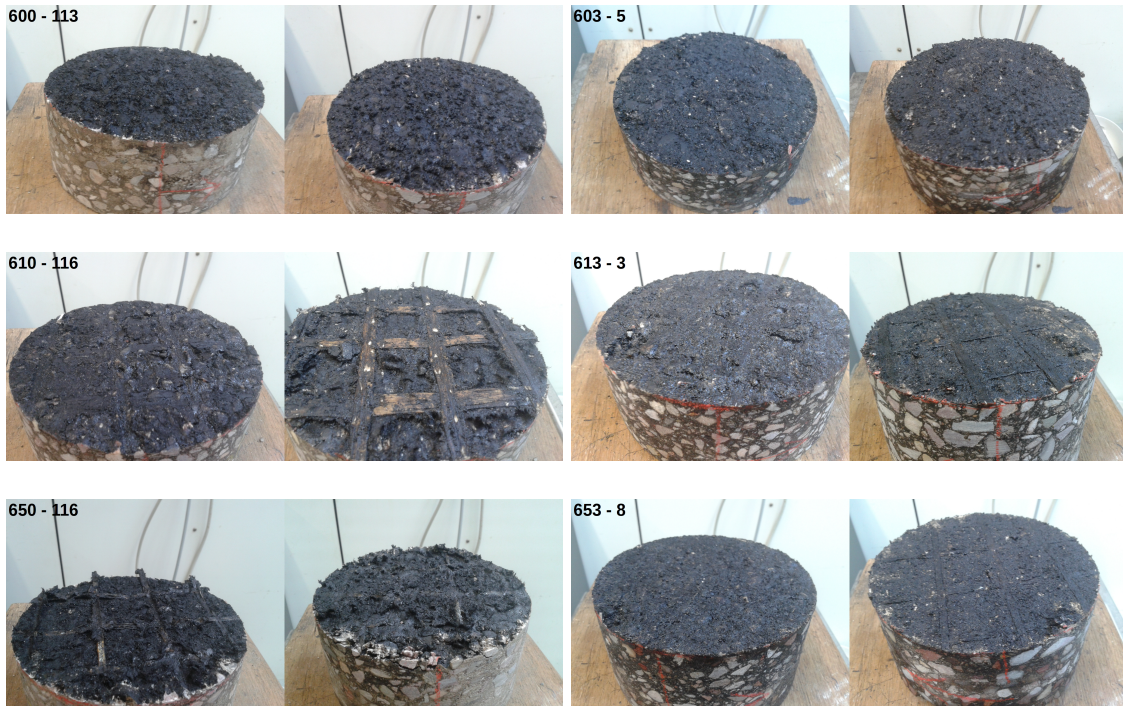
Figure III.2.9: Interfaces with high (0, left column) and low (3, right column) application rates (left of one picture: SC, right BC). First row: 60X, second row: 61X, third row: 65X

The difference in residual binder quantity on the different interfaces becomes visible

in the loss of evenness for the reinforced specimens, which can be due to the tearing of the non-woven. The difference in application rate was also noticeable by touching of the specimens, as specimens with higher contents of emulsion were still sticky.

III.2.4   Discussion of the results

III.2.4.1   Influence of glass fibre grids on the interlayer bonding

In figure III.2.10 the reinforced and unreinforced sections are marked. As mentioned before, it can be seen that no reinforced section (red box) can reach the minimum average values of the unreinforced sections (green box), apart from the strongly overdosed section 650 (1638 g/m^2 of residual binder).
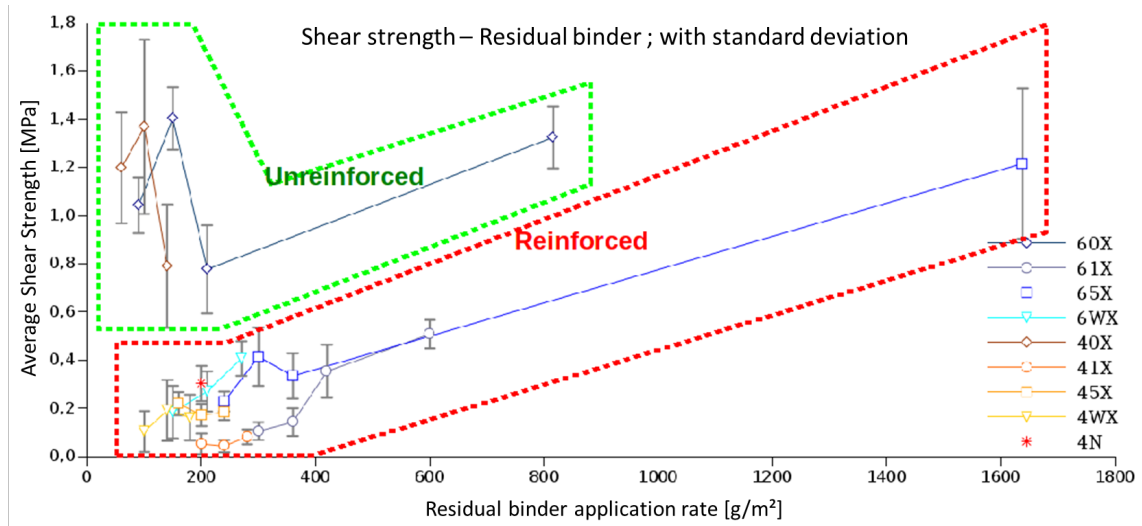
Figure III.2.10: Shear strength against residual binder with standard deviation with markings of reinforced and unreinforced sections

These results confirm the previous studies of Vismara et al. [VIS 12], Sokolov [SOK 07] and Ferrotti et al. (see section II.2)

As no recommendation about the use of C40B5-S is made on the reinforced section, comparison of the shear strength values of the sections coated with C60B4-S was made. The recommended application rates of the sections without grids as well as of the reinforced sections with the grids 1, 5 and W are listed in III.2.5 together with the corresponding shear strength achieved for the residual binder values. The last column shows the loss in shear strength compared to the section without a grid. A loss of at least 60 % can be observed on the reinforced sections compared with the reinforced section.

Table III.2.5: Loss in shear strength due to the insertion of grids in compared with unreinforced specimens

Grid	Recommended application rate (residual binder, C60B4-S)	Shear strength (5 & W: extrapolation)	Loss in comparison to 'no grid'
	[g/m^2]	[MPa]	[%]
No grid (0)	150	1.40	-
1	600	0.53	62
5	500	0.46	67
W	350	0.54	61

One year after the tests, the manufacturer increased the recommended residual binder application rates for the grids used in this study by 100 g/m.

III.2.4.2   Influence of the residual binder application rate on the interlayer bonding of reinforced and unreinforced sections

(a) (b) (c)
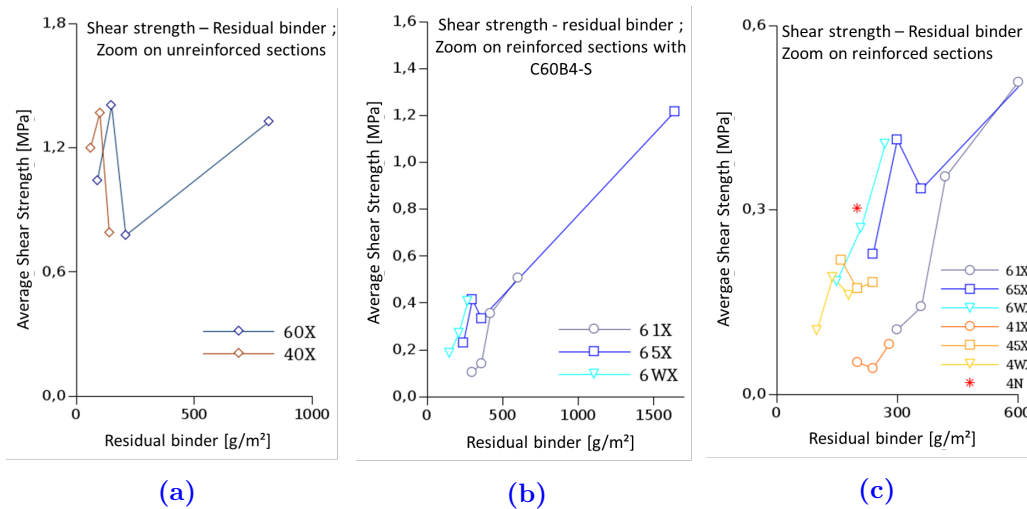
Figure III.2.11: Shear strength - Residual binder: A: Zoom on unreinforced sections 60X and 40X; B: Zoom on reinforced sections coated with C60B4-S; C: Zoom on reinforced sections

The observations made on the influence of the application rate can be divided into three points: influence on unreinforced sections (figure III.2.11a), influence on reinforced sections coated with C60B4-S (figure III.2.11b) and influence on all reinforced sections with low application rates (application rates 1 to 3, figure III.2.11c).

Figure III.2.11a shows the influence of residual binder of both emulsions on the bonding

between two layers without reinforcement. A first glance shows that the behaviour of both emulsions is very similar. For the lowest application rate, the shear strength observed is already above 1.0 MPa, which is mainly due to the interaction between the grains of both layers. By adding residual binder, the bonding strengthens until it reaches a maximum of about 1.4 MPa for application rates of 100 g/m^2 for C40B5-S (section 402) and 150 g/m^2 for C60B4-S (section 602). After these points, the bonding strength drops considerably to values slightly under 0.8 MPa. This effect is mostly explained by the creation of a slip plane caused by a surplus of residual binder, as described by Canestrari et al. [CAN 13]. This slip plane hinders the interlocking of the grains between the upper and lower layers by creating an interlayer, preventing the bonding of the layers.

However, section 600 with an application rate of 816 g/m^2 reaches an average shear strength of 1.32 MPa, which is almost as high as the peak value of 602. Here it seems that the loss of interlocking is compensated by a stronger adhesion due to the high amount of residual binder between the layers.

Figure III.2.11b showsthe reinforced sections coated with C60B4-S, being 61X, 65X and 6WX. It can be observed that all three sections show a tendency of 'more is more', meaning that the adding of residual binder improves the shear resistance of these specimens. Only section 652 seems to fall out of the series.

The general tendency for greater shear stress results with greater application rates can also be seen in their linear correlation coefficients, which are of 0.98 for 65X and 6WX, suggesting a nearly perfect linear correlation, and of 0.92 for 61X.

The zoom on all reinforced sections (except section 650) in figure III.2.11c shows the difference between sections coated with C60B4-S and sections coated with C40B5-S. As mentioned before, sections coated with C60B4-S show that the use of more residual binder leads to higher shear resistance values. Sections coated with C40B5-S show, on the contrary no tendency at all.

III.2.4.3   Influence of the emulsion type on the interlayer bonding of reinforced and unreinforced sections

The differences between the emulsions C60B4-S and C40B5-S are listed in III.1.2. The comparison between sections coated with C40B5-S and C60B4-S is based on the use of the same amount of emulsion, which results in different contents of residual binder, as C40B5-S has only 40 % and C60B4-S 60 %.

For the unreinforced specimens (figure III.2.12a), the use of a harder bitumen and the adding of the fluxing agent used in C40B5-S results in very similar shear strengths as well as a similar curve progression compared to the specimens coated with C60B4-S. A shear strength peak is visible for both emulsion types at 100 g/m^2 respectively 150 g/m^2 residual binder. This suggests the creation of a slip plane for both emulsions.

(a)   (b)
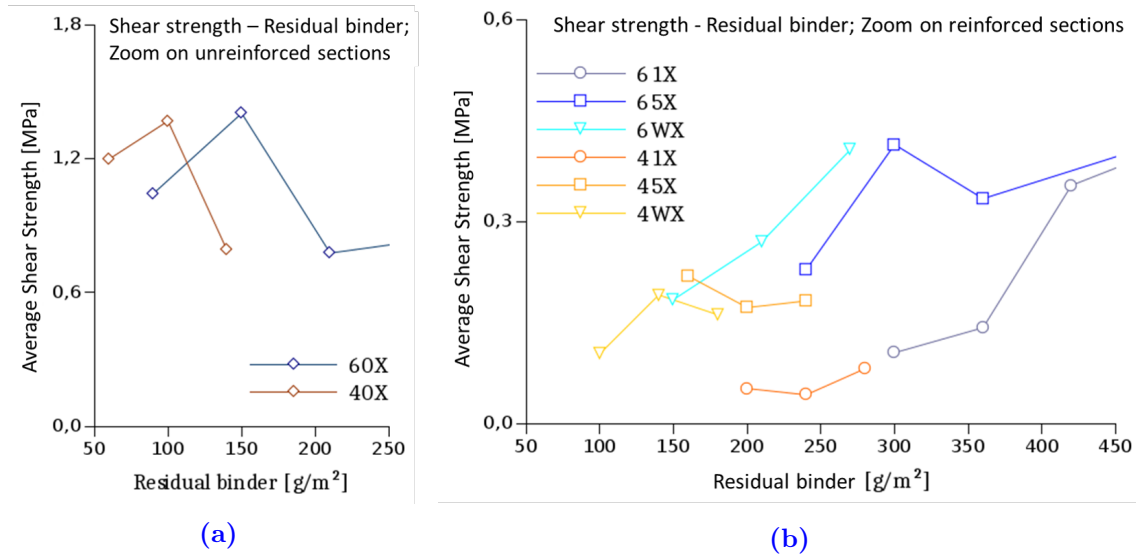
Figure III.2.12: Shear strength - Residual binder: A: Zoom on unreinforced sections 60X and 40X; B: Zoom on reinforced sections coated with C60B4-S; C: Zoom on reinforced sections

This similarity in behaviour between both emulsions is not to be found on reinforced sections. As figure III.2.12b shows, the differences in shear strength are relatively high, especially for the higher application rate 1. Analogies in curve progressions, as for unreinforced sections, cannot be found, because, as mentioned before, the C60B4-S coated sections show a rise for more residual binder while the C40B5-S do not.

It can be concluded that the change in emulsion properties, which is interesting for the bonding without grids, is not working on reinforced sections. Here, a softer binder seems to be of greater importance.

III.2.4.4   Influence of the non-woven on the interlayer bonding of reinforced sections
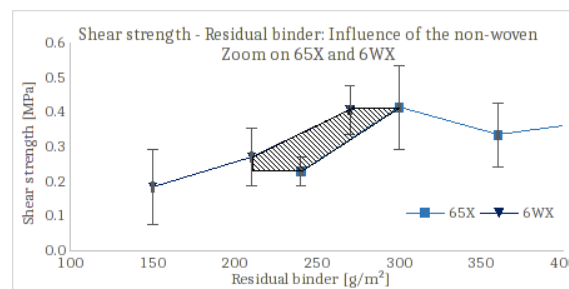
Figure III.2.13: Influence of the non-woven: Comparison of the results on sections 65X and 6WX

The grids W and 5 differ from each other only by the existence of a light non-woven between the strands of grid 5, whereas grid W has none. This non-woven can be necessary

to facilitate the installation of glass fibre grids on road surfaces. Figure III.2.13 shows the average results of the section 6W1,-2 &-3 and 651,-2 & -3. The hatched surface between the curves represents the difference in shear strength between the two, meaning that for the same amount of residual binder, the sections reinforced with grid W (without non-woven) reach a stronger shear resistance than sections reinforced with grid 5 having a non-woven. It can be concluded that the use of even a light non-woven between the strands has a negative influence on the bonding.

III.2.4.5 Influence of the resin and the form of the strands on the interlayer bonding of reinforced sections

The grids 5 and N differ only in the resin used to coat and protect the glass fibre of the grid. For grid N, only the emulsion C40B5-S with an application rate of 200 g/m^2 of residual binder was tested. This section can directly be compared with section 452, also coated with 200 g/m^2 of residual binder of C40B5-S. As shown in figure III.2.14 , we can observe that the shear stress results of section 4N are much higher than those of section 452. Further, on figure III.2.11c (zoom on reinforced sections), we can observe that the grid N reaches the highest shear stresses of all reinforced C40B5-S coated sections and achieves better results than C60B4-S coated sections for the same amount of residual binder.
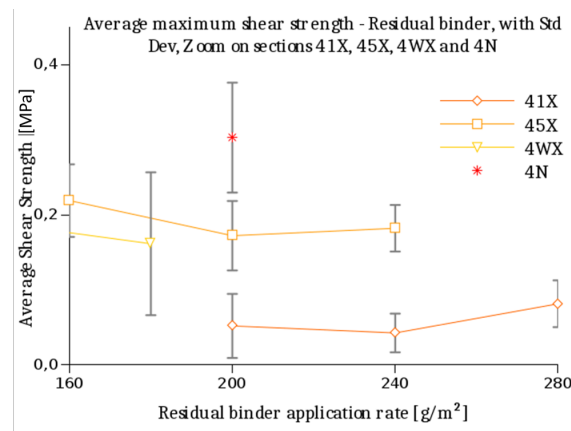
Figure III.2.14: Influencing components on the bonding: comparison of grids with resin A (grids 1 and 5) and B (grid N)

3D-scans of the strands of the grids were made in order to analyze their shapes. For this examination, nine strands of each grid direction (machine direction 'md' or warp yarn and cross machine direction 'cmd' or filling yarn) of the grids N, 5 (same as W) and 1 were scanned with a 3D-microscope. The average shapes can be seen in figure III.2.15 It can be observed that the strands of grid 1, having a tensile strength twice as high as 5 and N, are nearly twice as wide as the grids 5 and N, without being noticeably higher than the two other grids.

The comparison of the strands of grids 5 and N shows that the strands of grid N are slightly taller but also slightly thinner than the strands of grid 5, which can lead to a better interlocking with the granular of the upper layer, explaining partly the better results of 4N compared to 452 as discussed before.

(a)   **(b)**
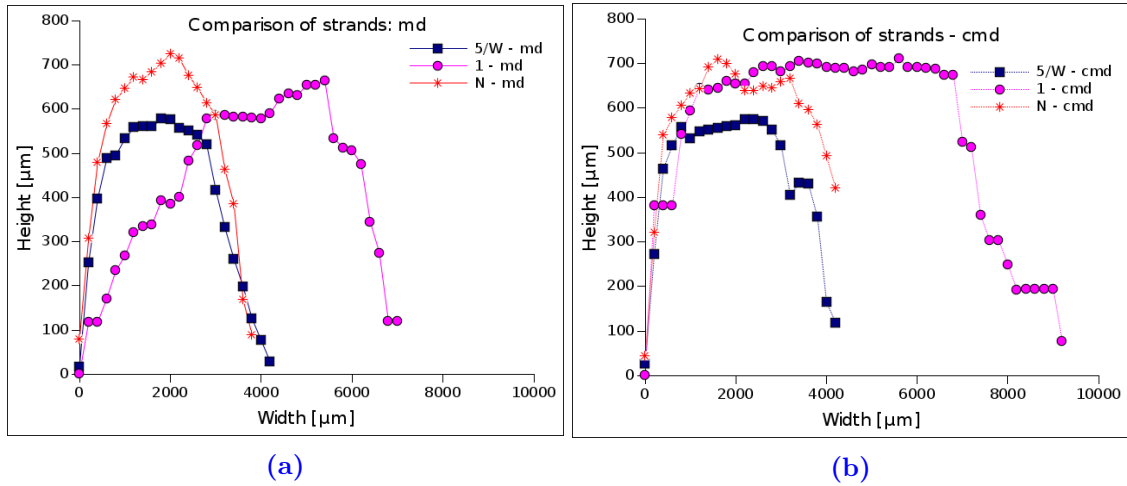
Figure III.2.15: Influencing components on the bonding: comparison of the shape of the strands of grids 1, 5 and N. Left: strands md, Right: strands cmd

As the resin used in grids 5 and N is different, it can be assumed that the resin has an impact on the shear strength, firstly as it leads to a different form of the strand, secondly because it can be in some cases self-adhesive. In our study, a self-adhesion was not noticed, however the behaviour of the resin under hot temperatures, as it is the case during construction, was not further investigated.

III.2.4.6   Microscopic examination

The pictures of figure III.2.16 were made with a 20-times magnification and show about 1 cm of the interface width of 6 observed cores. The upper part of the picture shows the wearing course, the lower part is the binder course. The cores were cut perpendicular to the interlayer in the direction of rolling, the strands coming out of the cores are therefore filling yarns (cmd). As only a few specimen scans were taken, the following pictures can only give a slight overview of the interlayer.

On the picture of the unreinforced specimens (600 and 602) the interface between the wearing course and the binder course is not clearly visible. This similarity in appearance can also be seen in the test results, as both achieve more than 1.1 MPa average shear strengths. No voids are visible in both samples.

The pictures of 610, 611 and 650 show a md-strand running along the interface, picture 651 shows a cmd-strands coming out of the core.

The existence of voids can be seen under the strands of picture 611 and 651. However,
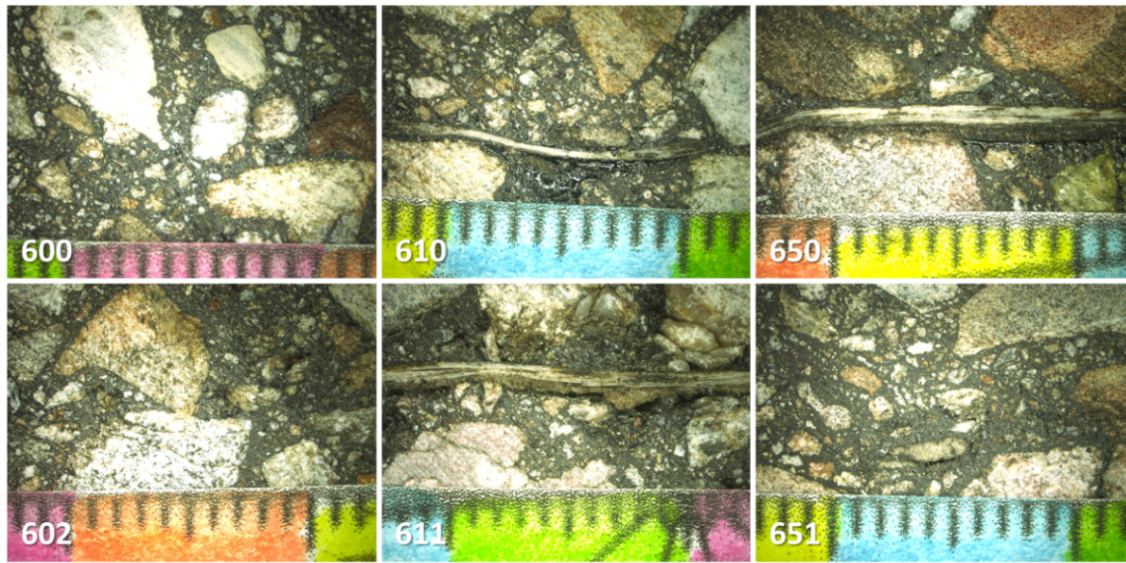
Figure III.2.16: Results of the microscopic examination of the interfaces of cores from the sections 600, 602, 610, 611, 650 and 651 with a 20-times magnification

no voids can be seen on picture 610 and 650. This may be caused by the more important amount of residual binder present on the specimens 650 and 610 compared with 611 and 651 (611: 420 g/m^2 and 651: 360 g/m^2 whereas 610: 600 g/m^2 and 650: 1638 g/m^2), which fills the voids with binder, leading to a higher binder content at the interface. This residual binder is visible in pictures 650 and 610 as shining black points under the strands. A high binder content together with no voids at the interface leads to the assumption that in this case, the load is mainly transmitted over the binder, instead of being held by aggregate and binder together.

III.2.4.7   Effect of different bonding conditions on the shear resistance

As observed before, the unreinforced section group 60X shows a peak for an amount of 150 g/m^2 (application rate 2) of residual binder. The negative slope starting after this point is the expected result of the creation of a slip plane as mentioned before, due to the excess of residual binder. This new plane created between the upper and the lower courses of the structure prevents a good interlocking between the granular of the upper and lower courses.

Knowing this, it can be assumed that the positive slope starting again from section 601 (210 g/m^2 of residual binder) and leading to section 600 (816 g/m^2 of residual binder) cannot be due to the interlocking between the aggregates, as it is disturbed through the excess of residual binder. The remaining influencing factor can then only be the adhesion due to the residual binder between the two layers.

The difference between the factor 'interlocking' and the factor 'adhesion' can be seen on the slope between 603 and 602 or 601 and 600. While the first ascension, due to interlocking

and adhesion, is relatively steep with an average slope of 6.01E-3, the second ascension, where the interlocking is lost and only the adhesion is working, is significantly flatter with an average slope of 9.04E-4.

Based on this result, a comparison was made between the average slopes of the different groups 61X, 65X and 6WX, 603-602 (positive slope before the slip plane appears) and 601-600 (positive slope after the slip plane appears).

The average slopes of each group were calculated using the method of least squares and can be seen in figure III.2.17.
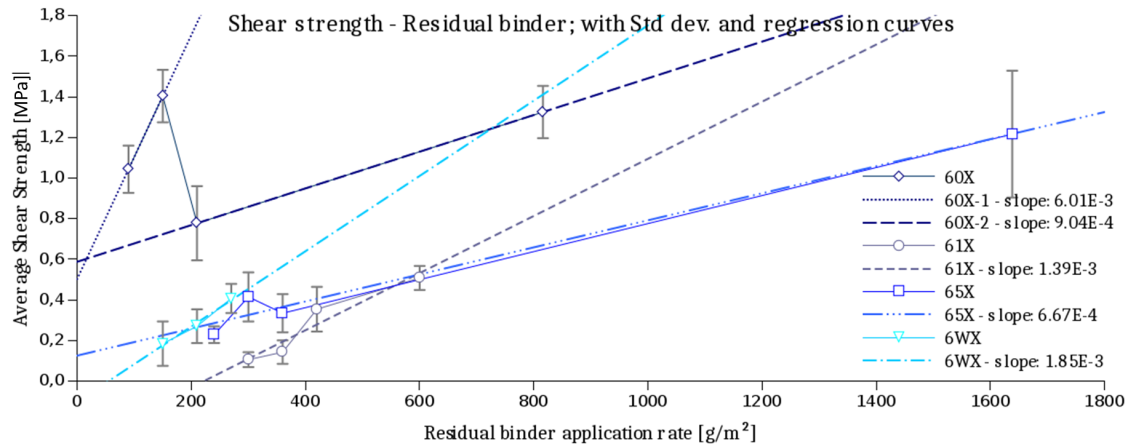
Figure III.2.17: Average slope of each section group

The tendency described before can be observed again on this graph. The group 6WX using grid W, without non-woven, shows the second steepest slope. Here the steep slope can be explained by the non-using of a non-woven, which enables a direct interlocking of the granular. However, as it was observed on the microscope picture, the grids strands are still disturbing the bonding by creating voids under the strands, explaining the difference of slope between the 6WX and 603-602.

Because of this possible interlocking, it can be assumed that with more residual binder a slip plane would appear and cause a fall of the curve as happens on the unreinforced specimens curves.

The groups 61X and 65X show both flatter slopes, having both a non-woven between the strands of their grids. It can be assumed that the interlocking of the aggregates is lightly disturbed by the non-woven so that the main bonding agent is the adhesion through the residual binder. In this case the residual binder fills the voids under the strands of the grids, leading to better shear strength results. It can be observed that a great amount of residual binder as used for section 650, leads to shear strength values equalling the best results of the unreinforced sections.

The representation of the curve as linear to infinity is most likely not correct, it should be assumed that the curves would more likely have a sigmoid form. However, the linearity of the curves is a good approximation for the middle part as represented.

In conclusion, it can be said that specimens without reinforcement and low residual binder content have an undisturbed interlocking of the grains, while test specimens with reinforcements are bonded together mainly through the residual binder.

This hypothesis is strengthened when looking at the microscope scans (see figure III.2.16), where the residual binder is visible under the strands of the grids on the pictures of the reinforced specimens, while the residual binder seems to be absorbed in the asphalt around the interface in the pictures of the unreinforced specimens.

The effect of interlocking is visible in the slope of the curves. The steeper the slope, the stronger the interlocking between the grains and on the contrary: the flatter the curve, the stronger the influence of the residual binder on the bonding.

Considering this fact with regard to the temperature dependency of the shear resistance (see section III.2.2, figure III.2.3), it can be observed that the reinforced specimens, in which the residual binder is primarily responsible for the interlayer bonding, are more temperature dependent than the unreinforced specimens, where the interlocking - which is widely temperature independent - has still a role to play.

III.2.4.8 Influence of reinforcement at the interface on the shear resistance - temperature behaviour

For comparative purposes, the results obtained in this study (see section III.2.2) were compared with the values obtained by Canestrari et al. [CAN 13] and Vismara et al. [VIS 12].

Leutner Test perfomed by Canestrari et al. In their study from 2013, Canestrari et al. [CAN 13] observed the influence of different interface treatments on the shear resistance of double layered specimens. For this purpose, a test surface was constructed consisting of a lower asphalt layer with a nominal maximum aggregate size of 16 mm and a 70/100 bitumen and an upper asphalt layer with a nominal maximum size of 11 and the same bitumen type.

The interface between the layer was treated in 3 different ways:

- Pavement 1: Without treatment (not hot on hot)

- Pavement 2: Pre-coated with a polymer modified emulsion

- Pavement 3: Pre-coated with a conventional cationic emulsion

The shear tests were carried out on 150 mm diameter with a displacement rate of 50 mm/min and at the temperatures 10 °C, 20 °C, 25 °C, 30 °C and 40 °C.

The shear stress values obtained for each section are listed in table III.2.6.

Table III.2.6: Shear strength results of specimens Canestrari et al. at different temperatures

Temperature [°C]	Pavement 1	Pavement 2	Pavement 3
	Shear stress [MPa]		
10	1.07	2.04	2.22
20	0.83	1.19	1.34
25	0.61	0.88	1.02
30	0.34	0.59	0.75
40	0.19	0.34	0.36

The slopes calculated with these results and using equation 1 are:

Pavement 1: a = -0.021

Pavement 2: a = -0.025

Pavement 3: a = -0.024

It can be observed that first the values of a are relatively close to each other for all 3 pavements, and second that all three values are almost identical to the value of section 600 with a= -0.025.

Leutner Tests performed by Vismara et al.   Vismara et al. observed in their study of 2012 [VIS 12] the influence of different reinforcements installed on the interface between two asphalt layers on the shear resistance and compared it with an unreinforced specimen variant.

The specimens (diameter 150 mm) were made in a laboratory and consisted of two asphalt layers with a nominal maximum aggregate size of 11 and a bitumen with penetration grade 60. The three different interlayer options were:

- Tack coat

- Reinforcement A: Polypropylene nonwoven and glass fibre with tensile strength of 50 kN/mm^2

- Reinforcement B: Polypropylene nonwoven and glass fibre with tensile strength of 100 kN/mm^2

The Leutner tests were carried out at 5 °C and 25 °C. The results of the tests are listed in table III.2.7.

Table III.2.7: Shear strength results of specimens Vismara et al. at different temperatures

Temperature [°C]	Tack coat	Reinforcement A	Reinforcement B
	Shear stress [MPa]		
5	5.566	1.932	1.669
25	1.159	0.302	0.314

The slope calculated with these results and using equation 1 are:

Tack coat: a = -0.0341

Reinforcement A: a = -0.0403

Reinforcement B: a = -0.0548

Comparison of parameter a, describing the influence of the temperature on the shear resistance   Figure III.2.18 plots all calculated a-parameters determined with the values of Canestrari et al., Vismara et al. and of this study. The different colours are a reference to the existing interface conditions: green columns indicate an interface without reinforcement, red with glass fibre grids and grey with polypropylene non-woven and glass fibres.
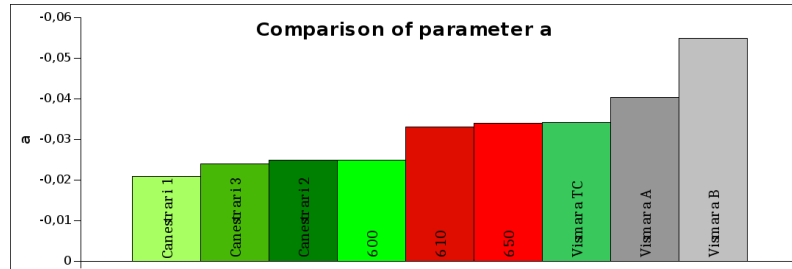
Figure III.2.18: Comparison of calculated parameter a, describing the influence of the temperature on the shear resistance, in ascending order. Shades of green: Interface without reinforcements, shades of red: Interface with different glass fibre grids, shades of grey: Interface with different polypropylene nonwoven and glass fibres

It can be observed that the first four columns represent interlayer without any type of reinforcement. The following two red columns represent the specimens with glass fibre grid reinforcement. A sharp increase of a can be seen, corresponding to a jump of 0.008. The last three columns represent the values based on the study of Vismara et al.. When viewed alone, a sharp increase between specimens without and with reinforcement can also be observed here. The fact that all three a-values of Vismara et al. are higher than the other values can be due to the different production methods, as the specimens used in Vismara et al.'s studies were prepared in a laboratory while the other specimens were

all extracted from test surfaces.

In conclusion, it can be observed that specimens built under the same conditions tend to have greater a-values when a reinforcement is laid on the interface, showing that the influence of the temperature on the shear resistance is higher for specimens with reinforcement than for specimens without reinforcement.

III.2.5   Conclusion about shear tests

28 different sections were built, varying types of grids (with and without non-woven, different resins), types of emulsions and emulsion application rates. The cylindrical cores extracted from the surface were tested with a monotonic shear test. The results are:

- The insertion of glass fibre grids has a negative influence on the bonding, as for the recommended application rates, the shear strength of reinforced specimens reach only about 60 % of the shear strength of unreinforced specimens

- The application rate on reinforced samples has a important effect on the bonding. For low application rates, no positive influence on the shear stress is visible. However high application rates can lead to shear stresses similar to the ones on unreinforced samples.

- Important variations can be observed between the different emulsions.

- The use of a non-woven between the strands leads to a loss of interlocking between the layers hence to lower shear stress results. For grids with non-woven, a high application rate is very important.

- The resin with which the glass fibres are coated can have a positive influence on the bonding.

- The form of the strands can lead to a better interlocking between the grid and the upper layer.

- The relation between temperature and shear resistance depends on the acting bonding effects: Interlocking: lower temperature dependency, bonding through residual binder: higher temperature dependency.

III.3   Stiffness modulus of reinforced and unreinforced specimens

The stiffness modulus is a mechanical value describing the resistance of a body against elastic deformation induced by a force or a moment. The stiffer the material, the greater the effort required to obtain a given deflection.The stiffness depends on the elastic property of the material, but also on its homogeneity.
In road construction, the stiffness modulus is used as a parameter to describe the asphalt materials. With the stiffness modulus of a layer material, it is possible to calculate the deformation and the stresses occurring in a layer when applyig a defined charge.

In Europe, the European standard EN 12697-26:2012 [EN12697-26] specifies the various methods used to determine the stiffness of asphalt. The tests described in the standard are shown in figure III.3.1. These tests are:

- Bending tests:

    - 2PB-TR: Two point bending tests on trapezoidal specimens

    - 2PB-PR: Two point bending tests on prismatic specimens

    - 3PB-PR: Three point bending tests on prismatic specimens

    - 4PB-PR: Four point bending tests on prismatic specimens

- Indirect tensile tests:

    - IT-CY: Indirect tensile tests on cylindrical specimens

    - CIT-CY: Test with indirect cyclic tensile load of the specimens

- Direct uniaxial tests

    - DTC-CY: Uniaxial tension-compression tests on cylindrical specimens

    - DT-CY: Direct tensile tests on cylindrical specimens

    - DT-PR: Direct tensile tests on prismatic specimens
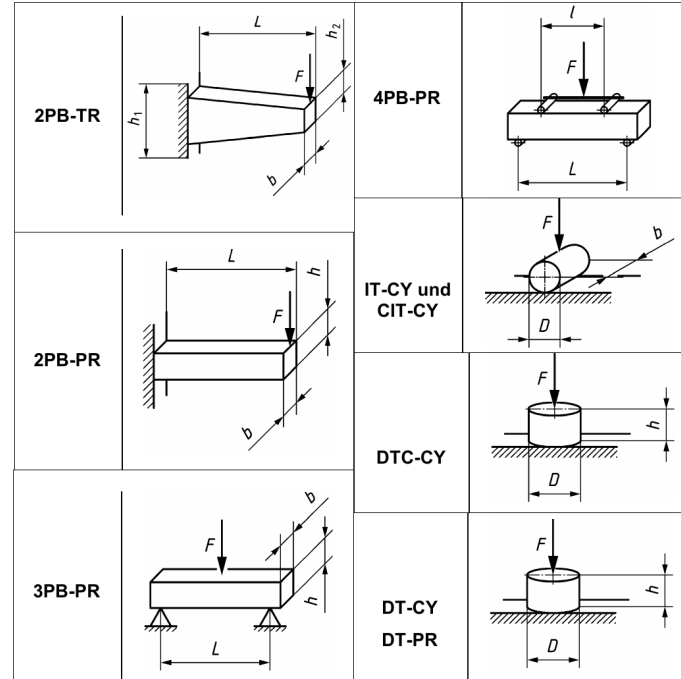
Figure III.3.1: Tests described in the european standard 12697:26-2012 for stiffness test on hot mix asphalt [EN12697-26]

In Germany, the test used to characterize the stiffness modulus of an asphalt mix is the indirect tensile test on cylindrical specimens, abbreviated IT-CY or ITT (Indirect Tensile Test). This value is used for the dimensioning of road structures. For this reason, it was decided to use the ITT test to investigate the influence of the grid on the stiffness modulus, in order to use the outcome of the tests for future dimensioning work - should the impact of the grid be measured.

III.3.1   Indirect tensile test - stiffness modulus

The indirect tensile test is a cyclic test during which a cylindrical asphalt specimen is submitted to sinusoidal cyclic compressive stress on its vertical diametric plane, inducing perpendicular tensile stresses in the specimens which will lead to the rupture of the specimens by splitting along the center in the vertical direction. The mechanisms of the tests are pictured in figure III.3.2.

This test is easily carried out as the cylindrical specimens needed for the test can be drilled directly from the road without the need for further preparation.

The implementation of the test is described in the German directive AL Sp-Asphalt 09 [AL-Sp 09].

Based on this directive, the stiffness modulus of a layer has to be determined at least at 4 different temperatures and at least at 3 different frequencies.

In this study, the chosen temperatures are: -10 °C, 0 °C, +10 °C and +20 °C. The chosen

frequencies are: 0.1 Hz, 1 Hz, 5 Hz and 10 Hz.

The test is a non-destructive test during which the specimen should not endure plastic deformations.
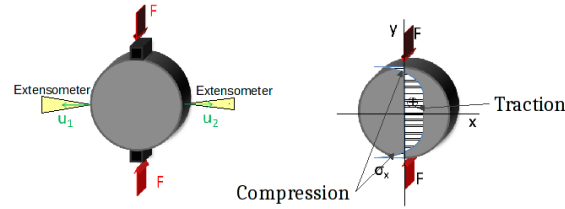
Figure III.3.2: Sketch and principle of the indirect tensile test

III.3.2   Extraction of specimens for ITT from sections 600, 610 and 650

The specimens used for the tests are double-layered cores extracted from the test surface described in paragraph III.1, from lane 600 (unreinforced, residual binder application rate: 816g/m^2), lane 610 (reinforced with grid 1, residual binder application rate: 600 g/m^2) and lane 650 (reinforced with grid 5, residual binder application rate: 1638 g/m^2).

In order to test the impact of the grids compared to the unreinforced samples, the specimens had to be extracted from the side. Their extraction was therefore conducted in two steps:

1. Extraction of rectangular slabs from the test surface (dimensions: 20 x 30 x 12 cm)

2. Extraction of cores (diameter 100 mm) from the slabs

Thus, it was possible to have the grids positioned where the tension stresses would occur, even if it was not completely possible to extract the specimens in such a way that the grid would be positioned exactly in the center.

Figure III.3.3 pictures the extraction steps as well as the specimen after extraction.
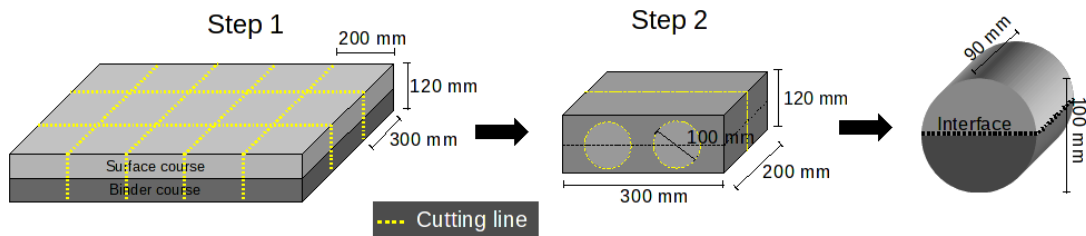
Figure III.3.3: Specimen preparation for indirect tensile test

As the maximal length usable in the testing device was 100 mm, the specimens had to be cut in half after extraction from the slabs. The short length led to a maximal amount of 3 strands in each specimen, as the mesh size of the 2 grids used is 4 x 4 cm^2.

III.3.3   Test implementation

The tests were carried out at four temperatures: -10 °C, 0 °C, +10 °C and 20 °C. At least four samples of each section were tested at each temperature. To ensure a good tempering of the samples, the specimens were laid in a temperature conditioning unit for at least 12 hours before starting the test.

Pre-test   Since the test is a non-destructive test, a first specimen was tested in a pre-test for each temperature. This enabled the determination of a suitable loading test to ensure the non-destructivity. During this pre-test, one temperature conditioned specimen of each section was subjected to an increasing maximal loading at 10 Hz, while a minimal compression stress of 0.035 MPa was always kept. After every 100 loading cycles, the maximal compression stress was increased by 0.2 MPa, starting from an initial maximum stress of 0.2 MPa and carried out until reaching maximum horizontal strains of 0.2 ‰.
The horizontal deformation of the specimen during the test was measured by two extensometers placed on the lateral surface (see figure III.3.2). The stress was selected in such a way that plastic deformations do not occur in the specimen. The resulting strains should correspond to approximately 0.10 ‰.

An example of the 3 cycles of the 3 first steps of the pre-test as well as the result of one pre-test is shown in figure III.3.4.

<div align="center">(a)</div>

<div align="center">(b)</div>
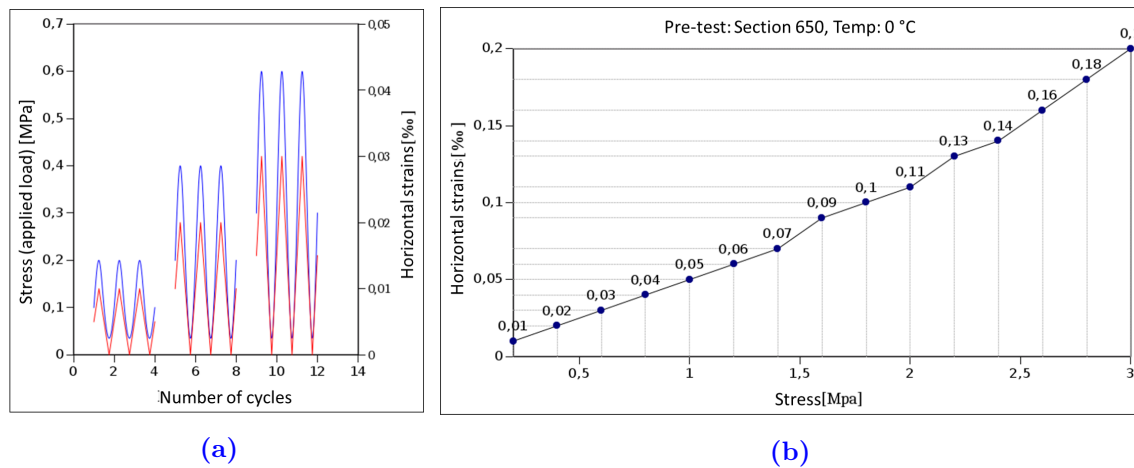
Figure III.3.4: (a) Principle of the pre-test and (b) results of the pre-test for section 650 at 0 °C

As the pre-test is carried out at 10 Hz, the chosen maximum loading stress has to be adapted for the other frequencies. A thumb rule is:

- At 5 Hz: Initial maximum loading stress - 0.1 MPa

- At 1 Hz: Initial maximum loading stress - 0.2 to 0.3 MPa

- At 0.1 Hz: Initial maximum loading stress -0.3 to 0.4 MPa

Main Test The main test is stress-controlled and composed of 5 different steps, in which sinusoidal loading cycles are applied at different frequencies and maximum loading stress, while the minimum compression stress is kept at 0.035 MPa. The maximum loading stress is determined during the pre-test, as described before, and depends on the different sections (600, 610 and 650) and on the temperature (-0 °C, 0 °C, +10 °C, +20 °C).

Step 1: 110 cycles at 10 Hz

↪ Step 2: 100 cycles at 5 Hz

↪ Step 3: 20 cycles at 1 Hz

↪ Step 4: 10 cycles at 0.1 Hz

↪ Step 5: 110 cycles at 10 Hz

The return to 10 Hz in step 5 was necessary to ensure that no damage and plastic deformation occurred during the test. If the variation in horizontal deformation between step 1 and step 5 is larger than 15 %, it must be assumed that damage has occurred and the test has to be rejected.

Output and calculation of stiffness modulus The output of the tests is the applied force and displacement measured by the extensometers on both sides of the shell surface of the specimens for each cycle at each frequency.

The stiffness modulus is calculated with equation (2).

$$|E| = \frac{\Delta F * (0.274 + \nu)}{h * \Delta u} \tag{2}$$

With

E: Stiffness modulus [MPa]

ΔF: Difference between minimum and maximum force [N]

Δu: Difference between minimum and maximum displacement [mm]

h: Height of the specimen [mm]

ν: Poisson's ratio [-]

The Poisson's ratio ν depends on the temperature and can be calculated with equation (3).

$$\nu = \frac{0.15 * 0.35}{1 + e^{[3.1849 - 0.04233 * (\frac{9}{5} * T + 32)]}} \tag{3}$$

With

T = Temperature [°C]

To determine ΔF and Δu, which are equal to the difference between minimum and maximum force and displacement, 5 cycles of each step are examined. For steps 1 and 5 (10 Hz) the examined cycles are cycles 98 to 102, for step 2 (5 Hz) cycles 93 to 97, for step 3 (1 Hz) cycles 13 to 17 and for step 4 (0.1 Hz) cycles 3 to 7.

Using the output of force against time or displacement against time of each previously named cycles, two regression curves are created. Their equations are shown in (4) (force) and (5) (displacement).

$$F(t) = A + B * sin(2 * \pi * f * t + C) \tag{4}$$

$$u(t) = a + b * sin(2 * \pi * f * t + c) \tag{5}$$

With

F(t): Measured force at time t [N]

u(t): Measured displacement at time t [mm]

t: time

f: test frequency

A resp. a: shift from the x-axis

B resp. b: Amplitude

C resp. c: phase shift

The parameter of the regression curves were calculated by searching for the minimum of residual sum of square.

$$\Sigma(F_i - \bar{F}_i)^2 \rightarrow min \quad \text{respectively} \quad \Sigma(u_i - \bar{u}_i)^2 \rightarrow min$$

Examples for regression curves are shown in figure III.3.5.
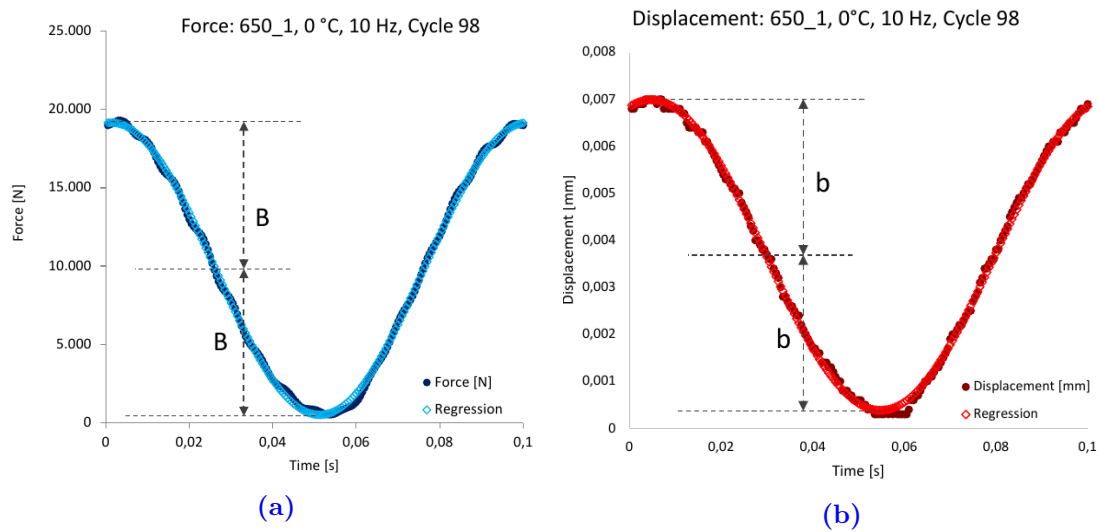
Figure III.3.5: Regression curves: Test at 0 °C, 10 Hz, cycle 98, section 650. (a): Force against time, (b): Displacement against time

III.3.4 Test results for specimens of sections 600, 610 and 650

Before carrying out the tests, some parameters of the test specimens were recorded, such as the diameter and the length of the specimens and the thicknesses of each layer. The data are listed in appendix III. Tables III.3.1 to III.3.4 show the resulting average stiffness modulus with standard deviation and coefficient of variation of each specimen for each temperature (see different tables) and frequency.

The diameter was measured at various points of the specimen. The height of the two layers was only measured on the two front sides of the specimens. Therefore the average diameter of the specimens may vary from the sum of their two layers.

Table III.3.1: Result Moduli at -10 °C, two-layered specimens 600, 610 and 650

	Temp. : -10 °C		600	610	650
10 Hz	Average	[MPa]	17,587	17,933	18,875
	Std. Dev.	[MPa]	750	2304	1649
	Coef of Variation		0.0348	0.1049	0.0714
5 Hz	Average	[MPa]	16,586	16,779	17,768
	Std. Dev.	[MPa]	780	2141	1474
	Coef of Variation		0.0384	0.1042	0.0677
1 Hz	Average	[MPa]	14,255	14,716	15,448
	Std. Dev.	[MPa]	826	1998	1341
	Coef of Variation		0.0473	0.1109	0.0709
0.1 Hz	Average	[MPa]	10,931	12,163	12,084
	Std. Dev.	[MPa]	908	2044	1190
	Coef of Variation		0.0678	0.1372	0.0804
10 Hz	Average	[MPa]	17,431	17,546	18,633
	Std. Dev.	[MPa]	932	2234	1758
	Coef of Variation		0.0436	0.1040	0.0771

Table III.3.2: Result Moduli at 0 °C, two-layered specimens 600, 610 and 650

	Temp. : 0 °C		600	610	650
10 Hz	Average	[MPa]	14,031	12,453	14,401
	Std. Dev.	[MPa]	1213	1597	561
	Coef of Variation		0.0706	0.1047	0.0318
5 Hz	Average	[MPa]	12,410	11,187	13,036
	Std. Dev.	[MPa]	1278	1448	692
	Coef of Variation		0.0841	0.1057	0.0434
1 Hz	Average	[MPa]	9,965	8,976	10,343
	Std. Dev.	[MPa]	1172	1175	663
	Coef of Variation		0.0960	0.1069	0.0523
0.1 Hz	Average	[MPa]	6,819	6,138	6,934
	Std. Dev.	[MPa]	949	995	583
	Coef of Variation		0.1137	0.1323	0.0686
10 Hz	Average	[MPa]	12,855	11,753	13,844
	Std. Dev.	[MPa]	1426	1554	584
	Coef of Variation		0.0906	0.1080	0.0345

Table III.3.3: Result Moduli at 10 °C, two-layered specimens 600, 610 and 650

	Temp. : 10 °C		600	610	650
	Average	[MPa]	8,131	7,853	10,376
10 Hz	Std. Dev.	[MPa]	579	327	1528
	Coef of Variation		0.0581	40.0360	0.1203
	Average	[MPa]	7,045	6,732	8,843
5 Hz	Std. Dev.	[MPa]	611	129	1135
	Coef of Variation		0.0708	40.0166	0.1047
	Average	[MPa]	4,907	4,748	6,554
1 Hz	Std. Dev.	[MPa]	475	151	814
	Coef of Variation		0.0791	40.0275	0.1014
	Average	[MPa]	2,707	2,620	3,821
0.1 Hz	Std. Dev.	[MPa]	324	116	413
	Coef of Variation		0.0977	40.0383	0.0882
	Average	[MPa]	7,836	7,762	9,887
10 Hz	Std. Dev.	[MPa]	614	200	1292
	Coef of Variation		0.0640	40.0223	0.1067

Table III.3.4: Result Moduli at 20 °C, two-layered specimens 600, 610 and 650

	Temp. : 20 °C		600	610	650
	Average	[MPa]	4,248	6,067	45,246
10 Hz	Std. Dev.	[MPa]	384	849	543
	Coef of Variation		0.0738	40.1212	40.0896
	Average	[MPa]	3,490	5,312	44,305
5 Hz	Std. Dev.	[MPa]	337	690	544
	Coef of Variation		0.0789	40.1125	40.1095
	Average	[MPa]	2,203	3,468	42,718
1 Hz	Std. Dev.	[MPa]	282	453	396
	Coef of Variation		0.1045	40.1131	40.1264
	Average	[MPa]	1,106	1,776	41,375
0.1 Hz	Std. Dev.	[MPa]	139	259	242
	Coef of Variation		0.1024	40.1264	40.1526
	Average	[MPa]	4,223	6,256	45,201
10 Hz	Std. Dev.	[MPa]	439	629	540
	Coef of Variation		0.0849	40.0870	40.0900

A graphical representation of the results is shown in figure III.3.6.

At first sight, it can be observed that the specimens reinforced with grid 5 (section 650) reach higher stiffness moduli for nearly every test combination except for the test temperature of 20 °C, where section 610 reaches higher values.

The influence of the temperature appears to be less negative on the specimens of section
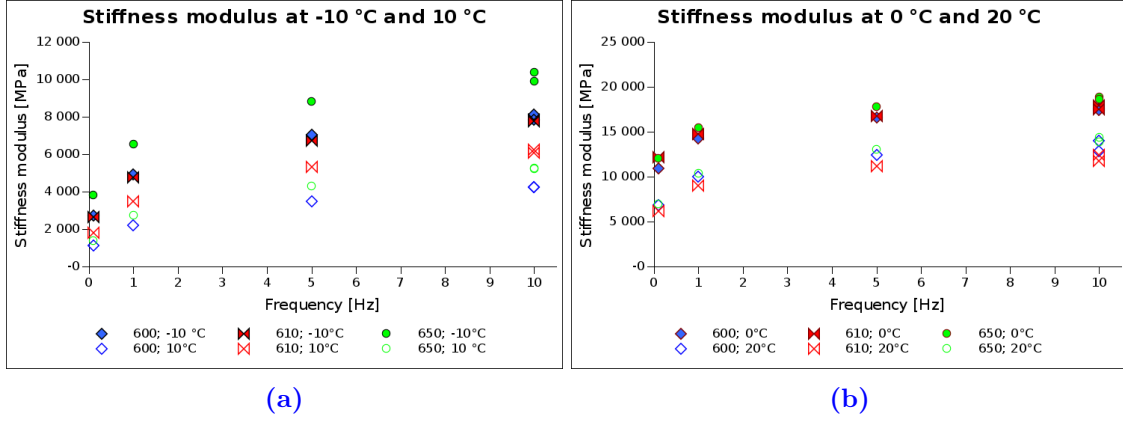
Figure III.3.6: (a) and (b) Average stiffness modulus of each step against frequency - (a): Temperatures -10 °C and 10 °C, (b) Temperatures 0 °C and 20 °C

610 than on the specimens of section 600 and 650, resulting in the best results of all at 20 °C.

Creation of the master curves   The creation of a master curve in accordance with the German directive [AL-Sp 09] is based on the calculation of a shift factor $log(\alpha_T)$ which moves the determined isotherms of the stiffness modulus in the direction of the frequency axis so as to produce a continuous function.
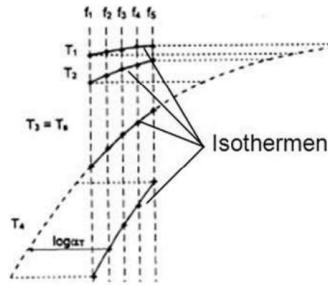
Figure III.3.7: Determination of the master curve by the displacement of the isotherms according to german directive [AL-Sp 09]

The calculation of the shift factor $log(\alpha_T)$ is based on equation 6.

$$log(\alpha_T) = \frac{E_a}{R}(\frac{1}{T} - \frac{1}{T_0})$$ (6)

With

α_T: Shift factor

E_a: activation energy [J/mol]

R: universal gas constant (R=8.314 J/mol) [J/mol]

T: Temperature of the wanted stiffness modulus to be calculated (actual temperature) [K]

T_0: Temperature of the master curve. The chosen reference temperature should be 20 °C (293.15 K). [K]

The master curve has the form of a sigmoid curve and can be constructed using a regression function going through the determined data points. The sigmoid function has the form of equation 7.

$$|E| = y_0 + \frac{w}{1 + e^{(\frac{x-x_0}{z})}} \tag{7}$$

With

E: Stiffness modulus [MPa]

y_0: Intersection of the function with the y-axis [Hz]

x_0: Intersection of the function with the x-axis [MPa]

x: arbitrary value on the x-axis, $log(\alpha_T)$ [Hz]

w: Material parameter [MPa]

z: Material parameter [-]

The five unknown parameters x_0, y_0, w, z and E_a are calculated by searching for the minimum residual sum of square with the solver function of Microsoft Excel. The master curve of section 650 with the determined and calculated data points and the values of the different parameters is shown in figure III.3.8.
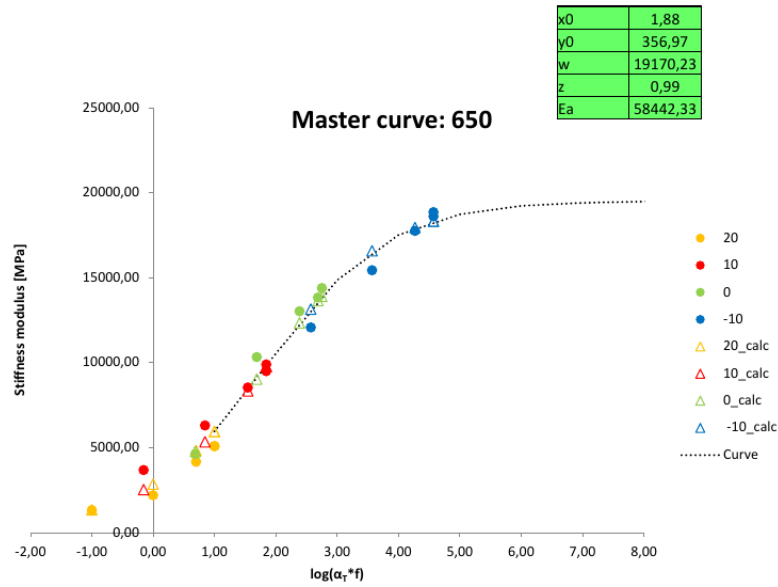
Figure III.3.8: Regression function of the master curve of section 650 with calculated parameters

The calculated parameters enable the calculation of the stiffness modulus for each frequency and temperature. This way it is possible to create a sigmoid curve showing the evolution of the stiffness modulus depending on the temperature for any frequency. The curves of all three section at 10 Hz are represented in figure III.3.9.
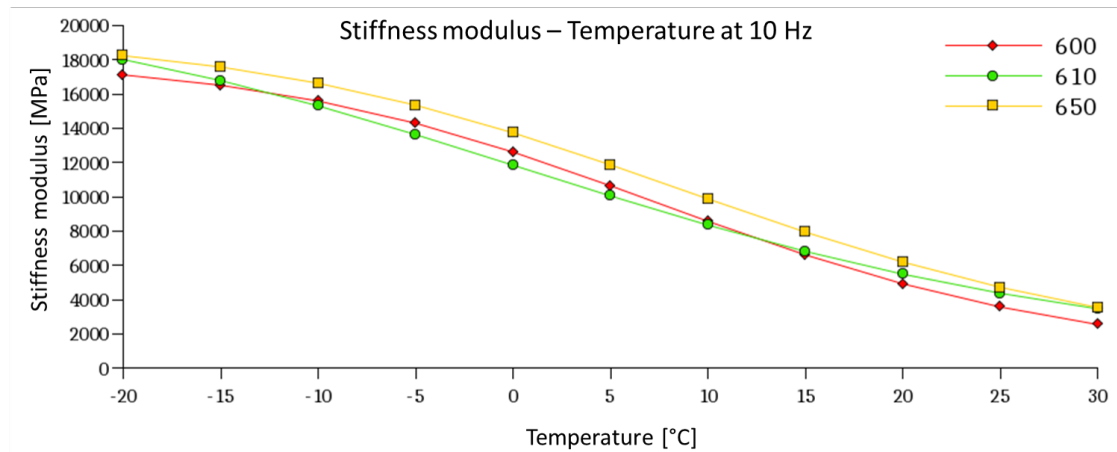
Figure III.3.9: Stiffness modulus - Temperature for section 600, 610 and 650

The values corresponding to the curves are listed in table III.3.5.

Table III.3.5: Parameters for the creation of the sigmoid curve and stiffness modulus values for different temperatures at 10 Hz - section 600, 610 and 650

	600	610	650
Parameters of sigmoid function			
x_0	2.13	2.65	1.89
y_0	5.09	5.09	5.02
w	18005	21240	19347
z	1.15	1.56	1.18
E_a	70526	67139	65116
Temp	Stiffness modulus [MPa]		
-20	17 131	18 027	18 251
-15	16 525	16 798	17 592
-10	15 606	15 320	16 645
-5	14 308	13 643	15 363
0	12 626	11 856	13 749
5	10 654	10 062	11 877
10	8582	8360	9888
15	6620	6824	7950
20	4930	5495	6203
25	3580	4383	4729
30	2558	3474	3549

III.3.5   Test on surface and binder courses: Specimen preparation and test results

In order to compare the results obtained for double-layered specimens with the layer composing the specimens themselves, indirect tensile tests were carried out on specimens composed of only the surface or binder layer.

Unlike the two-layer specimens, the specimens used to determine the stiffness modulus of the surface and binder courses were drilled directly from the test surface. The average diameter of the specimens was 99 mm, their average length was 55 mm. The extraction and cutting steps are shown in figure III.3.10.
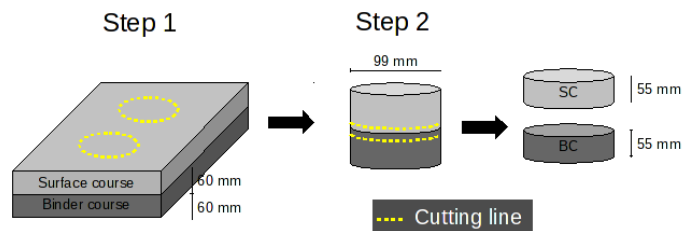
Figure III.3.10: Preparation of cylindrical specimens for stiffness modulus testing of the surface and binder courses of the test surface

The tests were carried out as described above. The diameter and length of each specimen as well as the achieved stiffness modulus for each frequency and each temperature, are listed in appendix III, table III.3.6 to III.3.9 show the average stiffness modulus for all specimens at one temperature for all frequency as well as the corresponding standard deviation and coefficient of variation.

Table III.3.6: Result Moduli at -10 °C, surface and binder courses

Temp. : -10 °C			SC	BC
10 Hz	Average	[MPa]	22961	21807
	Std. Dev	[MPa]	289	2719
	Coef. of Var.		0.0126	0.1247
5 Hz	Average	[MPa]	21635	20276
	Std. Dev	[MPa]	255	2732
	Coef. of Var.		0.0118	0.1347
1 Hz	Average	[MPa]	18617	17230
	Std. Dev	[MPa]	541	2542
	Coef. of Var.		0.0291	0.1475
0.1 Hz	Average	[MPa]	14943	13014
	Std. Dev	[MPa]	776	2197
	Coef. of Var.		0.0520	0.1688
10 Hz	Average	[MPa]	23011	21038
	Std. Dev	[MPa]	757	2625
	Coef. of Var.		0.0329	0.1248

Table III.3.7: Result moduli at 0 °C, surface and binder courses

Temp. : 0 °C			SC	BC
10 Hz	Average	[MPa]	16881	14860
	Std. Dev	[MPa]	1508	586
	Coef. of Var.		0.0893	0.0395
5 Hz	Average	[MPa]	13857	13024
	Std. Dev	[MPa]	251	453
	Coef. of Var.		0.0181	0.0348
1 Hz	Average	[MPa]	10790	9815
	Std. Dev	[MPa]	196	626
	Coef. of Var.		0.0182	0.0639
0.1 Hz	Average	[MPa]	7087	6110
	Std. Dev	[MPa]	125	651
	Coef. of Var.		0.0176	0.1066
10 Hz	Average	[MPa]	14415	13903
	Std. Dev	[MPa]	545	381
	Coef. of Var.		0.0378	0.0274

Table III.3.8: Result moduli at 10 °C, surface and binder courses

Temp. : 10 °C			SC	BC
10 Hz	Average	[MPa]	8264	11866
	Std. Dev	[MPa]	3241	1334
	Coef. of Var.		0.3922	0.1124
5 Hz	Average	[MPa]	7025	9869
	Std. Dev	[MPa]	2939	1874
	Coef. of Var.		0.4183	0.1899
1 Hz	Average	[MPa]	5012	7408
	Std. Dev	[MPa]	2176	931
	Coef. of Var.		0.4340	0.1257
0.1 Hz	Average	[MPa]	3051	4446
	Std. Dev	[MPa]	1451	557
	Coef. of Var.		0.4754	0.1253
10 Hz	Average	[MPa]	7574	11298
	Std. Dev	[MPa]	3412	898
	Coef. of Var.		0.4505	0.0795

Table III.3.9: Result moduli at 20 °C, surface and binder courses

Temp. : 20 °C			SC	BC
10 Hz	Average	[MPa]	6374	7067
	Std. Dev	[MPa]	247	822
	Coef. of Var.		0.0387	0.1164
5 Hz	Average	[MPa]	5441	5855
	Std. Dev	[MPa]	389	645
	Coef. of Var.		0.0714	0.1102
1 Hz	Average	[MPa]	3587	3809
	Std. Dev	[MPa]	256	452
	Coef. of Var.		0.0714	0.1188
0.1 Hz	Average	[MPa]	1818	1891
	Std. Dev	[MPa]	158	244
	Coef. of Var.		0.0867	0.1290
10 Hz	Average	[MPa]	6032	6509
	Std. Dev	[MPa]	219	713
	Coef. of Var.		0.0363	0.1096

The master curves were calculated as described before. The parameters of the regression curves, as well as the stiffness modulus of the surface and binder courses at 10 Hz, are listed in table III.3.10.

Figure III.3.11 represents the master curves of the surface and binder course together with the curves of sections 600, 610 and 650. For comparisons purposes, the curves of

the calibration binder and surface courses of the German guideline [RDO 09] are added to the graph. These two curves are shown solely to compare the waveform and the possible stiffness modulus values of the different binder and surface courses (RDO 09 and test surface).

Table III.3.10: Parameters for the creation of the sigmoid curve and stiffness modulus values for different temperatures at 10 Hz - surface and binder courses

	Surface Course	Binder Course
Parameters of sigmoid function		
x_0	4.18	9.45
y_0	2109	-6854
w	27470	126005
z	1.43	4.01
E_a	103246	74729
Temp	Stiffness modulus [MPa]	
-20	27391	29509
-15	25627	25249
-10	22950	21474
-5	19409	18149
0	15429	15231
5	11649	12678
10	8560	10449
15	6308	8504
20	4787	6807
25	3805	5326
30	3184	4032
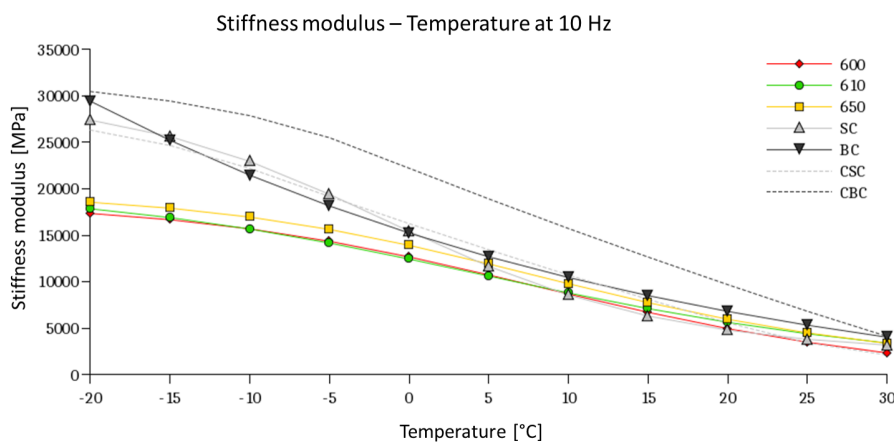
Figure III.3.11: Stiffness modulus - Temperature for surface and binder courses (SC and BC), two layered specimens 600, 610 and 650 and for comparison purposes calibrating binder and surface asphalt of RDO 09 (CBC and CSC)

III.3.6   Interpretation of the result

III.3.6.1   Sections 600, 610 and 650

When looking at the curves of 600, 610 and 650 (figure III.3.9), it first becomes apparent that the two curves 600 and 650 run parallel to one another and maintain a relatively constant distance of about 1100 MPa, which may be interpreted as a clear indication of the positive influence of the reinforcement.

Curve 610 does not hold to this parallelism. At low temperatures (-20 ° C) and high temperatures (from 30 ° C), grid 1 achieves the highest stiffness modulus, while the results at medium temperatures (-10 °C to +10 °C) are the smallest of all three. Here it seems that the influence of the grid is lost in some ways.

Considering the curves 600 and 650, a further common point can be found: the shear resistance determined with the Leutner test (see section III.2.3.1) at 25 °C is approximately the same for both sections.

As demonstrated in section III.2.4.8, the influence of temperature on the behaviour of the shear strength depends, inter alia, on whether or not a reinforcement is placed at the interface. This fact is explained by the influence of the residual binder, which is largely responsible for the shear strength in the case of reinforced test specimens. While the bitumen solidifies or liquefies with the temperature, the influence of the interlocking is to a large extent temperature-independent.

Sections 610 and 650 show a strong influence of the residual binder on the bonding of the two layers, as can be seen in section III.2.4.7.

Since 650 has a relatively high shear strength at normal temperatures, the difference between curves 600 and 650 remains essentially constant at all temperatures.

For 610, however, bonding improves massively at lower temperatures compared to its shear strength at 25 °C, which can lead to a displacement reduction within the specimen during the test and thus to higher resulting stiffness modulus.

The higher the temperatures, the more the bonding reduces in all three sections so that the bonding loses in significance. Calculating the shear strength of the three sections at different temperatures according to section III.2.2 results in the following values (table III.3.11):

Table III.3.11: Shear strength of sections 600, 610 and 650 at different temperatures

	600	610	650
Temperature [°C]	Shear strength [MPa]		
-20	17.62	15.60	41.30
-10	9.91	7.29	18.88
0	5.57	3.41	8.63
10	3.13	1.60	3.94
20	1.76	0.75	1.80
25	1.32	0.51	1.22
30	0.99	0.35	0.82

To investigate this theory, the stress-strains-graphs of all tests carried out at 10 Hz (1st step of the main test) and 0.1 Hz (4th step of the main test) and for all four temperatures are represented in figure III.3.12.
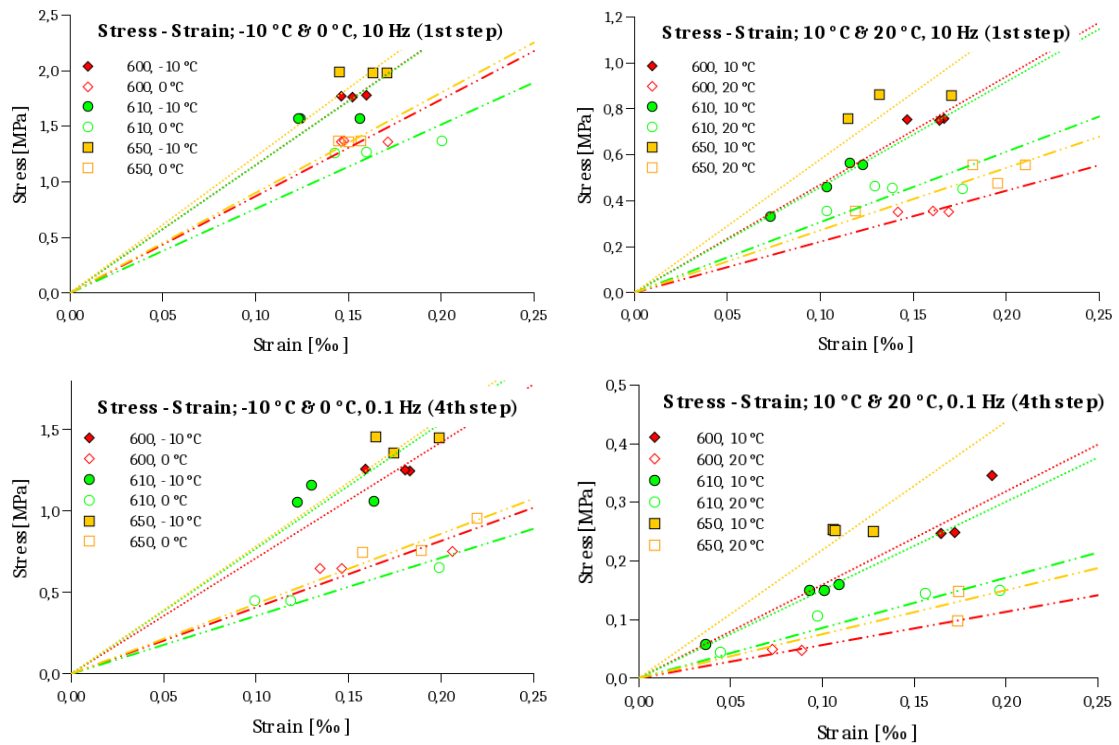
Figure III.3.12: Stress-strain graphs of the test carried out on the specimens of sections 600, 610 and 650 at 10 Hz (upper graphs) and 0.1 Hz (lower graphs) at -10 °C and 0 °C (left graphs) and 10 °C and 20 °C (right graphs)

Table III.3.12 lists the slopes of the linear regression curves drawn according to the strain-stress results obtained at each temperature and at 0.1 Hz and 10 Hz frequencies.

It can be observed that for both frequencies the slopes of section 610 are actually the

smallest for the temperatures from -10 ° C to 10 ° C, being relatively close to the slopes of section 600 at -10 ° C. This trends changes at 20 °C, meaning that from -10 °C to 10 °C, for a certain force, the responding deformations within the specimens of section 610 are greater than for 600 and 650.

On the other hand, the 650 curve remains the steepest at temperatures between -10 °C and 10 °C, indicating smaller deformations within the specimens.

Table III.3.12: Slopes of the stress-strain regression curve for every specimen at the four temperatures and two frequencies (10 Hz and 0.1 Hz). The cell colours represents the steepness of the slopes: green: flattest curve, more displacement in the specimen, yellow: middle curve, orange: steepest curve.

	0.1 Hz				10 Hz			
Temp. [°C]	-10	0	10	20	-10	0	10	20
600	7.118	4.088	1.594	0.566	11.517	8.703	4.702	2.218
R^2	0.996	0.985	0.99	0.997	0.999	0.995	0.997	0.995
610	7.074	3.568	1.505	0.857	11.486	7.574	4.586	3.065
R^2	0.978	0.984	0.998	0.982	0.987	0.989	0.999	0.981
650	7.842	4.308	2.188	0.751	12.276	9.009	5.797	2.714
R^2	0.994	0.996	0.991	0.988	0.995	0.999	0.983	0.992

III.3.6.2   Comparison of results of sections 600, 610 and 650 and results of surface and binder courses

In addition to the comparisons between sections 600, 610 and 650, these sections are compared with the binder and surface courses (BC and SC) used for the construction of the specimens.

Figure III.3.11 shows the curve of the respective stiffness moduli as a function of the temperature.

It can be observed that for lower temperatures from approximately 0 ° C on, the curves of sections 600, 610 and 650 move apart from the curves BC and SC. SC and BC remain relatively close to the curves of CBC and CSC (calibration asphalt, inserted for the sake of comparison). It can be concluded that a strong effect is produced between the two types of test specimens at lower temperatures.

The first question is whether this effect can be attributed to a possible anisotropy in the asphalt, as the test specimens of sections 600, 610 and 650 were taken perpendicularly to the specimens of SC and BC.

In their study of 2016, Hofko et al. [HOF 16] show the effects of asphalt anisotropy

on, inter alia, cyclic indirect tensile tests. For these purposes, asphalt slabs consisting of an asphalt with a nominal maximum aggregate size of 22 and a bitumen with penetration grade 50/70 were constructed. Specimens of 100 mm diameter and 60 mm length were extracted in two perpendicular directions (see figure III.3.13).

Figure III.3.13: Extraction of specimens from slabs in the study of Hofko et al. [HOF 16]

The results checked for are the fatigue and stiffness modulus tests. In their study, the authors were able to find out that the stiffness fatigue performances are highly sensitive to the material anisotropy, noting that the effects of anisotropy tend to increase with the increasing aggregate size of the asphalt.
They observed that the F-Z-Y orientation (left picture of figure III.3.13), which reflects the loading situation on a road, showed 23 % stiffer results and 36% better results in fatigue performance at 20 °C and 10 Hz than the F-X-Y orientation.

The results of this study cannot be transferred one-by-one to this study as the asphalt mixes are different: AC 11 and AC 16 in our study against AC 16 for Hofko et al., meaning that the influence of the anisotropy is lower for our specimens.

If for comparative purposes, one assumes a 23 percent change at 20 ° C anyway, one can see that the values of SC and BC increase as shown in figure III.3.14.
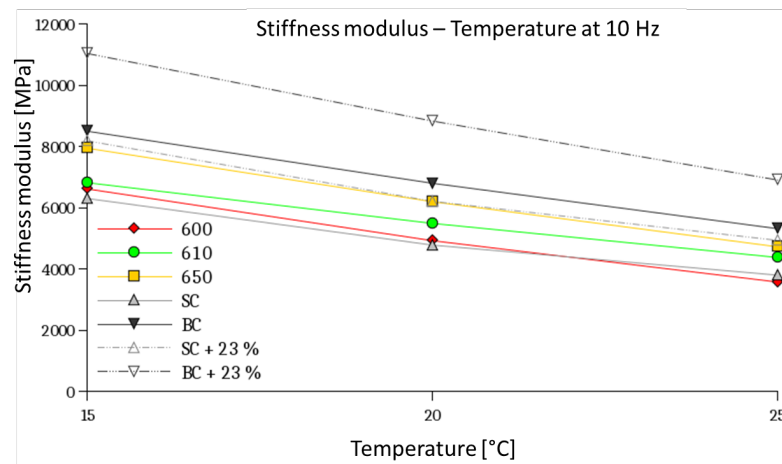
Figure III.3.14: Stiffness modulus - Temperature: Increased SC and BC values by 23 % due to anisotropy

However the difference between the values of 600, 610 and 650 and the values of SC

and BC increases and does not explain why the curves go apart at temperatures below 0 ° C.

The next point to be checked is the influence on the creation of cryogenic stresses at low temperatures. Cryogenic stresses are stresses occurring when low temperatures prevents the asphalt from relieving stresses by modifying its shape.

Transferred to our specimens, it would mean that deformations are strongly inhibited at low temperature in one layered specimen, although they are still possible in double layered specimens, leading to strongly different results in stiffness modulus.
This theory can be examined by looking at the deformation resulting from different stress levels. At low temperatures, these deformations should be greater for two-layered specimens than for uni-layered specimens. For higher temperature (from 0 °C on) the difference due to cryogenic stresses should become smaller.

To investigate this point, the stress-strains curves of the sections 600,610 and 650, defined as two-layered specimens, were opposed to the stress-strains curves of sections SC and BC, defined as uni-layered specimens, for all temperature and at 10 Hz and 0.1 Hz frequencies. The corresponding graphs are shown in figure III.3.15.
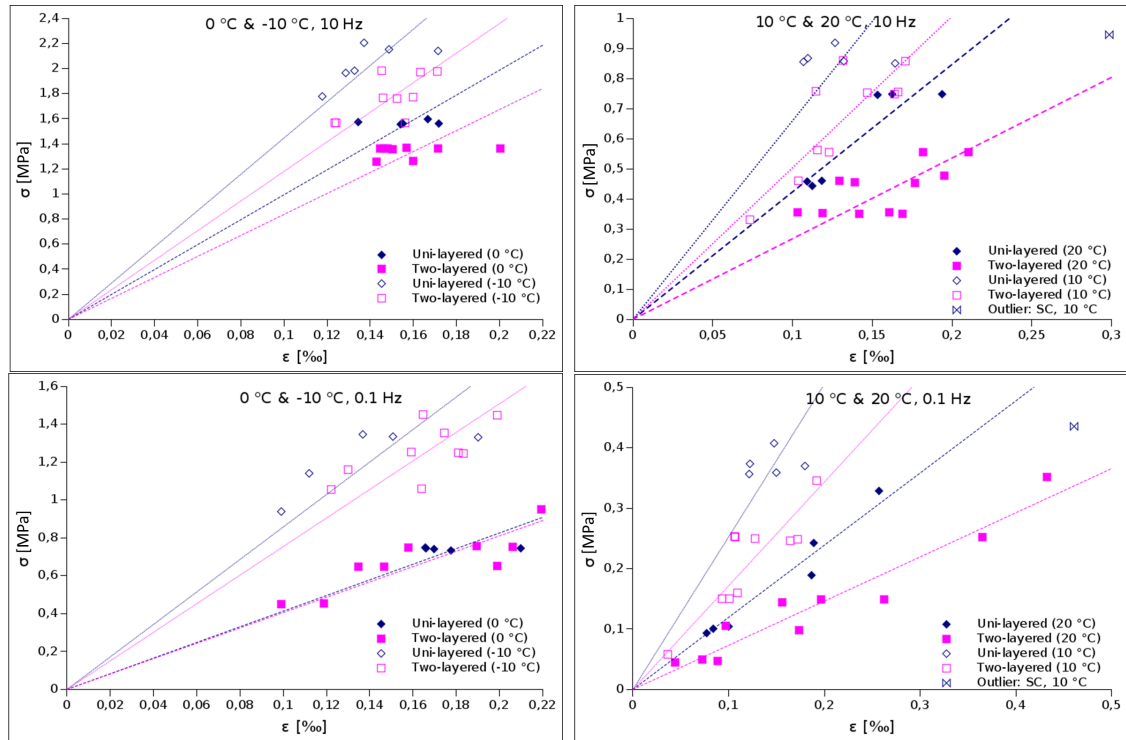
Figure III.3.15: Stress-strain graphs of the test carried out on the specimen of section 600, 610 and 650 (two-layered specimens) and SC and BC (uni-layered specimens) at 10 Hz (upper graphs) and 0.1 Hz (lower graphs) at -10 °C and 0 °C (left graphs) and 10 °C and 20 °C (right graphs)

Linear regression curves were drawn through the points of each section. The equation form of the lines was y = mx where m is the slope. The slopes and the coefficient of determination R^2 of each calculated regression curve are listed in table III.3.13.

Table III.3.13: Slope of the stress-strain regression curve of sections 600,610 and 650, summarized as two-layered specimens, and SC and BC, summarized as uni-layered specimens, for all temperatures and two frequencies (10 Hz and 0.1 Hz).

	10 Hz		0.1 Hz	
	Slope	R^2	Slope	R^2
Uni-layered, 20 °C	4.24	0.99	1.19	0.99
Two-layered, 20 °C	2.68	0.98	0.73	0.98
Uni-layered, 10 °C	6.60	0.97	2.53	0.98
Two-layered, 10 °C	5.04	0.98	1.72	0.97
Uni-layered, 0 °C	9.94	0.99	4.13	0.99
Two-layered, 0 °C	8.37	0.99	4.05	0.99
Uni-layered, -10 °C	14.46	0.99	8.58	0.98
Two-layered, -10 °C	11.80	0.99	7.54	0.99

It can be observed that for all temperatures and frequencies, except at 0 °C and 0.1 Hz, the slope of the uni-layered curve is clearly steeper than the slope of the two layered specimens. It can be concluded that the deformation achieved for the same stress levels are higher within two-layered specimens. For the mentioned exception of 0 °C, 0.1 Hz, it can be observed that the slopes are nearly equal, even though the slope of the uni-layered specimens is a little steeper than that of the two-layered.

If we observe the difference in percentage between the slopes of uni- and two-layered specimens at each temperature and frequency, as can be seen in figure III.3.16, it can be noticed that the slightest difference is to be found at 0 °C. Below and above this temperature, the differences are more important.
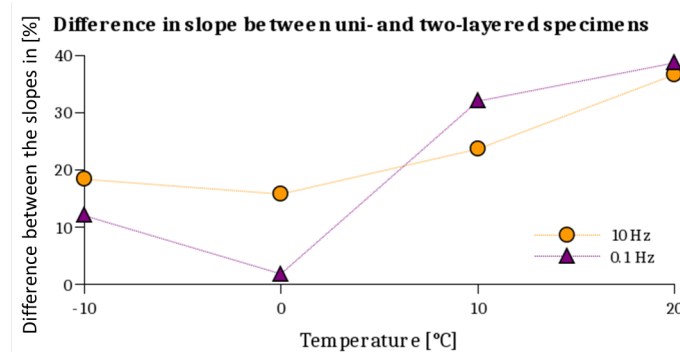
Figure III.3.16: Slope difference between uni-layered and two-layered specimens in percentage

These minima in the curves at 10 Hz and 0.1 Hz point out a change in behaviour at the transition between positive and negative temperature values, suggesting a different behaviour in deformations for positive and negative temperatures.

The fact that the difference is higher before 0 °C suggest an impact created by the low temperature, which could be due to the difficulty for the asphalt to change its shape at low temperatures.

At higher temperatures, we see quite high differences between the uni- and two-layered specimens, but as the slopes themselves are rather flat, the difference in stiffness modulus, in the end, is manageable, leading to relatively close stiffness modulus curves from 5 °C on (see III.3.11).

III.3.7   Conclusion: stiffness modulus

The indirect tensile tests on reinforced and unreinforced specimens give information on the acting of the reinforcement as well as on the acting of the interface inside the specimens.

The comparison of the two-layered specimens 600 and 650, with a rather similar shear strength, show the direct effect of the reinforcement by grid 5 compared to the specimens without grids. This led to a constant difference of approximately 1100 MPa for all temperatures.

The quite different shear resistance at the interlayer of the specimens of section 610 could be seen in the shape of its curve, which was different from the curves 600 and 650. Both courses were parallel on their entire length. The difference in shape showed the influence of the temperature on the displacement happening at the interface.

The comparison of the two-layered specimens with the uni-layered specimens SC and BC also show very different curve shape, especially at temperatures below 0 °C.

The observation of the strain-stress curves of the specimens at temperatures -10 °C, 0 °C, 10 °C and 20 °C and at 0.1 Hz and 10 Hz frequencies showed that, for same stress levels, more deformation took place in two-layered specimens than in uni-layered specimens, leading to different results in stiffness moduli. This difference was smallest at 0 °C, which leads to the assumption that different effects act on the interface of the specimens.

At higher temperatures it can be expected that the bonding between the interfaces becomes poorer, leading to more deformation. At lower temperatures it can be assumed that the differences are the results of cryogenic stresses, which in cases of two-layered specimens can be dissipated along the interface.

A comparison of the uni-layered and two-layered specimens is sadly not possible, as a quantification of the impact of the interface cannot be given. A possibility to investigate this special point could be to test two-layered specimens composed of the same asphalt mix on both sides and to compare with the results of uni-layered specimens made of the same asphalt mix. Such tests could additionally be carried out on two-layered specimens with different bonding characteristics, e.g. with different amount of emulsion or different surface treatments.

III.4   Fatigue testing of reinforced and unreinforced specimens

The fatigue of a material describes the effect of the repeated loading of a material with a load which, when applied a single time would perhaps cause no damage at all, but after a certain amount of loading can cause the fracturing of the material.

The application of a stress smaller than the rupture stress will lead to a progressive damaging, starting with microscopical damages, obliging a decreasing surface to support a constant stress. The damage due to fatigue will lead to the creation of cracks, which, in a composite material such as asphalt, can cause the loss of bonding between the individual materials being here the aggregate and the binder.

In their study of 2004, Di Benedetto et al. [DI BEN 04] divide the fatigue development into three characterizing phases:

- Phase I or adaptation phase: A strong loss of stiffness modulus and the creation of micro-cracks due to the repeated loading as well as to thixotropy and material warming.

- Phase II or quasi-stationary phase: The evolution of the stiffness modulus stays nearly constant, while the cracks spreads and distribute themselves inside the structure

- Phase III or failure phase: Phase during which the damage due to cracking accelerates. The micro-cracks become macro-cracks and spread through the structure, leading to failure of the structure.

These phases are illustrated in figure III.4.1.
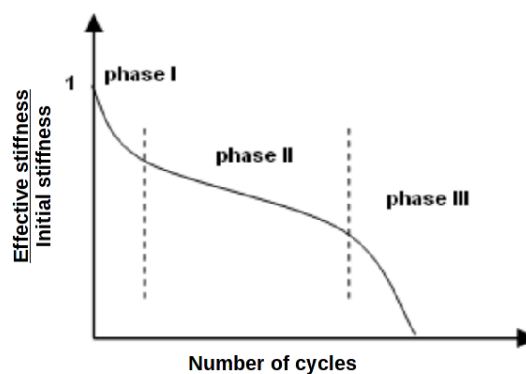
Figure III.4.1: Typical evolution of the modulus of a asphalt material under repeated loading [ARS 13]

The fatigue of asphalt materials can be determined with different tests, as described in section III.3. The test chosen for the investigations in this thesis is the indirect tensile

test (ITT). The description of the indirect tensile test can be found in section III.3.1.

The fatigue life of a specimen depends on various factors, for example, the load, as well as the loading mode, the material properties (Stiffness modulus, Poisson's ratio) and the form of the specimen [ARS 13].

It is to be noted that this tests adds a creep components, which is not rated in this study.

III.4.1 Specimens used for the fatigue tests

The specimens used for the fatigue tests are two layered, cylindrical specimens with a diameter of 100 mm, as described in section III.3.2.
The grids installed at the interface of the test-specimens were grids 1 and 5 extracted from the sections 610 and 650. The residual binder application rates used for the bonding were 600 g/m^2 and 1636 g/m^2 respectively. The unreinforced specimen was extracted from section 600 and was bonded with a residual binder application rate of 816 g/m^2. More information about the construction, the materials, the emulsion and the glass fibre grids can be found in section III.1.

III.4.2 Test implementation

The fatigue tests were carried out based on the German directive AL Sp-Asphalt 09 [AL-Sp 09].
The tests were performed at 10 °C and 20 °C, at a frequency of 10 Hz and were load controlled. To ensure a good tempering of the specimens, the specimens were laid in a climatic chamber for at least 12h before the beginning of the tests.

During the test, the cylindrical specimens were repeatedly loaded with cycles of a si-nusoidal form, going from a minimum compression stress of 0.035 MPa to a maximum compression stress, chosen so that the failure would occur between 1,000 and 1,000,000 cycles.
Extensometers positioned on each side of the specimen, as shown in figure III.4.2, mea-sured the horizontal displacement during the test.

The failure was defined as the cycle for which the stiffness modulus was only 50 % of the initial stiffness modulus:

$$Fatigue\,Criterium : \frac{E_N}{E_{init}} = 0.5 \tag{8}$$

With

E_N: Stiffness modulus at cycle N

E_{init}: Stiffness modulus measured at the beginning of the test, average of cycles 98 to 102

The stiffness modulus was calculated with equation (2) (see section III.3.3), using the displacements measured by the extensometers and the applied load levels.

Figure III.4.2: Test specimen inserted in the fatigue testing device

The fatigue curves of each section and for each temperature were constructed with the various results achieved for different maximum stress levels and their resulting deformations.

For 10 °C, the following stress levels were chosen:

Table III.4.1: Stress levels chosen for the fatigue tests at 10 °C

Stress levels [MPa]	0.4	0.6	0.9	1.0	1.5	1.6	
Section	**N° of specimens tested**						**Total**
600	1	2	1	2	2	1	9
610	1	2	2	-	3	-	8
650	1	2	3	-	3	-	9

For 20 °C, the variation of possible stress levels was limited by the load cell. For small stress levels (under 0.4 MPa), the stress application by the testing device could not be made exactly enough. The fatigue was therefore tested at only two stress levels.
At 20 °C the following stress levels were chosen:

Table III.4.2: Stress levels chosen for the fatigue tests at 20 °C

Stress levels [MPa]	0.4	0.6	
Section	N° of specimens tested		Total
600	3	3	6
610	3	3	6
650	3	3	6

III.4.3   Test results

III.4.3.1   Fatigue tests at 20 °C

The results of the fatigue tests made at 20 °C are listed in table III.4.3. The results are also represented in figure III.4.3, together with the determined regression curves and their equation.

Table III.4.3: Results of the fatigue tests made at 20 °C

Specimen	Max. stress σ	Initial strain ϵ_{init}	Initial stiffness modulus E_{init}	Failure stiffness modulus E_f	Cycle of failure N_f
	[MPa]	[%]	[MPa]	[MPa]	
600A	0.4	0.270	4662.3	2331.1	21197
600B	0.4	0.272	4639.5	2319.8	24692
600C	0.4	0.269	4680.9	2340.4	27491
600E	0.8	0.395	4203.2	2101.6	1591
600F	0.8	0.343	4837.0	2418.5	1795
600G	0.8	0.344	4821.3	2410.7	1896
610A	0.8	0.408	4071.5	2035.7	2299
610B	0.8	0.287	5794.9	2897.5	2197
610C	0.8	0.337	4925.6	2462.8	2796
610D	0.4	0.274	4602.2	2301.1	55100
610E	0.4	0.247	5106.4	2553.2	41692
610F	0.4	0.209	6048.5	3024.2	70594
650A	0.8	0.331	5014.8	2507.4	2697
650B	0.8	0.353	4705.1	2352.5	3200
650C	0.8	0.310	5347.5	2673.8	2800
650D	0.4	0.246	5124.0	2562.0	40995
650E	0.4	0.268	4703.8	2351.9	30296
650F	0.4	0.260	4842.2	2421.1	29797

It can be observed that, for both stress levels 0.4 MPa and 0.8 MPa, the reinforced specimens 610 and 650 achieve more cycles until failure than the unreinforced specimens 600.

The progression of the determined regression curves is not parallel, showing different influences based on the stress levels of the specimens.

When extended, it can be noted that curves 600 and 650 would meet at a stress level of 0.10 MPa after 2,349,217 cycles, curves 600 and 610 at a stress level of 1.24 MPa after 319 cycles and curves 610 and 650 at a stress level of 1.24 MPa after 3,494 cycles.
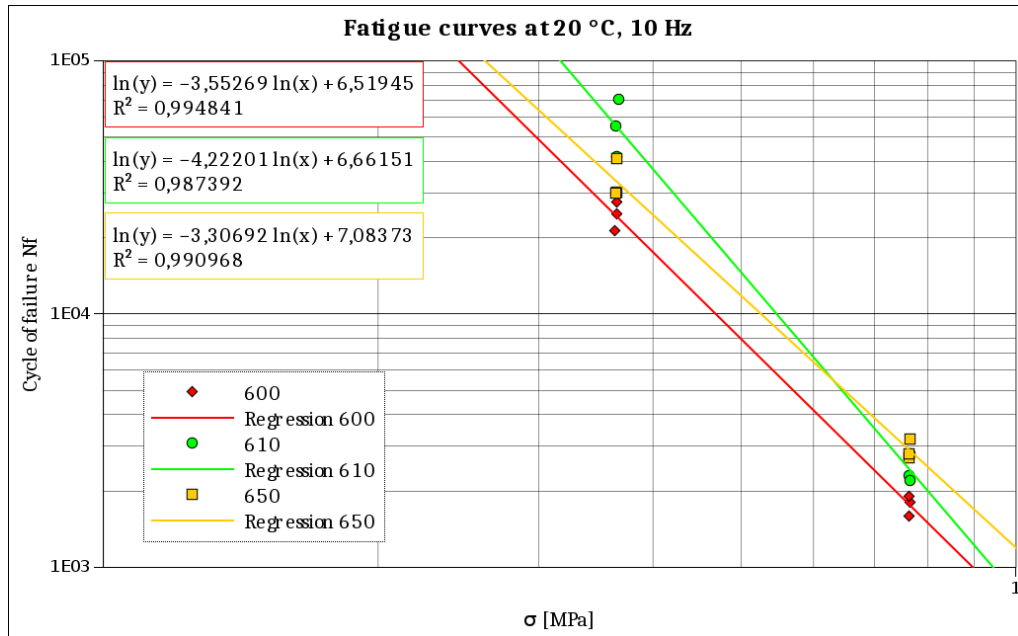
Figure III.4.3: Fatigue curves at 20 °C and 10 Hz

III.4.3.2 Fatigue tests at 10 °C

The results of the fatigue tests made at 10 °C are listed in table III.4.4. The results are also represented in figure III.4.4 together with the determined regression curves and their equations.

It can be observed that, unlike for the test-temperature 20 °C, the progression of the determined regression curves is nearly parallel. This can be seen in the very similar slopes of the curves (average: -4.6080, Std. dev.: 0.0711, coefficient of variation: -0.0154). It can also be observed that the axis intercepts of reinforced curves 610 and 650 are equally similar (Average: 9.554, Std. dev.: 0.045, coefficient of variation: 0.005), so that the two curves lie nearly on top of each other.

In contrast, the axis intercept of the unreinforced curve 600 shows a difference of 0.487 compared to the average value of the reinforced section.

Table III.4.4: Results of the fatigue tests made at 10 °C

Specimen	Max. stress σ	Initial strain ϵ_{init}	Initial stiffness modulus E_{init}	Failure stiffness modulus E_f	Cycle of failure N_f
	[MPa]	[%]	[MPa]	[MPa]	
600T	0.4	0.084	7435.7	3717.9	711444
600V	0.6	0.124	7864.9	3932.4	150539
600X	0.6	0.130	7472.5	3736.3	136567
600Q	0.9	0.237	6279.1	3139.6	8093
600R	1.0	0.172	9639.0	4819.5	19491
600W	1.0	0.218	7601.9	3800.9	16095
600M	1.5	0.341	7389.1	3694.5	1591
600P	1.5	0.457	5511.0	2755.5	995
600N	1.6	0.390	6883.5	3441.7	998
610Q	0.4	0.085	7436.5	3718.2	965489
610U	0.6	0.115	8451.4	4225.7	272817
610X	0.6	0.141	6901.9	3450.9	293768
610N	0.9	0.194	7666.3	3833.1	24599
610P	0.9	0.212	6997.1	3498.5	20298
610M	1.5	0.323	7776.3	3888.2	2691
610S	1.5	0.334	7549.2	3774.6	2698
610T	1.5	0.344	7316.5	3658.3	2495
650J	0.4	0.065	9734.1	4867.0	928075
650S	0.6	0.102	9520.2	4760.1	224711
650R	0.6	0.103	9428.5	4714.3	230788
650N	0.9	0.172	8680.5	4340.2	33192
650Q	0.9	0.178	8370.3	4185.1	43597
650U	0.9	0.201	7383.3	3691.7	25797
650M	1.5	0.263	9581.0	4790.5	1498
650P	1.5	0.304	8285.9	4143.0	2194
650W	1.5	0.328	7681.7	3840.9	2195
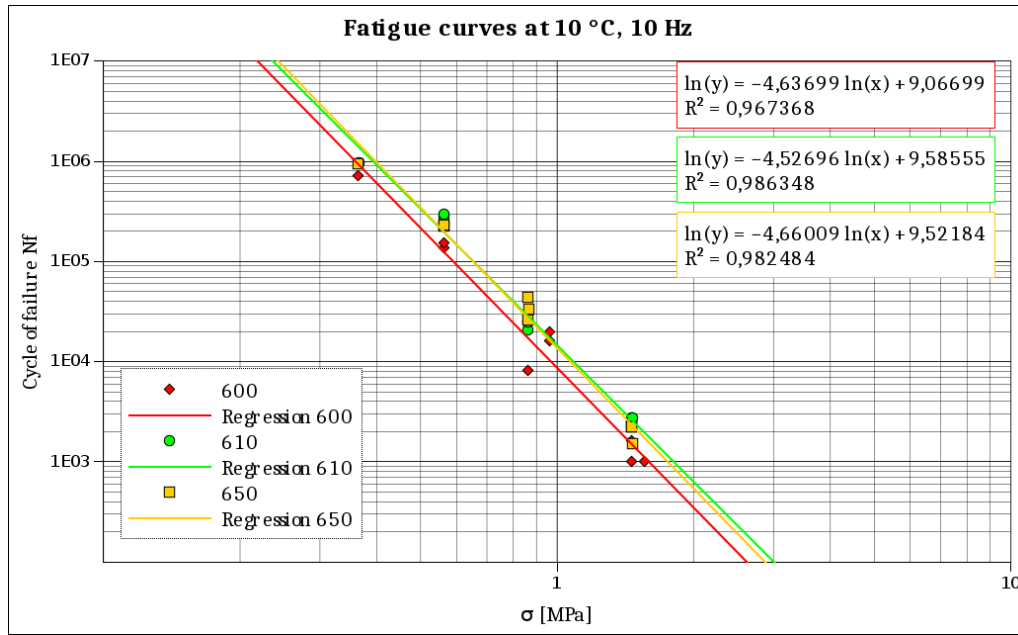
Figure III.4.4: Fatigue curves at 10 °C and 10 Hz

III.4.4   Interpretation

At 20 °C, it is observed that for both stress levels, the number of cycles reached by reinforced samples is always higher than by the unreinforced samples.

The graphical representation shows that the smaller the stress load, the greater the difference to both other curves, showing that the influence of grid 1 at 20 °C becomes particularly important, when small stresses occur, but is less noticeable for higher stress levels.

In contrast, the specimens of 650 show that the higher the stress level, the greater the positive influence of the grid in comparison to the two other groups.

At 10 °C the described behaviours are not shown anymore, as the progression of the three curves is nearly parallel, which leads to the assumption that here again, the temperature influence on the grid impact is great.

When looking at the slopes of the curves at both temperatures, we observe that only section 610 keeps a constant slope of -4.222 at 20 °C and -4.527 at 10 °C, while slopes 600 and 650 vary from -3.553 and -3.307 respectively at 20 °C to -4.637 and -4.660 respectively at 10 °C. Remembering the stiffness modulus testing, it can be noted that the behaviour of sections 600 and 650 keep a constant difference at all temperatures, while the results of section 610 vary compared to the two others.

Keeping this in mind, we can observe a parallelism in behaviour, as at this point again the specimens of section 610 behave differently from the specimens 600 and 650. This would mean that here again, the influence of the shear strength, or of the great amount

of residual binder at the interface on the fatigue life can be measured.

III.4.5   Observation made on uni-layered and two-layered tested cores

In order to observe the crack propagation during a repeated load test in reinforced and unreinforced specimens, it was decided to film some of the tests.
For good sight conditions and as the horizontal displacement was of secondary importance for these observations, the extensometers were not fixed on the cores.
The tests filmed with a were done with a high-resolution camera, allowing to see the details from crack initiation and propagation until failure occurred.

The cores tested here were two-layered specimens from the section 600, 610 and 650 as used for fatigue and modulus testing as well as uni-layered cores from the surface and binder course of the surface test used during the modulus tests.
The tests were carried out in a stress-controlled way with a constant stress of 0.8 MPa and a sinusoidal loading. In order to protect the test machine, the stopping criteria were set to be a maximum of 7 mm vertical displacement through the pressure cell.
In order to have a better view of the cracks, the specimens were sprayed with white colour, which however still enabled the seeing of aggregates through the colour. The black lines on the 600, 610 and 650 specimens represent the position of the interface.
The pictures represented in figure III.4.5 (see also appendix IV) show the 5 specimens at 5 different moments of the tests, showing the different advancements, beginning at the first cycle and ending when the maximum 7 mm vertical displacement was reached.

The first observation to be made is the form of the specimens at the end of the tests. It is clearly visible that the reinforced specimens did not break apart, in contrast to the unreinforced specimens. It can be observed that both glass fibre grids hold the specimens together in absolute contrast to the other specimens.
The second observation is of the crack propagation. When looking at the specimens of 600, 610 and 650 at 50 %, it can be observed that on specimen 600, a crack is in formation on both sides of the interface, while for the cores 610 and 650, the first signs of a crack are to be seen on only one of the two sides (upper side for 610 and lower side for 650). At 75 %, the cracks on the reinforced specimens are still strongly one-sided, while the two cracks visible on both sides of the interface of specimen 600 have already touched.

(a)600, 0 %   (b)610, 0 %   (c)650, 0 %   (d)SC, 0 %   (e)BC, 0 %

(f)600, 25 %   (g)610, 25 %   (h)650, 25 %   (i)SC, 25 %   (j)BC, 25 %

(k)600, 50 %   (l)610, 50 %   (m)650, 50 %   (n)SC, 50 %   (o)BC, 50 %

(p)600, 75 %   (q)610, 75 %   (r)650, 75 %   (s)SC, 75 %   (t)BC, 75 %

(u)600, 100 %   (v)610, 100 %   (w)650, 100 %   (x)SC, 100 %   (y)BC, 100 %
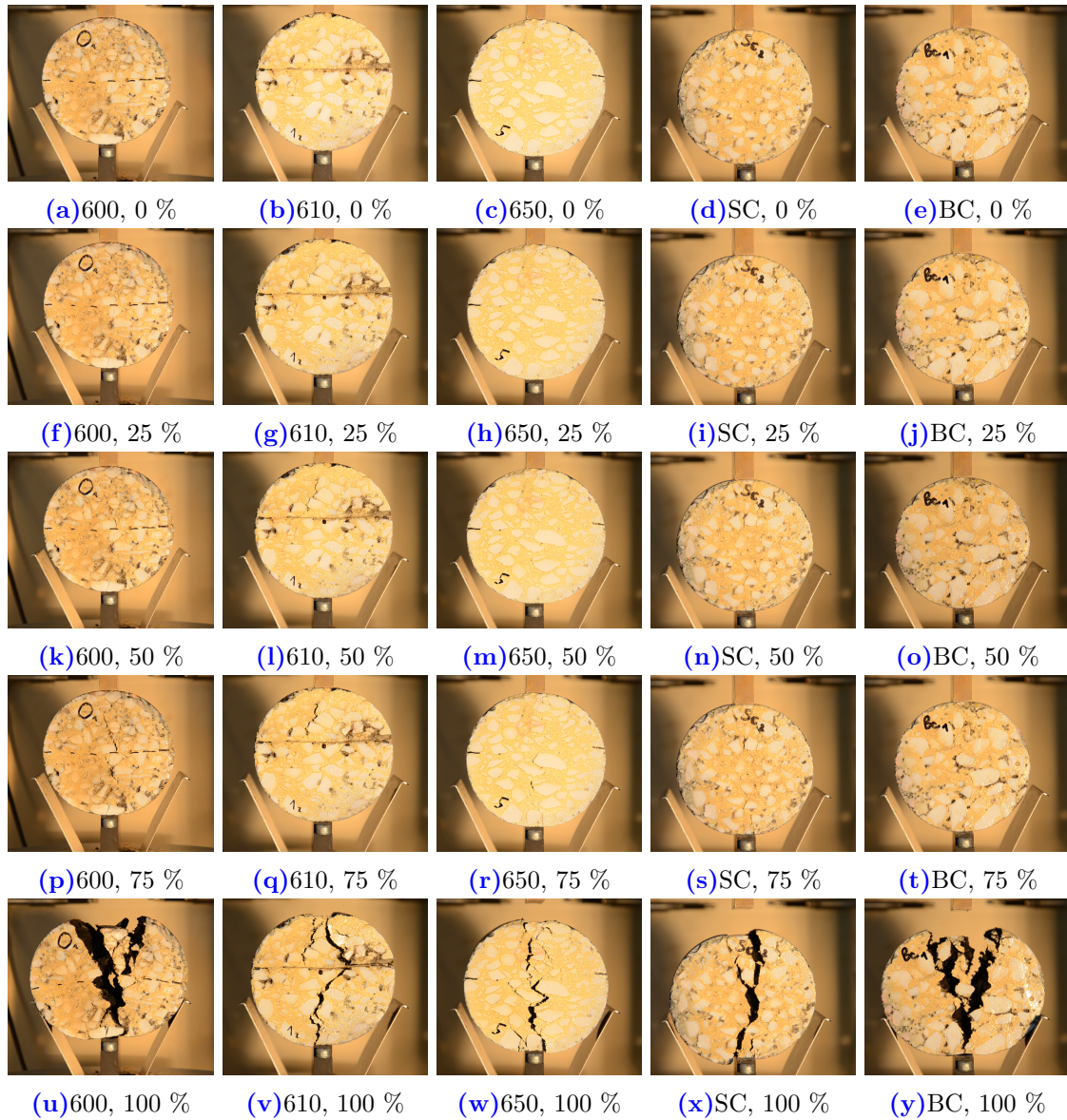
Figure III.4.5: Photos of uni-layered and two-layered reinforced and unreinforced specimens during repeated loading test

III.4.6   Conclusion - Fatigue testing

The fatigue tests conducted on reinforced and unreinforced cylindrical specimens under indirect tensile strength showed a positive effect of both reinforcement on the fatigue life time of the cores, compared to the unreinforced specimens. This was the case for both test temperatures 10 °C and 20 °C.

It was also observed that at 10 °C, the slopes of the fatigue curves were nearly the same for all three specimens types, showing three parallel progressing curves, only varied through their different intercept. It can be noted that at 10 °C, the results between the

specimens of section 610 and 650 are very similar.

At 20 °C however, the observed parallelism was non-existent and the curves of the reinforced specimens showed a different tendency: Compared to the unreinforced specimens, the specimens of section 650 showed the greatest difference for high-stress levels, but approached the results of 600 for lower stress levels. In contrast, the curve of section 610 showed a steeper slope and improved fatigue life results for low-stress levels.

The picture made during repeated load tests showed the different type of crack propagation, as on two layered, reinforced specimens, the cracks propagated first in one of both layers and crossed the interface only shortly before the end of the test, while the unreinforced specimen showed a crack propagation on both layer sides.
It was also observed that at the end of the test, i.e. after a vertical displacement of 7 mm of the pressure cell, the cores of the unreinforced specimens were falling in two parts, divided through the center, while the cores of the reinforced specimens kept together.

Part IV

In-situ observations

IV.1   In situ observations: RD4

IV.1.1   RD4: Informations and characteristics

The in-situ observations were carried out on a 800 m long road section in France, named RD4 ('Route Départementale' n° 4) near the town of Colmar. The purpose was to investigate the impact of the installation of grids on a cracked road section. To do so, the test section was monitored before and after road maintenance works, which took place in October 2015.

The section of the RD4 observed in this study is located in the department 'Haut Rhin' in the north east of France, between the villages of Holtzwihr/Wickerschwihr and Muntzenheim in an agricultural region. The road has one lane in each direction and a heavy traffic circulation of 300 a day (total of the two lanes). A map of the location and an aerial photograph of the section are shown in figure IV.1.1.

(a)   (b)
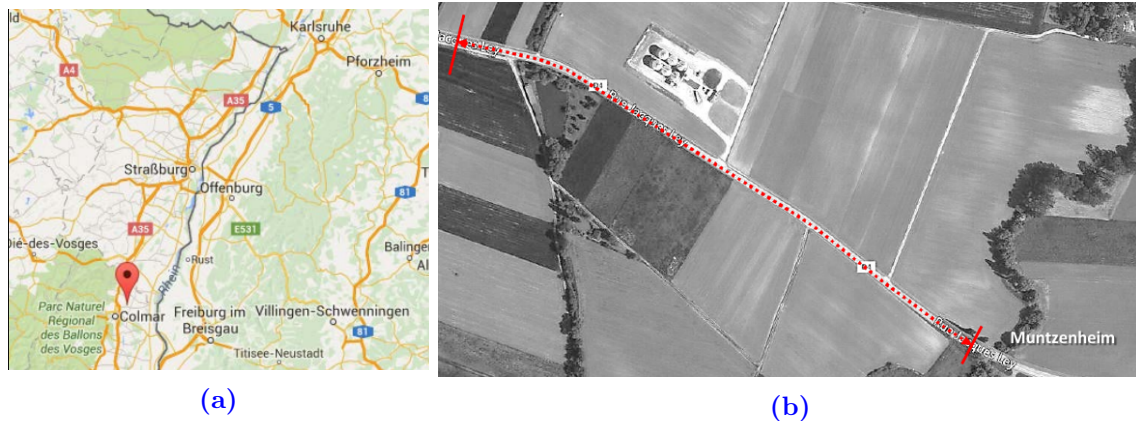
Figure IV.1.1: (a) Localisation of the RD4 and (b) aerial photograph of the RD4 (Map data ©2017 Google and ©2017 GeoBasis-DE/BKG (©2009), Google, Holtzwihr)

During former construction works, a test drilling was performed near Wickerschwihr, giving information about the structure of the road and the ground (see appendix V):

- 0.15 m of asphalt

- 1.15 m of embankment: sands, gravel, pebble

- 1.20 m of sandy clay and gravel

IV.1.2 Monitoring of the RD4 before road maintenance works

IV.1.2.1 Materials of the RD4

As no information could be found regarding the history of the RD4, characteristics of the road structure and materials used in the road had to be determined by different analyses. Therefore, a first core extraction campaign was ordered, during which 6 cores were extracted from the RD4. Four of these cores were sent to an external laboratory (core A to D), where the moduli of the different layers were determined (see results in section IV.1.4.4). One of the cores was not representative (core X), as its structure was clearly different from the structure of the other cores. One of the cores was examined in the laboratory of the Hochschule Karlsruhe (core H) in order to determine the binder content, the binder characteristics as well as the nominal maximum aggregate size used in the different layers.

Pictures of the extracted cores as well as the location of their extraction are shown in figure IV.1.2.
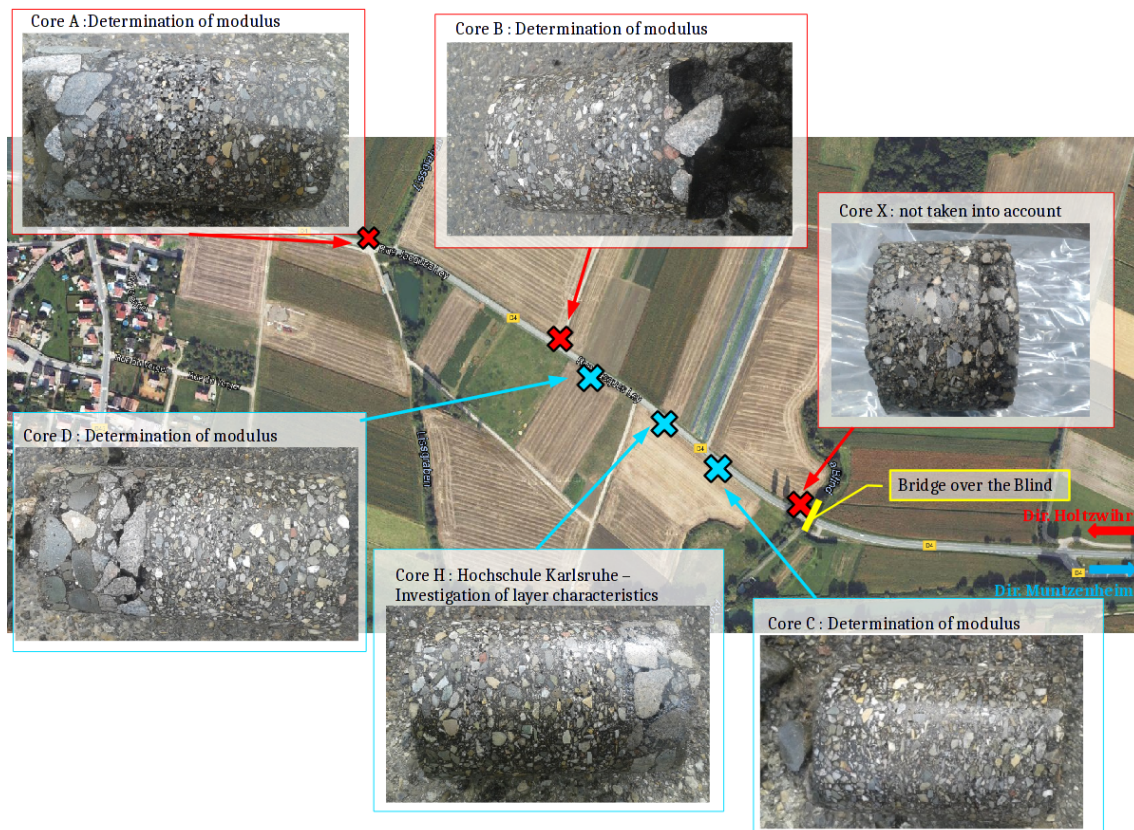
Figure IV.1.2: Cores, location of the cores and purpose of the cores extracted from the RD4 before road maintenance works

Except for core X, the cores extracted from the RD4 consisted of 4 different layers. It was observed that the three upper layers of the cores were asphaltic layers of approx-

imately the same heights and that the fourth layer was a macadam which in some cases fell apart during the drilling. The picture of a core with its different layers is shown in figure IV.1.3
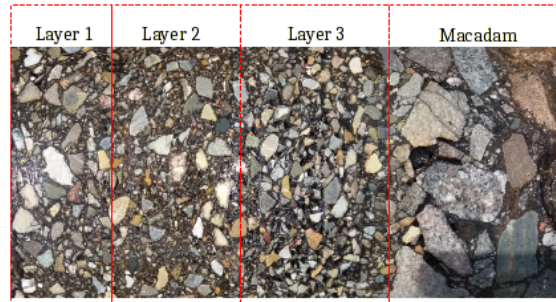
Figure IV.1.3: Core of the RD4 with the different layers

The layers of core H were cut apart from each other. The bitumen and the aggregates of each layer were extracted with an asphalt analyser using trichloroethylene as dissolvent.

Aggregates The extracted aggregates of layer 2 and 3 were sieved and the maximum aggregate size as well as the fine content were determined. They are listed in table IV.1.1.

Table IV.1.1: Maximum aggregate size and fine content of aggregates of layers 2 and 3 of the RD4

Layer	Passing at 16 mm	Passing at 11.2 mm	Fine content after extraction
2	100 %	98.86 %	10 %
3	100 %	98.60 %	7.6 %

Based on these results, it can be assumed that layers 2 and 3 had a nominal maximum aggregate size of 11 mm. This size is rather small and is mostly used in a surface course.

Bitumen After extraction the bitumen of layers 1, 2 and 3 were heated up at a temperature of 150 °C to 155 °C and filled in the respective forms for the needle penetration test and the ring and ball test.

The needle penetration test was performed in accordance with standard DIN EN 1426 [EN 1426]. The results are listed in table IV.1.2.

Table IV.1.2: Results of needle penetration test on the bitumen of the 3 asphalt layers of the RD4

Needle penetration [1/10 mm]							
Layer	Test 1	Test 2	Test 3	Test 4	Test 5	Test 6	Test 7	Average
1	20.3	20.8	19.1	17.9	21.2	21.0	20.5	**20.1**
2	36.9	33.8	24.9	35.0	29.9	30		**31.8**
3	17.3	18.5	17.2	19.7	21.8	18	16.2	**18.4**

The ring and ball tests were performed in accordance with standard DIN EN 1427 [EN 1427]. The results are listed in table IV.1.3.

Table IV.1.3: Results of Ring and Ball test on the bitumen of the 3 asphalt layers of the RD4

Softening point [°C]				
Layer	Test 1	Test 2	Test 3	Test 4	Average
1	66.6	66.8	66.2	66.5	**66.5**
2	59.7	59.5	60.0	60.1	**59.8**
3	64.7	64.6	64.7	65.0	**64.8**

It is known that no construction works were done on the RD4 in the past few years. It can therefore be assumed that the binder used in the different layers is at least 5 years old, and even 10 to 15 years in the lower layers. As explained in section I.1.3.3, bitumen oxides when it is in contact with air, leading to a stiffer and more brittle bitumen. In order to determine which bitumen was used at the time of the construction, a back-calculation is needed.

Based on the results published in Forschung Straßenbau und Straßenverkehrstechnik, issue 774, [FSS 99], the values of Ring and Ball and Needle Penetration of the bitumen 30/45, 50/70 and 70/100 varies over a time period of 15 years as follows (table IV.1.4):

Table IV.1.4: Change of different bitumens characteristics over 15 years

Bitumen	Δ RaB [°C]	Δ Pen [1/10 mm]
B 80 (70/100)	+ 19.9	- 52
B 65 (50/70)	+ 18.4	- 35
B 45 (30/45)	+ 15.1	- 26

As the bitumen 70/100 is rarely used in France, it can be assumed that the bitumen used on the RD4 was either a 50/70 or a 30/45 or a bitumen having a penetration grade in-between. The use of a polymer-modified bitumen is also excluded as it is improbable that such a bitumen was used on a road with such a traffic load.

Therefore it was chosen to use the average value of 30/45 and 50/70 as correction factor on the Ring and Ball and Needle Penetration values determined on the RD4-cores, resulting in the following values (table IV.1.5):

Table IV.1.5: Bitumen values of RD4 before and after the use of an ageing correction factor

	RaB now	RaB before 15 a	Pen now	Pen before 15 a
Layer	[°C]	[°C]	[1/10 mm]	[1/10 mm]
1	66.5	**49.8**	20.1	**50.6**
2	59.8	**43.1**	31.8	**62.3**
3	64.8	**48.0**	18.4	**48.9**

It is to be noted that these values are purely theoretical and shall give an idea of the possible state of the bitumen in new condition.

Void, binder, aggregate and fine content   The calculation of the void, binder, aggregate and fine contents is based on the values obtained after the extraction procedures. The different contents are listed in table IV.1.6.

Table IV.1.6: Void, binder, aggregate and fine contents of the three layers of the core extracted from the RD4

	Void content	Binder content	Granular content	Fine content
Layer	[Vol-%]	[M-%]	[M-%]	[M-%]
1	5.55	6.00	94	9.1
2	5.85	6.09	93.01	10.0
3	7.19	5.95	94.05	7.6

Based on the collected values and the national practices, it was assumed that the 3 upper asphalt layers of the RD4 are surface course of the type 'BBSG', standing for 'béton bitumineux semi-grenu' being a rather thick asphalt layer (3 cm to 9 cm) which is often used as a surface or a binder course with nominal maximum aggregate sizes of 0/6, 0/10 or 0/14.

In our case, we assume that the three layers have a nominal maximum aggregate size of 0/10 and a 35/50 or 50/70 bitumen.

The lowest layer is assumed to be a macadam layer. No other characteristics are known.

IV.1.2.2   Damage types observed on the RD4

The observation of the RD4 showed different damage types:

- Change in road structure

- Longitudinal cracks at the centre line

- Longitudinal cracks on the right wheel track

- Crocodile cracks (especially at the end of the section in direction Muntzenheim, on both lanes)

Pictures of the section before road maintenance works can be seen in figure IV.1.4.

Figure IV.1.4: Photographs of the RD4 before maintenance and location of the pictures taken (map on the right, second line)

IV.1.2.3   Deflection measurements with Flash Deflectograph

Before the maintenance works, deflection measurements with a Flash deflectograph were done on the entire road length.
The Flash deflectograph is the latest version of the Lacroix Deflectograph (see figure IV.1.5), used to measure the deflection basin of a surface under a heavy weight moving at a constant speed of 3.5 km/h or 7 km/h. [VEC 17]

The measurements take place between each double-wheel of the rear axle, which is loaded with a constant load of 13 tonnes. A measuring device consisting of two measuring beams is placed on the surface of the road while the truck is moving. A first deflection measurement is made in an unloaded state (under the truck) and a second measurement
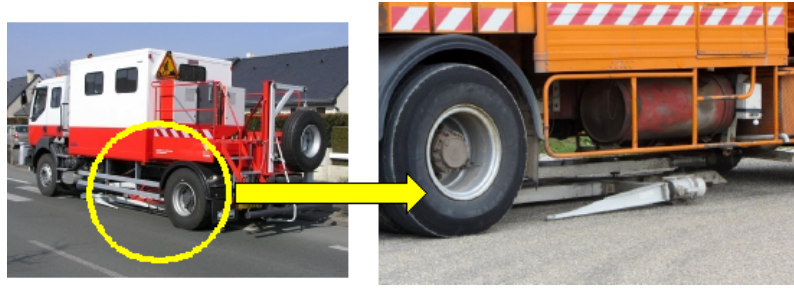
Figure IV.1.5: Deflectograph Flash and Lacroix: Truck and measuring device [VEC 17]

when the beams are positioned between the double wheels of the rear axle. The measuring device is lifted up and pulled back to the centre of the track, where it is placed on the surface again and the measurement restarts from the beginning. The difference between the two measurements is the deflection and is given in [1/100 mm]. The principle is highlighted in figure IV.1.6. This procedure enables to have measurement points every 5 m under each of the double-wheels. The measurements taken under the left double-wheel are described with the name 'Axis-side', the measurements under the right double-wheel are named 'Bank-side'.
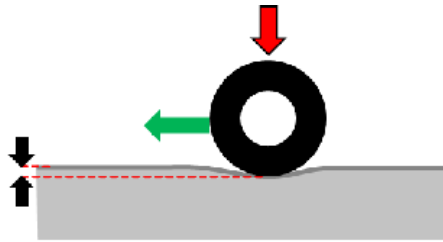
Figure IV.1.6: Principle of the deflection measurement

The measurements started at the eastern end of Holtzwihr and went until the junction with the road RD112, which is approximately 2 km. The observed section represents only a section of 650 m and only this section will be examined in the rest of this work.

Temperature adjustment The road surface temperature is also measured with the measurement device of the deflectograph at each measurement point. In order to compare the values obtained, a temperature adjustment is applied to on the values. The reference temperature is 15 °C. The adjustment is done based on the following equation given by the [CFTR 09]:

$$D_{15} = \frac{D_T}{1 + K * \frac{T-15}{15}} \tag{9}$$

With

D_{15}: Deflection at 15 °C (reference temperature) [1/100 mm]

D_T: Deflection at temperature T [1/100 mm]

T: Temperature [°C]

K: Coefficient depending on the structure type

Coefficient K is chosen depending on the existing structure type:

- Flexible structure: K = 0.15

- Thick asphalt structure: K = 0.2

- Mixed structure: K = 0.08

- Semi-rigid structure: K = 0.04

The coefficient corresponding to the RD4 is K = 0.2.

Deflection measurements June 2015 after temperature adjustment   Figure IV.1.7 shows the deflections measured June 2015, before the maintenance works were done, on both side of the RD4, where M15 stands for the measurements done in 2015 in the travel direction of Muntzenheim (eastbound) and H15 for the measurements done in 2015 in the travel direction of Holtzwihr (westbound). Figure IV.1.7a shows all values measured on both sides of the road and under both double-wheels of the deflectograph (bank and axis). Figure IV.1.7b shows the measurement made under the left double-wheel (axis) and figure IV.1.7c shows the measurements done under the right double-wheel (bank).

It can be observed that the form of the moving average curves on bank and axis sides is approximately the same, but that the curves of the bank-sides show a more pronounced form and the deflections on the bank sides are much higher than on the axis-side, indicating a more weakened edge of the road, which confirms the visual observation made on the RD4.

It can also be seen that after about 2/3rd of the distance, both bank and axis sides show higher deflections. This is especially visible when looking at the moving average curves.
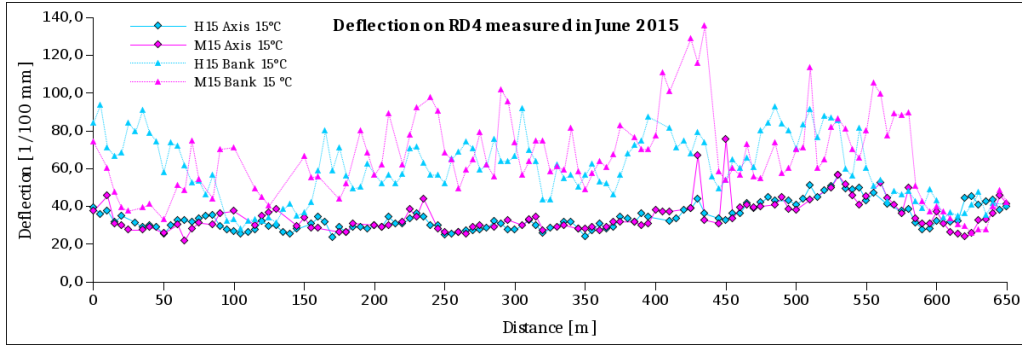
(a) Deflection measured in the direction Holtzwihr and Muntzenheim on axis and bank sides.
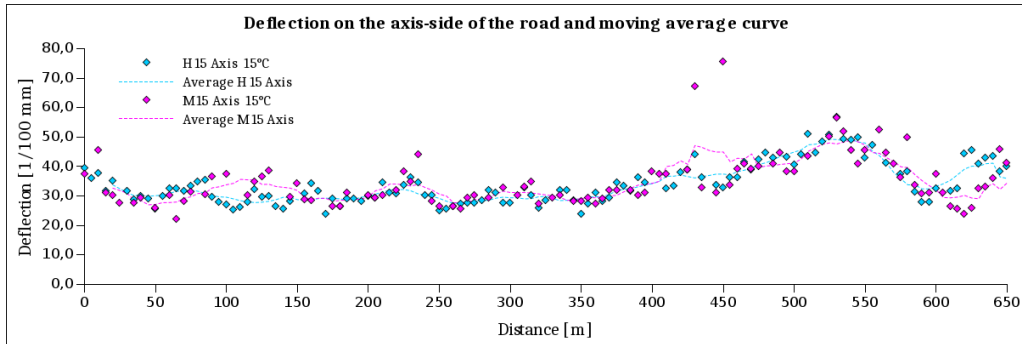
(b) Deflection measured in the direction Holtzwihr and Muntzheim on axis sides and moving average curves
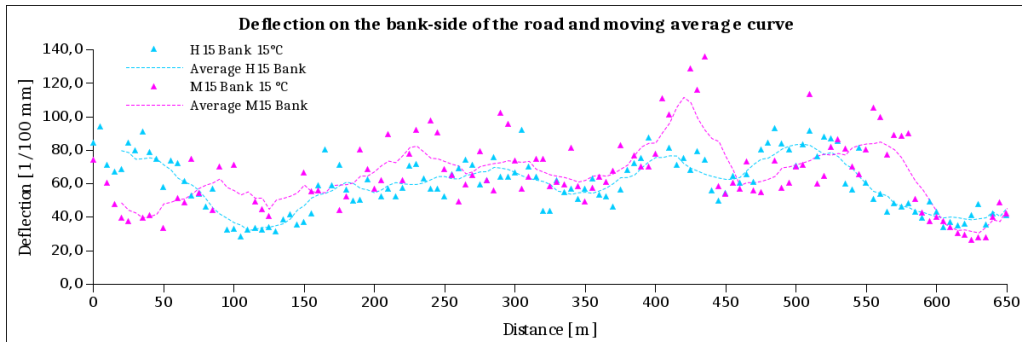
(c) Deflection measured in the direction Holtzwihr and Muntzheim on bank sides and moving average curves

Figure IV.1.7: Deflection measured on the RD4 in June 2015

The average values of the measurements of the bank and axis side in both directions are listed in table IV.1.7 , together with their standard deviations and coefficients of variation. As an increase in the deflection was observed after about 2/3rd of the distance, it was decided to divide the route into different sections as follows:

- Measurements on axis sides:

    Part 1: 0 m to 400 m,

    Part 2: 405 m to 580 m

    Part 3: 585 m to 650 m

- Measurements on bank sides:

  Part 1: 0 m to 350 m,

  Part 2: 355 m to 450 m

  Part 3: 455 m to 650 m

Table IV.1.7: Average values, standard deviations and coefficients of variation of the deflection measured on the RD4 in 2015

	Distance	Average deflection	Standard Deviation	Coefficient of variation
	[m]	[1/100 mm]	[1/100 mm]	
M15 Axis	0-400	31.0	4.39	0.142
	405-580	44.0	9.87	0.224
	585-650	32.4	6.21	0.192
	Total	34.9	8.7	0.2
H15 Axis	0-400	30.2	3.39	0.112
	405-580	42.1	6.13	0.145
	585-650	36.8	6.42	0.174
	Total	34.0	6.9	0.2
M15 Bank	0-350	62.6	16.50	0.264
	355-450	83.1	26.66	0.321
	455-650	61.4	23.20	0.378
	Total	65.2	21.9	0.3
H15 Bank	0-350	58.7	15.96	0.272
	355-450	65.5	12.23	0.187
	455-650	59.5	19.10	0.321
	Total	59.9	16.6	0.3

IV.1.3 Maintenance works on the RD4

The maintenance works on the RD4 were conducted between the eastern end of the village of Wickerschwihr and the junction of the RD4 with the RD112. The test sections are located in the middle of the route. The works were conducted on two different days: On the first day, the works were executed from the eastern end of Wickerschwihr to the beginning of the observed section, which is about 300 m later. On the second day, the rest of the road was done, which corresponds to about 1.7 km.

The construction of the observed section took place on October, 30th of 2015.

The maintenance works consisted in adding a new surface layer on the top of the present road. The height of the new surface layer was to vary between 6 cm and 4 cm, corresponding to a BBM and BBTM asphalt layer based on French classification.

The observed section was divided into 5 different sections: two reference sections with 6

cm of the new surface course at the beginning and the end of the observed section and 3 reinforced sections in the middle, as shown in figure IV.1.8:

- First section: 'Ref 6 cm' - unreinforced section with 6 cm overlay

- Second section: 'N1' - section reinforced with grid N1 with 4 cm overlay

- Third section: 'N5' - section reinforced with grid N5 with 4 cm overlay

- Fourth section: '5' - section reinforced with grid 5 with 4 cm overlay

- Fifth section: 'Ref 6 cm - 2' - unreinforced section with 6 cm overlay
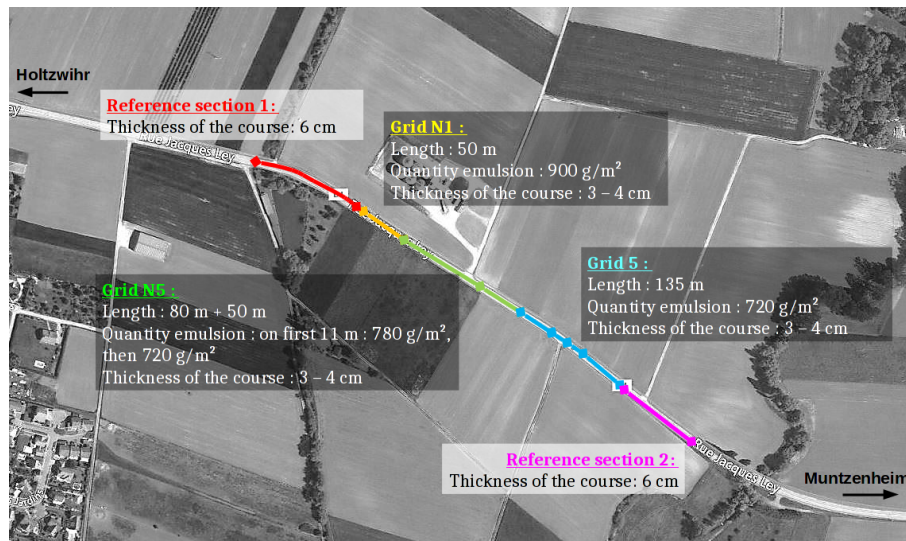
Figure IV.1.8: Five sections and characteristics of each of the observed RD4

IV.1.3.1 Materials used for the maintenance works

Asphalt The asphalt used for the new surface course was an AC 0/10 with a maximum nominal aggregate size of 10 mm and a 50/70 bitumen and the addition of 20 % of recycling materials with a maximum aggregate size of 14 mm.

The fine content represents 2.6 %, the binder content is 5.4 % with 1 % brought by the recycling materials. The bulk density of the asphalt was 2.429 to/m^3.

Emulsion The emulsion used for the bonding between the old structure and the new surface layer is C65B4-S with 65 % residual binder. The application rate varied depending on the section of the road. The application rate for every section is shown in figure IV.1.8.

Glass Fibre Grids The grids used in the section are N1, N5 and 5. Grids N5 and 5 correspond to grids N and 5 applied on the test surface described in section III.1. A description of the grids is given in table IV.1.8 .

Table IV.1.8: Characteristics of the glass fibre grids installed on the RD4

Grid Name	Non-woven	Resin	Tensile strength	Mesh size
			kN/m	cm^2
N1	Light polyester fibre	B	100	4 x 4
N5	Light polyester fibre	B	50	4 x 4
5	Light polyester fibre	A	50	4 x 4

IV.1.3.2 Construction steps

The construction was done under running traffic conditions, meaning that one lane remained open for traffic while the other was constructed. The construction was started in the morning with the lane towards of Muntzenheim. The lane towards Holtzwihr was constructed in the afternoon.

Before starting the construction, the surface of the old structure was swept with a road sweeper. Afterwards a bitumen sprayer started to spread the emulsion corresponding to the section (figure IV.1.9a). The junction between the road section made the day before and the new section was made by adding a greater amount of emulsion on the junction.
For the section reinforced with grids, the emulsion was always spread only a few meters ahead, so that the grids could be applied on the unbroken emulsion.
The grids were unrolled manually on their full length by pushing the roll with the foot. It was then pressed onto the road surface with the help of brushes until the non-woven was soaked with emulsion.
As the section of grid 5 is partly laid in a curve, the grid had to be cut in smaller parts of about 20 m length each (see figure IV.1.9c).
Grid N5 was laid in two parts: the first one had a length of 80 m, the second one of 50 m.
The overlapping of two grids was done over a length of about 50 cm to 1 m.
The laying of the asphalt layer was started when the installation of the grids was sufficiently advanced so that the laying had not to be interrupted.

(a)   (b)   (c)   (d)

Figure IV.1.9: RD4 maintenance works: Construction steps: (a): Emulsion sprayer at the beginning of the construction works; (b): Difference in emulsion application rate, left: section N1, right: section Ref 6 cm; (c) Application of grid 5 in the curve (d) Finished road

IV.1.4   Monitoring of the RD4 after maintenance works

IV.1.4.1   Visual inspection of the RD4 after maintenance works

The RD4 was inspected visually a few times between October 2015 and May 2017. The inspection showed no sign of cracks, neither on the reinforced nor on the unreinforced sections. However, other particularities were observed:

- **Small pull-outs and small bitumen accumulations**
  First observation: December 2015
  Location: continuously
  Possible explanation: Demixing of the asphalt-components in the trucks before installation; low temperatures on the construction day
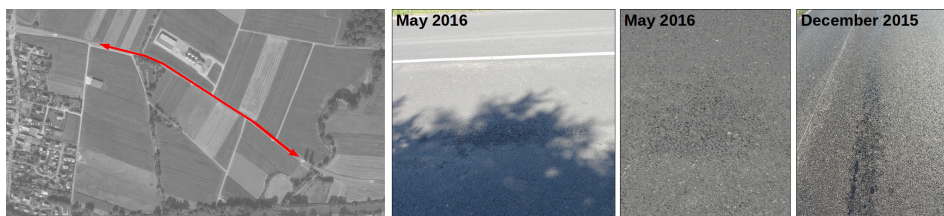
Figure IV.1.10: RD4: Small pull-outs and small bitumen accumulations

- **Medium and big bitumen accumulations**
  First observation: August 2016
  Location: In direction of Muntzenheim, second half of the observed section
  Possible explanation: Resulting from the high temperatures in the summer combined with the traffic load

Figure IV.1.11: RD4: Medium and big bitumen accumulations

- **Crack at the centre line**

  First observation: December 2015, constant deterioration

  Location: continuously

  Possible explanation: Bad bond between the two lanes, as they were built one after the other without reinforcing the centre with extra emulsion

Figure IV.1.12: RD4: Crack at the centre line

- **Big pull-outs**

  First observation: June 2016

  Location: Towards Muntzenheim, second half of the observed section

  Possible explanation: Demixing of the asphalt-components in the trucks before installation, weak bonding between the aggregates

Figure IV.1.13: RD4: Pull-outs

- **Superficial, very straight crack**

  First observation: February 2017

  Location: Continuously towards of Holtzwihr

  Possible explanation: mechanically created crack through metallic object cutting in

the road

Figure IV.1.14: RD4: Superficial, very straight crack

- **Crack between the section built 29/10/15 and the section built 30/10/15**
  First observation: February 2017
  Location: First half of the observed section, towards Muntzenheim
  Possible explanation: Bond between the two sections was not strong enough

Figure IV.1.15: RD4: Crack between the section built in on 29/10/15 and the section built on 30/10/15

IV.1.4.2   Extraction of cores after the maintenance works

9 cores were extracted from the RD4 in May 2017. These cores were used to determine the thickness of the new surface layer at different positions, to determine the elastic modulus of the new layer and to investigate the quality of the bonding between the new surface layer and the old structure.

For comparison purposes, all cores extracted before and after the maintenance works are represented in figure IV.1.16
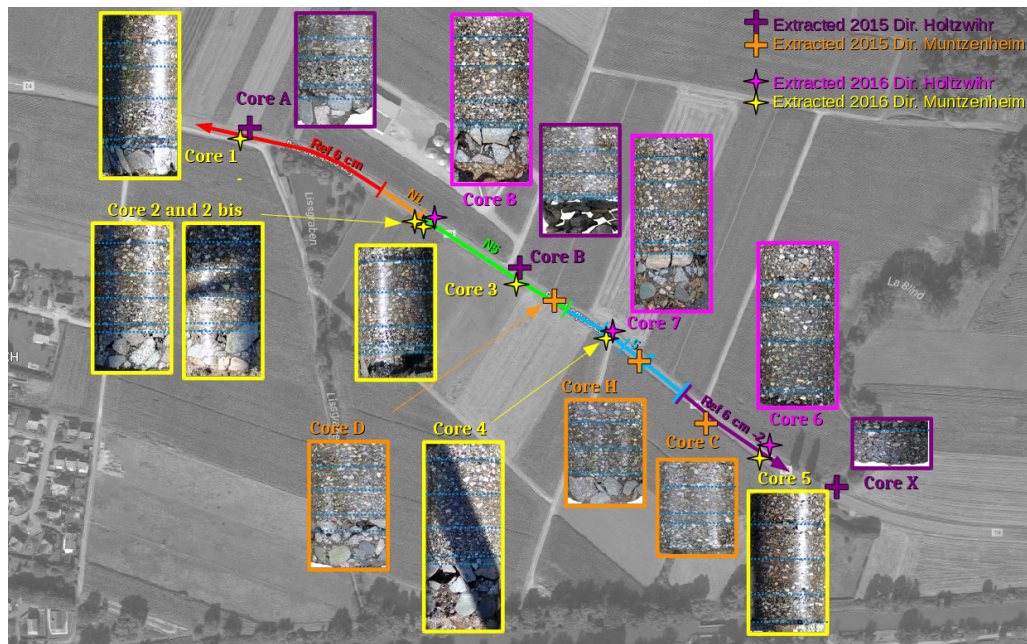
Figure IV.1.16: Cores extracted on the RD4; Cores with a letter as name: Extracted in 2015, Cores with a number: Extracted in 2017

As mentioned before, the cores extracted show a structure made of 3 older surface layers, topped with the new surface layer for the cores extracted in May 2017. Under the surface layers is a macadam layer, which can be seen in most cores. A very thin layer is to be found between the macadam and the surface layers, which was probably a surface dressing laid on the macadam.

However, it has to be noted that some of the cores extracted from the second half of the road section were extracted without the macadam layer. This is the case for cores C, 5 and 6. The picture of core B shows the macadam broken apart during drilling.

IV.1.4.3   Height of the different layers of the RD4

The thickness of the different layers was determined in the laboratory of Cerema, Direction territoriale Est and are represented in figure IV.1.17.
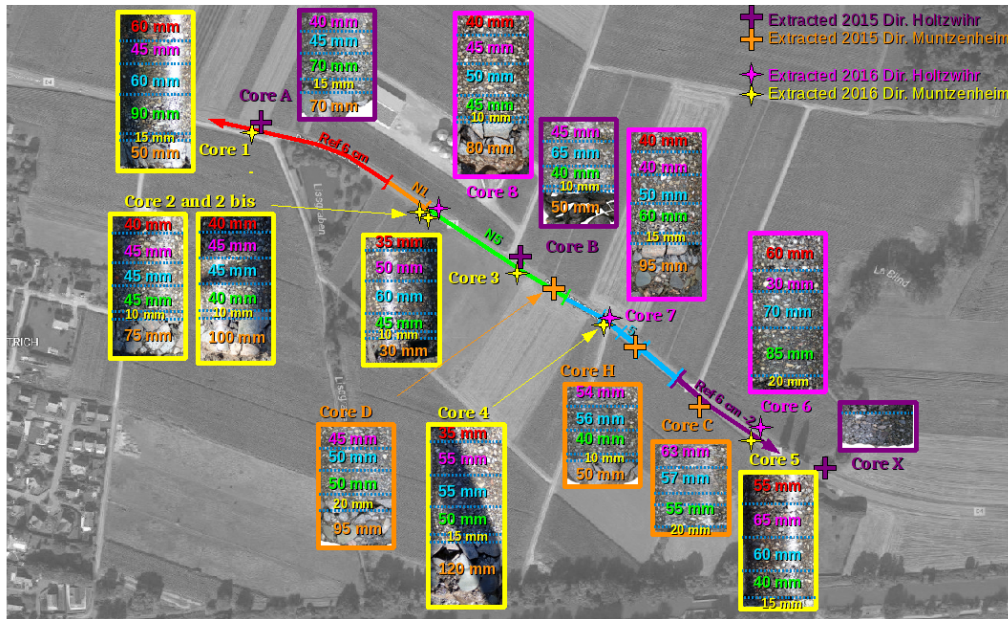
Figure IV.1.17: Thickness of the different layers of the cores extracted from the RD4

The calculated average thickness of the layers of the old structure, as well as the standard deviation and the coefficient of variation, are listed in table IV.1.9.
The highest coefficient of variation is to be found for the macadam, varying between 30 mm and 100 mm whenever the macadam is present. It can be assumed that in some cases, the macadam broke apart during drilling, leading to smaller layer thickness.
The second highest coefficient of variation was determined for the third surface course of the old structure, as it strongly varies especially between the two travel directions.

The thickness of the new surface layer was between 6 cm and 5.5 cm in the reference sections and 3.5 to 4 cm in the reinforced sections.

Table IV.1.9: Average thickness of the layers of the old structure with standard deviation and coefficient of variation

Layer		1	2	3	4	Macadam
Direction Muntzenheim						
Average	[mm]	51.9	54.2	50.6	13.9	74.3
Std Dev	[mm]	7.5	5.8	14.8	3.9	30.1
Coef of Var		0.14	0.11	0.29	0.28	0.40
Direction Holtzwihr						
Average	[mm]	40.0	56.0	60.0	14.0	73.8
Std Dev	[mm]	5.5	9.7	16.4	3.7	16.3
Coef of Var		0.14	0.17	0.27	0.27	0.22
Both directions						
Average	[mm]	47.6	54.9	53.9	13.9	74.1
Std Dev	[mm]	9.2	7.7	16.7	4.0	27.2
Coef of Var		0.19	0.14	0.31	0.29	0.37

IV.1.4.4   Elastic modulus of the different layers of the RD4

The moduli of the different layers were determined with the indirect tensile test in the laboratory of Cerema, Direction territoriale Est and are represented in figure IV.1.18, based on European standard NF EN 12697-26, appendix C [EN12697-26]. The tests were made at 10 Hz and at test temperatures of 10 °C and 15 °C. Based on the standard NF P 98-086 [NF P 98-086], the average of both values was taken as modulus at an equivalent temperature of 15 °C at 10 Hz.

The condition for testing a layer was a minimum thickness of 40 mm. For this reason, the modulus of the small layer 4 was not determined.

The average modulus of each layer together with the standard deviation and the coefficient of variation are listed in table IV.1.10.
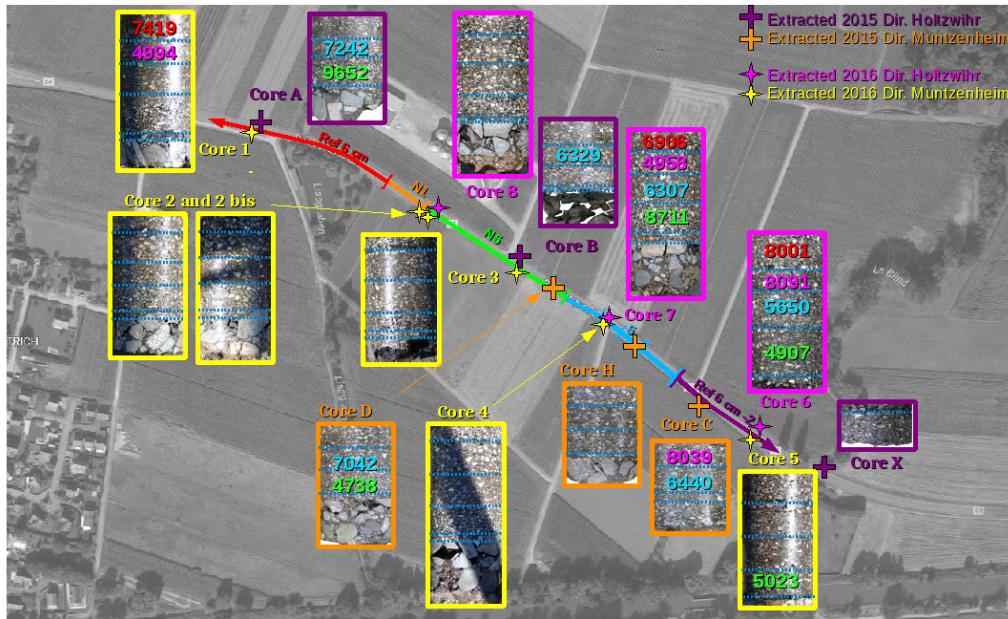
Figure IV.1.18: Modulus of the different layers of the RD4

Table IV.1.10: Average modulus of the layers with standard deviation and coefficient of variation

Modulus [MPa]				
Core / Layer	NSL*	1	2	3
A			7242	9652
B			6329	
C		8039	6440	
D			7042	4738
1	7419	4994		
5				5023
6	8001	8091	5650	4907
7	6906	4958	6307	8711
Average	**7442**	**6520**	**6502**	**6606**
Std Dev	548.1	1783.6	572.1	2376.3
Coef. of Var.	0.0737	0.2736	0.0880	0.3597

*NSL = New Surface Layer

It can be observed that the coefficient of variation of layers NSL and 2 is relatively small with 0.0737 and 0.0880 respectively. Layers 1 and 3, however, show the more important coefficient of variation. It can be concluded that the variation within the layer is quite important.

Normally the stiffness of an asphalt layer depends from:

- The bitumen

- The temperature

- The test speed or test frequency

- The mixture proportions used

As the testing parameters stay the same for all tests and the bitumen as well as the mixture proportions should actually not vary within the layer, it should be assumed that none of these points explain the changes within the layers.

When looking in figure IV.1.18, we observe that the changes in layer 1 take place between section Ref 6 cm -2 and the rest of the road: The modulus determined on cores 6 and C (section Ref 6 cm -2) are above 8000 MPa, while the modulus determined on cores 1 and 7 are below 5000 MPa.

For layer 3, we observe a change of modulus going along with a change in the material structure of the cores. When looking closely at layer 3 of cores A and 7 (see figure IV.1.19), we observe a strong presence of voids in the layer. On the other hand layer 3 of cores D, 6 and 5 shows no voids.
When comparing this fact with the modulus, we observe that cores A and 7 show a layer 3 modulus much higher (> 8000 MPa) than that of cores D, 6 and 5 (4738 MPa - 5023 MPa).

Core A : 9652 MPa   Core D : 4738 MPa   Core 6 : 4907 MPa

Core 7 : 8711 MPa   Core 5 : 5023 MPa
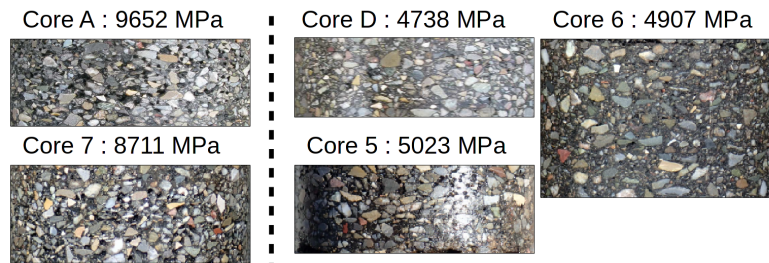
Figure IV.1.19: Layer 3 sorted depending on the visible porosity, with respective modulus

The porosity also seems to be depending on the position on the road. Further cores showing a porosity similar to the porosity of cores A and 7 are cores 1, 2, 8, 3 and 4. Only core C shows a structure similar to cores D, 6 and 5.
Cores 2 bis, B and H show a medium amount of voids.
Cores C, 5 and 6, both having a low amount of visible voids, are all positioned in the section Ref 6 cm -2. Core D is positioned at the end of section N5, which is the middle section.

All other cores are positioned in the sections west of section Ref 6 cm -2.

IV.1.4.5 Deflection measurements with Lacroix Deflectograph

In August 2016, deflections were again measured on the RD4, in order to see the effect of the maintenance works. The measurements were now done with a Lacroix Deflectograph, having basically the same working method as the Flash Deflectograph described above but for the measurement speed which is only 3 km/h.

The temperature adjustment was done as described before. The graphs representing the deflection on bank and axis sides in both directions, as well as the graphs showing the moving average curves of the axis and bank sides are shown in figure IV.1.20.
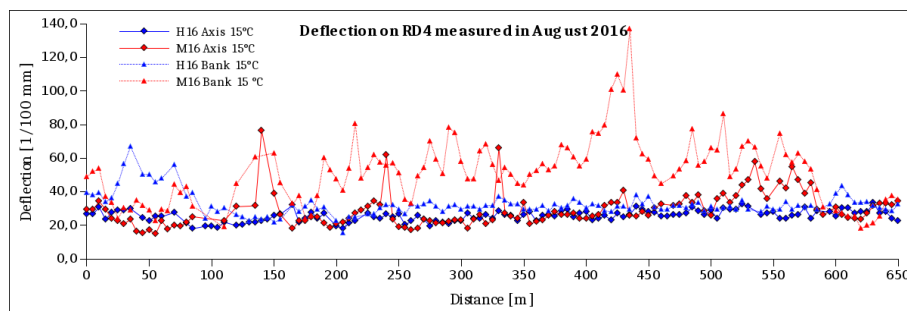
(a) Deflection measured towards Holtzwihr and Muntzenheim on axis and bank sides.
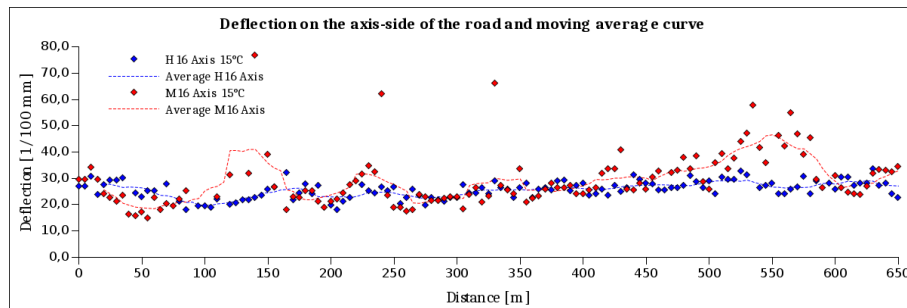
(b) Deflection measured towards Holtzwihr and Muntzheim on axis sides and moving average curves
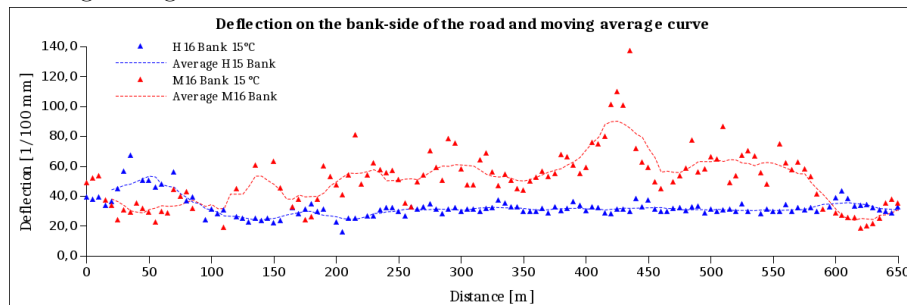
(c) Deflection measured towards Holtzwihr and Muntzheim on bank sides and moving average curves

Figure IV.1.20: Deflection measured on the RD4 in August 2016

It can be observed that the values of the bank side towards Muntzenheim are still greater than the other deflection values, pointing out that this side of the road is still strongly weakened compared to the rest of the road, especially the second half. The values of the bank side towards Holtzwihr are approximately the same as the deflections of the axis sides in both directions, except at a distance of about 50 m, where the curve shows a flat peak.

The results of the axis side towards Muntzenheim show 3 points which seem to be outliers. A closer look reveals that these outliers are located at places, where the shear resistance could be weakened: The first point, at a distance of 140 m, is the point where the structure built on October 29th and the structure built on October 30th meet (see figure IV.1.20a). It can be assumed that the high deflection at this position is related to a bad bonding between the two parts.

The second point at 240 m is at the position where grids N1 and N5 overlap, the third point at 330 m is at the position of the overlapping of the two grids N5. Here it can be assumed that the overlapping caused a particular poor bond between old and new pavement, leading to high deflections at these points.

As a whole, the axis side also shows a slight increase of the deflection on the second half of the route, as was already seen in the measurements of 2015.

The calculation of the average values, the standard deviations and the coefficient of variation will be made again for different parts of the roads. In contrast to the deflection determined in 2015, the axis and bank sides are now also divided in the travel direction, as the direction of Muntzenheim shows an important difference compared to the direction of Holtzwihr. The new section parts are:

- Axis side

    - **Direction Holtzwihr**

        Part 1: 0 m to 650 m

    - **Direction Muntzenheim**

        Part 1: 0 m to 100 m

        Part 2: 105 m to 170 m

        Part 3: 175 m to 500 m

        Part 4: 505 m to 600 m

        Part 5: 605 m to 650 m

- Bank side

    - **Direction Holtzwihr**

        Part 1: 0 m to 110 m

Part 2: 115 m to 650 m

– **Direction Muntzenheim**

Part 1: 0 m to 100 m

Part 2: 105 m to 360 m

Part 3: 365 m to 600 m

Part 4 605 m to 650 m

Table IV.1.11: Average values, standard deviations and coefficients of variation of the deflection measured on the RD4 in 2016

	Distance	Average deflection	Standard Deviation	Coefficient of variation
	[m]	[1/100 mm]	[1/100 mm]	
M16 Axis	0-100	22.5	5.5	0.2
	105-170	33.5	18.6	0.6
	175-500	27.3	8.4	0.3
	505-600	40.7	8.3	0.2
	605-650	29.0	4.2	0.1
	Total	29.1	10.2	0.4
H16 Axis	Total	25.6	3.3	0.1
M16 Bank	0-100	35.7	9.3	0.3
	105-360	51.1	13.3	0.3
	365-600	64.2	19.5	0.3
	600-650	27.1	6.8	0.3
	Total	51.7	19.4	0.4
H16 Bank	0-110	41.9 10.9 0.3		
	115-650	30.6	3.8	0.1
	Total	32.3	6.9	0.2

IV.1.5 Comparison of the deflections measured in 2015 and 2016

The comparison of the deflections is made on the different observed sections of the observed part of the RD4, which are:

- Reference 6 cm ('Ref 6 cm'): 0 m to 100 m:
  6 cm of new surface layer

- Grid N1: 195 m to 225 m:
  Grid N1 and 4 cm of new surface layer

- Grid N5: 245 m to 360 m:
  Grid N5 and 4 cm of new surface layer

- Grid 5: 390 m to 470 m:
  Grid 5 and 4 cm of new surface layer

- Second reference 6 cm ('Ref 6 cm - 2'): 510 m - 650 m:
  6 cm of new surface layer

The parts between the sections were cut out so that the influence of overlapping of different grids are not taken into account. For this reason, the outlier at 325 m (section Grid 5) was also removed.

The difference between the values of 2015 and 2016 shows the improvement brought by the new surface course. The corresponding graphs are shown in figure IV.1.21 (axis side) and figure IV.1.22 (bank side). The respective average values of each section are listed in tables IV.1.12 (axis side) and IV.1.13 (bank side), together with the standard deviation and the coefficient of variation of each section and the calculated difference between the deflection measured in 2015 and the deflection measured in 2016 on the respective sections, expressed in [1/100 mm] and in percentage of the initial 2015 deflection value.
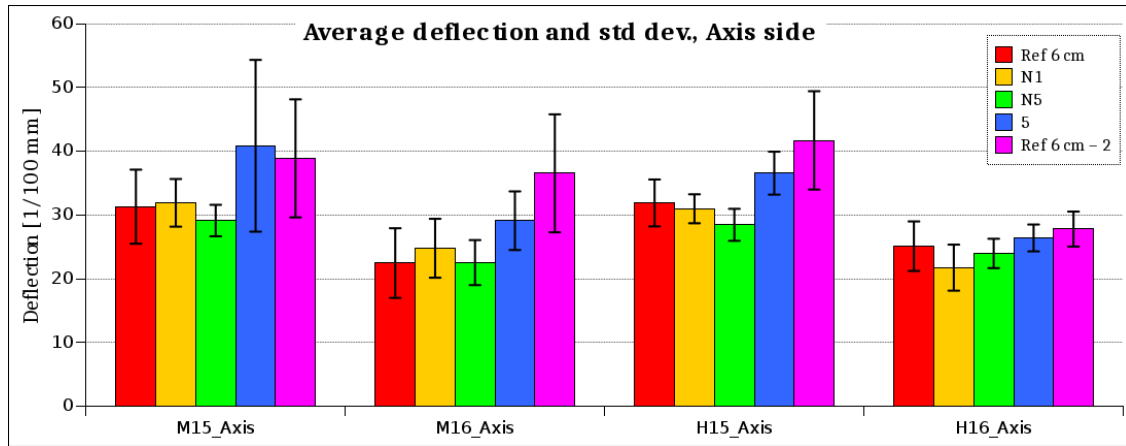
Figure IV.1.21: Average deflections of each section measured on the axis side in both directions in 2015 and 2016 with std dev.

Table IV.1.12: Comparison of the average deflection of each section measured in 2015 and 2016 on the axis side towards Muntzenheim and Holtzwihr, with standard deviation (Std Dev), coefficient of variation (Coef. of Var.) and the calculation of the difference between the two measurements in [1/100 mm] and [%] of the 2015-values

Axis						
			Muntzenheim		Holtzwihr	
Section			2015	2016	2015	2016
Ref 6 cm	Average	[1/100 mm]	31.3	22.5	31.9	25.1
	Std Dev	[1/100 mm]	5.8	5.5	3.7	3.9
	Coef. of Var.		0.1856	0.2433	0.1152	0.1547
	Difference	[1/100 mm]	8.8		6.8	
	Difference	[%]	28.2		21.3	
N1	Average	[1/100 mm]	31.9	24.8	31.0	21.8
	Std Dev	[1/100 mm]	3.7	4.6	2.3	3.6
	Coef. of Var.		0.1172	0.1863	0.0733	0.1659
	Difference	[1/100 mm]	7.1		9.2	
	Difference	[%]	22.3		29.8	
N5	Average	[1/100 mm]	29.1	22.5	28.5	24.0
	Std Dev	[1/100 mm]	2.5	3.5	2.5	2.3
	Coef. of Var.		0.0847	0.1566	0.0881	0.0960
	Difference	[1/100 mm]	6.6		4.5	
	Difference	[%]	22.6		15.8	
5	Average	[1/100 mm]	40.9	29.1	36.6	26.4
	Std Dev	[1/100 mm]	13.5	4.6	3.4	2.1
	Coef. of Var.		0.3296	0.1580	0.0921	0.0798
	Difference	[1/100 mm]	11.8		10.2	
	Difference	[%]	28.8		27.8	
Ref 6 cm - 2	Average	[1/100 mm]	38.9	36.6	41.7	27.8
	Std Dev	[1/100 mm]	9.3	9.3	7.7	2.7
	Coef. of Var.		0.2380	0.2531	0.1849	0.0987
	Difference	[1/100 mm]	2.3		13.9	
	Difference	[%]	6.0		33.4	
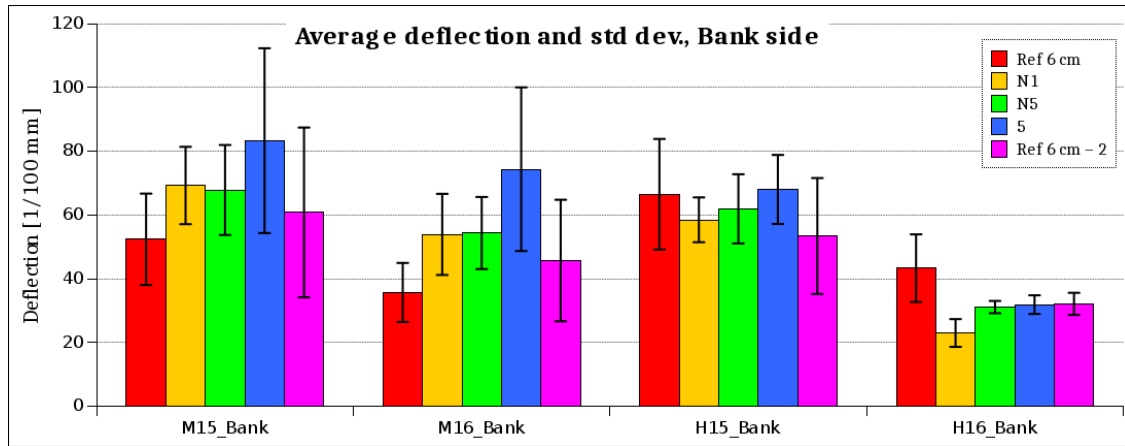
Figure IV.1.22: Average deflections of each section measured on the bank side in both directions in 2015 and 2016 with std dev.

Table IV.1.13: Comparison of the average deflection of each section measured in 2015 and 2016 on the bank side towards Muntzenheim and Holtzwihr, with standard deviation (Std Dev), coefficient of variation (Coef. of Var.) and the calculation of the difference between the two measurements in [1/100 mm] and [%] of the 2015-values

Bank						
			Muntzenheim		Holtzwihr	
Section			2015	2016	2015	2016
Ref 6 cm	Average	[1/100 mm]	52.4	35.7	66.5	43.3
	Std Dev	[1/100 mm]	14.3	9.3	17.4	10.6
	Coef. of Var.		0.2738	0.2590	0.2609	0.2447
	Difference	[1/100 mm]	16.7		23.2	
	Difference	[%]	31.8		34.8	
N1	Average	[1/100 mm]	69.3	53.9	58.5	23.0
	Std Dev	[1/100 mm]	12.1	12.7	7.0	4.3
	Coef. of Var.		0.1751	0.2359	0.1201	0.1890
	Difference	[1/100 mm]	15.3		35.5	
	Difference	[%]	22.2		60.7	
N5	Average	[1/100 mm]	67.9	54.4	62.0	31.1
	Std Dev	[1/100 mm]	14.1	11.3	10.9	1.9
	Coef. of Var.		0.2080	0.2081	0.1752	0.0623
	Difference	[1/100 mm]	13.5		30.8	
	Difference	[%]	19.9		49.8	
5	Average	[1/100 mm]	83.3	74.4	68.0	31.9
	Std Dev	[1/100 mm]	29.0	25.7	10.8	2.9
	Coef. of Var.		0.3479	0.3451	0.1591	0.0918
	Difference	[1/100 mm]	8.9		36.1	
	Difference	[%]	10.7		53.1	
Ref 6 cm - 2	Average	[1/100 mm]	60.8	45.7	53.4	32.1
	Std Dev	[1/100 mm]	26.6	19.1	18.2	3.5
	Coef. of Var.		0.4379	0.4169	0.3404	0.1080
	Difference	[1/100 mm]	15.1		21.3	
	Difference	[%]	24.8		39.8	

Figure IV.1.21 shows that on the axis side the distribution form of the deflection is equivalent in 2015 and 2016, with in both cases smaller values for sections Ref 6 cm, N1

and N5 and increased deflections for sections 5 and Ref 6 cm -2.

This observation can also be done on figure IV.1.22, as towards Muntzenheim, section 5 stands out with a higher average deflection for both years. Towards Holtzwihr, the deflections in 2015 are quite constant. For 2016, section Ref 6 cm sticks out lightly.

The difference in deflection between the measurements of 2015 and 2016, expressed in percentage of the deflections of 2015, are shown in figure IV.1.23.
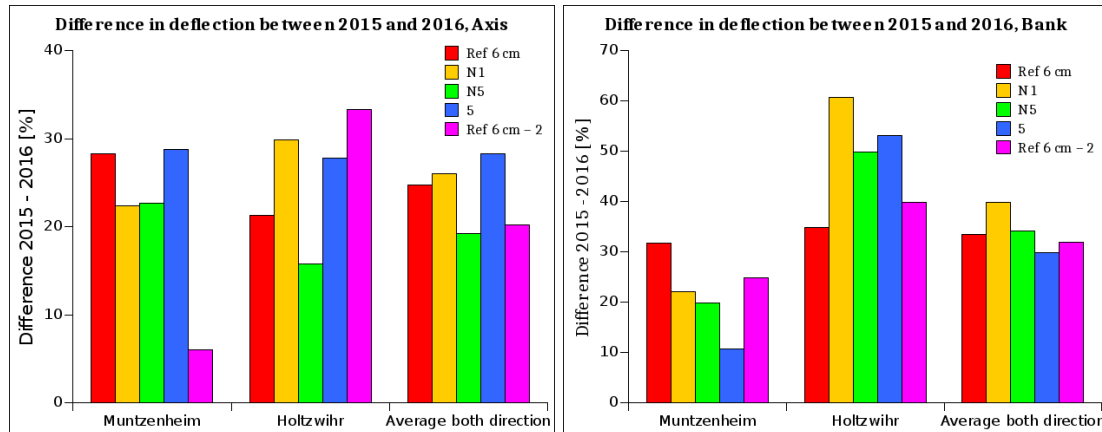
Figure IV.1.23: Difference [%] between the deflections measured in 2015 and 2016

We observe that the improvement due to the new surface layer is very different, depending on the direction of travel and on the side measured. The greatest distinction is noticeable between the values of section Ref 6 cm measured on the axis side. Towards Muntzenheim, the improvement due to the new surface layer is very low compared to the other sections. However, towards Holtzwihr we observe the best improvement of all.

Another great distinction is visible between the values on the bank side. Here, we see that towards Muntzenheim the greatest improvement made is smaller than the smallest improvement towards Holtzwihr.

A possible explanation for the smaller improvements could be a weaker or stronger bonding between the old surface and the new surface layer.

In the case of section 5 towards Holtzwihr, it should be noted that the deflection results of 2015 showed quite a weak structure. The weaker the structure at the beginning, the bigger the possible improvements after maintenance works.

The bank side showed also quite high deflection results in 2015 in both directions. A better bonding between the new layer and the old surface could have led to a stronger improvement of the deflections compared to the improvement towards Muntzenheim.

In both cases, the direction of Holtzwihr gives better results than the direction of Muntzenheim. It can also be noted that the new layer towards Muntzenheim was built in the early morning of the 30th of October 2015, while the layer towards Holtzwihr was built in the afternoon of the same day. Knowing this, it could be assumed that the bonding has suffered from the lower temperature in the morning (about 5 °C) compared with the temperatures of the afternoon (> 10 °C).

To investigate this possibility, it was decided to extract again some specimens from the RD4. Some of them were to be used for the determination of the shear resistance between the old structure and the new layer and some for the determination of the modulus of the different courses (especially the new surface layer).

The results of the shear tests can be seen in section IV.1.5.1, the modulus of the layers are listed in section IV.1.4.4.

IV.1.5.1 Shear resistance between the old structure and the new surface layer

The test used to determine the shear resistance between the new layer and the old surface was the Leutner test, which was already described in this study (see section III.2.1). This test requires cylindrical specimens with at least two layers and a diameter of (150 ± 2) mm.

Unfortunately, the cores extracted from the RD4 only had a diameter of 140 mm to 142 mm, which hinders a comparison of the results achieved here with cores from other projects. Nevertheless, it was decided to test the cores, as a comparison between them was still interesting.

The test procedure remained identical to the normal Leutner test. The test-temperature was 20 °C.

The calculation of the shear strength was done in two different ways:

1. By dividing the determined shear force through the whole surface of the core

2. By dividing the determined shear force through a reduced surface (calcul of the reduced surface see appendix VI)

The cores extracted for this test were taken at locations where a weaken bond was awaited or where the results would be interesting for comparison purposes. Figure IV.1.24 shows the location of the extracted specimens.

Cores 1, 6 and 7 were extracted only for modulus-testing (see section IV.1.4.4).

Cores 2 to 5 were extracted from the lane towards Muntzenheim. Core 2 is positioned slightly beneath the place where grid N1 and N5 overlap, core 2 bis is exactly at the overlapping emplacement. Core 3 is at the overlapping of the two N5 grids, core 4 was extracted from section 5, core 5 from section Ref 6 cm -2. Core 8 is at the same height as

core 2, but on the other lane (direction Holtzwihr).

The cores were always extracted from the middle of one lane.
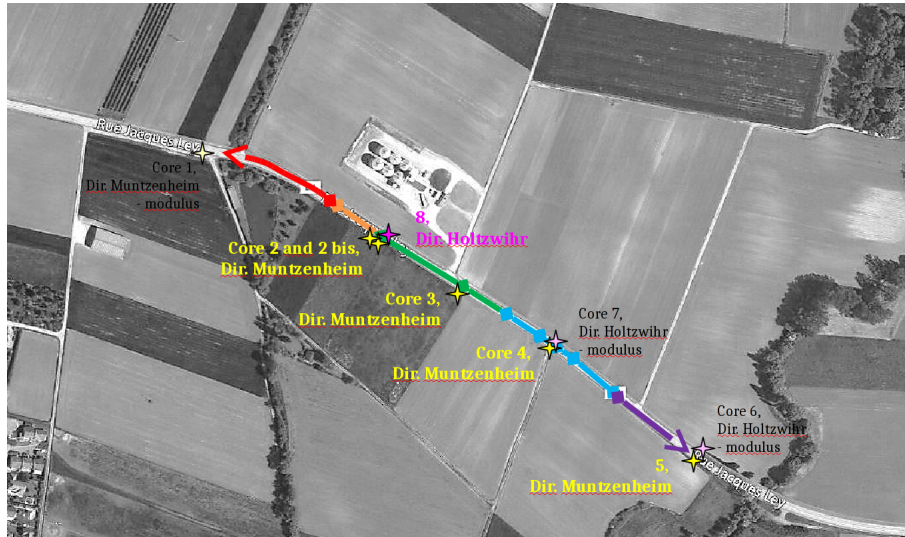
Figure IV.1.24: Emplacement of the cores extracted for Leutner test on the RD4

The results of the test for each core are listed in table IV.1.14.

Table IV.1.14: Shear strength results of the cores extracted from the RD4

	Core	2	2 bis	3	4	5	8
Grid at this position		N1	N1 & N5	N5	5	-	N5 or N1
Diameter	[mm]	141.3	141	141.1	141.1	140.1	142.2
Displacement	[mm]	1.4	1.4	1.5	1.8	0.8	1
Shear strength [1]	[N/mm^2]	0.39	0.47	0.47	0.49	0.52	0.58
Shear strength [2]	[N/mm^2]	0.50	0.61	0.60	0.59	0.85	0.80

[1]: Calculated using the whole surface, [2] Calculated using a reduced surface

Figure IV.1.25 shows the graphical representation of these results.
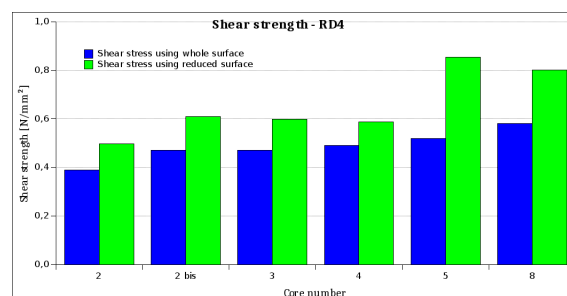
Figure IV.1.25: Graphical representation of the shear strength achieved by the cores of the RD4

Regarding the shear strengh calculated with the reduced surface, the highest shear strength is achieved by core n° 5, which is the only core without grid between the new surface layer and the old structure. This result confirms the investigations made in this study, concluding in the fact that grids can disturb the bonding between two asphalt layers.

The second best result is achieved by core n°8, which is the only core on the lane towards Muntzenheim. This could confirm the idea that the warmer temperatures in the afternoon had a beneficial effect on the bonding.

The shear strength achieved by core n° 2 bis is unexpectedly high, as it was assumed that the overlapping had a particularly negative effect on the bonding. The result of core n° 2 bis is even slightly higher than the result of core n°2, which is positioned only one meter beneath core n° 2 bis.

The results of the cores n° 2 bis, 3 and 4 are very similar.

IV.1.6 Deflections measured with the Benkelman Beam

Measurements with the Benkelman beam were made in October 2016.

The Benkelman beam (BB) is a simple deflection test. The Benkelman beam consists of a frame with an arm on a hinge, which is attached to a dial gauge, measuring the displacement of the arm in the vertical direction.

For this measurement, the rear axle of a truck with double-wheels loaded with a specific charge (here 13 tonnes rear axle load) is positioned on the point at which the deflection is sought. The arm is then positioned between the double-wheels of the truck and the value showed by the dial gauge is recorded. The truck moves forward, leading to the discharge of the point. The value showed by the dial gauge is recorded again. The difference between the loaded and unloaded value is the deflection at this position point.

Other variants exist, depending on national standards. One other possibility, for example, is to measure the point in its unloaded form first and then to reverse slowly with the truck so that the arm of the beam is positioned exactly under the double wheel. This variant is interesting regarding the unloaded measurements but its implementation is quite difficult.

Figrue IV.1.26 illustrates the principle of the Benkelman beam.
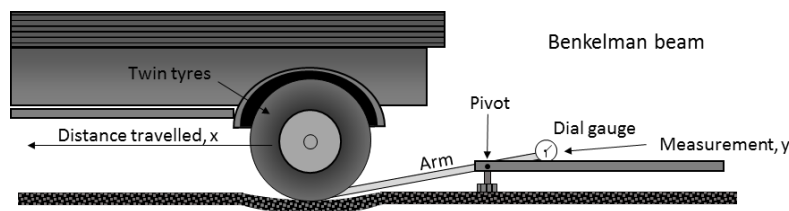
Figure IV.1.26: Principle of the Benkelman beam [THO 14]

As the measurements done with the Benkelman beam are static, the deflection measured this way cannot be compared directly to the deflections determined with the Lacroix and Flash deflectograph, which are made at a constant speed of 5 km/h. For this reason, only tendencies were compared, noting that according to Romero et al. [ROM 94] the deflection decreases with the measurement speed. This fact should result in lower deflections when measured with the Lacroix Deflectograph compared to the deflections measured with the Benkelman beam.

Deflections were measured at 5 points per section, in each direction and on both sides of the rear axle (axis and bank side). Simultaneously the temperature of the road surface was determined. The temperature adjustment was done as described in section IV.1.2.3.

The deflections measured with the Benkelman beam as well as the standard deviation are listed in table IV.1.15.

Table IV.1.15: Average deflections and standard deviations measured with the Benkelman beam on each section

			BB M Bank	BB M Axis	BB H Bank	BB H Axis
	Average	[1/100 mm]	45.1	8.3	51.0	15.7
Ref 6 cm	Std Dev	[1/100 mm]	11.9	3.4	17.5	2.0
	Coef. of Var.		0.3	0.4	0.3	0.1
	Average	[1/100 mm]	79.3	20.2	65.1	18.0
N1	Std Dev	[1/100 mm]	19.1	3.3	3.6	2.3
	Coef. of Var.		0.2	0.2	0.1	0.1
	Average	[1/100 mm]	59.3	13.6	66.0	9.7
N5	Std Dev	[1/100 mm]	9.8	7.1	21.1	0.6
	Coef. of Var.		0.2	0.5	0.3	0.1
	Average	[1/100 mm]	74.5	20.3	86.4	11.6
5	Std Dev	[1/100 mm]	22.9	2.7	23.1	6.7
	Coef. of Var.		0.3	0.1	0.3	0.6
	Average	[1/100 mm]	59.0	23.8	72.7	21.0
Ref 6 cm - 2	Std Dev	[1/100 mm]	11.8	2.6	28.4	1.4
	Coef. of Var.		0.2	0.1	0.4	0.1

The graphical representation of the average deflection values determined with the Benkelman beam as well as, for comparison purposes, the graphical representation of the average deflection values determined with the Lacroix deflectograph in 2016 are shown in figure IV.1.27.
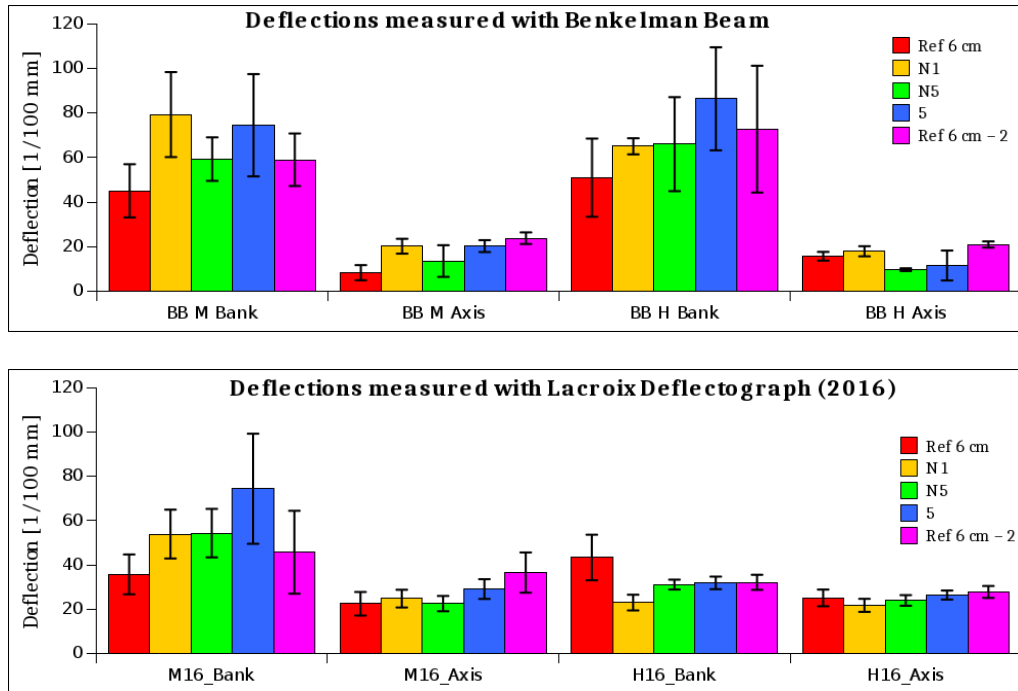
Figure IV.1.27: Average deflections of the different sections measured with Benkelman beam (upper graph) and Lacroix deflectograph (lower graph)

As said before, the deflection values themselves cannot be compared, as the measurement devices are very different. Nevertheless, the different tendencies detected with the different devices can be compared.

Compared to each other, it can be observed that the deflections measured on the bank sides are greater than the deflections measured on the axis sides, confirming the observation that the bank side is weaker than the axis side.

On the bank side towards Holtzwihr, we can also observe that the deflections of sections 5 and Ref 6 cm -2 are higher than those of the other three sections, showing again this weakening in the second half of the route. The bank side of the Muntzenheim lane shows higher results for the last two sections but has also higher values for section N1.

The axis sides show more constant deflections. Towards Muntzenheim, the smallest deflections are to be found in section Ref 6 cm, followed by section N5, with a rather high standard deviation value. The other sections show very similar deflections.
Towards Holtzwihr, section N5 shows the lowest average deflection, followed by sections 5 and Ref 6 cm with very similar deflection values and then sections N1 and Ref 6 cm -2.

Based on Romero et al. [ROM 94] the comparison of the tendencies of the deflections

measured with the Benkelman beam in October 2016 and the deflections measured with the Lacroix deflectograph in August 2016 should show lower deflections for the measurements done with the Lacroix deflectograph, as the Lacroix deflectograph is a measurement device moving at a constant speed of 5 km/h.

Yet the comparison of our values shows that this is only the case for the deflections on the bank sides of the lanes. For the axis side, the deflections measured with the Benkelman beam are smaller than the deflections measured with the Lacroix deflectograph.

Apart from that, there are similarities:

Both measurement devices show rather low deflections on the axis side on both lanes. When looking more specifically, it can be noted that for both devices, section Ref 6 cm -2 always shows the highest deflection, followed by section 5 - except for the axis side towards Holtzwihr measured with the Benkelman beam.

Towards Muntzenheim, both devices show that section Ref 6 cm has the smallest deflections on the axis side.

The bank side of the lane towards Muntzenheim shows higher deflections with both measurement devices.

However the bank side towards Holtzwihr shows much greater results with the Benkelman beam than with the Lacroix deflectograph.

Besides the difference in the measurement method, the differences observed between the two methods can also be the result of different climatic conditions on the days of the measurements, as the measurements with the Lacroix deflectograph were done on the 11th of August at a temperature of about 30 °C while the measurements made with the Benkelman beam were made after the summer, on the 27th of October with a surface temperature being of around 9 °C .

The precipitations in the month before the measurements were in both case of about 50 mm [1]. However, it also as to be noted that nearly no rain (4 mm) felt in the week before the Lacroix measurements, while the week before the Benkelman measurement had 31 mm rain.

A softening of the soil under the structure, which could influence the deflections, can, therefore, be considered, explaining the higher values of the bank side, towards Holtzwihr measured in October, compared to the values measured in August.

---

[1]http://www.wetteronline.de, Wetterdaten, Rückblick, search of the precipitation on the Basel-Mulhouse Airport, Sept 4th, 2017

IV.1.7   Conclusion: Observation of the RD4

A 650 m long part of the RD4 was observed from June 2015 until the end of this thesis. The road is located near Colmar, between the villages of Holtzwihr and Muntzenheim. Maintenance works were made on the road in October 2015, consisting in the installation of a new surface layer on the old structure. Some parts of the road were reinforced with different grids, recovered with 4 cm of the new surface layer, the rest of the road was recovered with 6 cm surface layer. As a whole, 5 sections were observed, named 'Ref 6 cm', 'N1', 'N5', '5' and 'Ref 6 cm -2'.

Deflections were measured before and after the maintenance works. The measurement before the maintenance works was done with a Flash deflectograph in June 2015. The measurements after the maintenance works were done with a Lacroix deflectograph in August 2016 and a Benkelman beam in October 2016.

The visual inspection of the RD4 before the works stated primarily different types of cracks such as cracks at the centerline and crocodile cracks, especially on the bank side of the lanes.

The deflection made in June 2015 showed a weakened bank side in both travel directions with average deflections of around 60 [1/100 mm] on the banks side versus 34 [1/100 mm] on the axis sides. It was also observed that the deflections went up on the last third of the observed route, showing a weakened structure on the eastern part of the road.

Deflection measured after the maintenance works in August 2016 showed an improvement of the deflections on all parts of the roads. Yet, this improvement was not constant on all parts. The measurements made on the bank side of the lane towards Holtzwihr showed an improvement of 46.1 %, while the measurements on the bank side towards Muntzenheim and the measurements on the axis sides in both directions showed improvements of only 15.7 % to 24.7 %.

Any special distinction of a section, showing that its characteristics (e.g. reinforcement) brought especially good or bad improvements compared to the old structure, could not be observed.

Deflections measured in October 2016 with the Benkelman beam confirmed the results obtained with the Lacroix deflectograph except for the bank side towards Holtzwihr. The deflections of the bank sides towards Holtzwihr measured with the Lacroix deflectogaph were at a similar height as the deflections on the axis sides. The deflections measured with the Benkelman beam on the bank side towards Holtzwihr were at a similar height as the deflections on the bank side towards Muntzenheim and higher than the deflections measured on the axis sides.

The shear test performed on the cores of the RD4 confirmed the results obtained in this study in section III.2.1, showing that a grid at the interface will lower the shear strength of the interlayer. However, a negative influence of an overlapping of two grids on the bonding was not found.

IV.2   Modelling of the RD4 with the modelling program BISAR

The aim of this chapter is to use the program BISAR to model the structure of the RD4 using the known deflections in the different sections as well as the thicknesses and moduli for each layer of the RD4 to distil the possible effects of the glass fibre grids on the deflections.

As the modulus of the sub-grade under the RD4 is not known and the modulus of the macadam can only be guessed, the first step of the modelling is to determine both moduli using back-calculation based on the known moduli and deflections of the unreinforced sections.

Having all moduli at 15 °C, the model is used for the reinforced sections. The modelled deflections are then be compared to the actual deflections measured with the Lacroix Deflectograph and adjusted to 15 °C.

The structure is changed until the actual and modelled deflections match, thus showing the impact of the glass fibre grids on the structure.

IV.2.1   BISAR: functioning

The program BISAR ('BItumen Structure Analysis in Roads') is a program developed by Shell research in 1970's to calculate stresses, strains and displacements in an elastic multi-layered system. The configurations and material properties required for modelling are [BISAR 98]:

- The system consists of a horizontal layer with uniform thickness resting on a semi-infinite base or half space

- The layers extend infinitely in horizontal directions

- The material of each layer is homogeneous and isotropic

- The materials are elastic and have a linear shear-strain relationship

IV.2.2   Required input for calculation

The input parameters needed for the calculation with BISAR are:
Load:

- One of the following combinations to indicate the vertical normal components of the load:

  - Stress and load

  - Load and radius (used in this study)

   – Stress and radius

- Number of loads

- Position of the load carrying point

Layers:

- Number of layers

- Layer thickness (except for the lowest one)

- Elasticity modulus of each layer

- Poisson's ratio of every layer and the soil

Others:

- Interface shear spring compliance at each interface (a factor defining the bonding between two layers. In cases of full bonding the factor is zero)

- The coordinates of the positions for which an output is required

IV.2.2.1   Load type

The load used for structure modelling is the load of the double-wheel of the rear axle of the Flash/Lacroix deflectograph used to determine the deflections on the RD4.
As the rear axle was loaded with a total load of 13 tonnes, each double wheel was loaded with 6.5 tonnes, i.e. 3.25 tonnes or 32.5 kN per wheel.
The contact surface of the double wheel on the road is described as a circle with a radius of 0.105 m. The distance between the centre of the circles is defined as 0.315 m.

IV.2.2.2   Poisson's ratio

The Poisson's ratio is a material parameter describing the ratio between transverse contraction strain and axial extension strain in an elastically stretched or compressed sample. The ratio is mostly written ν and calculated as follows:

$$\nu = -\frac{d\epsilon_{trans}}{d\epsilon_{axial}} \tag{10}$$

With

   ν: Poisson's ratio

   ϵ_{trans}: Transverse strain

   ϵ_{axial}: Axial strain

When a material is incompressible, the Poisson's ratio is 0.5.
According to the German Directive RDO Asphalt 09 [RDO 09], the Poisson's ratio for asphalt layers was taken at 0.35 while the Poisson's ratio for the sub-grade was taken at 0.5.

IV.2.2.3 Bonding between layers

BISAR enables the modelling of a non-fully bonded interlayer. To do so, the program proposes the value AK, being the standard shear spring compliance, calculated by means of the following equation:

$$AK = \frac{Relative\ horizontal\ displacement\ of\ layers}{Stresses\ acting\ at\ the\ interface}[m^3/N] \tag{11}$$

The value of the relative horizontal displacement and the stress acting at the interface can be taken from the results of the Leutner test with the displacement and stress at fracture. As the Leutner-tests made on the cores of the RD4 were made under non-standard conditions, these values were not taken into account for the modelling. Therefore the bonding between the Layers was taken as full (AK = 0).

IV.2.2.4 Modulus

The moduli used for modelling the structure of the RD4 are the ones given in section IV.1.10. As the deflection is to be calculated for each section, but we do not have measurements for each section, the moduli have to be assigned appropriately.

Layers NSL and 2 Layers NSL ('New Surface Layer') and 2 showed very little variation along the road. It was therefore decided to take the determined average modulus as reference modulus:

- Layer NSL: 7442 MPa (Std. Dev.: 548.5 MPa)

- Layer 2: 6502 MPa (Std. Dev. 572.1 MPa)

Layer 1 Layer 1 showed strong variations between the determined moduli, depending on the position of the tested layers. It was observed that layers tested in section Ref 6 cm -2 (eastern end of the observed road part) had a stronger modulus than the layers of the other sections. The modulus of layer 1 used for modelling was therefore made dependent on the modelled section:

- Section Ref 6 cm -2: 8064.8 MPa (Std. Dev.: 25.1 MPa)

- Other sections: 4975.8 MPa (Std. Dev.: 37.1 MPa)

Layer 3   Layer 3 showed variations due to the structure of the layer. Layers showing a high amount of voids also showed a stronger modulus (9181 MPa), while layers with nearly no voids reached feebler moduli (4889 MPa). The moduli of the untested layers were therefore taken depending on their visible amount of voids.

When the cores were sorted according to the sections from which there were extracted, the following table can be constructed:

Table IV.2.1: Layer 3: Assignment of the cores depending on their porosity

Porosity	Section				
	Ref 6 cm	N1	N5	5	Ref 6cm -2
High	A, 1	2, 8	3	7, 4	
Medium			B, 2bis	H	
Low			D		5, 6, C

The corresponding moduli for each section were calculated by taking a modulus of 9181 MPa for layers with a high porosity, 4889 MPa for layers with a low porosity and 7035 MPa for layers with a medium porosity (average of high and low porosity).

It results in the following moduli:

- Section Ref 6 cm: 9181 MPa (Std. Dev. 665.4 MPa)

- Section N1: 9181 MPa (Std. Dev. 665.4 MPa)

- Section N5: 7035 MPa (Std. Dev. 1752,1 MPa)

- Section 5: 8466 MPa (Std. Dev. 1239 MPa)

- Section Ref 6 cm -2: 4889 MPa (143 MPa)

Layer 4   The thickness of layer 4 is too small to be tested with the indirect tensile test. Therefore the thickness of the layer 4 is added to the thickness of the macadam.

Macadam   The modulus of the macadam was not determined. Therefore an empirical value had to be taken. It was chosen as 800 MPa.

IV.2.2.5   Layer thickness

The thicknesses taken for modelling are calculated using the thicknesses of the layers of the cores extracted from the respective sections, in both travel direction. This would be:

- Ref 6 cm: Holtzwihr: A,   Muntzenheim: 1
- N1:   Holtzwihr: 8,   Muntzenheim: 2
- N5:   Holtzwihr: B,   Muntzenheim: 2bis, 3, D
- 5:   Holtzwihr: 7,   Muntzenheim: 4, H
- Ref 6 cm -2:   Holtzwihr: 6,   Muntzenheim: C, 5

The thickness of layer 4 is added to the thickness of the macadam.

IV.2.2.6   Summary: Modulus and Thickness

Table IV.2.2: Modulus and thickness used for modelling

			NSL	Layer 1	Layer 2	Layer 3	Macadam
Ref 6 cm	Thickness	[mm]	60	43	53	80	75
	Std Dev.	[mm]	0.0	3.5	10.6	14.1	14.1
	Modulus	[MPa]	7442	4975.8	6502	9181	800
	Std Dev.	[MPa]	548.1	25.1	572.1	665.4	0.0
N1	Thickness	[mm]	40	45	48	45	87.5
	Std Dev.	[mm]	0.0	0.0	3.5	0.0	3.5
	Modulus	[MPa]	7442	4975.8	6502	9181	800
	Std Dev.	[MPa]	548.1	25.1	572.1	665.4	0.0
N5	Thickness	[mm]	35	46.3	55	43.8	81.2
	Std Dev.	[mm]	3.5	2.5	9.1	4.8	37.1
	Modulus	[MPa]	7442	4975.8	6502	7035	800
	Std Dev.	[MPa]	548.1	25.1	572.1	3034.8	0.0
5	Thickness	[mm]	37.5	49.7	53.7	50	101.67
	Std Dev.	[mm]	3.5	8.4	3.2	10.0	38.2
	Modulus	[MPa]	7442	4975.8	6502	8466	800
	Std Dev.	[MPa]	548.1	25.1	572.1	1492.4	0.0
Ref 6 cm -2	Thickness	[mm]	57.5	52.7	62.3	60	18.3
	Std Dev.	[mm]	3.5	19.7	6.8	22.9	2.9
	Modulus	[MPa]	7442	8064.8	6502	4889	800
	Std Dev.	[MPa]	548.1	37.1	572.1	143.3	0.0

IV.2.3   Output

The program BISAR gives as output the radial, tangential and vertical displacements, stresses and strains at any point in the structure.

The output required in our case is the total vertical displacement on the surface of the structure, in the centre of the double-wheel. The displacement is given in [m] and is then converted in [1/100 mm] in order to be compared to the deflections measured on the RD4.

IV.2.4 Results of modelling

IV.2.4.1 First step: Determination of the deformation modulus E_v2 of the sub-grade

The first modelling step consists in the determination of the sub-grade modulus using back-calculation.

For this purpose, we used the modulus of the known layers as well as the obtained deflections for each section measured in 2015 (before the works) and changed the modulus of the sub-grade until finding satisfactory values.

The following sub-grade moduli were determined: (table IV.2.3)

Table IV.2.3: Sub-grade moduli determined using back-calculation with BISAR

2015		Ref 6cm	N1	N5	5	Ref 6cm-2
Modulus Sub-grade	[MPa]	160	190	220	130	125
Measured deflections	[1/100 mm]	31.6	31.45	28.8	38.75	40.3
Calculated deflections	[1/100 mm]	31.12	31.8	28.97	38.91	40.56
Difference	[1/100 mm]	-0.48	0.35	0.17	0.16	0.26
Coef. of Var.		0.011	0.008	0.004	0.003	0.005

It is observed that the variation of the sub-grade moduli throughout the road section is quite important, starting with a modulus corresponding to a gravel sub-grade (150 to 250 MPa [RDO 09]), but falling to a modulus corresponding to a sub-grade made of a sand-gravel mixture after section N5 (100 MPa to 150 MPa [RDO 09]).

As mentioned in section IV.1.1, the sub-grade is known to be made of a sand, gravel and pebble mixture, which corresponds to the calculated values.

IV.2.4.2 Second step: Confirming the sub-grade modulus

To confirm the sub-grade moduli determined in the first step, the deflections are calculated using the determined sub-grade moduli, but now adding the new surface layer (NSL). This new structure is then compared to the deflections measured on the unreinforced sections (Ref 6 cm and Ref 6 cm -2) in 2016.

The results of this comparison can be found in the following table (table IV.2.4):

Table IV.2.4: Confirmation of the back-calculated sub-grade modulus

2016		Ref 6cm	Ref 6cm-2
Modulus Sub-grade	[MPa]	160	125
Measured deflections	[1/100 mm]	23.8	32.2
Calculated deflections	[1/100 mm]	24.22	32.03
Difference	[1/100 mm]	0.42	-0.17
Coef. of Var.		0.012	0.004

It can be observed that the differences between the deflections determined with the back-calculated sub-grade moduli and the deflections measured on the RD4 in 2016 are very small.

A calculated p-value of 0.914 shows that the null-hypothesis cannot be rejected, leading to the assumption that no significant difference can be found between the differences determined in 2015 and 2016.

IV.2.4.3   Third step: Calculation of the deflections on reinforced sections and comparison with measured deflections

Now that the moduli of the sub-grade are confirmed, it can be used to model the reinforced structure, in order to see if a difference between calculated and measured deflections exists. If it exists, it can be assumed that this difference is based on the insertion of the grid in the structure.

The deflections calculated for the 2016-structures are shown in table IV.2.5, together with the measured deflections, the difference and the coefficient of variation between the two values.

Table IV.2.5: Comparison of the deflections measured in 2016 on the RD4 and the modelled deflections for the 2016 structure

2016		Ref 6cm	N1	N5	5	Ref 6cm-2
Modulus Sub-grade	[MPa]	160	190	220	130	125
Measured deflections	[1/100 mm]	23.8	23.3	23.25	27.75	32.2
Calculated deflections	[1/100 mm]	24.22	26.57	24.5	32.46	32.03
Difference	[1/100 mm]	0.42	3.27	1.25	4.71	-0.17
Coef. of Var.		0.012	0.093	0.037	0.111	0.004

The coefficient of variation shows important differences between the unreinforced and reinforced sections, as the differences between the measured deflections and the calculated deflections in unreinforced sections is lower than 0.5 [1/100 mm] whereas the differences between the measured deflections and the calculated deflections in reinforced sections are larger than 1 [1/100 mm].

The p-value used to compare the differences between the measured and calculated deflections is 0.0015, showing a rejection of the null-hypothesis, suggesting a significant difference between the reinforced and unreinforced values.

We also observe that the differences between the two deflection values on the reinforced sections are positive, showing that the calculated deflections are higher than the measured ones. This means that for the known structure characteristics, the structure should actually achieve higher deflections, and therefore be weaker, as it effectively is.

IV.2.4.4   Fourth step: Comparison of the deflections using best and worst structure characteristics

Up to now the comparison was based only on the average values of the deflection measured on the RD4 as well as on the average thickness and modulus values.

However, we know that variations were observed in all three parameters. In order to include these points in the comparison, the deflections were calculated using the moduli and thicknesses $\pm$ their standard deviations and compared to the measured deflections $\pm$ their standard deviations on the respective sections. The moduli of the sub-grade and the macadam were kept as given.

The standard deviations of the calculated deflections were then calculated with their average, their worst and their best results. The outcome is shown in figure IV.2.1.
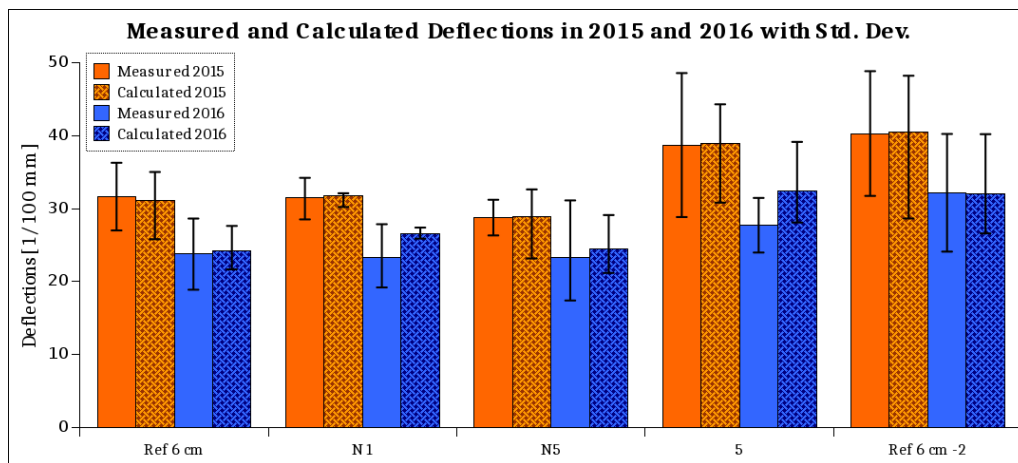
Figure IV.2.1: Comparison of measured and calculated deflections with standard deviation

We observe a difference between the unreinforced sections and the reinforced sections, as the calculated deflections where no grid is placed correspond to the actually measured deflections on the RD4, while the calculated deflections of the reinforced sections show a significant difference to the actually measured deflections.

Therefore it can be assumed that all three glass fibre grids have a positive influence on the deflections. The grid showing the greatest difference is thereby grid 5, followed by grid N1

and N5.

IV.2.4.5   Fifth step: Modelling the surface course of the reinforced sections in order to achieve the actual measured deflection values

Knowing the actual measured deformation, the next step is to determine the effect that the grid has on the stiffness of the surface course. Three methods shall be used:

1. Increasing the stiffness of the new surface layer until reaching the actual measured deflection values

2. Building a new layer out of the NSL and Layer 1, by adding the thickness of both and changing their stiffness until reaching the actual measured deflection values

3. Increasing the thickness of the NSL until reaching the actual measured deflection values.

Increasing the stiffness of the new surface layer until reaching the actual measured deflection values   For this part, the modulus values of all other layers, as well as the thickness of all layers, remain the same, only the modulus of the NSL is modified. The moduli of the reinforced section, with which the actual measured deflection values are reached, are listed in table IV.2.6.

Table IV.2.6: Calculation of an equivalent modulus for layer NSL, in order to reach the actual measured deflections on reinforced sections

	N1		N5		5	
	D	Mod	D	Mod	D	Mod
	[mm]	[MPa]	[mm]	[MPa]	[mm]	[MPa]
NSL	40	35000	35	14000	37.5	45000
1	45	4975.8	46.3	4975.8	49.7	4975.8
2	48	6502	55	6502	53.7	6502
3	45	9181	43.8	7035	50	8466
Macadam	87.5	800	81.2	800	101.7	800
Sub-grade		190		220		130
Def calculated	23.27		23.28		27.73	
Def actual	23.3		23.25		27.75	

The results show that for section N1, the modulus of the NSL had to be increased by 370 %, for section N5 of 88 % and for section 5 of 505 %. At this point it has to be noted that a modulus of 45 000 MPa is only theoretical and cannot be achieved practically.

Constructing a new upper layer consisting of layers NSL, 1 and glass fibre grids
For this part, the thickness of layers NSL and 1 are added in order to model a unique first

layer made of the first two layers and the glass fibre grid in between. The moduli of the newly built layer, with which the actual measured deflection values are reached, are listed in table IV.2.7.

Table IV.2.7: Calculation of an equivalent moduli for a new layer (NSL + 1) in order to reach the actual measured deflections on reinforced sections

	N1		N5		5	
	D	Mod	D	Mod	D	Mod
	[mm]	[MPa]	[mm]	[MPa]	[mm]	[MPa]
NSL + 1	85	22000	81.3	10500	87.2	28000
2	48	6502	55	6502	53.7	6502
3	45	9181	43.8	7035	50	8466
Macadam	87.5	800	81.2	800	101.7	800
Sub-grade		190		220		130
Def calculated	23.25		23.29		27.71	
Def actual	23.3		23.25		27.75	

Compared to the average modulus of the two upper layer, being of 6209 MPa, it can be noted that the modulus of the new first layer in section N1 had to be increased by 254 %, the modulus of section N5 by 69 % and the modulus of section 5 by 351 %.

Increasing the thickness of the new surface layer until reaching the actual measured deflection values   For this part, the modulus values of all other layer as well as the thickness of all layers remain the same, only the thickness of the NSL is modified. The thickness of the reinforced section with which the actual measured deflection values are reached are listed in table IV.2.6.

Table IV.2.8: Calculation of an equivalent thickness for layer NSL, in order to reach the actual measured deflections on reinforced sections

	N1		N5		5	
	D	Mod	D	Mod	D	Mod
	[mm]	[MPa]	[mm]	[MPa]	[mm]	[MPa]
NSL	74	7442	48	7442	81	7442
1	45	4975.8	46.3	4975.8	49.7	4975.8
2	48	6502	55	6502	53.7	6502
3	45	9181	43.8	7035	50	8466
Macadam	87.5	800	81.2	800	101.7	800
Sub-grade		190		220		130
Def calculated	23.34		23.28		27.76	
Def actual	23.3		23.25		27.75	

Compared to the initial thickness of NSL, the new thicknesses are an improvement of 85 % in section N1, 37 % in section N5 and 116 % in section 5.

IV.2.5   Conclusion of modelling

Using the structure modelling of the RD4, we were able to see the reinforcement impact due to inserted grids, which were not visible by only looking at the deflections measured before and after the maintenance works on the RD4.

It was observed that, for the back-calculated sub-grade modulus, the differences between the calculated deflections and the measured deflections were quite important in the reinforced sections, while the unreinforced sections showed differences of less than 0.5 [1/100 mm]. The greatest difference was found in section 5 (grid with a tensile strength of 50 kN/m), followed by sections N1 (tensile strength of 100 kN/m) and N5 (tensile strength of 50 kN/m).

The structure modelling in order to reach the actual measured deflection values was possible by increasing both the stiffness of the NSL as well as the thickness of the NSL. The determined modulus values showed that the NSL would have to have a modulus of 35 000 MPa for section N1, 14 000 MPa for section N5 and 45 000 MPa for section 5. However, a stiffness modulus of more than 20 000 MPa as modulus at 15 °C seems very unlikely.

The description of the impact of the reinforcement as an equivalent to increasing thickness seems more suitable. In this case, it was calculated that the modelled new surface layer would have to be thicker by 85 % forr section N1, by 37 % for section N5 and by 116 % for section 5 in order to achieve the actual measured deflections.

Part V

General conclusion

Glass fibre grids are composite materials installed in pavements in order to lengthen their lifetime by hindering crack initiation and propagation inside the structure. However, the insertion of glass fibre grids at an interface between two layers is also known to create a weakening of the interlayer bonding, which is a crucial value for the good reduction of traffic induced stresses through the structure.

This study, carried out from 2014 to 2017, dealt on the one hand with the impact of different glass fibre grids, coated with different emulsions and different emulsion application rates on the interlayer bonding strength, and on the other hand with the impact of glass fibre grids as reinforcement in asphalt structures.

The study was divided in 3 experimental parts:

Laboratory tests:

- Investigation of the shear strength

- Investigation of the stiffness modulus and fatigue life using indirect tensile tests

In-situ tests:

- Observation of the RD4 with reinforced and unreinforced road sections

Shear test In the first part, shear tests carried out with the Leutner device on double layered cores extracted from an in-situ test surface showed that:

- For recommended emulsion application rates, the specimens reinforced with glass fibre grids achieved low results compared to the unreinforced specimens

- The emulsion application rate had a strong influence on the shear strength, leading to the possibility of equally strong bonds for reinforced specimen and for unreinforced specimens when enough residual binder was added at the interface

- The use of a non-woven between the strands of a grid had a negative influence on the bonding

- The form of the grid strands had an influence on the bonding

- The type of emulsion used for coating have a strong influence on the bonding

- The temperature dependence of the shear resistance differs with the acting bonding effects: Interlocking: lower temperature dependency, bonding through residual binder: higher temperature dependency

Stiffness modulus In the second part, the indirect tensile tests on reinforced and un-reinforced specimens gave information on the acting of the reinforcement as well as on the acting of the interface inside the specimens.

Using the indirect tensile test to investigate the stiffness modulus of two-layered re-inforced and unreinforced specimens, it was observed that, with a similar shear strength, the specimens of sections 600 and 650 showed a constant stiffness modulus difference of about 1100 MPa at all tested temperatures.
Specimens of section 610 on the other hand, having a weakened shear resistance compared to 600 and 650, showed a different curve shape. This differences in shape showed the influence of the temperature on the displacement happening at the interface.

The two-layered specimens were also compared to uni-layered specimens. It was observed that for temperatures under 0 °C, the moduli of the uni-layered specimens were much stiffer than the moduli of the two-layered specimens.
By comparing the strain-stress curves of all the tested specimens at all tested tempera-tures, it was observed that the interlayer within the two-layered specimens enabled more displacement, and so led to lower stiffness modulus, prohibiting a direct comparison of the two-layered specimens with the uni-layered specimens.

A possibility to investigate this special point could be to test two-layered specimens composed of the same asphalt mix on both sides and to compare it with the results of uni-layered specimens made of the same asphalt mix. Such tests could additionally be carried out on two-layered specimens with different bonding characteristics, e.g. with different amounts of emulsion or different surface treatments.

Fatigue tests Fatigue tests performed with the cyclic indirect tensile test on the same two-layered specimens at 10 °C and 20 °C showed that for both temperatures, the rein-forcement had a positive influence on the fatigue life.
While for 10 °C, the behaviour of all three sections 600, 610 and 650 was the same, show-ing very similar fatigue curve slopes, distinguished only by their different axis intercept, the curves at 20 °C were very different.

The visual observations made during the tests highlighted the different crack initiation and propagation progress in the reinforced specimens compared to unreinforced specimens. It was seen that on reinforced specimens, the cracks expanded mainly on one side, while for unreinforced specimens, cracks could be found on both sides of the interface.
It was also observed that even for great vertical deformations, the grids of the reinforced specimens were able to hold the specimens together, while the unreinforced specimens

were falling in two parts.

In-situ-observations The RD4 is an in-situ test road, on which maintenance works were done in 2015, implying the installation of various grids at the interface between the old, cracked structure and the new surface layer.
Deflection measurements with a Flash deflectograph were made before road maintenance works and with a Lacroix deflectograph as well as with a Benkelman beam after road maintenance works.

The deflection measurements made after the maintenance works showed an improvement in the deflections on all parts of the roads, but a special distinction of a section, showing that its characteristics (e.g. reinforcement) brought especially good or bad improvements compared to the old structure, could not be observed.

The measurements made with the Benkelman beam mainly confirmed the results determined with the Lacroix deflectograph. Shear tests, performed on the cores of the RD4, confirmed the results achieved in this study, showing that a grid at the interface weakens the shear strength of the interlayer.

Modelling of the RD4 The elastic moduli of the layers of the RD4 were determined by an external laboratory. The values were used for the modelling of the road structure with the program BISAR. The modelling was divided into 5 different steps:

1. Determination of the modulus of the sub-grade under the asphalt structure using the known deflections, measured in 2015 and the modulus of the other layers

2. Confirming the sub-grade modulus by adding the new surface layer and compare the outcoming deflections with the actual deflections measured on the RD4

3. Calculation of the deflections on the reinforced sections

4. Comparing the deflections using best and worst structure characteristics

5. Modelling the surface course of the reinforced sections in order to obtain the actual measured deflection values

It was observed that the effects of the reinforcement due to the inserted grids, which were not visible on the deflections measured before and after the maintenance works on the RD4, became visible through modelling: For the reinforced sections, the deflections calculated with BISAR were significantly higher than the actual measured deflections on the RD4.

In order to model the structure so that the same calculated deflections were obtained, the modulus of the new surface layer had to be increased by 370 % for section N1, 88 % for section N5 and 505 % for section 5 or the thickness of the new surface layer had to be increased by 85 % in section N1, 37 % in section N5 and 116 % in section 5.

Perspectives   While clearing a few points, the study uncovered a lot of new questions, especially regarding the possibilities of connecting the different investigation points together.

The influence of the interlayer on the stiffness modulus, for example, was clearly visible on the strain-stress curves, showing that it authorized more displacements within the specimen. As the stiffness modulus is crucial for the design of road structures, it would be interesting to be able to model the influence of the interlayer, as to be able to put it apart for tests with reinforcements.
In order to better understand the debonding caused through grids, it would also be very interesting to study the behaviour of specimens under cyclic shearing tests at different temperatures. This way, it would be possible to test the specimens under more in-situ-like conditions.

The observation of the RD4 can also provide the possibility of further investigations regarding long time behaviour of the road.
Shear tests made on cores extracted from the road showed that the unreinforced section achieved the strongest shear resistance when calculated with the reduced surface, while the reinforced sections were weakened. Based on this information, it would be interesting to observe the shear strength behaviours at different time periods of the year, for example during the winter or after the summer. These observations could give an impression of possible de-bonding of the reinforced sections during the winter and possible re-bonding after the summer.
Deflection measurements, which would be done at about the same time than the extraction of the cores for shear tests, could also enable the connection between the bonding between the layers and the measured deflections.

Also, the modelling of the RD4 showed the existing influence of the grids on the deflections of the structure under a certain load. Here, it would be interesting to check how to take into account this influence, e.g. by adding a new layer in-between or by increasing the stiffness of one or more layers which could be affected by glass fibre grids.

References

[AIF 07]   Wellner, F., Ascher, D., 'Schlussbericht zum AiF-Projekt Nr 13589 BR/1: Untersuchungen zur Wirksamkeit des Haftverbundes und dessen Auswirkungen auf die Lebensdauer von Asphaltbefestigungen', 2007, Professur für Straßenbau, Technische Universität Dresden

[AL-Sp 09]   Forschungsgesellschaft für Straßen- und Verkehrswesen (FGSV), 'Arbeitsanleitung zur Bestimmung des Steifigkeits- und Ermüdungsverhaltens von Asphalten mit dem Spaltzug-Schwellversuch als Eingangsgröße in die Dimensionierung AL Sp-Asphalt 09', November 2009, FGSV-Verlag, ISBN: 978-3-941790-06-03

[AP9 15]   Forschungsgesellschaft für Straßen- und Verkehrswesen (FGSV), 'Arbeitspapier Nr. 9/K2.3 zur Systematik der STraßenerhaltung, Reihe K: Kommunale Belange, Abschnitt K2: Zustandserfassung, Unterabschnitt K2.3: Schadenskatalog für die messtechnische und visuelle Zustandserfassung', 2015, FGSV-Verlag, ISBN: 978-3-86446-126-2

[ARS 13]   Arsenie, I.M., 'Etude et modélisation des renforcements de chaussés à l'aide de grilles en fibre de verre sous sollicitations de fatigue', 2013, PhD-Thesis, Université de Strasbourg

[ARS 16]   Arsenie, I.M., Chazallon, C., Duchez, J.-L., Hornych, P., 'Laboratory characterisation of the fatigue behaviour of glass fibre grid-reinforced asphalt concrete using 4PB tests', 2016, Road Materials and Pavement Design, DOI: 10.1080/14680629.2016.1163280

[BAT 09]   Bathias, C. et coll., 'Matériaux composites', , 2009, 2nd edition, L'Usine nouvelle Dunod, Paris, ISBN: 978-2-10-052608-6

[BISAR 98]   Bitumen Business Group, 'BISAR 3.0 User Manual', 1998, Shell International Oil Products B.V.

[CAN 13]   Canestrari, F., Ferrotti, G., Lu, X., Millien, A., Partl, M. N., Petit, C., Phelipot-Mardelé, A., Piber, H., Raab, C., 'Mechanical Testing of Interlayer Bonding in Asphalt Pavements', 2013, Volume 9 of the series RILEM State-of-the-Art Reports, pp. 303-360., Springer ISBN 978-94-007-5104-0

[CFTR 09]   CFTR (Comité francais pour les techniques routières), 'Guide technique: Les renforcements de chaussées - Diagnostic et conception', 2009, Collection 'Les outils', Sétra

[DI BEN 04]   Di Benedetto, De La Roche, C., Baaj, H., Pronk, A., Lundstrom, R., 'Fatigue of bituminous mixtures', 2004, RILEM TC 182-PEB Perfomance testing and evaluation of bituminous materials, Materials and Structures, Vol. 37, pp 202-216

[EN12697-26]   European Committee for Standardization, 'European Standard 12697-26, Bituminous mixtures - Test methods for hot mix asphalt - Part 26: Stiffness', 2012, ICS 93.080.20

[EN 1426]   European Committee for Standardization, 'European Standard 1426, Bitumen and bituminous binders- Determination of needle penetration, German version prEN 1426:2013', 2013, ICS 75.140; 91.100.50

[EN 1427]   European Committee for Standardization, 'European Standard 1426, Bitumen and bituminous binders- Determination of the softening point - Ring and Ball method, German version EN 1427:2007', 2007, ICS 75.140; 91.100.50

[FER 12]   Ferrotti, G., Canestrari, F., Pasquini, E., Virgili, A., 'Experimental evaluation of the influence of surface coating on fiberglass geogrid performance in asphalt pavements', 2012, Geotextiles and Geomembranes, Volume 34, pp. 11-18, DOI: 10.1016/j.geotexmem.2012.02.011

[FSS 99]   IFTA GmbH, Essen, 'Veränderung von Bindemitteleigenschaften während längerer Liegezeiten von Asphalten', ('Changes of binder characteristics during longer lifetime of asphalt'), 1998, Forschung Straßenbau und Straßenverkehrstechnik, Heft 774, Number 07.177

[HAK 12]   Hakimzadeh, S., Kebede, N.A., Buttlar, W.G., 'Comparison between Optimum Tack Coat Application Rates as obtained from Tension- And Torsional Shear-Type Tests' 2012, University of Illinois at Urbana Champaign, 7th RILEM International Conference on Cracking in Pavements

[HOF 16]   Hofko, B., Blab, R., Alisov, A., 'Influence of compaction direction on performance characteristics of roller-compacted HMA specimens', 2016, International Journal of Pavement Engineering, pp 39-41, DOI: 10.1080/10298436.2014.925550

[JAC 10]   Jacobs, D., 'Application of asphalt interlayers for road maintenance management', 2010, Conference paper, 10th Swiss Transport Research Conference (STRC)

[LAV 03]   Lavin, P.G., 'Asphalt Pavements. A practical guide to design, production, and maintenance for engineers and architects', 2003, Spon Press, Talor & Francis Group, ISBN: 0-415-24733-0

[NEJ 14]   Njead, F.M., Noory, A., Tooabi, S., Fallah, S., 'Effect of using geosynthetics on reflective crack prevention', 2014, International Journal of Pavement Engineering, DOI: 10.1080/10298436.2014.943128

[NF P 98-086]   AFNOR, 'French Standard NF P 98-086 : Dimensionnement des structures de chaussées routières', 2011

[NGU 13]   Nguyen, M.-L., Blan, J., Kerzého, J.-P., Hornych, P., 'Review of glass fibre grid use for pavement reinforcement and APT experiments at IFSTTAR', 2013, Road Materials and Pavement Design, Volume 14, sup. 1, pp. 287-308, DOI: 10.1080/14680629.2013.774763

[PLUG 10]   Plug, C.P., de Bondt, A.H., 'Adhesion of reinforcement grids in asphalt overlays', 5th world congress on emulsion, Lyon, France, October 2010

[RIC 11]   Richter, H.P., 'Die Pohris-Glasfaser - Ein vorteilhafter Werkstoff', 2011, MultiFas Aktuell, Volume 2011, www.multifas.de

[RAAB 04]   Raab, C., Partl, M., 'Interlayer shear performance: Experience with different pavement structures', 2004, 3rd Eurasphalt & Eurobitume Congress, Vienna, Paper 081, pp. 535-545

[RAAB 07]   Raab, C., 'Auswirkungen von Geotextilien auf den Schichtverbund bei bitumenhaltigem hocheinbau auf Betonstraßen', 2007, Presentation at the Empa-Akademie conference 'Asphaltverstärkungen mit Einlagen. Erfahrungen und Perspektiven', May 15th, 2007

[RAAB 16]   Raab, C., Arraigada, M., Partl, M.N., 'Effect of reinforced asphalt pavements on reflective crack propagation and interlayer bonding performance', 2016, 8th International conference on Mechanism of Cracking and Debonding Pavements, RILEM

[RDO 09]   Forschungsgesellschaft für Straßen- und Verkehrswesen (FGSV), 'Richtlinien für die rechnerische Dimesionierung des Oberbaus von Verkehrsflächen mit Asphaltdeckschicht - RDO Asphalt'; December 2009, FGSV-Verlag, ISBN: 978-3-941790-15-5

[ROM 94]   Romero, R., Ruiz, A., Rodil, R., Lechuga, M.A., 'Variation of Deflection with Measuring Equipment and Load Speed on Test Track', 1994, Transportation Research Record No. 1448: 'Strength and Deformation Characteristics of Pavement Sections', Transportation Research Board, National Academy Press, ISBN: 0-309-06057-5

[ROM 14]   Romeo, E., Freddi, F., Montepara, A., 'Mechanical behaviour of surface layer fibreglass-reinforced flexible pavements', 2014, International Journal of Pavement Engineering, Volume 15:2, pp. 95-109, DOI 10.1080/10298436.2013.828838

[SOK 07]   Sokolov, K., 'Laboruntersuchungen an unterschiedlichen verstärkten Asphaltschichten, 2007, Presentation at the Empa-Akademie conference 'Asphaltverstärkungen mit Einlagen. Erfahrungen und Perspektiven', May 15th, 2007

[STR 09]   Straube, E., Krass, K., 'Straßenbau und Straßenerhaltung - Ein Handbuch für Studium und Praxis, 2009, 9th edition, Erich Schmidt Verlag, Berlin, ISBN: 978-3-503-11254-8

[THO 14]   Thom, N., 'Principles of Pavement Engineering', 2014, 2nd Edition, ICE Publishing, ISBN: 978-0-7277-5853-8

[TP-A 12]   Forschungsgesellschaft für Straßen- und Verkehrswesen (FGSV), 'TP Asphalt StB, Teil 80: Abscherversuch' (Technical testing regulation for asphalt: Shear test), 2012, FGSV Verlag, ISBN: 978-3-939715-78-8

[VEC 17]   Vectra France, 'FLASH DEFLECTOGRAPH mlpc® - Deflection', website: http://vectrafrance.com/materials-and-solutions/worksite-testing/flash-deflectograph-mlpcR-deflection?L=6 , visited on August 29th, 2017

[VEL 13]   Velske, S., Mentlein, H., Eymann, P., 'Strassenbau - Strassenbautechnik', 2013, 7th Edition, Werner Verlag, ISBN: 978-3-8041-3883-4

[VIR 09]   Virgili, A., Canestrari, F., Grilli, A., Santagata, F.A., 'Repeated load test on bituminous systems reinforced by geosynthetics', 2009, Geotextiles and Geomembranes, Volume 27, pp. 187-195, DOI: 10.1016/j.geotexmem.2008.11.004

[VIS 12]   Vismara, S., Molenaar, A.A.A., Crispino, M., Poot, M.R., 'Characterizing the Effects of Geosynthetics in Asphalt Pavements', , 2012, 7th RILEM International Conference on Cracking in Pavements, pp. 1199-1207, RILEM 2012

[ZAM 10]   Zamora-Barraza, D., Calzada-Pérez, M.A., Castro-Fresno, D., Vega-Zamanillo, A., 'New procedure for measuring adherence between a geosynthetic material and a bituminous mixture', 2010, Geotextiles and Geomembranes, Volume 28, pp. 483-489, DOI:10/1016/j.geotexmem.2009.12.010

[ZAM 11]   Zamora-Barraza, D., Calzada-Pérez, M.A., Castro-Fresno, D., Vega-Zamanillo, A., 'Evaluation of anti-reflective cracking systems using geosynthetics in the interlayer zone', 2011, Geotextiles and Geomembranes, Volume 29, pp. 130-136, DOI:10.1016/j.geotexmem.2010.10.005

List of communications

- Published articles:

Sagnol, L., Chazallon, C., Stöckner, M., 'Effect of glass fibre grids on the bonding strength between two asphalt layers', 2017, Th 10th International Conference on the Bearing Capacity of Roads, Railways and Airfields (BCRRA 2017), pp. 1537-1542, DOI: 10.1201/9781315100333-220

- Articles in correction (state: 29/09/17):

Sagnol, L., Quezada, J.C., Chazallon, C., Stöckner, M., 'Effect of glass fibre grids on the bonding strength between two asphalt layers and its DEM modelling', Draft, Road Materials and Pavement Design

- Poster presentations:

Sagnol, L., 'Experimentelle ud numerische Betrachtung der Verstärkung von Straßenaufbauten durch Glasfasergitter', 15/16 February 2017, FGSV Veranstaltung, Arbeitsgruppentagung Infrastrukturmanagement 2017, Duisburg, DE

Sagnol, L., Quezada, J.C., Chazallon, C., Stöckner, M., 'Effect of glass fibre grids on the bonding strength between two asphalt layers and its DEM modelling', 12-14, June 2017, 7th International EATA Conference, EMPA, Zürich, CH

Sagnol, L., 'Experimental and numerical study of the reinforcement of infrastructure by glass fibre grids', 04/05, May 2017, HAWtech-Tagung 2017 - Bauen für die Zukunft, Berlin, DE

Part VI

Appendix

Appendix I: Construction of the test surface: Materials parameters

Materials used for the lower and upper course (by manufacturer)

SWA Südwest Asphalt GmbH & Co. KG
Josef-Herrmann-Straße 1-3
76473 Iffezheim

SWA Südwest Asphalt · Josef-Herrmann-Straße 1-3 · 76473 Iffezheim

REIF GmbH & Co. KG
- Herrn Steinbrunn
Hohlohstr. 9

76437 Rastatt

Ihr Zeichen:	Ihre Nachricht:	Unser Zeichen:	Unser Hausruf:	Datum:
		ga-sr	604.26	02.06.2015

Prüfzeugnisse für Asphaltmischgut

Baumaßnahme :   Lagerplatz Rastatt (17928)
Lieferwerk :   Iffezheim (SWA)
Auftragsnummer : lfd. Bedarf

Sehr geehrte Damen und Herren,

als Anlage erhalten Sie für Ihre oben genannte Baumaßnahme Prüfzeugnisse für die angebotenen Artikel

Art.-Nr.	EP-Nr.	Mischgutart/-sorte
32384	02425 00	AC 16 B S 25/55-55 RC
32322	03337 00	AC 11 D S 25/55-55 A.

Die Prüfzeugnisse entsprechen inhaltlich dem geltenden Technischen Regelwerk. Es gelten die in den ZTV Asphalt-StB 07/13 für Asphaltmischgut angegebenen Grenzwerte und Toleranzen.

Die Prüfung der Eignung des angebotenen Asphaltmischgutes für den genannten Verwendungszweck obliegt Ihnen. Sie können die Eignung gegenüber Ihrem Auftraggeber bestätigen (Eignungsnachweis) in dem Sie auf Seite 3 der Prüfzeugnisse die Baumaßnahme benennen, die entsprechende OZ-Nummer ergänzen und das Ganze mit Ihrer Unterschrift versehen.

Sofern wir nicht rechtzeitig vor Beginn der Baumaßnahme einen schriftlichen Änderungsvorschlag von Ihnen erhalten, gehen wir davon aus, dass wir das Mischgut nach der Konzeption unserer Prüfzeugnisse liefern werden. Wird eine andere Zusammensetzung des Mischgutes verlangt, so tragen wir keine Verantwortung für die Gebrauchseigenschaft der damit hergestellten Schichten.
                                                                                          .../...

Wir weisen darauf hin, dass die Angaben in den Prüfzeugnissen, die über die geforderten Angaben der ZTV Asphalt-StB 07/13 hinausgehen, rein informellen Charakter haben, nicht bindend sind und nicht Bestandteil des Liefervertrages werden.

Bitte geben Sie dem Mischwerk den voraussichtlichen Termin über die Probenahme im Rahmen der Kontrollprüfung bekannt. Das betreffende Labor wird Sie dann nach Möglichkeit unterstützen. In jedem Fall erwarten wir, dass uns die nach TP Asphalt-StB, Teil 27 zustehende Mischgutprobe mit der zugehörigen Niederschrift über die Probenahme zur Verfügung gestellt wird. Bitte übergeben Sie uns auch eine Kopie der Prüfberichte der Kontrollprüfung. An uns gerichtete Mängelrügen aufgrund der Ergebnisse der Kontrollprüfung erkennen wir nicht an, wenn die Grundsätze der TP Asphalt-StB, Teil 27 nicht eingehalten werden.

In den ZTV Asphalt-StB 07/13 sind Anforderungen an die Griffigkeit von Asphaltdeckschichten enthalten. Diese Anforderungen werden Bestandteile der Bauverträge, wenn die ZTV Asphalt-StB 07/13 dort vereinbart wird. Zur Erzielung einer sachgerechten Rauheit der Deckschicht im Sinne der ZTV Asphalt-StB 07/13 sind Abstumpfungsmaßnahmen erforderlich und von Ihnen durchzuführen. Für eine Sachgerechte Durchführung der Abstumpfungsmaßnahmen übernehmen wir keine Verantwortung. Wir erklären, dass das gemäß dem beigefügten Prüfzeugnis zusammengesetzte Asphaltmischgut zur Herstellung einer Deckschicht geeignet ist, welche die Anforderungen der Griffigkeit gemäß ZTV Asphalt-StB 07/13 erfüllt.

Geben Sie bei Mischgutabruf bitte die Auftragsnummer, die Artikelnummer sowie die Erstprüfungsnummer der auf dem Prüfzeugnis angegebenen Erstprüfung an. Wir sichern Ihnen eine einwandfreie und termingerechte Lieferung zu.

Mit freundlichen Grüßen

SWA Südwest Asphalt GmbH & Co. KG

ppa.   i.A.
    (Garthe)   (Scherrer)

SWA Südwest Asphalt GmbH & Co. KG
Josef-Herrmann-Str. 1–3
76473 Iffezheim
labor@suedwest-asphalt.de

Telefon (0 72 29) 604-0
Telefax (0 72 29) 604-44

Zentrallaboratorium Karlsruhe

Prüfzeugnis für Asphaltmischgut

Datum: **02.06.2015**

Erstprüfungsnummer: 02425 00 6721 00 vom 17.09.2013

Mischgutart/-sorte: **AC 16 B S nach TL Asphalt-StB 07 u. ARS 11/2012**

Zugegeb. Bindemittelart/-sorte: 25/55-55 RC

Zusätze:

resultierende Bindemittelsorte: 25/55-55 A

Lieferwerk: Iffezheim (SWA Südwest Asphalt GmbH & Co.KG)

Grundlagen: TL Asphalt-StB 07, TP Asphalt-StB 07, TL Gestein-StB 04, TL Bitumen-StB 07, ARS 11/2012

Artikel: **32384 AC 16 BS MOR 25/55-55 RC**

Auftragsnummer: Iffezheim (SWA) - SAP

Kornzusammensetzung des Gesteinskörnungsgemisches für die Vordosierung an der Asphaltmischanlage

Nr	M.-%	Bezeichnung	Lieferkörnung	Gewinnungsstätte	Hersteller
M 1	3,4	Kalkstein	Füller	Roßwag	Gebr. Zimmermann GmbH
M 2	16,1	Moräne	Feine Gesteinsk. 0/2	Iffezheim	KBI Kern GmbH & Co. KG
M 3	12,5	Moräne	Gr. Gesteinsk. 2/5	Iffezheim	KBI Kern GmbH & Co. KG
M 4	12,0	Moräne	Gr. Gesteinsk. 5/8	Iffezheim	KBI Kern GmbH & Co. KG
M 5	15,0	Moräne	Gr. Gesteinsk. 8/11	Iffezheim	KBI Kern GmbH & Co. KG
M 6	21,0	Quarzporphyr	Gr. Gesteinsk. 11/16	Ottenhöfen	W. Bohnert GmbH & Co. KG
Asphaltgranulat					
G 1	20,0	Asphaltfräsgut RA 16 (Deck- und Binderschichten diverser Baumaßnahmen)			

Kornzusammensetzung der Lieferkörnungen

		Siebrückstand M.-%							
	M 1	M 2	M 3	M 4	M 5	M 6	G 1		
mm	Füller	0/2	2/5	5/8	8/11	11/16			
31,50									
22,40									
16,00						8,9	2,0		
11,20					6,9	88,4	8,0		
8,00				8,9	84,8	2,5	14,0		
5,60			6,1	79,4	7,1	0,1	15,2		
2,00		6,1	87,4	10,6	0,6	0,1	15,5		
1,00		24,7	5,0	0,3	0,1	0,0	14,5		
0,25		40,5	0,9	0,3	0,1	0,0	14,0		
0,125	2,2	10,4	0,3	0,2	0,1	0,0	5,5		
0,063	10,6	6,0	0,1	0,1	0,1	0,0	2,4		
< 0,063	87,2	12,3	0,2	0,2	0,2	0,0	8,9		
Überkorn	12,8	6,1	6,1	8,9	6,9	8,9			
Sollkorn	87,2	93,9	87,4	79,4	84,8	88,4			
Unterkorn			6,5	11,7	8,3	2,7			
Rohdichte (g/cm³)	2,724	2,649	2,649	2,645	2,647	2,586	2,488		
Fließkoeffizient		36							

SWA Südwest Asphalt GmbH & Co. KG
Josef-Herrmann-Str. 1–3   Telefon (0 72 29) 604-0
76473 Iffezheim   Telefax (0 72 29) 604-44
labor@suedwest-asphalt.de

Zentrallaboratorium Karlsruhe

SÜDWEST ASPHALT

Seite 2/3   der Rezeptur Nr.   02425 00 6721 00

Kornzusammensetzung des Gesteinskörnungsgemisches			
mm	Rückstand	Durchgang	M.-%
> 45,00			
45,00			
31,50			
22,40		100,0	
16,00	2,3	97,7	grobe GK 71,6
11,20	21,3	76,4	
8,00	17,2	59,2	
5,60	14,4	44,8	
2,00	16,4	28,4	
1,00	7,5	20,9	feine GK 21,6
0,25	9,4	11,5	
0,125	2,9	8,6	
0,063	1,8	6,8	
< 0,063	6,8	Füller	

Sieblinienbereich für   AC 16 B S
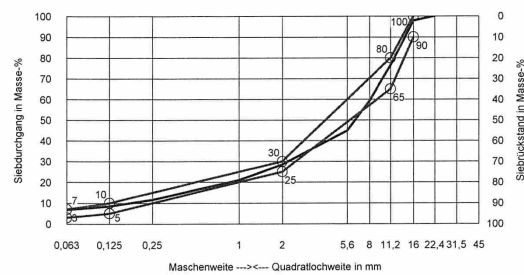
Gesteinskörnungsanteile		Istwert	Sollwert	
			min	max
Füller <0,063 mm (Siebdurchgang)	M.-%	6,8	3,0	7,0
<0,125 mm (Siebdurchgang)	M.-%	8,6	5,0	10,0
feine Gesteinskörnung	M.-%	21,6		
grobe Gesteinskörnung >2 mm (Siebrückstand)	M.-%	71,6	70,0	75,0
Größtkorn (Siebrückstand)	M.-%	23,6	20,0	35,0
Überkorn (Siebrückstand)	M.-%	2,3		10,0

Bindemittel / Asphaltgranulat / Zusätze				
Material: AC 16 B S		Asphaltmischgut-zusammensetzung	Sollwert	
			min	max
rechn. Mindestbindemittelgehalt	M.-%		4,5	
Gesamt-Bindemittelgehalt	M.-%	**4,8**	4,4	
Bindemittelgehalt Frischbitumen	M.-%	3,7		
Gesamt-Bindemittelgehalt	Gew.-T	5,04		
Bindemittelanteil	Vol.-%	10,9		
EP RuK (Asphaltmischgut)	°C	62,7	55,0	
EP RuK (Frischbitumen)	°C	63,0	55,0	63,0
EP RuK (aus Ausbauasphalt)	°C	61,8		
EP RuK (extrahiertes Bitumen)	°C			

SWA Südwest Asphalt GmbH & Co. KG
Josef-Herrmann-Str. 1–3   Telefon (0 72 29) 604-0
76473 Iffezheim   Telefax (0 72 29) 604-44
labor@suedwest-asphalt.de

Zentrallaboratorium Karlsruhe

Seite 3/3 der Rezeptur Nr.   02425 00 6721 00

Asphaltmischguteigenschaften				
Material: AC 16 B S		Asphaltmischgut-zusammensetzung	Sollwert	
			min	max
Rohdichte des Asphaltmischgutes	g/cm³	2,463		
Rohdichte des Gesteinskörnungsgemisches	g/cm³	2,649		
Raumdichte am Marshall-Probekörper	g/cm³	2,342		
Hohlraumgehalt (ber.)	Vol.-%	4,9	3,5	6,5
Hohlraumausfüllungsgrad	%	69,0		
Verdichtungstemperatur der Marshall-Probekörper	°C	145,0		
Proportionale Spurrinnentiefe	%	2,7		

Das nach dieser Rezeptur hergestellte Asphaltmischgut erfüllt die Anforderungen der TL Asphalt - StB 07/13.
Für die Gesteinskörnungen und den Füller liegen die CE-Kennzeichnungen vor. An den verwendeten groben Gesteinskörnungen wurde das Haftverhalten nach 24 h mit >=60 % ermittelt.
Die Asphaltmischgutuntersuchungen wurden gemäß TP Asphalt - StB durchgeführt.
Es gelten die in den ZTV Asphalt-StB 07/13 für Asphaltmischgut angegebenen Toleranzen.
Die Angaben der Rezeptur, die über die geforderten Angaben der ZTV Asphalt-StB 07/13 hinausgehen, haben rein informellen Charakter, sind nicht bindend und werden nicht Bestandteil des Liefervertrages.
Nur durch die Unterschrift des Auftragnehmers wird die Eignung des Asphaltmischgutes für den unten genannten Verwendungszweck nachgewiesen.

SWA Südwest Asphalt
GmbH & Co. KG
Zentrallabor

Dipl.-Ing. F. Garthe
(Prüfstellenleiter)

Eignungsnachweis
im Sinne der ZTV Asphalt - StB 07/13

Hiermit erklärt der Auftragnehmer:

gegenüber dem Auftraggeber:

für die Baumaßnahme:

folgendes:

a) Die Angaben zur Zusammensetzung und zu den im Rahmen der Erstprüfung nach TL Asphalt - StB 07/13 durchgeführten Prüfungen sind der oben aufgeführten Rezeptur zu entnehmen.
b) Das Asphaltmischgut ist für den vorgesehenen Verwendungszweck, wie er sich aus den im Bauvertrag festgelegten Anforderungen, insbesondere aus den OZ - Nummern ergibt, geeignet.

OZ-Nummern:

....

_____   _____
Ort, Datum   Auftragnehmer

Prüfzeugnis für Asphaltmischgut

Datum: 02.06.2015

Erstprüfungsnummer: 03337 00 6721 00 vom 10.08.2012

Mischgutart/-sorte: **AC 11 D S nach TL Asphalt-StB 07 u. ARS 11/2012**

Zugegeb. Bindemittelart/-sorte:	25/55-55 A
Zusätze:	
resultierende Bindemittelsorte:	
Lieferwerk:	Iffezheim (SWA Südwest Asphalt GmbH & Co.KG)
Grundlagen:	TL Asphalt-StB 07, TP Asphalt-StB 07, TL Gestein-StB 04, TL Bitumen-StB 07, ARS 11/2012
Artikel:	**32322 AC 11 DS MOR 25/55-55 A**
Auftragsnummer:	Iffezheim (SWA) - SAP

Kornzusammensetzung des Gesteinskörnungsgemisches für die Vordosierung an der Asphaltmischanlage

Nr	M.-%	Bezeichnung	Lieferkörnung	Gewinnungsstätte	Hersteller
M 1	4,0	Kalkstein	Füller	Roßwag	Gebr. Zimmermann GmbH
M 2	9,0	Kies	Feine Gesteinsk. 0/2	Iffezheim	KBI Kern GmbH & Co. KG
M 3	27,5	Moräne	Feine Gesteinsk. 0/2	Iffezheim	KBI Kern GmbH & Co. KG
M 4	10,5	Moräne	Gr. Gesteinsk. 2/5	Iffezheim	KBI Kern GmbH & Co. KG
M 5	18,0	Moräne	Gr. Gesteinsk. 5/8	Iffezheim	KBI Kern GmbH & Co. KG
M 6	21,0	Moräne	Gr. Gesteinsk. 8/11	Iffezheim	KBI Kern GmbH & Co. KG
Asphaltgranulat					
G 1	10,0		Asphaltfräsgut RA 8 (diverse Maßnahmen)		

Kornzusammensetzung der Lieferkörnungen

			Siebrückstand M.-%						
	M 1	M 2	M 3	M 4	M 5	M 6	G 1		
mm	Füller	0/2	0/2	2/5	5/8	8/11			
31,50									
22,40									
16,00									
11,20						6,9			
8,00					8,9	84,8	6,0		
5,60				6,1	79,4	7,1	14,4		
2,00		3,9	6,1	87,4	10,6	0,6	23,3		
1,00		14,3	24,7	5,0	0,3	0,1	17,0		
0,25		57,7	40,5	0,9	0,3	0,1	16,1		
0,125	2,2	22,6	10,4	0,3	0,2	0,1	6,2		
0,063	10,6	1,2	6,0	0,1	0,1	0,1	3,1		
< 0,063	87,2	0,3	12,3	0,2	0,2	0,2	13,9		
Überkorn	12,8	3,9	6,1	6,1	8,9	6,9			
Sollkorn	87,2	96,1	93,9	87,4	79,4	84,8			
Unterkorn				6,5	11,7	8,3			
Rohdichte (g/cm³)	2,724	2,643	2,649	2,649	2,645	2,647	2,431		
Fließkoeffizient		29	36						

SWA Südwest Asphalt GmbH & Co. KG

Josef-Herrmann-Str. 1–3   Telefon (0 72 29) 604-0
76473 Iffezheim   Telefax (0 72 29) 604-44
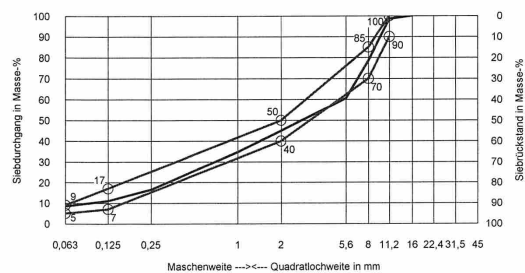labor@suedwest-asphalt.de

Zentrallaboratorium Karlsruhe

Seite 2/3   der Rezeptur Nr.   03337 00 6721 00

Kornzusammensetzung des Gesteinskörnungsgemisches

mm	Rückstand	Durchgang	M.-%
> 45,00			
45,00			
31,50			
22,40			
16,00		100,0	grobe GK 55,0
11,20	1,5	98,5	
8,00	20,1	78,4	
5,60	17,8	60,6	
2,00	15,6	45,0	
1,00	10,3	34,7	
0,25	18,2	16,5	feine GK 36,6
0,125	5,6	10,9	
0,063	2,5	8,4	
< 0,063	8,4	Füller	

Sieblinienbereich für AC 11 D S

Gesteinskörnungsanteile		Istwert	Sollwert	
			min	max
Füller <0,063 mm (Siebdurchgang)	M.-%	8,4	5,0	9,0
<0,125 mm (Siebdurchgang)	M.-%	10,9	7,0	17,0
feine Gesteinskörnung	M.-%	36,6		
grobe Gesteinskörnung >2 mm (Siebrückstand)	M.-%	55,0	50,0	60,0
Größtkorn (Siebrückstand)	M.-%	21,6	15,0	30,0
Überkorn (Siebrückstand)	M.-%	1,5		10,0

Bindemittel / Asphaltgranulat / Zusätze				
Material: AC 11 D S		Asphaltmischgut-zusammensetzung	Sollwert	
			min	max
rechn. Mindestbindemittelgehalt	M.-%		6,1	
Gesamt-Bindemittelgehalt	M.-%	**6,1**	6,0	
Bindemittelgehalt Frischbitumen	M.-%	5,5		
Gesamt-Bindemittelgehalt	Gew.-T	6,50		
Bindemittelanteil	Vol.-%	13,9		
EP RuK (Asphaltmischgut)	°C	63,0	55,0	
EP RuK (Frischbitumen)	°C	63,0	55,0	
EP RuK (aus Ausbauasphalt)	°C	62,9		
EP RuK (extrahiertes Bitumen)	°C			

SÜDWEST ASPHALT

Seite 3/3 der Rezeptur Nr.   03337 00 6721 00

Asphaltmischguteigenschaften				
Material: AC 11 D S		Asphaltmischgut-zusammensetzung	Sollwert	
			min	max
Rohdichte des Asphaltmischgutes	g/cm³	2,418		
Rohdichte des Gesteinskörnungsgemisches	g/cm³	2,652		
Raumdichte am Marshall-Probekörper	g/cm³	2,336		
Hohlraumgehalt (ber.)	Vol.-%	3,4	2,5	3,5
Hohlraumausfüllungsgrad	%	80,3		
Verdichtungstemperatur der Marshall-Probekörper	°C	145,0		

Das nach dieser Rezeptur hergestellte Asphaltmischgut erfüllt die Anforderungen der TL Asphalt - StB 07/13.
Für die Gesteinskörnungen und den Füller liegen die CE-Kennzeichnungen vor. An den verwendeten groben Gesteinskörnungen wurde das Haftverhalten nach 24 h mit >=60 % ermittelt.
Die Asphaltmischgutuntersuchungen wurden gemäß TP Asphalt - StB durchgeführt.
Es gelten die in den ZTV Asphalt-StB 07/13 für Asphaltmischgut angegebenen Toleranzen.
Die Angaben der Rezeptur, die über die geforderten Angaben der ZTV Asphalt-StB 07/13 hinausgehen, haben rein informellen Charakter, sind nicht bindend und werden nicht Bestandteil des Liefervertrages.
Nur durch die Unterschrift des Auftragnehmers wird die Eignung des Asphaltmischgutes für den unten genannten Verwendungszweck nachgewiesen.

SWA Südwest Asphalt
GmbH & Co. KG
Zentrallabor

_____
Dipl.-Ing. F. Garthe
(Prüfstellenleiter)

Eignungsnachweis
im Sinne der ZTV Asphalt - StB 07/13

Hiermit erklärt der Auftragnehmer:

gegenüber dem Auftraggeber:

für die Baumaßnahme:

folgendes:

a) Die Angaben zur Zusammensetzung und zu den im Rahmen der Erstprüfung nach TL Asphalt - StB 07/13 durchgeführten Prüfungen sind der oben aufgeführten Rezeptur zu entnehmen.
b) Das Asphaltmischgut ist für den vorgesehenen Verwendungszweck, wie er sich aus den im Bauvertrag festgelegten Anforderungen, insbesondere aus den OZ - Nummern ergibt, geeignet.

OZ-Nummern:

....

_____   _____
Ort, Datum   Auftragnehmer

Dateiname: EPr C60B1-S 130306

Datum: 20.03.2013

Erstprüfungszeugnis – CE – Zertifizierung
Produkt: C60B1-S

Angaben zur Prüfung:

Firma:	Süddeutsche Teerindustrie GmbH & Co. KG
Produktionsstätte:	Werk Malsch
Art der Probe:	C60B1-S / Bitumenemulsion zur Herstellung des Schichtenverbundes.
Fertigungsdatum:	06.03.2013
Probenahmedatum:	06.03.2013
Freigabedatum:	06.03.2013
Zugrundeliegende Norm:	TL BE-StB 07

Laboruntersuchungen:

Prüfeigenschaft	Prüfnorm	Sollwert	Istwert
pH – Wert Emulsion	interne Prüfung	< 3,0	2,7
Äußere Beschaffenheit	DIN EN1425	braun, homogen	braun, homogen
Brechverhalten [g]	DIN EN 13075-1	IA	122
Bindemittelgeh. [%]	DIN EN 1428	58 – 62	62
Ausflußzeit 2 mm [sek.]	DIN EN 12846	≤ 20	16
Siebrückstand [%]	DIN EN 1429	≤ 0,5	0,1
Siebrückstand n. 7 Tg.[%]	DIN EN 1429	≤ 0,5	0,2
Haftverhalten [%]	DIN EN 13614	≥ 75 %	90
Nadelpenetr. (25 °C) [0,1 mm]	DIN EN 1426	≤ 220	172
EP R.u.K [°C]	DIN EN 1427	≥ 35	42,8
Nach Alterung:			
Nadelpenetr. (25 °C) [0,1 mm]	DIN EN 1426	IA	160
EP R.u.K [°C]	DIN EN 1427	IA	43,8

Zusammenfassung:

Das geprüfte Produkt C60B5-REP erfüllt die Anforderungen an eine Bitumenemulsion zur Herstellung des Schichtenverbundes im Straßenbau nach TL BE-StB 07.

Malsch, 20.03.2013

Boy

Süddeutsche Teerindustrie GmbH & Co. KG - Otto – Eckerle – Str. 7 – 11 - 76316 Malsch

C60B4-S (old name: C60B1-S)

Erstprüfungszeugnis – CE – Zertifizierung
Produkt: C40BF1-S

Angaben zur Prüfung:

Firma:	Süddeutsche Teerindustrie GmbH & Co. KG
Produktionsstätte:	Werk Malsch
Art der Probe:	C40BF1-S / Bitumenemulsion zur Herstellung des Schichtenverbundes.
Fertigungsdatum:	11.07.2012
Probenahmedatum:	12.07.2012
Freigabedatum:	12.07.2012
Zugrundeliegende Norm:	TL BE-StB 07

Laboruntersuchungen:

Prüfeigenschaft	Prüfnorm	Sollwert	Istwert
pH – Wert Emulsion	interne Prüfung	< 3,0	1,6
Äußere Beschaffenheit	DIN EN1425	braun, homogen	braun, homogen
Brechverhalten [g]	DIN EN 13075-1	IA	> 180
Eindringfähigkeit [min.]	DIN EN 12849	IA	17
Bindemittelgeh. [%]	DIN EN 1428	38 - 42	41
Ausflußzeit 2 mm [sek.]	DIN EN 12846	$\leq$ 20	14
Siebrückstand [%]	DIN EN 1429	$\leq$ 0,5	< 0,1
Siebrückstand n. 7 Tg. [%]	DIN EN 1429	$\leq$ 0,5	0,1
Haftverhalten [%]	DIN EN 13614	$\geq$ 75 %	90
Nadelpenetr. (25 °C) [0,1 mm]	DIN EN 1426	$\leq$ 220	100
EP R.u.K [°C]	DIN EN 1427	$\geq$ 35	46,2
Nach Alterung:			
Nadelpenetr. (25 °C) [0,1 mm]	DIN EN 1426	IA	78
EP R.u.K [°C]	DIN EN 1427	IA	48,9

Zusammenfassung:

Das geprüfte Produkt C40BF1-S erfüllt die Anforderungen an eine Bitumenemulsion zur Herstellung des Schichtenverbundes im Straßenbau nach TL BE-StB 07.

Malsch, 14.08.2012

Boy

Süddeutsche Teerindustrie GmbH & Co. KG - Otto – Eckerle – Str. 7 – 11 - 76316 Malsch

C40B5-S (old name: C40BF1-S)

Appendix II: Leutner test results

Shear strengh results of all sections with standard deviation dependent from the residual binder application rate.

Shear strength - Residual binder; with Standard deviation
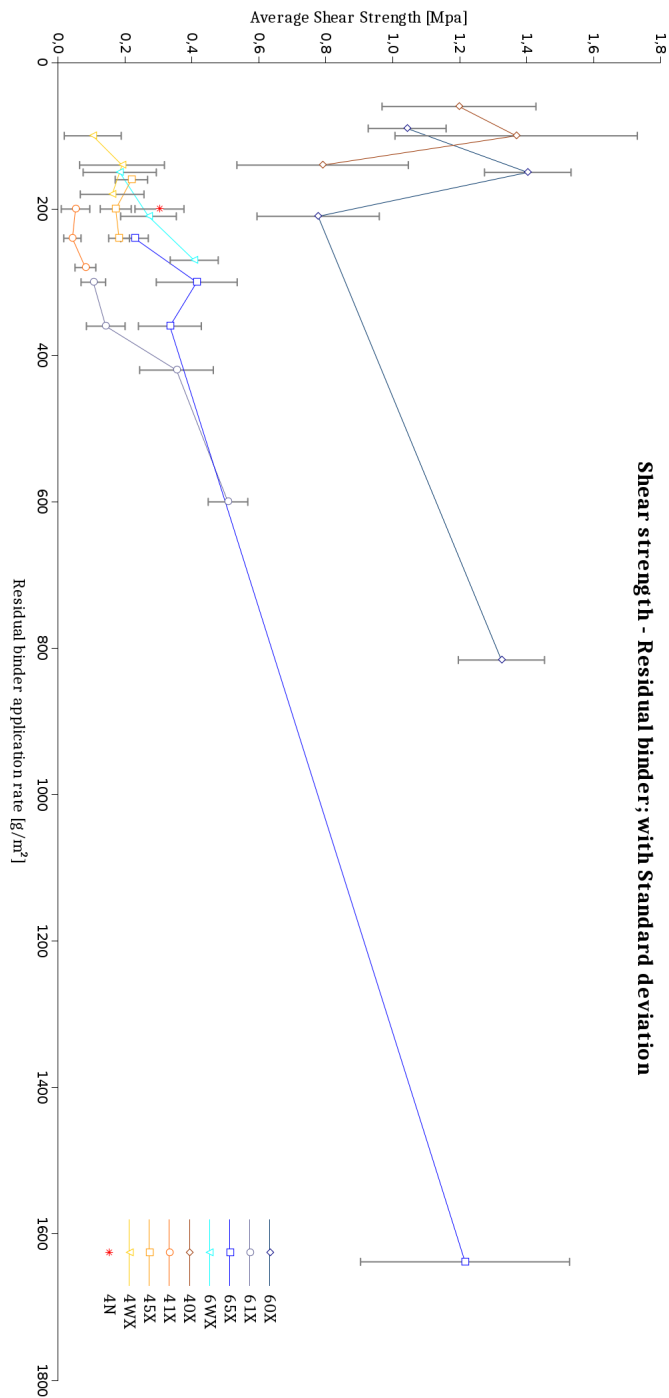
Shear strength results of all tested specimens. White rectangles: specimen not tested. Rectangles with X: Specimen broke during drilling

Shear Strength [MPa]

Average shear strength of all sections

Shear Strength [MPa]

Section	Average	Standard Dev.	Coef. of Var.
603	1.04	0.116	0.192
403	1.20	0.230	0.112
602	1.40	0.129	0.265
402	1.37	0.362	0.092
601	0.78	0.183	0.324
401	0.79	0.256	0.235
6W3	0.18	0.109	0.822
4W3	0.10	0.085	0.594
6W2	0.27	0.083	0.663
4W2	0.19	0.127	0.308
6W1	0.41	0.072	0.589
4W1	0.16	0.095	0.176
653	0.23	0.041	0.221
453	0.22	0.048	0.180
652	0.41	0.121	0.269
452	0.17	0.046	0.292
651	0.33	0.094	0.170
451	0.18	0.031	0.281
613	0.11	0.037	0.822
413	0.05	0.043	0.349
612	0.14	0.058	0.603
412	0.04	0.026	0.406
611	0.35	0.110	0.382
411	0.08	0.031	0.311

Section	Average	Standard Dev.	Coef. of Var.
610	0.51	0.059	0.117

Section	Average	Standard Deviation	Coefficient of Variation
650	1.22	0.312	0.257

Section	Average	Standard Dev.	Coef. of Var.
600	1.32	0.129	0.097

Section	Average	Standard Deviation	Coefficient of Variation
4N	0.30	0.073	0.242

Displacement until failure of all tested specimens. White rectangles: specimen not tested. Rectangles with X: Specimen broke during drilling

Displacement at failure [mm]

Average displacement until failure of all sections

Displacement at failure [mm]

Section	Average	Standard Dev.	Coef. of Var.
603	2,18	0,542	0,192
602	3,00	0,358	0,265
601	3,00	1,091	0,324
6W3	1,02	0,544	0,82
6W2	1,05	0,340	0,603
6W1	1,42	0,107	0,382
653	0,82	0,157	0,22
652	1,15	0,293	0,269
651	1,32	0,167	0,17
613	1,05	0,222	0,822
612	1,17	0,213	0,663
611	1,87	0,229	0,589

Section	Average	Standard Dev.	Coef. of Var.
403	1,85	0,541	0,112
402	2,20	0,785	0,092
401	1,30	0,346	0,235
4W3	2,19	2,241	0,594
4W2	0,70	0,294	0,308
4W1	0,74	0,444	0,176
453	0,78	0,146	0,18
452	0,76	0,185	0,292
451	1,08	0,453	0,281
413	0,73	0,094	0,0349
412	0,69	0,131	0,311
411	1,40	0,235	0,117

Legend boxes:

610		
Average	1,70	
Standard Dev.	0,276	
Coef. of Var.	0,162	

650		
Average	2,10	
Standard Deviation	0,206	
Coefficient of Variation	0,098	

600		
Average	2,73	
Standard Dev.	0,281	
Coef. of Var.	0,103	

4N		
Average	1,20	
Standard Deviation	0,238	
Coefficient of Variation	0,198	

Dirt contamination degrees of all tested specimens. White rectangles: specimen not tested. Rectangles with X: Specimen broke during drilling

Earth on the interface - Dirt contamination degree (0: No contamination, 3: Strong contamination)

Appendix III: Stiffness modulus: Test results

Two-layered specimens

Table VI.2.9: Result Moduli, -10 °C

Temp. : -10 °C	600			610			650		
Specimen number	1	2	3	1	2	3	1	2	3
Diameter [mm]	98.5	99	98.5	99	98.5	98.5	98.5	98.5	98.5
Heigth SC [mm]	43.5	51.5	47.5	45	47.5	45	52.5	47.5	48
Heigth BC [mm]	56	46.5	52.5	53.5	51.5	52.5	47	52	50.5
Length [mm]	90	88.5	89	98.5	91	102.5	94.5	96.5	98.5
10Hz E [MPa]	18,363	16,866	17,533	15,273	19,209	19,316	20,718	17,539	18,367
Average [MPa]		17,587			17,933			18,875	
Std. Dev. [MPa]		750			2304			1649	
Coef of Variation		0.0348			0.1049			0.0714	
5Hz E [MPa]	17,400	15,844	16,514	14,332	17,695	18,310	19,429	16,617	17,258
Average [MPa]		16,586			16,779			17,768	
Std. Dev. [MPa]		780			2141			1474	
Coef of Variation		0.0384			0.1042			0.0677	
1Hz E [MPa]	15,172	13,569	14,024	12,438	15,538	16,172	16,952	14,379	15,012
Average [MPa]		14,255			14,716			15,448	
Std. Dev. [MPa]		826			1998			1341	
Coef of Variation		0.0473			0.1109			0.0709	
0.1Hz E [MPa]	11,975	10,325	10,494	9,819	13,576	13,092	13,393	11,068	11,790
Average [MPa]		10,931			12,163			12,084	
Std. Dev. [MPa]		908			2044			1190	
Coef of Variation		0.0678			0.1372			0.0804	
10Hz E [MPa]	18,459	16,642	17,192	14,998	18,471	19,168	20,640	17,366	17,891
Average [MPa]		17,431			17,546			18,633	
Std. Dev. [MPa]		932			2234			1758	
Coef of Variation		0.0436			0.1040			0.0771	

Table VI.2.10: Result Moduli, 0°C

Temp. : 0 °C	600			610			650		
Specimen number	1	2	3	1	2	3	1	2	3
Diameter [mm]	99	99	98.5	99	98.5	99	98.5	99	98.5
Height SC [mm]	46.5	44.5	48.5	48	49.5	46.5	45.5	45.5	51.5
Height BC [mm]	52.5	53.5	50	50.5	50	52	53	54	48
Length [mm]	90	90.5	89.5	91.5	92.5	99	89	93.5	103.5
10Hz E [MPa]	12,632	14,670	14,790	10,812	14,001	12,545	14,991	14,337	13,874
Average [MPa]	14,031			12,453			14,401		
Std. Dev. [MPa]	1213			1597			561		
Coef of Variation	0.0706			0.1047			0.0318		
5Hz E [MPa]	10,961	13,373	12,897	9,656	12,535	11,369	13,469	13,403	12,238
Average [MPa]	12,410			11,187			13,036		
Std. Dev. [MPa]	1278			1448			692		
Coef of Variation	0.0841			0.1057			0.0434		
1Hz E [MPa]	8,658	10,922	10,315	7,819	10,169	8,941	10,538	10,886	9,604
Average [MPa]	9,965			8,976			10,343		
Std. Dev. [MPa]	1172			1175			663		
Coef of Variation	0.0960			0.1069			0.0523		
0.1Hz E [MPa]	5,787	7,655	7,014	5,198	7,180	6,038	6,910	7,529	6,364
Average [MPa]	6,819			6,138			6,934		
Std. Dev. [MPa]	949			995			583		
Coef of Variation	0.1137			0.1323			0.0686		
10Hz E [MPa]	11,208	13,660	13,697	10,190	13,298	11,771	14,256	14,101	13,176
Average [MPa]	12,855			11,753			13,844		
Std. Dev. [MPa]	1426			1554			584		
Coef of Variation	0.0906			0.1080			0.0345		

Table VI.2.11: Result Moduli, +10°C

Temp. : 10 °C	600			610				650		
Specimen number	1	2	3	1	2	3	4	1	2	3
Diameter [mm]	99	99	99	98.5	98.5	99	99	98.5	98.5	99
Height SC [mm]	49	49	49	46	46	44.5	49.5	45.5	53.5	49
Height BC [mm]	50	49.5	50	53.5	53.5	54.5	49	54	45.5	49.5
Length [mm]	90	89.5	89	102.5	102.5	104	95	99.5	95.5	107.5
10Hz E [MPa]	8,800	7,794	7,800	7,748	7,605	7,723	8,334	11,314	11,201	8,612
Average [MPa]	8,131			7,853				10,376		
Std. Dev. [MPa]	579			327				1528		
Coef of Variation	0.0581			0.0360				0.1203		
5Hz E [MPa]	7,741	6,600	6,793	6,818	6,772	6,540	6,796	9,434	9,561	7,535
Average [MPa]	7,045			6,732				8,843		
Std. Dev. [MPa]	611			129				1135		
Coef of Variation	0.0708			0.0166				0.1047		
1Hz E [MPa]	5,454	4,597	4,669	4,895	4,835	4,556	4,704	7,038	7,010	5,614
Average [MPa]	4,907			4,748				6,554		
Std. Dev. [MPa]	475			151				814		
Coef of Variation	0.0791			0.0275				0.1014		
0.1Hz E [MPa]	3,077	2,478	2,564	2,697	2,740	2,537	2,505	4,086	4,031	3,345
Average [MPa]	2,707			2,620				3,821		
Std. Dev. [MPa]	324			116				413		
Coef of Variation	0.0977			0.0383				0.0882		
10Hz E [MPa]	8,530	7,364	7,614	7,865	7,823	7,465	7,894	10,632	10,635	8,395
Average [MPa]	7,836			7,762				9,887		
Std. Dev. [MPa]	614			200				1292		
Coef of Variation	0.0640			0.0223				0.1067		

Table VI.2.12: Result Moduli, +20°C

Temp. : 20 °C		600			610				650			
Specimen number		1	2	3	1	2	3	4	1	2	3	4
Diameter [mm]		99	99	99	98.5	98.5	99	98.5	98.5	98.5	99	99
Height SC [mm]		51.5	53.5	48	40	47	46	44.5	44.5	50	45	47.5
Height BC [mm]		47.5	46	50.5	59	52.5	53.5	54.5	54	48.5	54.5	52.5
Length [mm]		90	90	90	95	94.5	103	99.5	88	99	88	90
10Hz	E [MPa]	4,174	3,906	4,663	6,493	6,202	4,836	6,736	4,990	4,607	5,765	5,621
Average [MPa]		4,248			6,067				5,246			
Std. Dev. [MPa]		384			849				543			
Coef of Variation		0.0738			0.1212				0.0896			
5Hz	E [MPa]	3,304	3,286	3,879	5,682	5,192	4,397	5,976	4,126	3,613	4,743	4,736
Average [MPa]		3,490			5,312				4,305			
Std. Dev. [MPa]		337			690				544			
Coef of Variation		0.0789			0.1125				0.1095			
1Hz	E [MPa]	2,110	1,979	2,519	3,621	3,384	2,893	3,973	2,587	2,215	3,014	3,055
Average [MPa]		2,203			3,468				2,718			
Std. Dev. [MPa]		282			453				396			
Coef of Variation		0.1045			0.1131				0.1264			
0.1Hz	E [MPa]	1,069	989	1,259	1,880	1,745	1,434	2,045	1,308	1,062	1,536	1,593
Average [MPa]		1,106			1,776				1,375			
Std. Dev. [MPa]		139			259				242			
Coef of Variation		0.1024			0.1264				0.1526			
10Hz	E [MPa]	4,123	3,843	4,704	6,781	5,976	5,500	6,766	5,009	4,523	5,612	5,660
Average [MPa]		4,223			6,256				5,201			
Std. Dev. [MPa]		439			629				540			
Coef of Variation		0.0849			0.0870				0.0900			

Unilayered specimens

Table VI.2.13: Result Moduli at -10 °C, surface and binder courses

Temp. : -10 °C		SC			BC	
Specimen number	1	2	3	1	2	3
Diameter [mm]	99	99	99	99	99	99
Length [mm]	55	65.6	74.5	52.5	49.5	59
10Hz E [MPa]	22913	22699	23271	18976	22049	24397
Average [MPa]		22961			21807	
Std. Dev [MPa]		289			2719	
Coef. of Var.		0.0126			0.1247	
5 Hz E [MPa]	21734	21346	21827	17378	20645	22804
Average [MPa]		21635			20276	
Std. Dev [MPa]		255			2732	
Coef. of Var.		0.0118			0.1347	
1 Hz E [MPa]	18628	18071	19153	14491	17687	19513
Average [MPa]		18617			17230	
Std. Dev [MPa]		541			2542	
Coef. of Var.		0.0291			0.1475	
0.1Hz E [MPa]	14394		15492	10635	13440	14967
Average [MPa]		14943			13014	
Std. Dev [MPa]		776			2197	
Coef. of Var.		0.0520			0.1688	
10Hz E [MPa]	22794	22387	23853	18044	22122	22946
Average [MPa]		23011			21038	
Std. Dev [MPa]		757			2625	
Coef. of Var.		0.0329			0.1248	

Table VI.2.14: Result moduli at 0 °C, surface and binder courses

Temp. : 0 °C		SC			BC	
Specimen number	1	2	3	1	2
Diameter [mm]	99.1	99	99	99	99
Length [mm]	56	63.7	63.5	42.5	40.5
10Hz E [MPa]	15985	18622	16037	14446	15275
Average [MPa]		16881			14860	
Std. Dev [MPa]		1508			586	
Coef. of Var.		0.0893			0.0395	
5 Hz E [MPa]	13961	13571	14039	12704	13344
Average [MPa]		13857			13024	
Std. Dev [MPa]		251			453	
Coef. of Var.		0.0181			0.0348	
1 Hz E [MPa]	11001	10613	10755	9372	10258
Average [MPa]		10790			9815	
Std. Dev [MPa]		196			626	
Coef. of Var.		0.0182			0.0639	
0.1Hz E [MPa]	7183	6946	7132	5650	6571
Average [MPa]		7087			6110	
Std. Dev [MPa]		125			651	
Coef. of Var.		0.0176			0.1066	
10Hz E [MPa]	15020	13963	14263	13634	14173
Average [MPa]		14415			13903	
Std. Dev [MPa]		545			381	
Coef. of Var.		0.0378			0.0274	

Table VI.2.15: Result moduli at 10 °C, surface and binder courses

Temp. : 10 °C		SC			BC		
Specimen number	1	2	3	1	2	3
Diameter [mm]	99	99	99	99	99	99
Length [mm]	48.2	71	45	47.5	76	43.5
10Hz E [MPa]	5040	11522	8230	10327	12571	12700
Average [MPa]		8264			11866	
Std. Dev [MPa]		3241			1334	
Coef. of Var.		0.3922			0.1124	
5 Hz E [MPa]	4026	9900	7149	7706	10873	11026
Average [MPa]		7025			9869	
Std. Dev [MPa]		2939			1874	
Coef. of Var.		0.4183			0.1899	
1 Hz E [MPa]	2752	7092	5191	6336	8013	7875
Average [MPa]		5012			7408	
Std. Dev [MPa]		2176			931	
Coef. of Var.		0.4340			0.1257	
0.1Hz E [MPa]	1502	4378	3274	3812	4668	4857
Average [MPa]		3051			4446	
Std. Dev [MPa]		1451			557	
Coef. of Var.		0.4754			0.1253	
10Hz E [MPa]	4122	10945	7654	10307	11527	12058
Average [MPa]		7574			11298	
Std. Dev [MPa]		3412			898	
Coef. of Var.		0.4505			0.0795	

Table VI.2.16: Result moduli at 20 °C, surface and binder courses

Temp. : 20 °C		SC			BC		
Specimen number	1	2	3	1	2	3
Diameter [mm]	99	99	99	99.1	99	99.2
Length [mm]	62.2	51.5	50	57	51	43
10Hz E [MPa]	6199	6656	6267	7313	7739	6150
Average [MPa]		6374			7067	
Std. Dev [MPa]		247			822	
Coef. of Var.		0.0387			0.1164	
5 Hz E [MPa]	5112	5870	5342	5953	6446	5167
Average [MPa]		5441			5855	
Std. Dev [MPa]		389			645	
Coef. of Var.		0.0714			0.1102	
1 Hz E [MPa]	3326	3838	3596	3958	4168	3301
Average [MPa]		3587			3809	
Std. Dev [MPa]		256			452	
Coef. of Var.		0.0714			0.1188	
0.1Hz E [MPa]	1637	1892	1926	2034	2030	1609
Average [MPa]		1818			1891	
Std. Dev [MPa]		158			244	
Coef. of Var.		0.0867			0.1290	
10Hz E [MPa]	5901	6285	5910	6766	7058	5703
Average [MPa]		6032			6509	
Std. Dev [MPa]		219			713	
Coef. of Var.		0.0363			0.1096	

Appendix IV: Fatigue: Pictures of the cores

Core 600: two-layered, without reinforcement
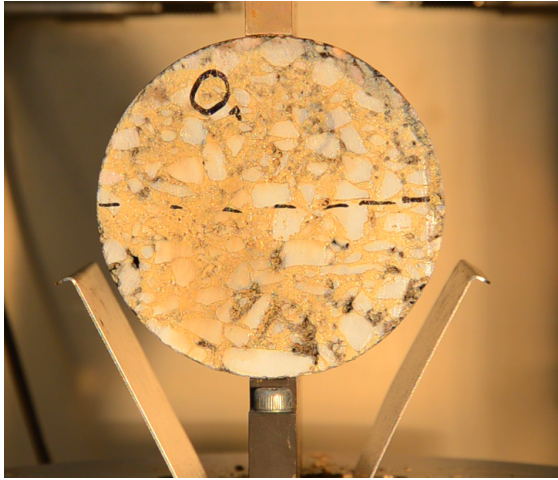
(a)600, 0 %
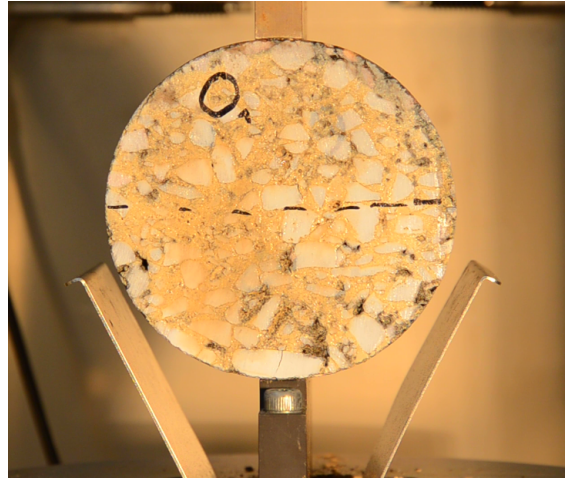
(b)600, 25 %
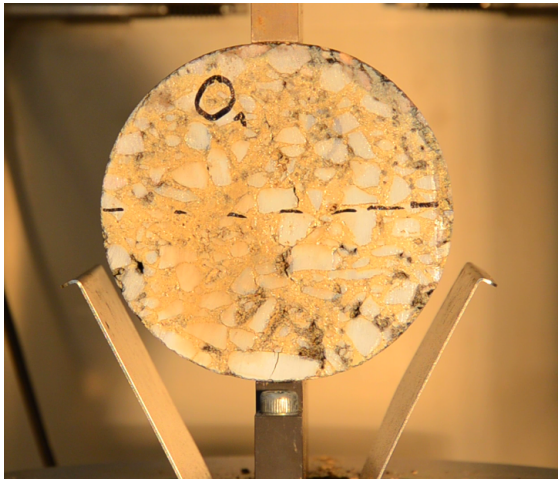
(c)600, 50 %
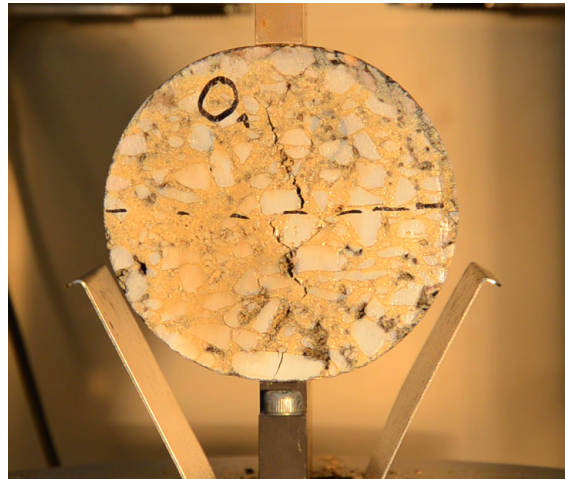
(d)600, 75 %
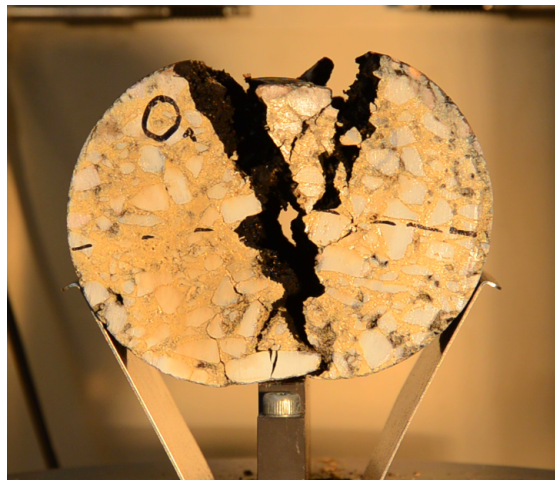
(e)600, 100 %

Core 610: two-layered, with reinforcement (Grid 1)
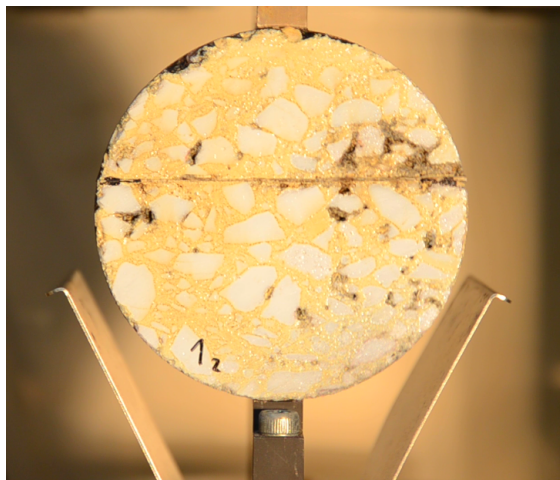
(a)610, 0 %
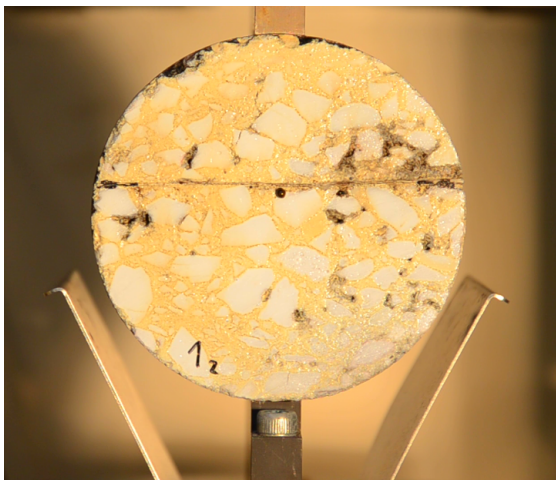
(b)610, 25 %
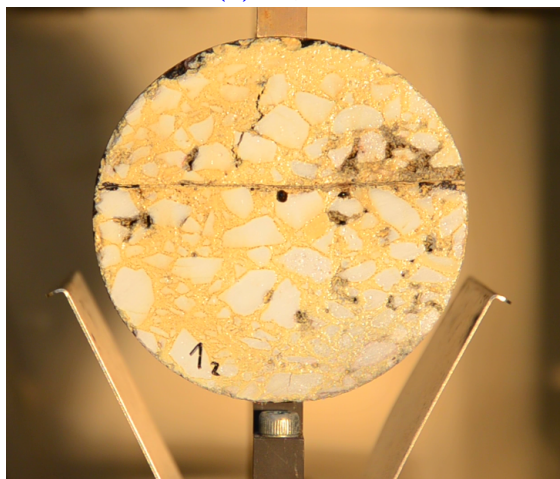
(c)610, 50 %
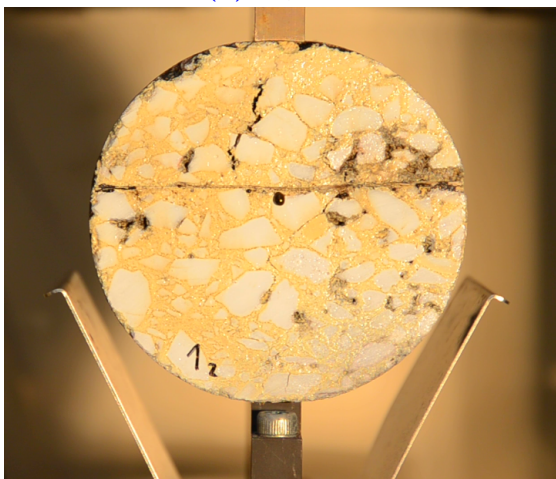
(d)610, 75 %
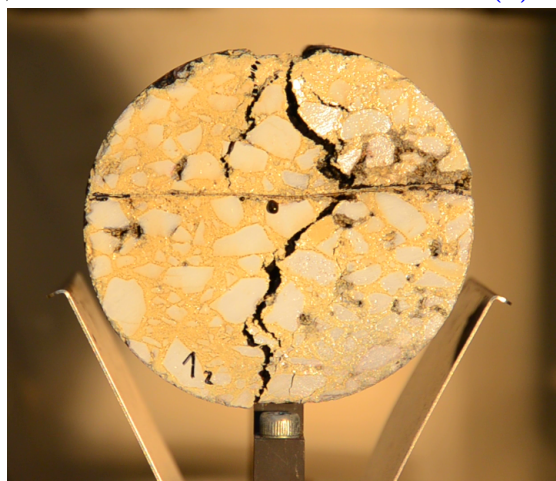
(e)610, 100 %

Core 650: two-layered, with reinforcement (Grid 1)
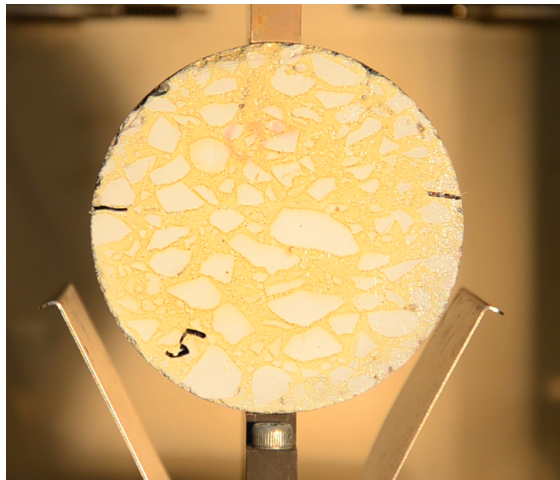
(a)650, 0 %
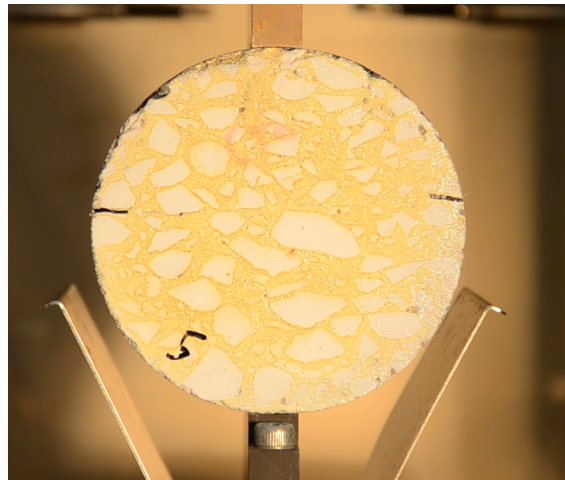
(b)650, 25 %
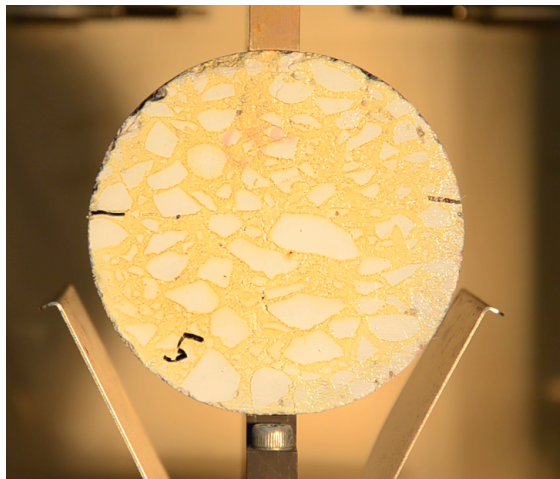
(c)650, 50 %
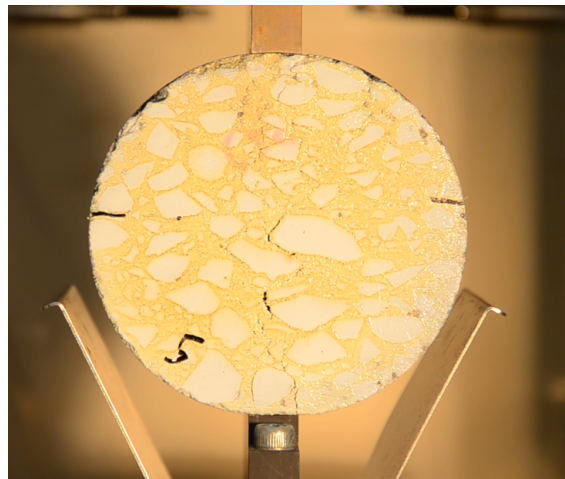
(d)650, 75 %
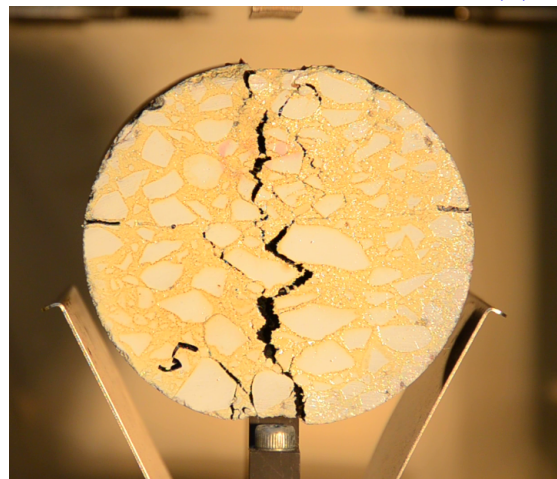
(e)650, 100 %

Core SC: Unilayered, upper layer of the test surface

(a)SC, 0 %
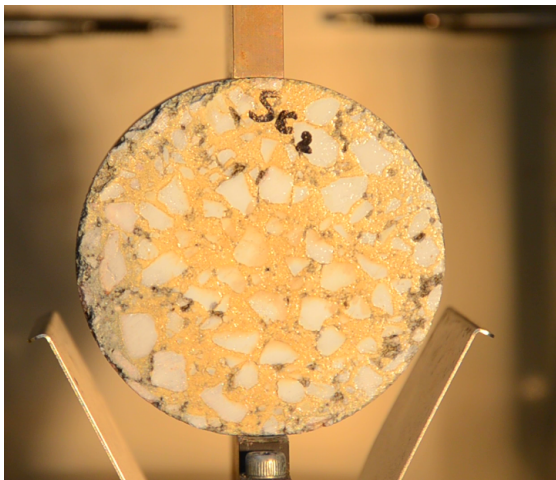
(b)SC, 25 %

(c)SC, 50 %

(d)SC, 75 %
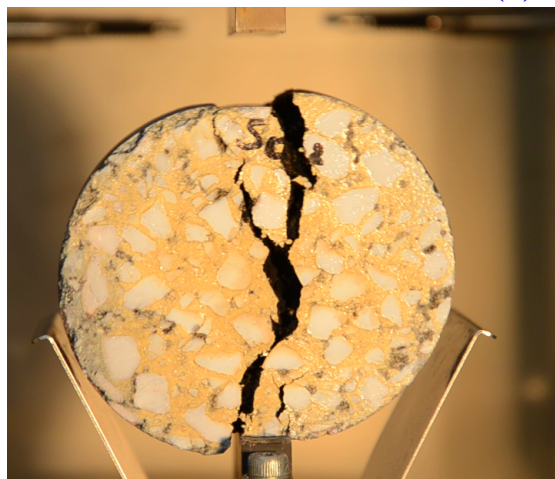
(e)SC, 100 %

Core BC: Unilayered, lower layer of the test surface
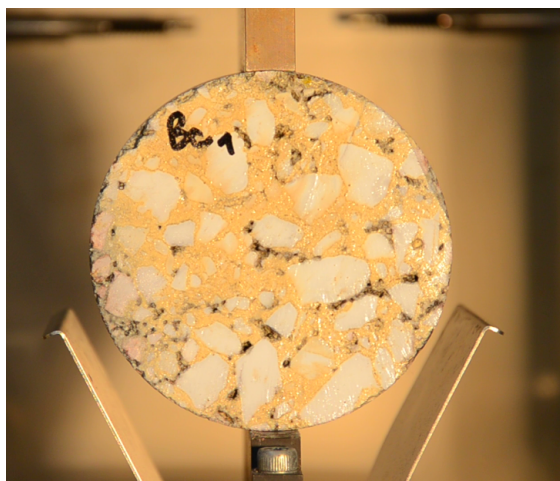
(a)BC, 0 %
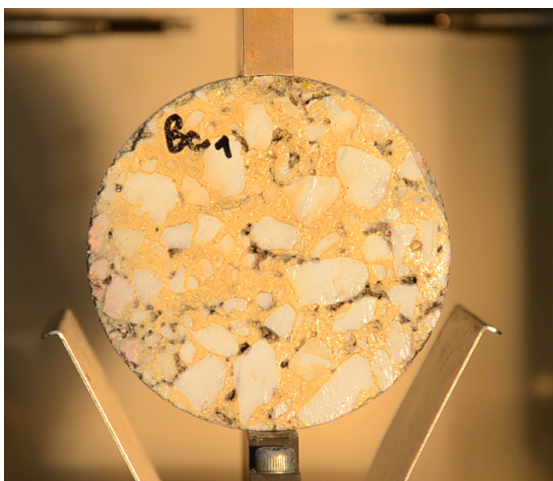
(b)BC, 25 %
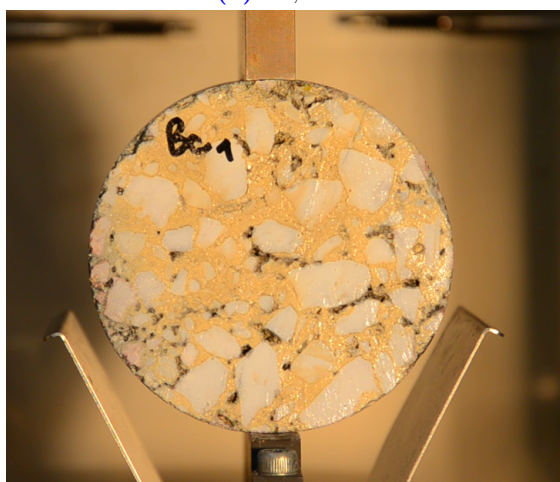
(c)BC, 50 %
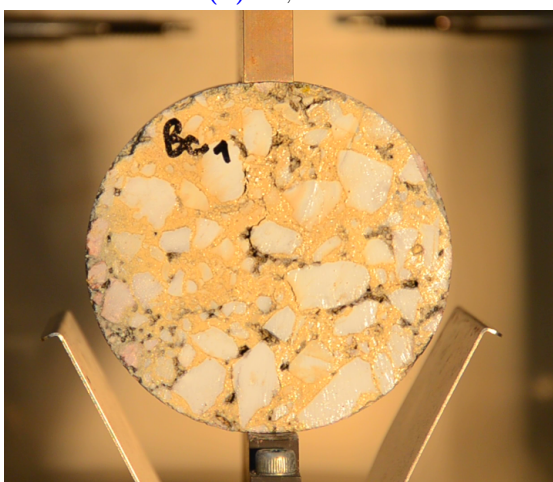
(d)BC, 75 %
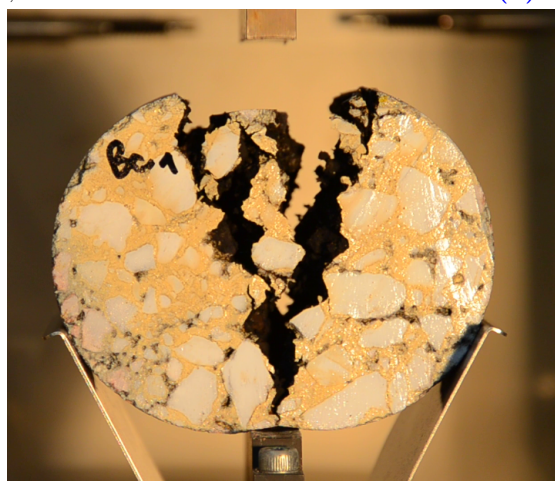
(e)BC, 100 %

Appendix V: RD4

Soil survey

Calcul of smaller surfaces for Leutner tests

Normally the shear strength resulting from the Leutner test is calculated by dividing the shear force through the surface of the core, while the surface is calculated by $A = \pi * r^2$. In our case, the stressed surface is smaller than for normal cores, as the shearing form cannot have continuous contact with the core.

Therefore the working surface was calculated depending on the diameter of the core as well as on the fracture displacement determined during the test. Figure VI.2.7 represents the working surface A of a core, consisting in a rectangle in the middle and a circle segment on each side. Its surface is calculated by means of:

$$A = A_R + 2 * A_C \tag{12}$$

With:

$\quad$ A: Working surface $[mm^2]$

$\quad$ A_R : Surface of the rectangle $[mm^2]$

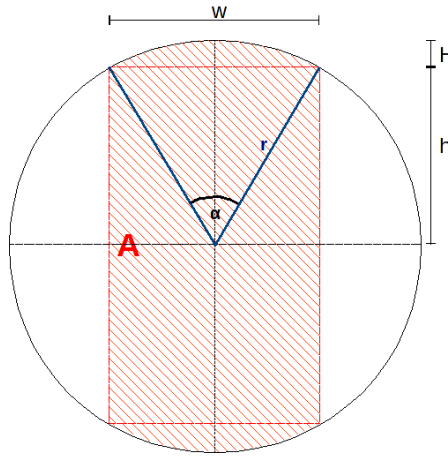$\quad$ A_C : Surface of the circle segment $[mm^2]$

Figure VI.2.7: Leutner: Calculation of the working surface A

$\quad$ The surface of the circle segment is calculated by means of:

$$A_C = \frac{r^2}{2} * \alpha - sin(\alpha) \tag{13}$$

With:

$\quad$ A_C : Surface of the circle segment $[mm^2]$

$\quad$ r: Radius of the core [mm]

α: Inscribed angle [rad]

The inscribed angle α is calculated by means of:

$$\alpha = 2 * arccos(1 - \frac{H}{r})$$ (14)

With:

α: Inscribed angle [rad]

r: Radius of the core [mm]

H: segment height [mm]

The segment height H is calculated by means of:

$$H = \frac{150}{2} - \frac{r}{2} + d$$ (15)

With:

H: segment height [mm]

r: Radius of the core [mm]

d: Displacement at break [mm]

The surface of the rectangle is calculated by means of:

$$A_R = 2 * (r - H) * w$$ (16)

With:

A_R : Surface of the rectangle $[mm^2]$

r: Radius of the core [mm]

H: segment height [mm]

w: Chord length [mm]

The chord length w is calculated by means of:

$$w = 2 * r * sin(\frac{\alpha}{2})$$ (17)

With:

w: Chord length [mm]

r: Radius of the core [mm]

α: Inscribed angle [rad]

Part VII
Résumée de la thèse en Francais

**Résumée de la thèse 'Experimental and numerical study of
the reinforcement of infrastructure by glass fibre grids'**

Étudiante: Loba Sagnol

Directeur de thèse : Cyrille Chazallon, INSA de Strasbourg, Markus
Stöckner, Hochschule Karlsruhe

Début : 01 septembre 2014, soutenance : 15 décembre 2017

1. Introduction

La construction et la réparation des infrastructures routières dans une optique de développement durable, se doivent de nos jours d'intégrer les problèmes de rareté future des matières premières tels que les produits dérivés du pétrole. Compte-tenu du patrimoine routier existant, la réparation est un enjeu majeur. Le vieillissement des infrastructures nécessite de développer des solutions abordables de ré-ingénierie écologique, qui vont permettre leur rénovation totale ou partielle, voire graduelle.

Les grilles, notamment en fibre de verre, constituent une solution performante, et économique pour le renforcement des chaussées bitumineuses, afin d'augmenter leur durée de vie et ralentir la remontée des fissures, tant en chaussées neuves, qu'en renforcement. Les grilles sont utilisées en tant que renfort, pour améliorer les performances en traction, et la résistance à la fissuration.

Cependant, l'utilisation de grilles signifie également une couche supplémentaire entre les deux couches en béton bitumineux. Cette couche supplémentaire peut affecter fortement la liaison entre les deux couches en béton bitumineux et conduire à un décollage. Une mauvaise liaison conduit à une mauvaise transmission des forces et des tensions introduites par le trafic à travers les couches, puisque chaque couche fonctionne comme une seule, plutôt qu'ensemble. En conséquence, des tensions peuvent apparaitre dans les parties inférieures et des compressions dans les parties supérieures des couches.

Des études faites sur les effets positifs des grilles en fibre de verre lors du renforcement des couches, la rétention de la propagation de fissures de réflexion et donc la prolongation de la durée de vie de la route, ainsi que sur les effets négatifs des grilles sur la liaison entre les différentes couches de la route, pouvant conduire à un raccourcissement de la durée de vie, sont les thèmes de cette thèse.

1.1 Chaussée routière : Matériaux et construction

Une structure routière est généralement composée de plusieurs couches, collées ensemble de façon a créer une unité complexe. Chaque couche a sa propre fonction, permettant à la structure de réduire les tensions et les contraintes induit par le trafic.

On différencie essentiellement entre les chaussées souples et rigides, les premières étant généralement construites avec des liants hydrauliques comme le ciment, les deuxièmes avec des liants bitumineux. Dans cette thèse, que les chaussées souples sont étudiées.

1.1.1 Chaussée souple en béton bitumineux

Les matériaux utilisés pour la construction de béton bitumineux sont :

1. Les granulats

2. Le bitume

Les granulats utilisés peuvent être classés en trois groupes, dépendant de leur taille : Gros granulats, allant d'un diamètre de 2 mm à un diamètre maximum de 45 mm, Agrégats fins, d'un diamètre de 0,063 mm à un diamètre de 2 mm, Fines, ou filler, ayant un diamètre inférieur à 0,063 mm.

La forme des granulats est importante pour la résistance contre la déformation d'une chaussée. Une forme angulaire apportera de meilleures résistances.

Le bitume utilisé est une mixture de différentes substances organiques, extraites pendant le reconditionnement de différents pétroles bruts. Ses propriétés viscoélastiques ainsi que sa dureté dépendes du pétrole utilisé.

Le bitume peut être modifié avec des polymères, par exemple des élastomères et des thermoplastiques.

1.1.2 Différentes couches de la chaussée

Une chaussée est constituée de plusieurs couches, comme représenté dans la figure VII.1.1.
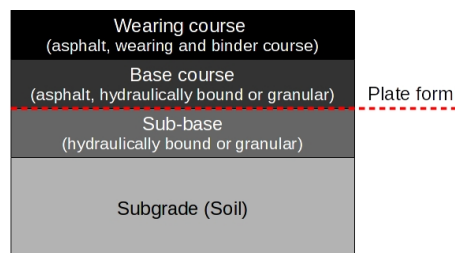

Figure VII.1.1: Chaussée constitué de plusieurs couches

La première couche est la couche de surface, qui sert de couche de roulement pour les véhicules. Cette couche a comme devoir d'assurer une bonne friction entre la surface de la route et les pneus des véhicules. Elle doit également empêcher l'infiltration d'eau de pluie dans la structure, être assez rigide pour empêcher la création d'ornières et avoir une pente de façon à ce que l'eau de pluie puisse s'écouler sur les côtés.

La deuxième couche, nommée couche de liaison, est construite pour des chaussées a fort trafic est doit assurer la transmission des contraintes de la couche de surface à la couche de base.

La couche de base est principalement responsable de la force de la structure. Sa tâche la plus importante est l'absorption de contraintes horizontales et verticales induits par le trafic. La couche de base peut être divisée en plusieurs couches dont les matériaux peuvent être liés avec différents liants, comme des liants hydrauliques ou bitumineux ou ne pas être liés du tout.

La couche de forme fait la transition entre la structure de la chaussée et la partie supérieure des terrassements. Son interface avec la couche de base est dénommées plate-forme de chaussée et a la fonction de répartir sur le sol les efforts dus au trafic.

1.2 Liaison entre les couches d'enrobées

La liaison entre les couches est d'une importance cruciale pour la transmission des tensions et des contraintes à travers la chaussée. Elle est constituée des trois facteurs majeurs : l'indentation, l'adhésion et la friction (voir figure VII.1.2).
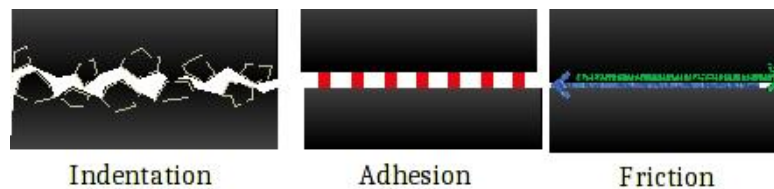

Figure VII.1.2: Facteurs de la liaison entre les couches

L'indentation décrit l'emboîtement entre les granulats de la couche du haut et de la couche du bas. Elle se crée pendant le compactage de la chaussée, pendant lequel les granulats de la couche du haut sont partiellement enfoncés dans la couche du bas.

L'adhésion dépend du type de liant bitumineux utilisé dans et entre les couches.

L'adhésion est particulièrement importante par temps froids, mais perd de son importance sous haute température, dû au ramollissement du bitume.

La friction a lieu entre les matériaux des deux couches et peut être gêné par un trop de bitume entre les couches.

1.3 Mécanisme d'endommagement et possibilité d'entretien.

Les causes d'endommagements les plus importantes sont :

- Le trafic (charges et mouvements)

- Les changements climatique (hivers/été)

- Le temps

Les endommagements pouvant apparaitre sont principalement des déformations dans la chaussée, visible en tant qu'orniérage, et la création de fissures dû à la fatigue.
La maintenance de la chaussée se fait majoritairement par le remplacement d'une ou de plusieurs couches de celle-ci, soit en ajoutant de nouvelles couches sur l'ancienne structure. Cependant, une structure ayant une couche de base fissurée montrera rapidement de nouveau signe de fissuration sur sa surface, nommé fissure de réflexion. L'utilisation de grille en fibre de verre posée entre l'ancienne structure fissurée et la nouvelle couche de surface permet de stopper la propagation des fissures de réflexions.

1.4 Grille en fibre de verre

Une grille en fibre de verre est un matériau composite fait d'une matrice, étant dans ce cas une résine, et d'un renfort, ici les fibres de verre. Le nouveau matériau composé de ses deux composants non-miscibles possède des propriétés que les composants seuls n'ont pas.
Les grilles en fibre de verre utilisées dans cette étude sont faites avec du verre type E ainsi qu'une résine thermodurcissable.
Elles sont installées sur la chaussée à l'aide d'un léger non-tissé positionné entre les fils de la grille . La grille a un maillage de 4 cm x 4 cm (voir figure VII.1.3).
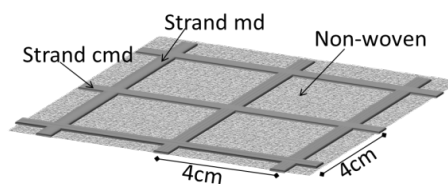

Figure VII.1.3: Croquis d'une grille en fibre de verre

2. Synthèse bibliographique

Les produits de renforcement comme les grilles en fibre de verre ont gagné en importance ces dernières années. Leurs avantages, surtout par rapport au ralentissement de la remonté des fissures et de leur effet positives sur la durée de vie d'une chaussée bitumineuse a été démontré dans différentes études [ARS 16][NGU 13][NEJ 14]. Néanmoins, il est également connu que les grilles entant que couche intermédiaire, peuvent aussi avoir un effet négatif sur la liaison entre les couches [VIS 12][SOK 07]. L'objet de cette thèse est l'étude des différents effets des grilles en fibre de verre sur la résistance au cisaillement, la fatigue et sur le comportement d'une section de route in-situ. La thèse a été basée sur trois piliers :

1. Les tests en laboratoire :

   Sur la liaison entre les couches, en utilisant un test de cisaillement du nom de Leutner

   Sur le module de rigidité d'éprouvettes renforcées et non renforcées

   Sur la fatigue d'éprouvettes renforcées et non renforcées

2. L'observation d'une route in-situ avant et après des travaux de maintenance

   Mesures des déflexions avant et après les travaux de maintenance

   Observation de la route pendant près d'un an et demi

3. Modélisation d'une structure renforcée basé sur les données de la route in-situ

3. Essais en laboratoire

Les éprouvettes utilisées pour les tests en laboratoire ont été extraites d'une surface d'essai extérieure à deux couches, construite juste pour ce but en Juin 2015 à Raststatt, Allemagne.

Cette structure consistait d'une couche inférieure AC 16 avec un bitume 25/55-55 RC et une couche supérieure AC 11 avec le même bitume est faisait 22 m de long et 5,8 m de large.

Au total, 24 interfaces différentes ont été construites, en utilisant deux émulsions différentes, trois à quatre taux d'application d'émulsion différents, 4 grilles (1, 5, W, N) et des sections de référence.

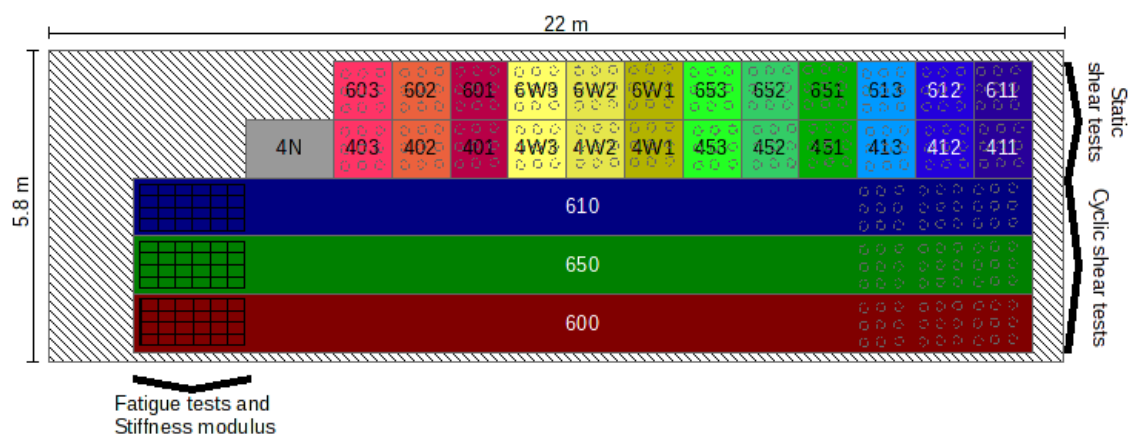La figure VII.3.4 montre le croquis de cette surface de test ainsi que les différentes sections.

Figure VII.3.4: Croquis de la surface de test

3.1 Détermination de la résistance au cisaillement

La détermination de la résistance au cisaillement a été effectuée sur toutes les variantes d'interface (24 variantes) avec le test Leutner , un test de cisaillement destructif impliquant le cisaillement d'une couche de l'échantillon avec un taux de déplacement constant de 50 mm/min tandis que l'autre couche est maintenue (voir figure VII.3.5).
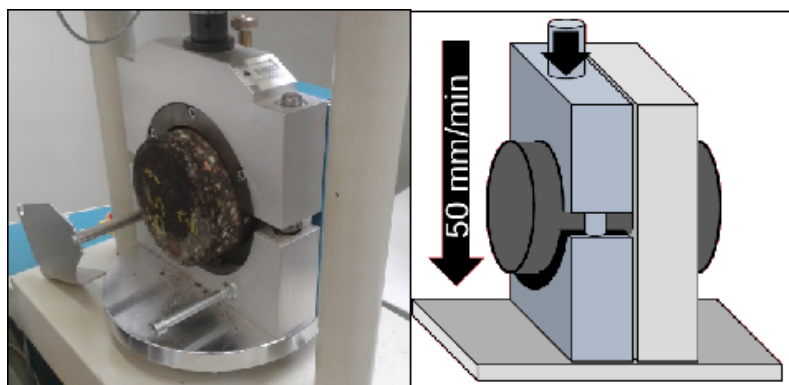
Figure VII.3.5: Essai Leutner

Il a été démontré que les essais sur éprouvettes non renforcées ont atteint des valeurs de résistance au cisaillement plus importantes que les éprouvettes renforcées.

Il a également été observé qu'en augmentant les taux d'application d'émulsion sur les éprouvettes renforcée, la résistance au cisaillement augmentée également, alors que les éprouvettes non-renforcée montre un premier pic pour un optimum d'émulsion, ensuite une perte en résistance et après un certain niveau d'émulsion de nouveau une augmentation de la résistance. Concernant le taux d'application d'émulsion, il a été observé qu'avec un taux d'application très élevé, une éprouvette renforcée était capable d'atteindre les même bonnes résistances que les éprouvette non-renforcée pour les taux d'application optimum.

De plus, il a été noté qu'un non-tissé entre les fils des grilles en fibre de verre, installé pour faciliter l'installation des grilles sur la chaussée, a une influence négative sur le collage et que les grilles ayant des fils avec une section plus hautes peuvent atteindre de plus grandes résistance au cisaillement.

3.2 Détermination du module de rigidité

La détermination du module de rigidité a été faite uniquement sur les éprouvettes renforcées avec la grille 1 et 5 et le taux d'émulsion le plus élevé ainsi que sur les sections de référence non renforcées également avec le taux d'émulsion le plus élevé. Le test utilisé est l'essai en traction indirecte, au cours duquel un échantillon cylindrique est soumis à une contrainte de compression cyclique sinusoïdale sur son plan diamétral vertical, ce qui provoque la rupture des éprouvettes par le biais du milieu dans la direction verticale (voir figure VII.3.6).

En ce qui concerne le module de rigidité, il a été démontré que les éprouvettes renforcées avec la grille 5 donnaient des résultats plus élevés pour des températures de - 20 °C à + 30 °C que les éprouvettes non renforcées. Il a également été observé qu'à basse
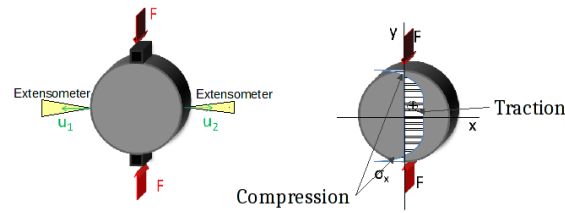
Figure VII.3.6: Essai en traction indirecte

température, l'influence de l'interface provoque un module de rigidité fortement affaiblie par rapport aux éprouvettes homogènes.

3.3 Détermination de la durée de vie en fatigue

La détermination de la durée de vie en fatigue a été faite uniquement sur les éprouvettes renforcées avec la grille 1 et 5 et le taux d'émulsion le plus élevé ainsi que sur les sections de référence non renforcées également avec le taux d'émulsion le plus élevé. Le test utilisé est l'essai en traction indirecte, comme pour la détermination du module de rigidité.

En ce qui concerne la durée de vie en fatigue, il a été démontré que les éprouvettes renforcées atteignaient une durée de vie plus longue que les éprouvettes non renforcées, mais que la différence dépend également de la température d'essai, étant plus constante pour 10 °C que pour 20 °C (voir figure **??**).

(a)(a)   **(b)**(b)
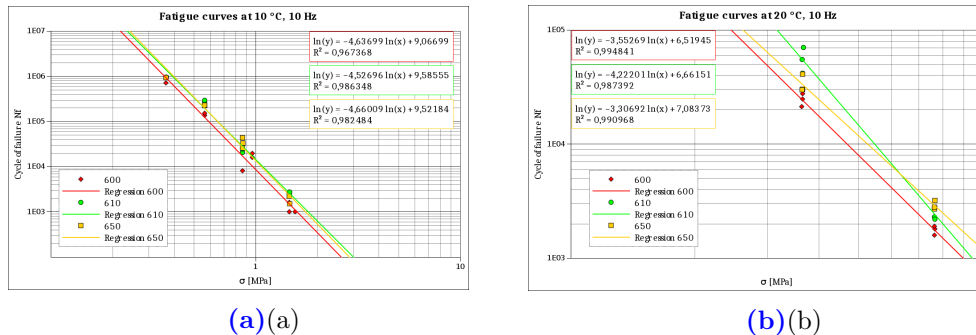
Figure VII.3.7: Courbe de fatigue à 10 °C (a) et 20 °C (b)

Les observations des essais en fatigue ont également montré une propagation différentes des fissures dans les éprouvettes.

Sur les éprouvettes non-renforcées les fissures se crée des deux côté de l'interface et se rejoignait au milieu, menant à la rupture de l'éprouvette en deux parties. Les éprouvettes non-renforcées montrait une fissure se formant pendant longtemps que sur un côté de l'éprouvette. A la fin de l'essai, les éprouvettes renforcées étaient encore tenues ensemble par les fils, même si la rupture était bien visible sur toute la hauteur.

4. Route in-situ

La route utilisée pour les observations est une section de la RD4, proche de Colmar, entre les villages Holtzwihr/Wickerschwihr et Muntzenheim, avec un trafic poids lourds de 300 par jour.

Des mesures de déflexions ont été faites avec une déflectographe Flash en 2015, avant que des travaux de maintenance est lieu sur cette route.

Les travaux de maintenacne comprenaient la construction d'une nouvelle couche de surface AC 10 sur l'ancienne structure routière. Quelques parties de la route ont été renforcées avec trois différentes grilles en fibre de verre sur lesquelles 4 cm de nouvelle couche de surface ont été posé ainsi que deux sections de référence non renforcées, construites avec 6 cm de nouvelle couche de surface (voir figure VII.4.8).
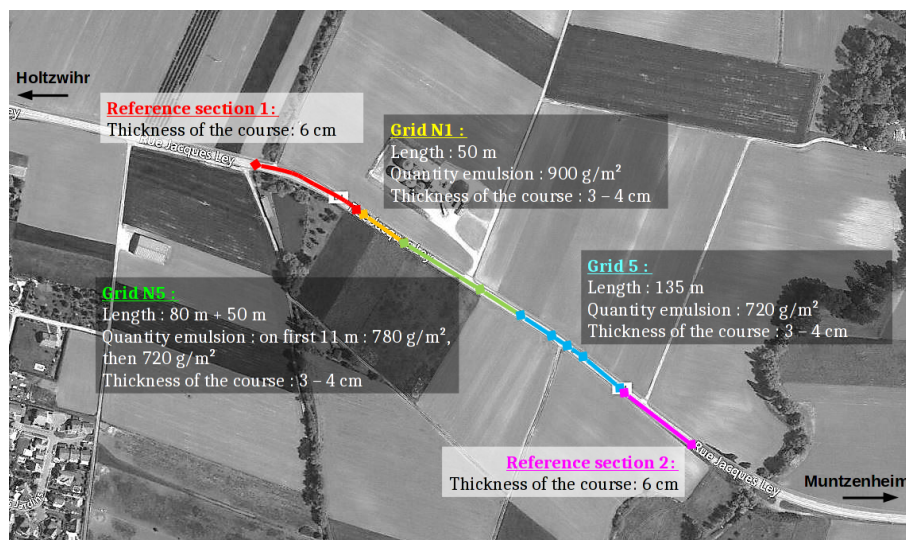

Figure VII.4.8: RD4 avec différentes sections

Les déflexions mesurées après les travaux de maintenance en 2016 à l'aide d'un déflectographe Lacroix ont montré une amélioration des déflexions sur toutes les parties de la route. Une distinction particulière d'une section, montrant que ses caractéristiques (par exemple, le renforcement) aient apporté une amélioration particulièrement bonne ou mauvaise par rapport à l'ancienne structure, n'a pas pu être observée.

La RD4 a été observé pendant un ans et demi. Après ce temps, la route ne montrait pas de fissuration.

Des éprouvettes ont été extraites de la RD4 avant et après les travaux, de façon à déterminer le module ainsi que les épaisseurs de chaque couche. Les modules ont était déterminés dans un laboratoire externe.

Ces valeurs ont ensuite été utilisées pour la modélisation de la structure.

4.1 Modélisation BISAR

Le programme BISAR ('BItumen Structure Analysis in Roads') est un programme utilisé pour calculer les contraintes, tension et déformation dans un système élastique et multi-couches.

La modélisation de la structure a été faites baser sur les propriétés connues de la RD4, c'est-à-dire :

- Le module de chaque couche sauf du macadam comme déterminer basé sur les essais de module (effectué dans un laboratoire externe)

- Le module du macadam en tant que 800 MPa (valeur empirique)

- Les hauteurs de chaque couche

- Les valeurs de déflexions mesurées avant et après les travaux de maintenance

La valeur du sol n'étant pas connue, la première modélisation a été une modélisation de calage, basé sur les modules et les hauteurs de chaque couche ainsi que les déflexions connues de la RD4 avant les travaux. Ici, les valeurs du sol pour chaque section ont été varié jusqu'à obtenir les déflexions mesurées.

La deuxième étape de modélisation a été la confirmation du modèle en ajoutant les valeurs de la nouvelle couche de surface sur les structures des sections non-renforcée de la route et de comparer les déflexions calculées avec les déflexions mesurées en 2016 sur les sections correspondante. Les différences entre les valeurs calculées et les valeurs mesurées se sont avérés très petites.

Dans une troisième étape, la même procédure a été effectuée avec les sections renforcées. La différence entre les valeurs calculées et les valeurs mesurées c'est avéré grandes. Les déflexions mesurées étant plus petites que les déflexions calculées, il en a été conclu que les grilles avaient un effet positif sur les déflexions.

Dans une quatrième étape, les meilleurs valeurs ainsi que les moins bonne valeurs ont été utilisé, de façon a ne pas juste comparer les valeurs moyennes mais aussi les meilleurs et moins bon scénario. Les résultats peuvent être vu dans la figure VII.4.9.
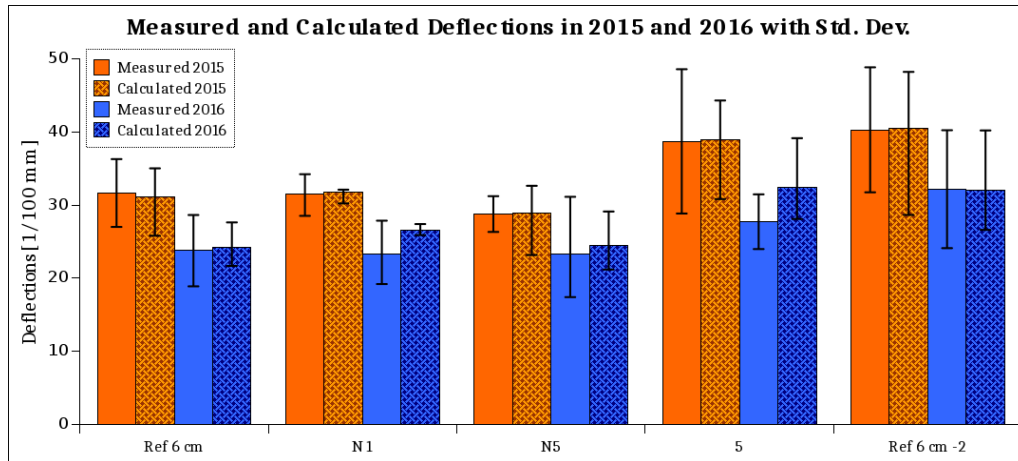
Figure VII.4.9: Resulats de la modélisation: orange: Valeurs de 2015, bleu: Valeurs de 2016

La section 5 montre les plus grandes différences.

Dans une cinquième étape, les modules et les hauteurs de la nouvelle couche de surface ont été augmenté jusqu'à ce que les résultats mesurés sur la RD4 soit atteint. Regardant le module de la nouvelle couche de surface, il a fallu l'augmenter de 370 % dans la section N1, de 88 % dans la section N5 et de 505 % das la seciton 5 afin d'atteindre les valeurs mesurées. Regardant la hauteur de la couche de surface, il a fallu l'augmenter de 85 % dans la section N1, de 37 % dans la section N5 et de 116 % dans la section 5.

5. Conclusion

Les tests en laboratoire ont montré un affaiblissement de la résistance de cisaillement pour les éprouvettes renforcées, mais également qu'en utilisant assez d'émulsion entre les couches, une résistance aussi bonne que sans grille pouvait être atteinte. Il a également pu être observé que la forme des grilles ainsi que l'utilisation d'un non-tissé avait une influence importante par rapport au cisaillement.

Les tests de module ont montrés une amélioration du module des éprouvettes renforcées par rapport aux éprouvettes non-renforcées quand la résistance aux cisaillement est la même. Il a également été observé que le comportement d'éprouvettes deux-couches est différentes que celui des éprouvettes uni-couches.

Les tests de fatigue ont montrés que l'insertion de grille augmenté la résistance de l'éprouvette. Il a également été observé que le comportement de rupture des éprouvettes est différentes selon si elles ont une grille ou non.

L'observation de la section de route RD4 entre Holtzwihr est Muntzenheim est la modélisation de cette section avec le programme BISAR ont montré que les déflexions de la route été plus petites sur les sections renforcées que ce qu'elle serait sans grille. Ainsi, il a pu être observé que les grilles ont une influence positive sur la déflexion de la route.